UNIVERSITY OF OKLAHOMA

GRADUATE COLLEGE

REAL TIME DISTRIBUTION NETWORK PROTECTION CONSIDERING THE IMPACT OF RENEWABLE ENERGY

A DISSERTATION

SUBMITTED TO THE GRADUATE FACULTY

in partial fulfillment of the requirements for the

Degree of

DOCTOR OF PHILOSOPHY

By

WANGHAO FEI
Norman, Oklahoma
2021

REAL TIME DISTRIBUTION NETWORK PROTECTION
CONSIDERING THE IMPACT OF RENEWABLE ENERGY

A DISSERTATION APPROVED FOR THE
SCHOOL OF ELECTRICAL AND COMPUTER ENGINEERING

BY THE COMMITTEE CONSISTING OF

Dr. Paul Moses, Chair

Dr. John Jiang, Co-Chair

Dr. Choon Yik Tang

Dr. Jie Cai

Dr. Chad Davis

Acknowledgements

Five years fly like a shuttle. The moment I finished this thesis, I had mixed feelings in my heart: both excited and grateful.

I wish to express my sincere gratitude to my research advisor, Professor Paul Moses, for teaching me a great deal of electrical engineering, for encouraging to explore and work in power system protection, for supporting me unconditional during all these years of graduate school and for being an excellent mentor. His support and leadership have been the primary contributing factors in my becoming the researcher that I am today. I am grateful for having had the opportunity to work with him.

I would like to express my deepest appreciation to Professor John Jiang for co-supervising my thesis and encouraging me to explore the topology identification method in the early stage of my PhD. His immense knowledge and plentiful experience have encouraged me in all the time of my academic research and daily life.

I would like to extend my gratitude to Professor Thordur Runolfsson who took me in as a PhD student at the beginning. Although he deceased last year, his rigorous academic attitude and profound knowledge of mathematical theory will and will always affect me.

I am especially indebted to my thesis committee members: Dr. Choon Yik

Tang, Dr. Chad Davis and Dr. Jie Cai. Without their guidance, I would not have made it.

I would like to thank my friends, lab mates, colleagues, research and administrative team in the Electrical and Computer Engineering Department at University of Oklahoma – Dr. Xin Li, Dr. Lihua Zhao, Dr. Qiushi Bo, Dr. Dhruv Sharma, Dr. Guomin Ji, Dr. Di Wu, Jonathan Devadason, Daniel Glover, Clint Keele, Stephanie Gill, Abe Hartley, Lisa Wilkins and Emily Barrios for a cherished time spent together in the lab, office and in social settings.

I would like to give my special gratitude to my uncle Dr. Yuelong Wang. It was him who encouraged me to pursue a PhD back in 2014 when I could never imagine about the moment I make it.

Finally, I am deeply grateful to my mom Zhengyan Wang. She only had a middle school diploma. However she always does her best to make my life better and receive a better education. Without her support, I would not be able to achieve what I am today.

Contents

List of Figures

List of Tables

Abstract

To achieve the net-zero carbon dioxide emissions goal, the penetration rate of distributed energy resources has been increasing in modern power distribution networks for the past decade. Although these energy resources are environmentally friendly, they raise challenges for distribution network protection. Distribution networks are typically designed based on the single power flow direction principle, where power is flowing from the substation transformer to the load following a tree-like topology. In this way, power lines that are closer to the substation may have higher current flows. For distribution network feeder protection, particularly overcurrent relays, coordination is achieved based on the above principle, such that the downstream power lines closer to the fault have equal or higher level of fault currents compared to the upstream power lines.

With distributed energy resources, the distribution network can work in either grid connected mode as is most common or islanded mode as in emerging microgrids. This indicates that the electrical topology of the distribution network can be changed in real time. Moreover, when a fault happens, the downstream relay can see higher level of fault current compared to the upstream relay, causing malfunctions of the relay, such as blinding or sympathetic tripping.

The main focus of this thesis is on the development and the implementation of a new current tracing decomposition method to address the above issues. Specifically, a very detailed grid model is proposed, which has sufficient information of the current flows both from each distributed energy source to the power lines and between each distributed energy source and loads.

With the results of the current flow information from the current tracing method, this research highlights the implementation of machine learning for fault

current identification. Specifically, the current tracing method is taken as the kernel function that can be used to improve the performance of the support vector machine for the detection of low level faults that may be below the sensitivity of conventional overcurrent relays in the presence of DERs.

This research also highlights the implementation of the new current tracing method on primary and backup protection schemes in distribution feeders. Specifically, decomposed currents are used as a substitute of the measurement currents to better coordinate the upstream and downstream relays. To demonstrate the effectiveness of the proposed method, the current tracing method is implemented in a Matlab-Simulink platform and imported to EMTP-MATLAB simulation interface. The simulation results show that using the decomposed current can improve the sensitivity and dependability of primary and backup protection in the presence of multiple DERs. It can also address the issue of protection relay blinding caused by the injection of distributed energy resources.

Chapter 1

Introduction

The past few decades have witnessed a growing number of distributed energy resources (DER) penetrating into the customer side, which has caused distribution grids to evolve into large, complex and interconnected networks. While these changes have made positive impacts to the sustainability of energy and helped in reducing the emission of greenhouse gases, they also present new challenges to the protection of distribution networks that have been working stably for more than 100 years.

One of the major challenges caused by the penetration of DERs into electricity grids is that, although the geographic topology of the power system is not changing, the electrical topology is changing dynamically due to the irregular changing of the DERs power injection. For example, the distribution network which operates under the current topology may switch to the other topologies due to the operating conditions and performance requirements. These complex electrical typologies are often not fixed, but subject to different factors such as environment and weather, for example, hot temperature, thunder storm, sleet storm, etc. Customer habits can also contribute to the topology change [1]. Such dynamic

change of distribution networks' topology disrupts the normally designed protection relay tripping sequence in feeders where the topology is unknown for each individual relay with limited local metering information.

At the other end of the spectrum, the conventional relay coordination strategy is designed to accommodate the traditional distribution networks which originally was intended to support feeder overcurrent protection for single direction power flow from the upstream substation to the downstream customer. With the rising amount of distributed and intermittent DERs, bidirectional power flow is introduced to the distribution networks. Currents may flow in either direction at any time. In addition, the current magnitude is also affected by the injection of DERs. This increases the likelihood of disrupting the protection relay tripping sequence as the upstream usually requires higher tripping current thresholds and longer time delays for backup coordination with downstream protection elements.

The accepted approach of feeder protection schemes is to isolate only the faulty sections, while leaving the majority of the healthy parts of the network still functioning. Investigating protection schemes in such complex networks requires a strong understanding of the interaction of different irregular and intermittent DERs through the dynamically changed distribution grids topology.

Given the requirement of designing protection schemes described above, the overarching goals of this thesis are initially to estimate the distribution networks' topology in real time considering the individual DER source and substation interactive contributions to the fault current. With the estimated topology information, a very detailed current tracing model is developed to decompose the current flow between different DERs and loads connected through the same power line. As a result, each protection relay on the distribution feeder typically has the information of current magnitude flowing between these DERs and loads. Pro-

tection schemes are then devised based on the newly proposed decomposed traced current flow information.

1.1 Motivation

The impact of DERs to the distribution grids has received a fair amount of attention in power system protection studies, especially in the aspect of bidirectional power flow from DERs such as solar photovoltaic farms and rooftop panels. The distribution network may also be reconfigured with sectional switches to modify its topology for improving performance. For example, it has been shown that the network may be reconfigured to cause the distribution transformers to electrically be relocated more centrally with respect to the loads to prevent higher line losses [2]. In addition, reverse power flow can lower the fault current detected by the upstream current transformer (CT) and corresponding protection relay [3]. If a wire is shorted to ground in the right conditions of reverse power flow, the protection system may not see the downed wire and so it remains in the ground fully energized and a hazard to the public.

One other uncertainty is the contribution of the inverter based DERs to the fault current. Due to the overload handling characteristic of inverters, for example, the fault current limiter [4, 5] and blocking the inverter [6], currents coming from DERs are much less than normal fault currents, but still contribute to the fault. High penetration of inverters may cause issues of blinding of protection relays from seeing a fault, sympathetic tripping for faults not within a relay's intended zone of operation, unintentional islanding and fuse-recloser miscoordination [7].

Reclosers, relays and other protection equipment may fail to protect distri-

bution feeders against the above changes and need to be readjusted to handle these changes [8, 9]. Proper planning and interconnection studies can provide an alternative way to partly fix these issues [10, 11] before they become problems. However, this is not practical for an already established distribution system where the location of DERs is installed on an ad-hoc basis.

Most of these problems can be addressed or partly remedied only in a case by case scenario. For example, the protection relay settings should be adjusted every time the topology is changed or the reverse power flow happens [12]. However, stringent reliability standards and regulations make it difficult to change protective relay settings easily and requires significant approval processes and protection coordination checks. Different types of protection relays also apply to particular schemes. The economics of the investment in protection system play a significant factor, which in many cases even outweigh the capital costs of the power being generated over the life of the generator.

Given the situation, a new general topological model which can accommodate the impact caused by the variable injection of DERs to distribution grids is proposed. This model should not only be easily integrated into different relays' processing algorithms, but also establish the connection between these relays while DERs are injected into the distribution network even though the DERs contribution to the fault current is weak.

1.2 Objective of the Work

The thesis is mainly focused on developing advanced models for relay coordination considering the impact of DERs on a distribution level power grid. Specifically, the study concentrates on the over current relay coordination issue under the im-

pact of DERs since the DERs may also contribute to the fault current. Thus the main objective is to develop a method for identifying the contribution of DERs, loads and the substation to different types of faults without additional relaying measurement points. To achieve this objective, for the first time, a decompositional current tracing method is proposed for application in overcurrent feeder protection relaying. This methods highlights the active and reactive current contributions of DERs, loads and the substation on their connected distribution lines. Therefore, in this research, one of the assumptions is that current, voltage and line impedance meter data can be obtained in real time, which can be achieved through the data concentrator system in wide area protection [13]. Once the contribution of the fault current on the distribution line are traced through the proposed method, the primary protection scheme of the distribution line can be established by either setting up the tripping threshold of the fault current contribution or using a machine learning method to identify the fault [14].

Another objective is in the area of backup protection scheme design. In this research, the distribution networks' topology is assumed to remained the same. Thus, the over current relay coordination is mainly how the backup protection relay reacts to the fault current when the primary protection relay fails to react to the same fault in a fixed topology distribution feeder. The backup protection scheme can be affected by higher penetration of DERs, causing problems like blinding of protection and sympathetic tripping, etc. This is illustrated with and without the proposed current tracing method. The application of current tracing in solving the blinding of protection relays is the main focus of this thesis.

Further results of the application of current tracing method in protection schemes are presented. These applications demonstrate the advantages of using current tracing over traditional overcurrent relaying in distribution power system

protection under the penetration of DERs.

This thesis is organized as follows: A literature review of current research in the area of feeder protection is provided in Chapter 2. Chapter 3 describes the known impacts of DERs to distribution networks protection. Chapter 4 describes the theoretical development of the proposed current tracing method. Chapter 5 demonstrates simulation results of the proposed current tracing method applied to distribution networks' primary protection. Chapter 6 introduces the application of current tracing method on distribution networks' backup protection. Conclusions are made in Chapter 7 along with future work.

1.3 Publications

Some results of this thesis have already been published and the details are given below.

[1] Fei, Wanghao, Paul Moses, and Chad Davis. "Identification of Smart Grid Attacks via State Vector Estimator and Support Vector Machine Methods." In 2020 Intermountain Engineering, Technology and Computing (IETC), pp. 1-6. IEEE, 2020.

[2] Fei, Wanghao, and Paul Moses. "Fault current tracing and identification via machine learning considering distributed energy resources in distribution networks." Energies 12, no. 22 (2019): 4333.

[3] Fei, Wanghao, and Paul Moses. "Modeling power distribution grids through current tracing method." In 2019 IEEE 7th International Conference on Smart Energy Grid Engineering (SEGE), pp. 196-200. IEEE, 2019.

[4] Ji, Guomin, Dhruv Sharma, Wanghao Fei, Di Wu, and John N. Jiang. "A Graph-theoretic Method for Identification of Electric Power Distribution System Topology." In 2019 1st Global Power, Energy and Communication Conference (GPECOM), pp. 403-407. IEEE, 2019.

[5] Fei, Wanghao, John N. Jiang, and Di Wu. "Impacts of modeling errors and randomness on topology identification of electric distribution network." In 2018 IEEE International Conference on Probabilistic Methods Applied to Power Systems (PMAPS), pp. 1-6. IEEE, 2018.

Some results that are not directly related to this thesis but published during the PhD. The details are given below.

[6] Devadason, Jonathan, Paul Moses, and Wanghao Fei. "Bifurcation analysis of weak electrical grids considering different load representations." In 2019 IEEE 7th International Conference on Smart Energy Grid Engineering (SEGE), pp. 208-212. IEEE, 2019.

[7] Aravinthan, Visvakumar, Thanatheepan Balachandran, Mohammed Ben-Idris, Wanghao Fei, Mohammad Heidari-Kapourchali, Anton Hettiarachchige-Don, John N. Jiang et al. "Reliability modeling considerations for emerging cyber-physical power systems." In 2018 IEEE International Conference on Probabilistic Methods Applied to Power Systems (PMAPS), pp. 1-7. IEEE, 2018.

[8] Sharma, Dhruv, Guomin Ji, Wanghao Fei, Di Wu, Paul Moses, and John N. Jiang. "Electric circuit foundation of structural analysis for power systems from a network perspective." (2018): 84-5.

[9] Fei, Wanghao, Guomin Ji, Dhruv Sharma, and John N. Jiang. "A new traveling wave representation for propagation of energy transients in power lines from a quantum perspective." In 2018 North American Power Symposium (NAPS), pp. 1-6. IEEE, 2018.

Chapter 2

A Critical Review of Existing Power System Protection Technologies

2.1 Overview

Power system protection has been an active research topic since the commercialization of electricity. Previously, researchers have proposed many methods to deal with various power system protection issues. In [15], a transmission line distance protection scheme was proposed using the communication aided method to mitigate the impact of series capacitor and adjacent lines such as the increased voltage. A unit protection scheme was proposed using the superimposed current for fault current detection [16]. This method provides improved performance for DC micro grid protection. To speed up the tripping of the second zone protection of the distance relay, an accelerated trip scheme was proposed based on the variations of the sequence currents and voltages caused by the faults [17].

This method can increase the sensitivity, avoid improper operation and alleviate the communication barrier. In [18], an overcurrent protection strategy was proposed considering the impact of DERs and fault current limiters (FCLs). In this method, each IED can calculate its own fault index, thus the fault location can be identified following the decision tree.

Traveling wave based method is another way to deal with the protection problem [19, 20, 21]. This method is proposed based on the fact that a fault would generate traveling waves (current and voltage) that propagate from the fault position to the busbar along the transmission line [22]. When the traveling wave impedance changes, it will get reflected and refracted. If a reference point is selected, the transient voltage and current could therefore be calculated according to the telegraph equations [23].

Wide area protection is becoming a popular topic in the past decades. It is used to save the system from a blackout or brownout when the system is in normal operational conditions such that no particular equipment is faulted or operated over its limitations[24]. The wide area protection is developed based on modern sensors or transducers, for example phasor measurement units (PMUs), along with a data concentrator [13], for example energy management system (EMS), such that a system wide communication infrastructure is established as shown in Fig. 2.1.

Such communication infrastructure is integrated with the traditional self contained protection system which can obtain real-time synchronized measurement data provided by GPS[13].

Transmission and distribution networks protection are usually handled differently. Distribution network tends to focus mainly on overcurrent protection, however, some technologies could potentially cross between transmission and dis-

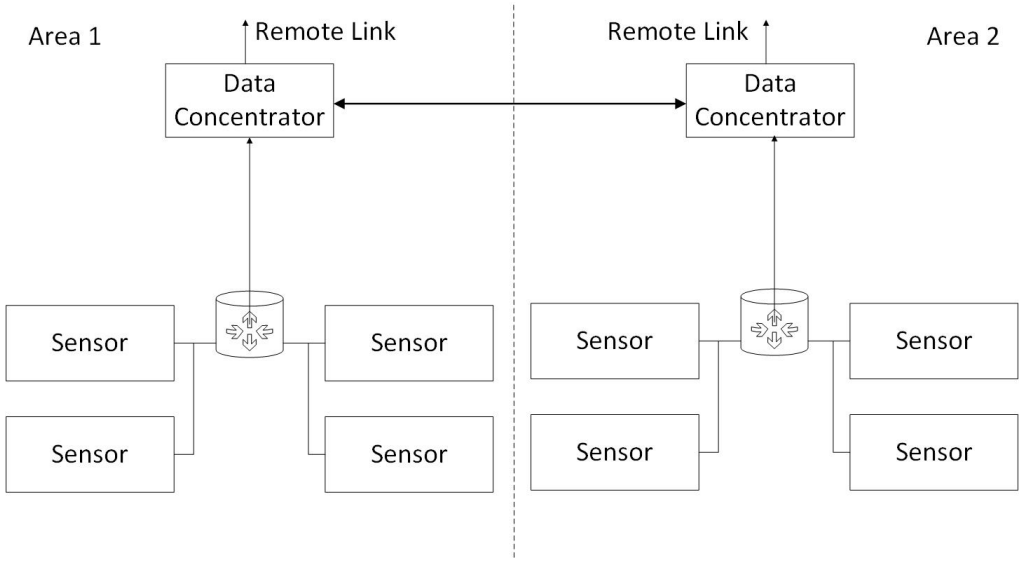

Figure 2.1: Substation data concentrator and sensor network.

tribution.

For distribution feeder protection without DERs, fuses and conventional reclosers are the two commonly used protection devices. They do not have directional features, but modern digital relays do [25]. Furthermore, it is economically impractical to replace all the fuses and conventional reclosers with advanced digital relays. However, it is still practical to use digital relays in medium voltage (MV) distribution protection. In a system that uses fuses, if a fault happens, replacing fuses would require extensive equipment outage times [26], which will impact more customers. With digital relay, the breaker can be reset through the EMS automatically.

Power distribution network protection schemes are continuously being challenged by the highly distributed and stochastic DERs. With the benefits of the communication infrastructure provided by wide area protection, energy contributions from DERs could be measured more accurately through PMU compared to SCADA system [27]. More data are available when a fault happens to assist

in making relay tripping decisions. In the light of that, many researchers have proposed more advanced protection schemes.

2.2 Implementation of Machine Learning in Distribution Network Protection

Since more data are available through PMU or any advanced meter infrastructure, advanced algorithms such as machine learning or deep learning can be implemented in power system protection for fault identification[28, 29]. In [30], a spatiotemporal patterns based machine learning method is proposed. This method uses the graph Laplacian to recognize the spatiotemporal patterns based on system wide measurements against cyber attacks. In [31], a Support Vector Machine embedded Layered Decision Tree based anomaly detection and adaptive load rejection within the set-up of multi-agent system integrity protection was investigated. Furthermore, this method does not rely on wide area communication, but data sets are still available for decentralized agents. A least square support vector machine Bayesian network decision tree is proposed in [32]. This method can be used to fill the missing meter data as well as improve the detection accuracy of relay protection.

Most of the machine learning based methods for power system protection are focusing on combining different machine learning algorithms and adjusting hyperparameters such as detecting a fault signature [33], improving the fault detection accuracy [34, 35], taking advantage of the advanced meter infrastructure and predicting the potential of faults [36] for the primary side protection.

Very limited research has focused on exploring insights from meter data and

finding the physical meaning from the kernel data. The difficulty also lies in the coordination of the primary and the back-up protection when it comes to power system planning and operation.

2.3 Distribution Network Protection Schemes

There are many different protection devices that are installed to protect particular equipment and components. Various protection schemes are embedded in these protection devices, each of them is suitable for a particular application and every type has some advantages over the other. The primary protection schemes along with the apparatus they are protecting are summarized in Table 2.1.

Table 2.1: Summary of the Primary Protection Schemes

Apparatus	Overcurrent	Directional	Differential	Distance
Alternator	0	1	1	1
Busbar	0	0	1	0
Transformer	0	0	1	0
Power Line	1	1	0	1
Large Induction Motor	1	0	1	0

In Table 2.1, "1" represents the corresponding protection scheme is suitable for the apparatus. Alternatively, "0" means that the protection scheme might not be a good fit for the apparatus. Sometimes, two protection schemes can be embedded into the same protection devices. For example, the "SEL 421 Protection, Automation, and Control System" has both the distance and overcurrent protection schemes. In the rest of the thesis, it is assumed that one primary protection device has only one protection scheme.

At the other end of the spectrum, backup protection scheme is invented to provide an extra layer of protection to the primary protection, particularly for

the overcurrent and the distance protection. Typically, the backup of these two protection schemes are realized through the inverse time overcurrent protection [37] and time stepped distance protection [38], respectively.

A good relay backup protection scheme should consider the impact caused by the injection of DERs, including the bidirectional flow and the lower sensitivity of the protection system.

Using adaptive protection schemes is one of the solutions proposed in literature to alleviate the impact of injection of DERs [39, 40]. In such methods, relay settings must be updated with the change of the distribution feeder status and usually includes the shifting of inverse definite minimum time (IDMT) curve to deal with the change of fault current [41]. In this way, the coordination between relays can be maintained. However, when the system becomes more complicated, there is little room for the relays to shift the IDMT curve as the shifting of the IDMT of one relay would disrupt the coordination with the other adjacent relays.

In [39], the relay setting is set to be adaptive based on all down-stream relays' pick up time and identify the status of the relay that picked up. A wide area backup protection scheme is proposed in [42]. This method defines the backup protection zones of the subsets of lines and buses which has a significant zero- and/or positive-sequence. Linear least squares method is then used to determine the faulted line and location using the current and the voltage phasors. An innovative hardware-in-the-loop adaptive protection scheme is presented in [43]. This method provides a continuously tuned protection scheme to the variable system operating modes. In [44], an adaptive multi-stage definite time over current protection scheme for ungrounded distribution systems with DERs is presented based on optimized thevenin equivalent parameters estimation. A centralized adaptive protection scheme is proposed in [45] to deal with the communication

system failures between relays. It provides optimal relays settings for varying operating conditions of the distribution networks with DERs.

Sometimes, the fault current cannot be seen by the measurement current transformers (CTs), particularly when the DERs are injecting into the grid. Furthermore, the backup protection relays cannot see as much fault current and may not trip for a failure in the primary protection. In addition, when the system becomes more complicated, there is little room for the relays to change their settings adaptively as it would disrupt the coordination with the other adjacent relays. There is not a fixed way to adjust all the relays adaptively using the same manner.

Chapter 3

Impact of Distributed Energy Resources to Distribution Grid Protection

3.1 Introduction

The increasing penetration rate of DER has led to some serious protection coordination problems which do not ordinarily occur in conventional distribution grids without DERs. One of the key problems is that the rising amount of distributed and intermittent DERs can lead to bidirectional power flow in the distribution grid and contribute to fault currents which may also flow in either direction based on its location. The traditional distribution grid was designed for single direction power flow from the substation to the customers. Almost all of the feeder protection schemes are designed based on this traditional concept. The intermittent DERs at the customer end can now generate power that is consumed by the customer or feed back excess power to the rest of the distribution feeder. In a

very high penetration scenario, the back feed may affect transmission level power flows as well. This raises new challenges to grid modeling methods in practical problems of system protection where the impacts of DERs have to be considered.

3.2 Fundamentals of Distribution Network Protection

3.2.1 Principles of System Protection in Power Networks

Fundamentally, the objective of power system protection is to provide quick response to a fault in a power system, so that the outage area can be minimized and the rest of the power system will remain working in normal condition. To achieve this objective, power system protection has long since followed the following basic design principles: Reliability, Selectivity, Sensitivity and Speed of operation [46, 47]. These are discussed in turn as follows:

Reliability

Reliability is the property that is used to evaluate if the relay scheme is performing consistently well in different scenarios. There are typically two ways to improve the system reliability. One may be through duplicating the relay and sometimes its associated switchgear. This is usually too expensive to be achieved particularly for distribution protection. The other most common method is through backup protection equipment utilizing another feeder zone's equipment to increase the reliability if the current zone protection fails. The reliability can be quantified

by the following expression

$$Reliability = \frac{NCT}{NDT + NIT} \times 100\%, \tag{3.1}$$

where NCT stands for the number of correct trips, NDT is the number of desired trips and NIT is the number of incorrect trips.

Reliability can also be evaluated through dependability and security. Dependability is used to evaluate the correctness of relay operation. It can be quantified as

$$Dependability = \frac{NCT}{NDT} \times 100\%. \tag{3.2}$$

Security is used to quantify the degree of certainty that the relay will trip incorrectly.

$$Security = \frac{NCT}{TNT} \times 100\%, \tag{3.3}$$

where TNT stands for the total number of trips.

Dependability can be improved by increasing the sensitivity of the protection system. However, this comes at the cost of increasing the likelihood of nuisance trips. Security of the protection system can be improved by increasing selectivity. These are explained further in the next subsections.

Sensitivity

In a low to medium voltage power distribution network, fault levels are sometimes lower compared to the transmission system, particularly for those feeders that lose connection to the distribution grid [48]. Therefore, the protection system must be sensitive enough to see the faults. Using the fault signature is a way to see these lower level faults in some cases [49], but it is also depends on the fault type.

For example, negative phase sequence filtering has been used in the past to detect low level unsymmetrical faults that normal positive sequence protection would not be sensitive enough to detect. If the low level unsymmetrical faults are sensitive enough to be detected, the dependability can be improved. However, there are issues with protection relay sensitivity when renewable DERs are injecting power into the system during faults. This has not been adequately addressed in existing research, but will be studied in this thesis.

Selectivity

Selectivity is defined as the ability to differentiate the normal condition and the fault condition. For example, the inrush current of transformers and large motors in a power system may surge up to 20 times of their rated currents, resembling a short circuit. In this case, the relay has to be able to discriminate the inrush from a genuine fault. One method in this example is identifying the large second order harmonic of the inrush current and restraining the operation of the relay. Therefore the inrush current and the fault current can be distinguished and the selectivity of the relaying system is increased.

In addition, the relay must also be set to decide whether the fault happens within its jurisdiction, previously referred to as the zone of protection. Thus the relay should ideally only should only operate for faults in its zone or sometimes back up the next zone, causing minimum impact to the system.

Speed of operation

Ideally, the relay should isolate the fault as quickly as possible to minimize disturbance to the system. For example, instantaneous overcurrent relays operate in one to one and a half cycles and the breaker mechanism takes an additional

operating time of one and a half to three cycles (on a 60 Hz basis) [50]. Based on [51], a high speed relay operates in less than 3 cycles. On the other hand, it is sometimes advantageous to not operate too quickly in order for the protection system to ride through transients or temporary overloads that can be tolerated for a short duration.

It is difficult to achieve all of the aforementioned requirements at the maximum level. For example, if the protection relay sensitivity increases, its selectivity may reduce as more relays will pickup the same fault. Thus, in practical real world protection system design, compromises have to be made and some requirements are prioritized at the expense of others.

3.2.2 Overcurrent Protection

To maintain the safety of the power system, current flow should be restricted based on the current handling ability of the power line, conductors, switches, load and transformers, etc. When the power system is operating at the normal condition, current in each circuit should be restricted to equal or less than the rated current. When a fault happens in the system, higher current level is expected known as the overcurrents. Overcurrents are expected to happen when there are short circuits, overloading or inrush current in the system. This thesis is mainly focusing on short circuits as it is more common and may lead to severe consequences.

There are mainly two protective devices employed in distribution feeders to isolate the power system fault current, either using fuses or overcurrent relays. According to IEEE Standard C37.2-2008 [52], an overcurrent relay can be divided into two subclasses: instantaneous overcurrent and inverse time overcurrent relay

with device code 50 and 51 respectively. A type 50/51 relay initiates its operation when the predetermined current setting is reached. This threshold is defined as the pickup. If the fault does not clear itself after the relay picks up, the relay will then trip the circuit breaker based on its time current curve (TCC).

Some of the overcurrent relays may include a reclosing function known as the recloser with device code 79. A 79 type recloser could close the opened circuit when the fault current is cleared. Overcurrent relays can also be fitted with a directional feature which improves the selectivity by being able to ascertain the vector direction of the fault current. This has been used in the past to selectively trip parallel feeders when a reverse current flow is detected.

Fuses on the other hand have no directional feature or tripping logic. They are selected to not operate under the rated current and are supposed to carry the normal maximum load current without melting. However, it needs to be replaced once the fault current has started melting the fuse element. However, like an overcurrent relay, fuses do have fuse melting characteristics that is time-current dependent based on the rate of melting and arc extinguishing time for a given fault current.

Both of these protective devices have the time current characteristic which is used to coordinate the multiple relays operating sequence when faults happen. In a distribution grid, these two devices are often used together. Since fuses cannot measure the fault current level directly, this research mainly focuses on expanding upon overcurrent relay protection which uses current transformers (CTs) to monitor the feeder currents in a distribution grid.

3.2.3 Feeder Protection Coordination

To achieve the maximum protection, all protection relays need to be coordinated. In a distribution grid, it is common for each single relay to be set up to not only protect its own zone (known as the primary protection zone), but also protect downstream zones (known as the backup protection zone). Thus the backup protection zone of one relay can be overlapped with the primary protection zone of downstream relay(s). In this case, if one downstream relay fails to pickup its primary protection zone faults or there is a failed circuit breaker, the upstream relay can pickup and trip its associated breaker for the backup protection zone and isolate all of the downstream zone.

The diagram of a typical overcurrent protection coordination on a single line distribution feeder is shown in Fig. 3.1.

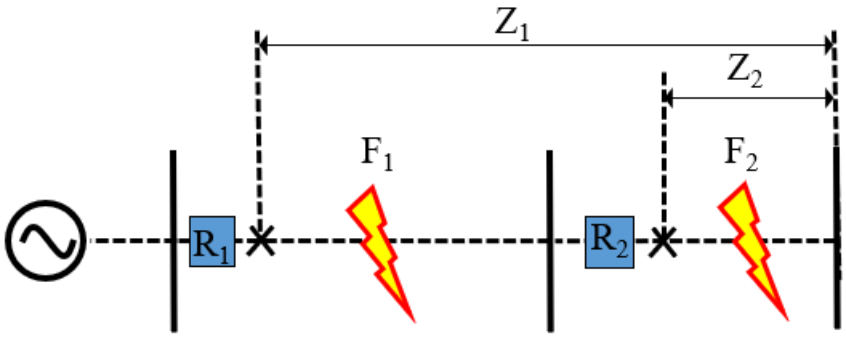

Figure 3.1: An example of a common protection system scheme for primary and backup protection of a radial distribution feeder

For this feeder, it can be observed that Relay R_1 can see the fault F_1 on its primary protection zone Z_1 or the fault on its downstream backup protection zone Z_2. Relay R_2 can only see the fault F_2 on its downstream backup protection zone Z_2. Thus the backup protection zone of R_1 is overlapped with the primary protection zone of R_2.

If F_2 fault happens, both R_1 and R_2 will pickup at the same time. However R_1 will be set up to delay its operation relative to R_2. In normal conditions, if R_2 trips and the fault is cleared, R_1 will dropout and not trip. If R_2 fails to pickup F_2, R_1 will trip after a delay. This whole process can be realized using the time current curve.

Time Current Curve

Time current curve plots the interrupting time of a relay. It is used to show how fast a relay will trip a breaker at any magnitude of fault current. With different TCC, different relays can pick up at different times for the same fault. The three types of TCCs are Instantaneous (INST), Definite Time (DT) and Inverse Time Overcurrent (ITO). Their relationships can be explained by Fig. 3.2.

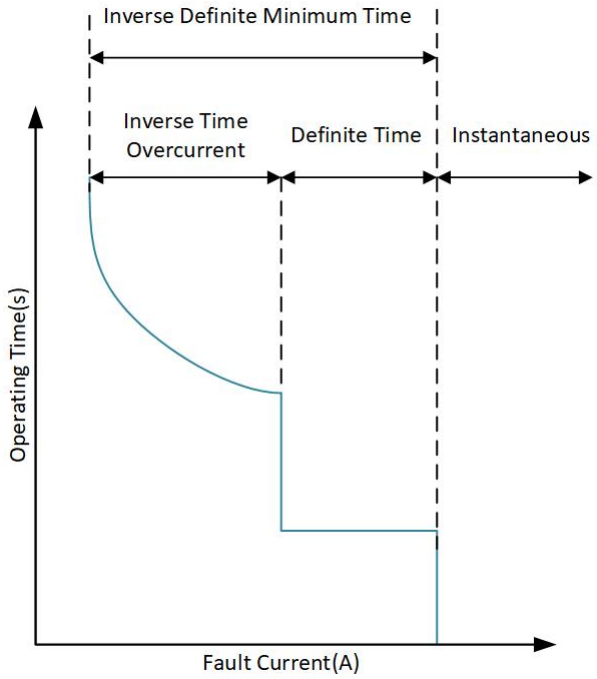

Figure 3.2: Relationship of different TCCs

The ITO can be explained by the following equation as defined by IEC 60255,

$$t = TMS \frac{A}{\left(\frac{I}{I_s}\right)^B - 1}, \tag{3.4}$$

where t is the operating time of the relay, TMS stands for the time multiplier setting of the relay, $\frac{I}{I_s}$ is the ratio of magnitude of fault current and the relay pickup current known as the Plug Setting Multiplier (PSM), A and B are the two constants that relate to the type of relay and its specific characteristic.

DT is a straight line that is in parallel with the x axis, meaning that if the fault current reaches a certain threshold, the relay will trip the breaker in a fixed time duration. It is usually implemented for the backup protection.

INST is similar to DT, but the relay operating time is moved to 0 seconds (no intentional time delay). It has the least sensitivity of all relays and does not need any coordination. Usually, INST is used if the fault level is very high and a trip is needed immediately without waiting.

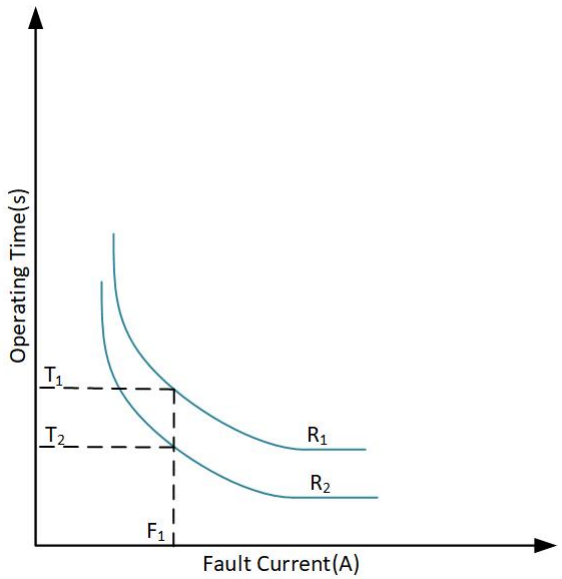

Figure 3.3: Coordination of R_1 and R_2 using IDMT curve

DT and ITO are often used together known as the IDMT curve. By setting the IDMT curve, R_1 and R_2 could be coordinated as shown in Fig. 3.3. It can be observed that if F_2 happens, the trip time of R_2 is faster than that of R_1.

3.2.4 Symmetrical Components in Power System Protection

Normally, medium voltage power lines in distribution grids consists of three phases, and sometimes in rural areas, it is more economical to run single phase lateral lines. Ideally, the three phases of the power distribution line have a balanced load. However, the three phases can become unbalanced caused by unbalanced load or unsymmetrical fault current in the distribution grid, causing unbalanced current or voltage. In this case, the symmetrical coordinate is proposed in [53]. Essentially, it describes how to transfer the three phases unbalanced current or voltage into three sets of balanced components known as positive, negative and zero sequence current or voltage components. These balanced components are defined as the symmetrical components. The balanced and unbalanced three-phase phasors are shown in Fig. 3.4.

It is convenient to use the unit phasor a with an angle displacement of $\frac{2}{3}\pi$ rads to describe the balanced sequence component angle such that,

$$\begin{aligned} a &= 1\underline{/120^\circ} \\ a^2 &= 1\underline{/240^\circ} \\ a^3 &= 1\underline{/360^\circ}. \end{aligned} \tag{3.5}$$

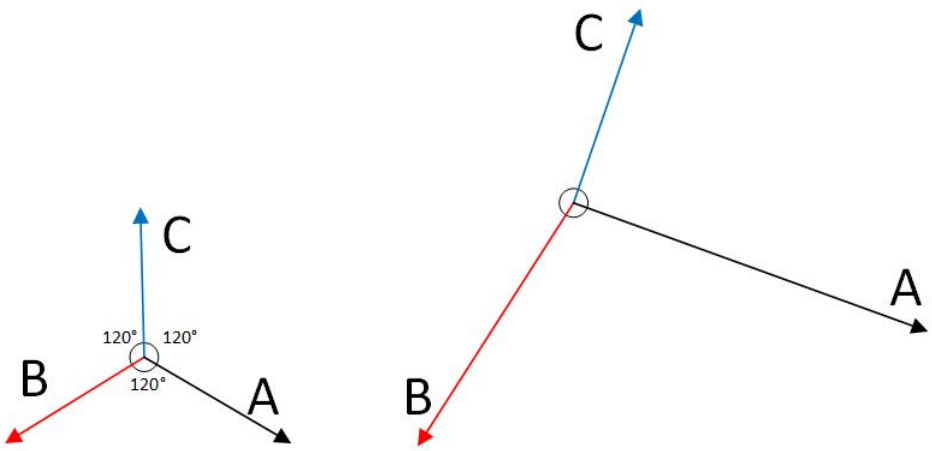

(**a**) Balanced System (**b**) Unbalanced System

Figure 3.4: Balanced and unbalanced three-phase phasor

The unbalanced three phase current can be expressed as

$$\begin{aligned} I_a &= I_1 + I_2 + I_0 \\ I_b &= a^2 I_1 + a I_2 + I_0 \\ I_c &= a I_1 + a^2 I_2 + I_0, \end{aligned} \tag{3.6}$$

where I_a, I_b and I_c are the phasor representation for the three phase currents. I_0, I_1 and I_2 represent the zero sequence, positive sequence and negative sequence currents as shown in Fig. 3.5.

Physically speaking, in a three phase system, a positive sequence set of currents produces a normal rotating field, a negative sequence set of currents produces a rotation field that is opposite to the positive sequence set of currents, and the zero sequence current set produces a field that oscillates but does not rotate in space.

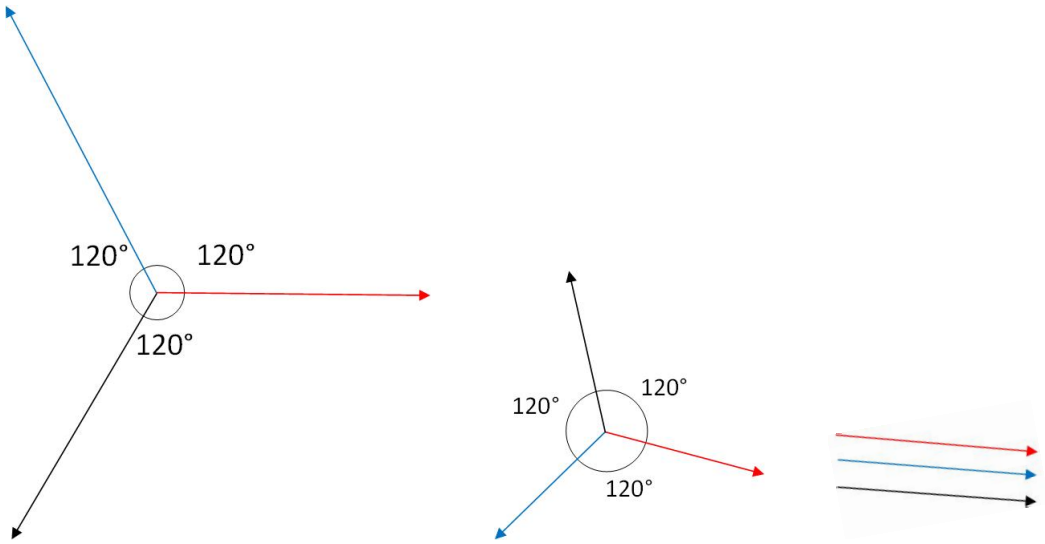

(**a**) Positive Sequence (**b**) Negative Sequence (**c**) Zero Sequence

Figure 3.5: Sequence Components

Based on Eq.(3.6), the current sequence component could be written as,

$$\begin{aligned} I_0 &= \frac{1}{3}(I_a + I_b + I_c) \\ I_1 &= \frac{1}{3}(I_a + aI_b + a^2 I_c) \\ I_2 &= \frac{1}{3}(I_a + a^2 I_b + aI_c), \end{aligned} \tag{3.7}$$

Based on Eq.(3.7), the three phase unbalanced currents become a linear combination of a balanced set of sequence components. The unbalanced three phase voltage can be expressed with a similar equation. In practice, the overcurrent relays operate based on the root mean square (RMS) value or the phasor magnitude value of the positive sequence components. Negative phase sequence is used in special applications such as detecting high impedance unbalanced faults on heavily loaded feeders which may not be detected with normal overcurrent positive sequence quantities.

3.2.5 Fault Types

In this thesis, the fault of interest is of the short circuit kind and not the open circuit type. Not all of the fault types can cause unbalanced currents or voltages. Essentially, there are two categories of fault types, either symmetrical fault or unsymmetrical fault.

Symmetrical faults

When symmetrical faults happen in a three phase system, all the phases are short circuited. They could either short circuit to each other, or to earth. When the three phase conductors connect to each other, it is defined as a line-to-line-to-line (LLL) fault. Similarly, when the three phases short circuit together and connect to earth, it is defined as a line-to-line-to-line-to ground LLLG fault. The LLL and LLLG faults are symmetrical since the fault is balanced. They are the most severe kinds of faults in power system, but are less common because multiple-point failures are required to cause this.

Unsymmetrical faults

Unsymmetrical faults are more common than symmetrical faults. A line-to-ground (LG) fault happens when one of the three phase lines is grounded or comes in contact with the neutral conductor. A line-to-line (LL) fault happens when two of the three phase lines are short circuited. A line-to-line-to-ground (LLG) fault happens when two of the three phase lines come in contact with the neutral conductor or ground. More than 95% of faults in the power system are these three types of faults, but they are not as severe as the symmetrical faults. Moreover, sometimes their fault levels are very small and hard to detect due to

high impedances bridging the connections such as debris or tree limbs. On the other hand, unsymmetrical faults may lead to more severe symmetrical faults if they are not isolated in time.

3.3 Main Protection Issues Considering the Integration of DERs on Distribution Feeders

3.3.1 Blinding of Protection

One of the emerging problems with the rise in DER in distribution grids is the issue of protection system blinding. The following scenario demonstrates this phenomena. In Fig. 3.6, an inverter based solar photovoltaic (SPV) system is connected to a distribution feeder. Relay 1 and Relay 2 are two IDMT overcurrent relays. The currents seen by Relays 1 and 2 are $\vec{I}_1$ and $\vec{I}_2$, respectively.

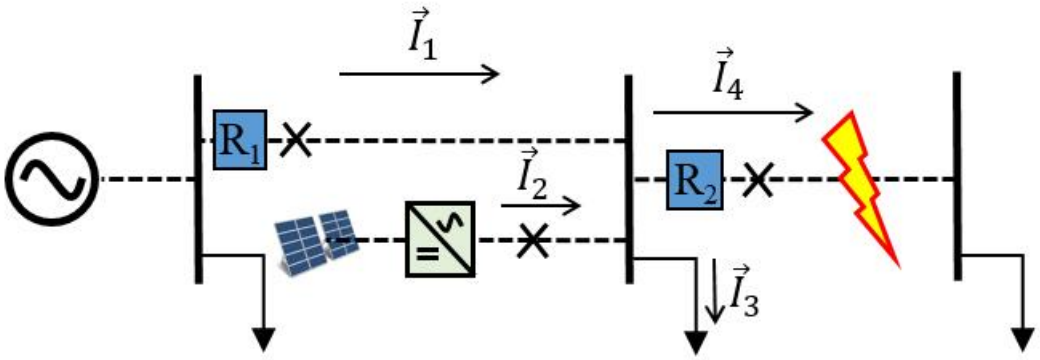

Figure 3.6: Blinding of Protection

Due to Kirchhoff's current law, $\vec{I}_1 = \vec{I}_4 + \vec{I}_3 - \vec{I}_2$. In the case of a fault happening at the end of the feeder, as shown in Fig. 3.6, $\vec{I}_3$ is decreased, $\vec{I}_4$ rises up to twice its rated current [54]. The fault current seen by Relay 1, defined as the backup relay, is less than that of Relay 2 defined as the primary relay.

Depending on the fault level and the rating of the SPV system, if Relay 2 fails to isolate the fault, Relay 1 may not pickup in time or trip for the fault after a while due to the partial blinding effect of seeing a reduced fault current.

3.3.2 Sympathetic tripping

Another problem is the issue of sympathetic tripping with DERs. This is demonstrated in the following scenario. In Fig. 3.7, two feeders are connected in parallel with each feeder equipped with a non-directional IDMT relay. The current seen by Relay 1 is $\vec{I}_1$ and $\vec{I}_2$ is seen by Relay 2.

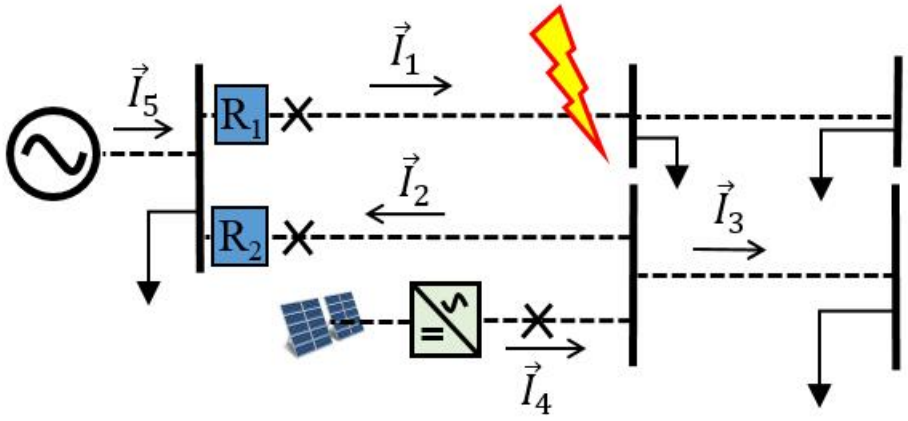

Figure 3.7: Sympathetic Trapping

In the case when a fault happens downstream of Relay 1, as shown in Fig. 3.7, $\vec{I}_2$ flows towards Relay 2, $\vec{I}_3 \approx 0A$, and $\vec{I}_4$ is increased. The fault current seen by Relay 2 is higher than the situation without DERs (assuming the DERs are generating some level of power). This would lead to the tripping of Relay 2 ahead of Relay 1.

Although this thesis is mainly focusing on the blinding of protection relay issue, the proposed method could potentially be used for alleviating sympathetic

tripping as well.

3.4 EMTP Simulation of Blinding Issue in Feeder Protection

In this section, the blinding of protection issue is reproduced with simulations to show the impact of DERs to the distribution feeder protection. These set of simulations are intended to not only highlight the problems, but also establish a known baseline to compare the benefits of alternative protection system solutions.

3.4.1 Distribution Feeder Protection Circuit

The simulation of a distribution feeder with DER is conducted in EMTP simulation software. EMTP is used to model the time-domain electromagnetic transient behavior of the power system in the normal and faulted conditions. The circuit diagram that is being simulated is shown in Fig. 3.8.

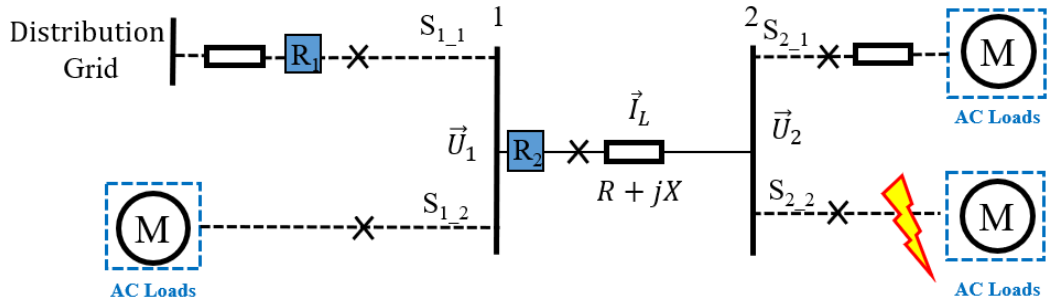

Figure 3.8: Distribution Feeder Protection Circuit

In Fig. 3.8, S_{i_j} stands for the j^{th} current source that connects to bus i. In this thesis, the current source is defined as any DERs, loads or substations that are connected to the buses. Each current source is connected to the bus with its

corresponding circuit breaker labeled as "X". $\vec{U}_1$ and $\vec{U}_2$ represents the voltage on bus 1 and bus 2 respectively. The line impedance between bus 1 and bus 2 is specified as a short line model with $R + jX$. The distribution grid that connects to bus 1 is considered as an infinite bus.

The simulation parameters are shown as follows. The total simulation time is 3 seconds with a time step of 10^{-5} second. A fault happens at 1.5 seconds as shown in Fig. 3.8. The faults are initiated with the build in fault component in EMTP. They are all set to the directly short fault without resistances between lines or line to the ground. The same fault setting is used throughout this thesis. The rated voltage of the distribution grid is set to be 34.5 kV. Current source S_{1_2} has an AC load of 24 MW and 9 MVAR; S_{2_1} has an AC load of 6 MW and 1.5 MVAR; S_{2_2} has an AC load of 9 MW and 3 MVAR. The line impedance is set to $2.478 + 6.742j\Omega$.

The EMTP simulation diagram of the distribution feeder protection circuit is shown in Fig. 3.9.

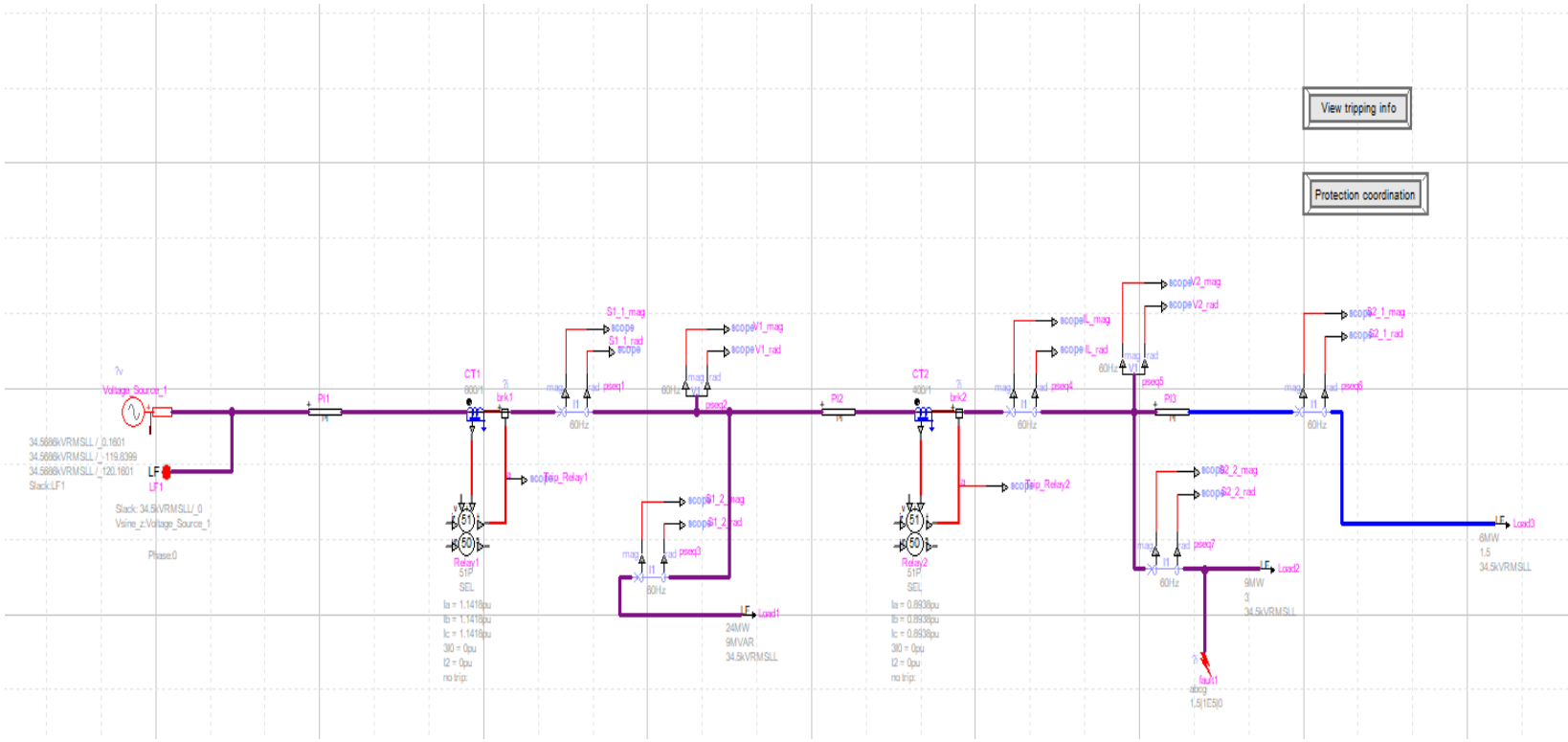

Figure 3.9: Distribution Feeder Protection Circuit in EMTP

In this simulation, both R_1 and R_2 relays are enabled. The relay models are all set to be the SEL 721 overcurrent relay. Based on the protection principle that was introduced in this chapter, R_2 should trip for its downstream faults ahead of R_1. All types of fault are tested, including LG, LL, LLG, LLL and LLLG. Only the positive sequence of current and voltage are measured in this simulation. All the relays are set to be tripped based on the phasor magnitude value of the positive sequence current. The phasor angle value of the positive sequence current and voltage are also included. This is used as a comparison to the results in the following chapters. The simulation result of the distribution feeder protection circuit is shown in the following figures.

Primary Protection

The voltage magnitude and angle of both buses are shown in Fig. 3.10 and 3.11. The current magnitude and angle of each of the sources are shown in Fig. 3.12, 3.13, 3.14 and 3.15. The line current I_L is shown in Fig. 3.16. The tripping signal captured by the both relays is shown in Fig. 3.17.

In the distribution feeder primary protection, when the fault happens at 1.5 seconds, both R_1 and R_2 picked up. However, the TCC of R_2 has less tripping time compared to R_1 at this fault level, thus it trips before R_1. R_1 will not operate for this fault in this case. The magnitude of S_{2_1}, S_{2_2}, V_2 and I_L are all zero because of the tripping of R_2. The tripping time of all types of faults is between 0.27 and 0.31 second.

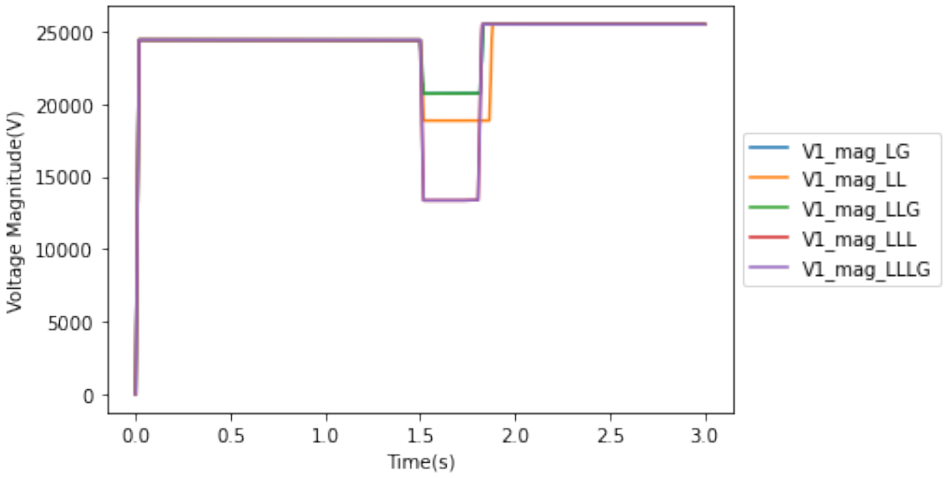

(**a**) Voltage V_1 magnitude

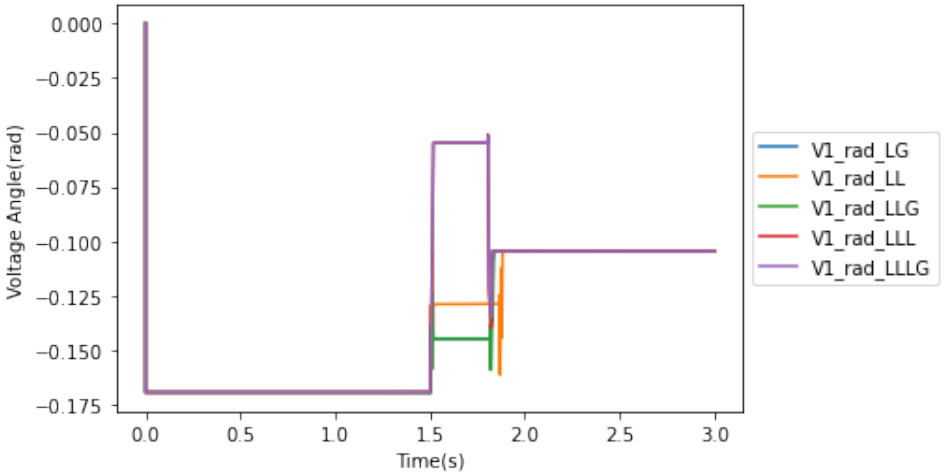

(**b**) Voltage V_1 angle

Figure 3.10: Primary Protection Voltage on Bus 1 of Distribution Feeder Protection Circuit

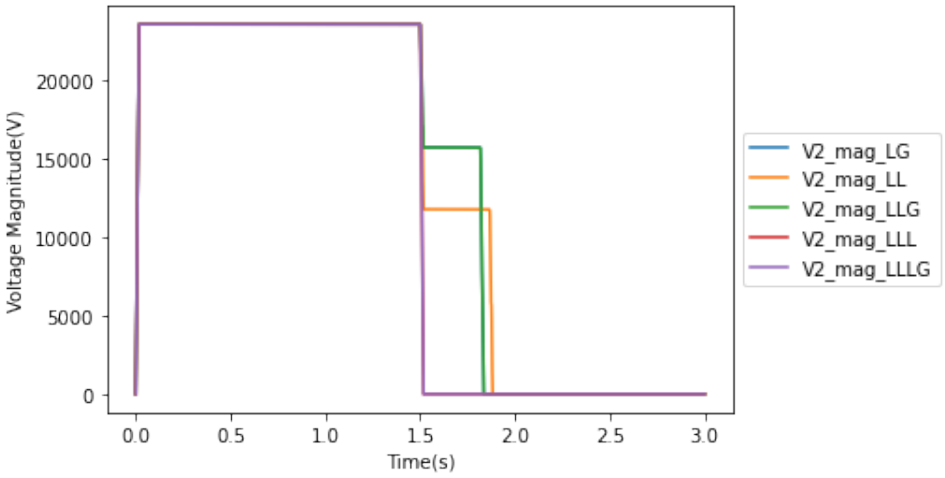

(**a**) Voltage V_2 magnitude

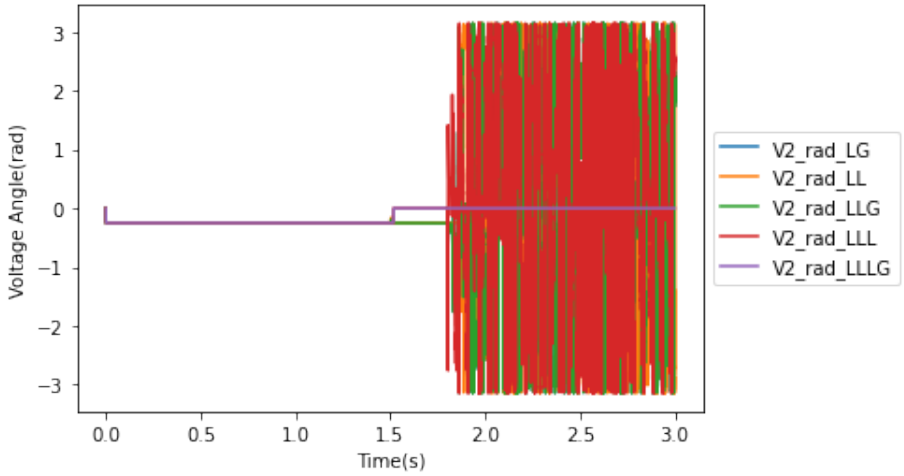

(**b**) Voltage V_2 angle

Figure 3.11: Primary Protection Voltage on Bus 2 of Distribution Feeder Protection Circuit

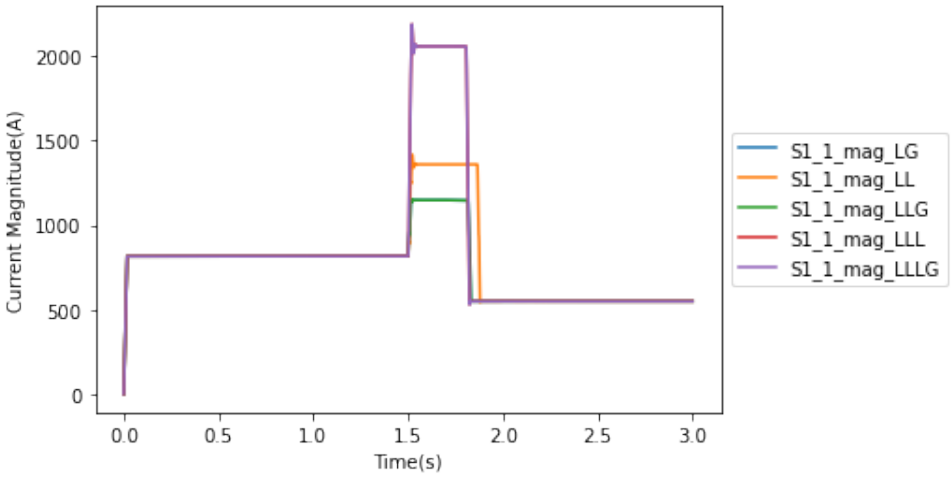

(**a**) Current source S_{1_1} magnitude

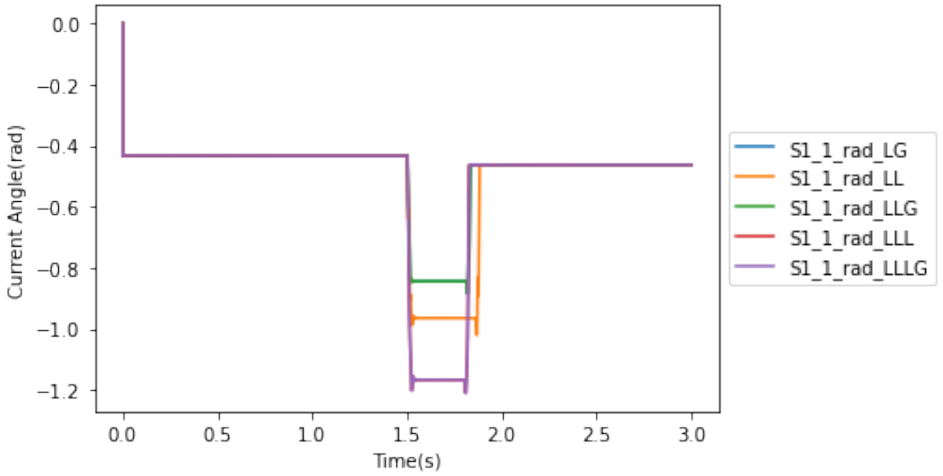

(**b**) Current source S_{1_1} angle

Figure 3.12: Primary protection current sources 1 connected to bus 1

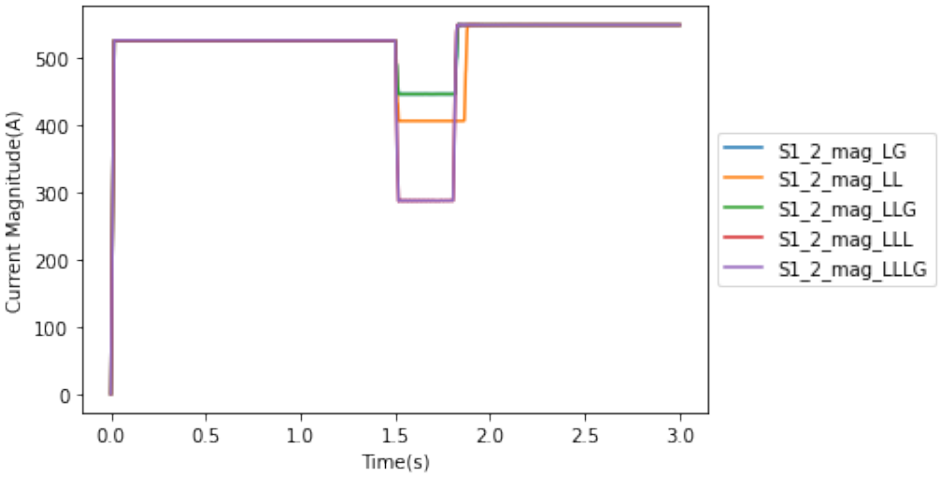

(**a**) Current source S_{1_2} magnitude

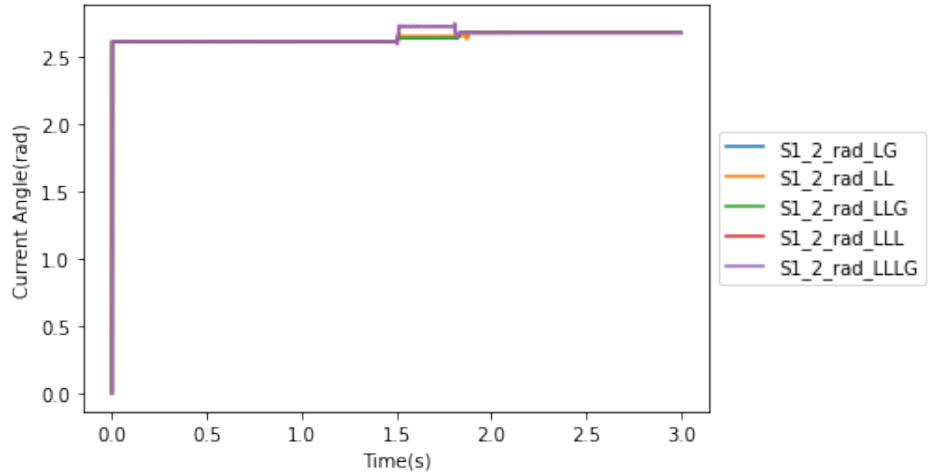

(**b**) Current source S_{1_2} angle

Figure 3.13: Primary protection current sources 2 connected to bus 1

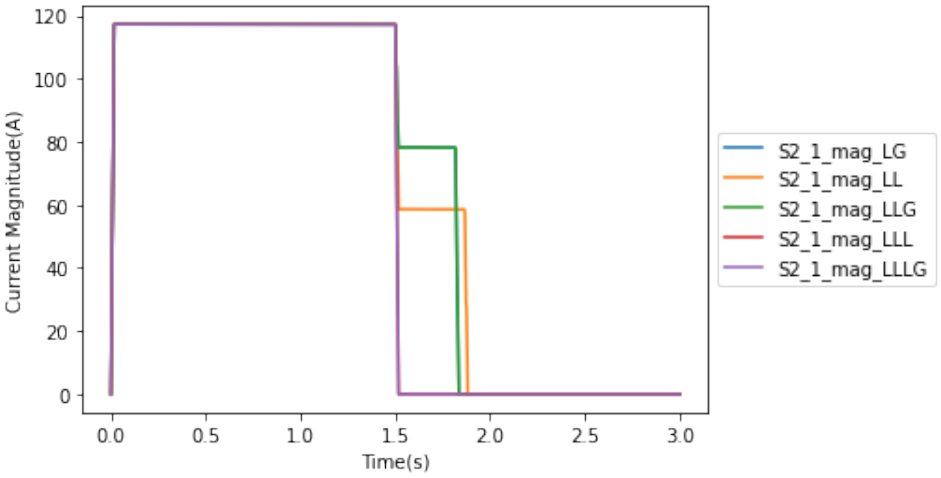

(**a**) Current source S_{2_1} magnitude

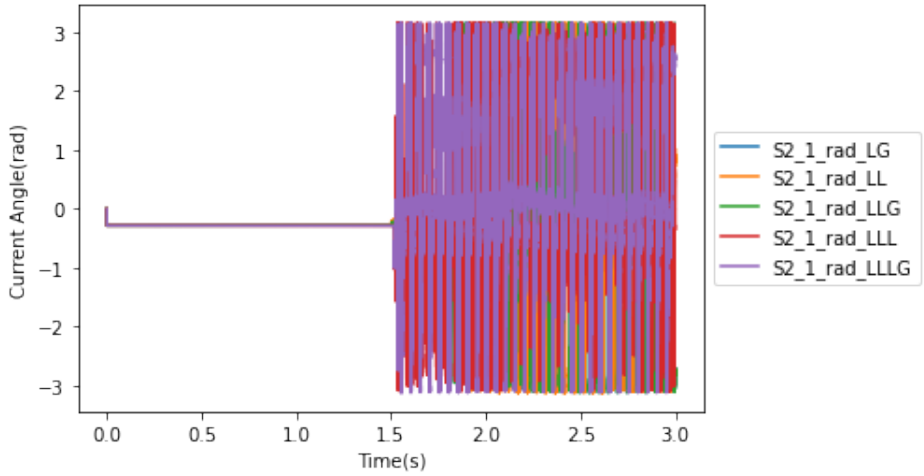

(**b**) Current source S_{2_1} angle

Figure 3.14: Primary protection current source 1 connected to bus 2

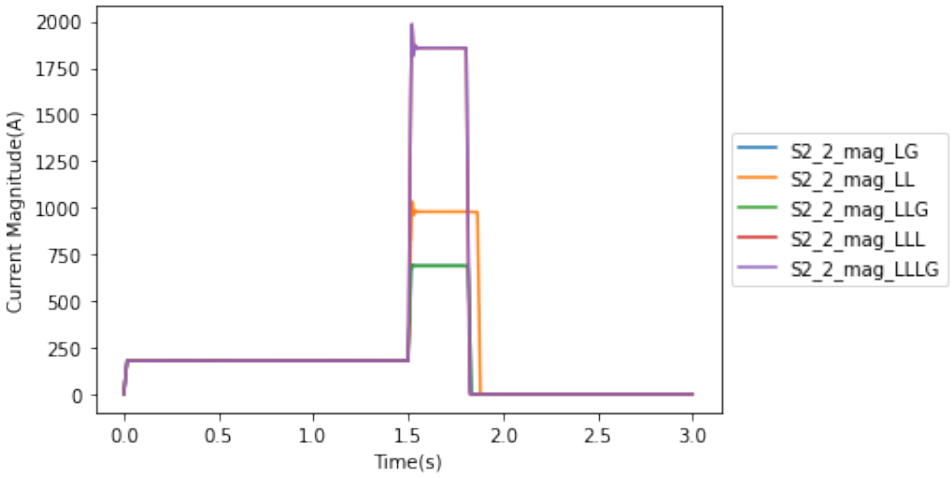

(**a**) Current source S_{2_2} magnitude

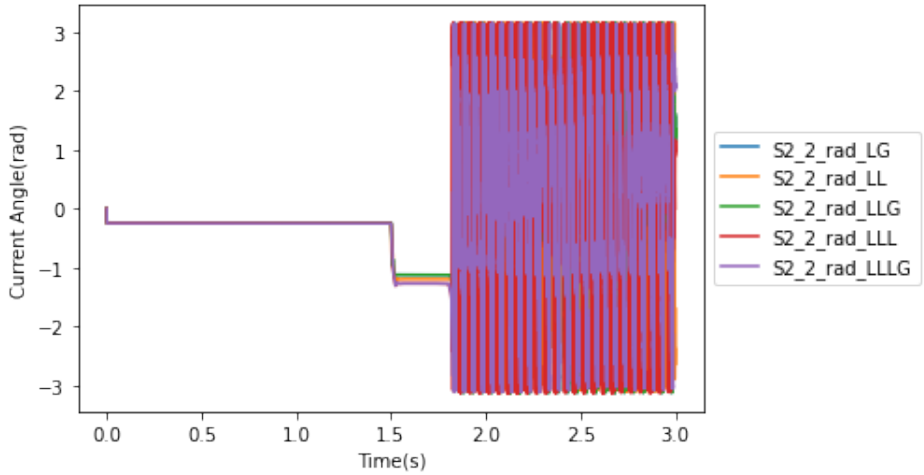

(**b**) Current source S_{2_2} angle

Figure 3.15: Primary protection current source 2 connected to bus 2

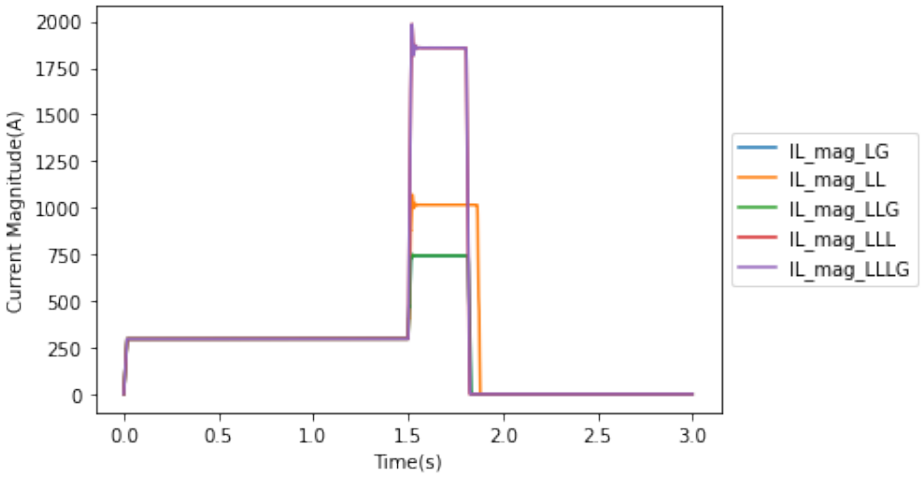

(**a**) Line current I_L magnitude

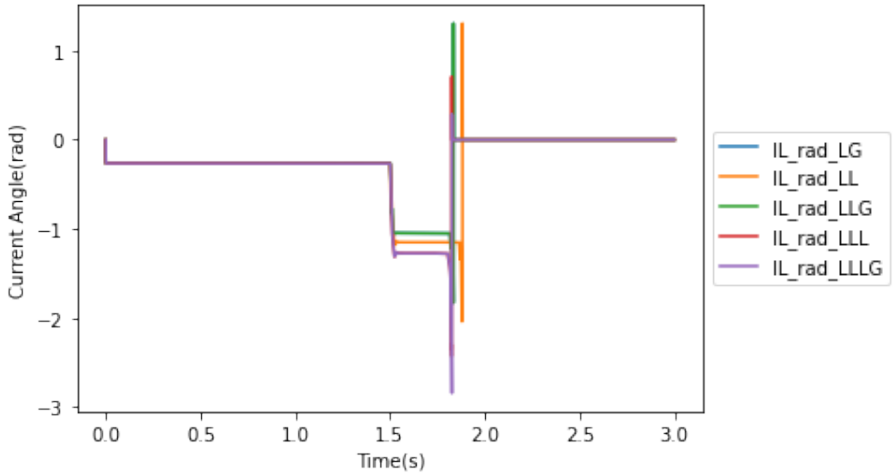

(**b**) Line current I_L angle

Figure 3.16: Primary Protection Line Current of Distribution Feeder Protection Circuit

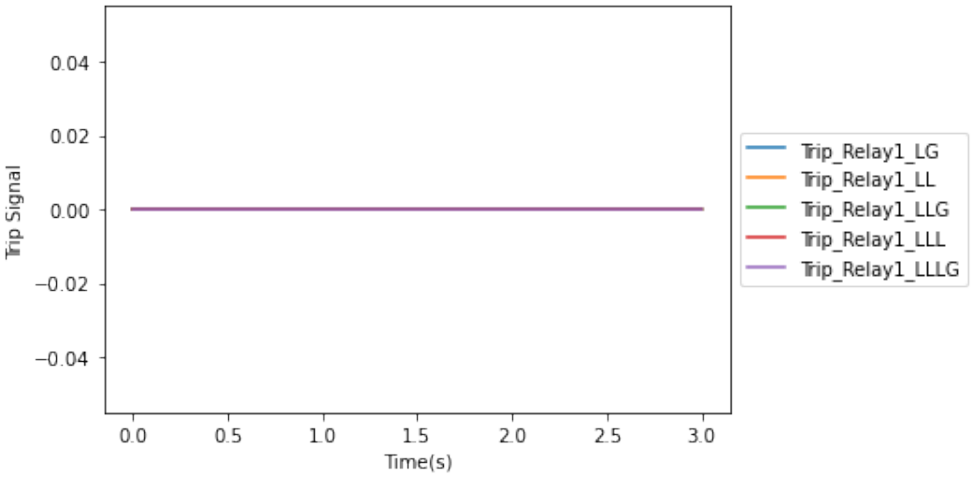

(**a**) Relay R_1 tripping signal

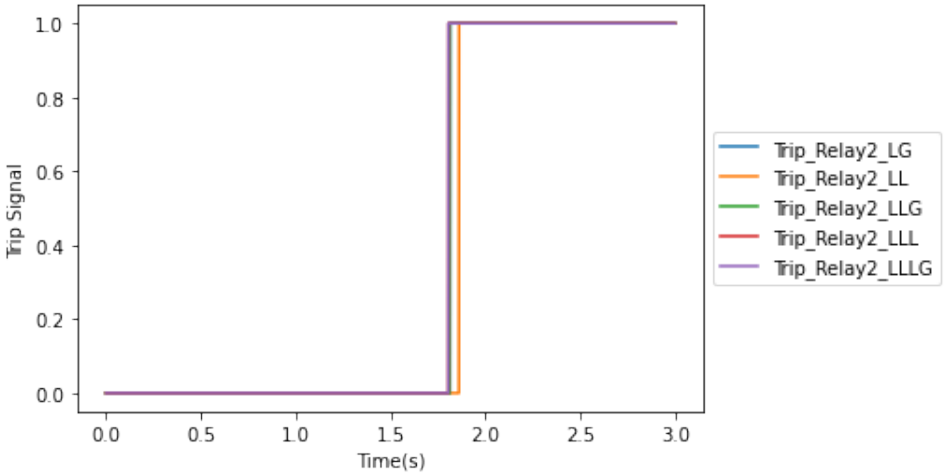

(**b**) Relay R_2 tripping signal

Figure 3.17: Primary Protection Tripping Signal of Distribution Feeder Protection Circuit

Backup Protection

In this simulation, the primary protection relay is assumed to have failed. This is done in the simulation by disabling R_2 and observing how the upstream relay functions. The backup is set to have a higher time delay and sensitivity so that it can see faults in its own zone and next zone. Ideally, R_1 should pickup when fault occurs at 1.5 seconds.

The voltage magnitude and angle of both buses are shown in Fig. 3.18 and 3.19. The current magnitude and angle of each source are shown in Fig. 3.20-3.23. The line current I_L is shown in Fig. 3.24. The tripping signal captured by the both relays is shown in Fig. 3.25.

It can be observed from the above figures that, when the fault happens at 1.5 seconds and the primary protection is disabled in the distribution feeder protection circuit, R_2 will not pick up. R_1 will trip for its downstream faults. Thus it can be observed that R_1 trips all types of faults at approximately 0.35 second which is later compared to the tripping time of R_2 in the primary protection. Since R_1 trips, the magnitudes of S_{1_2} and V_1 also becomes zero indicating the faulted section has been isolated from the source.

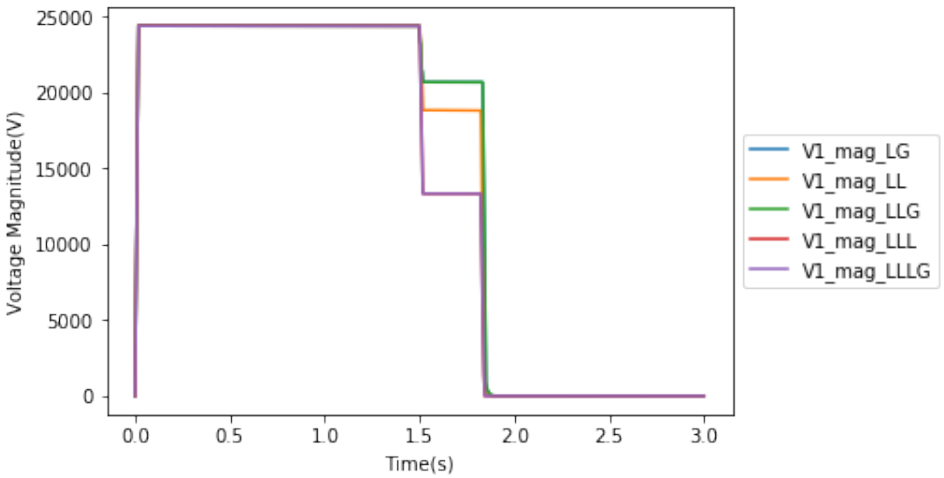

(**a**) Voltage V_1 magnitude

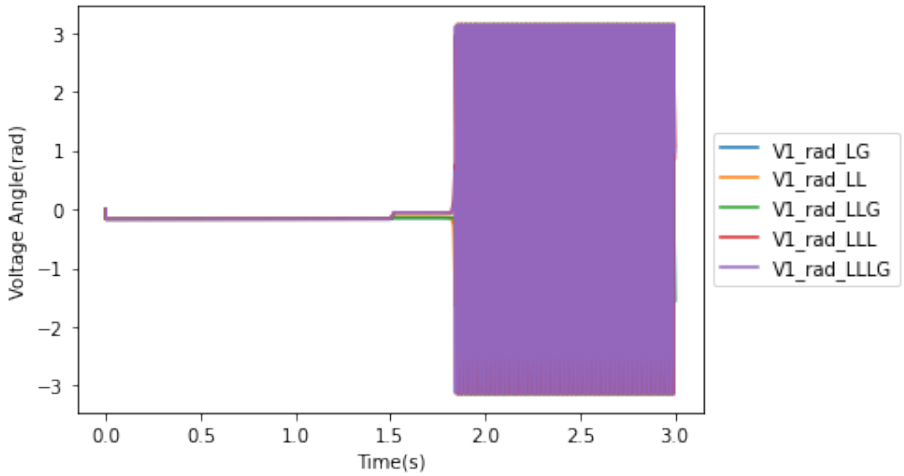

(**b**) Voltage V_1 angle

Figure 3.18: Backup protection voltage on bus 1 of distribution feeder protection circuit

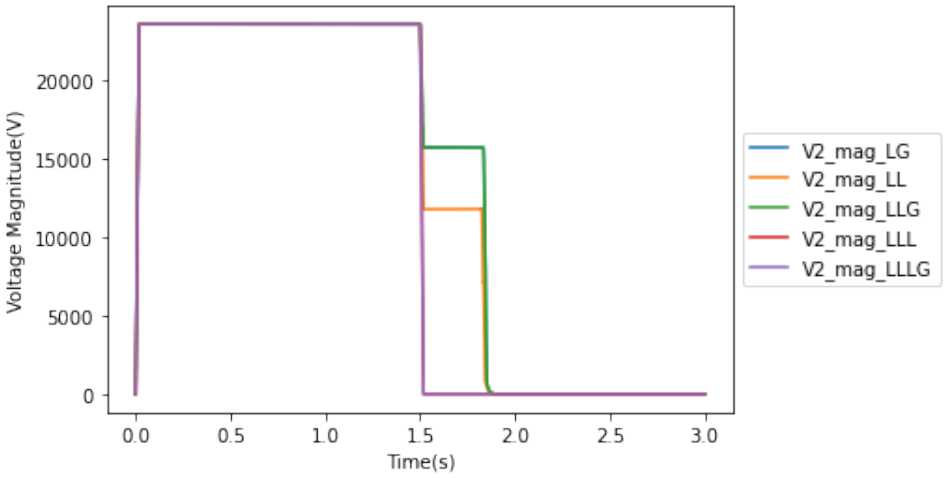

(**a**) Voltage V_2 magnitude

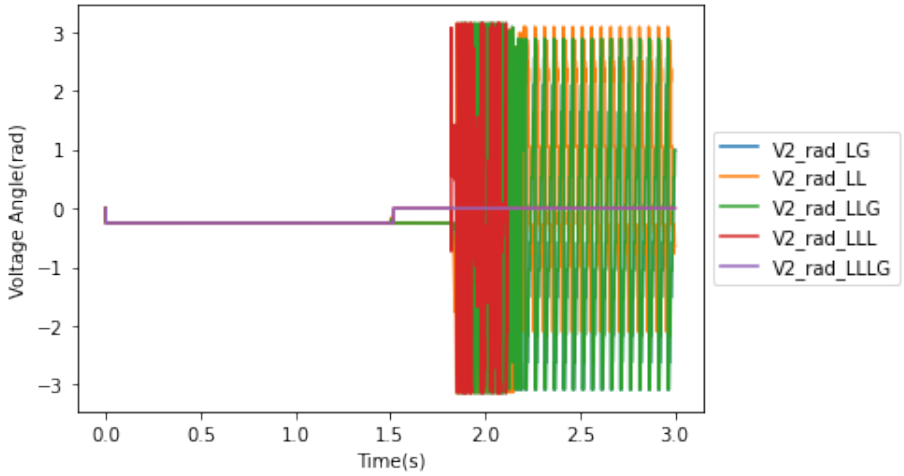

(**b**) Voltage V_2 angle

Figure 3.19: Backup protection voltage on bus 2 of distribution feeder protection circuit

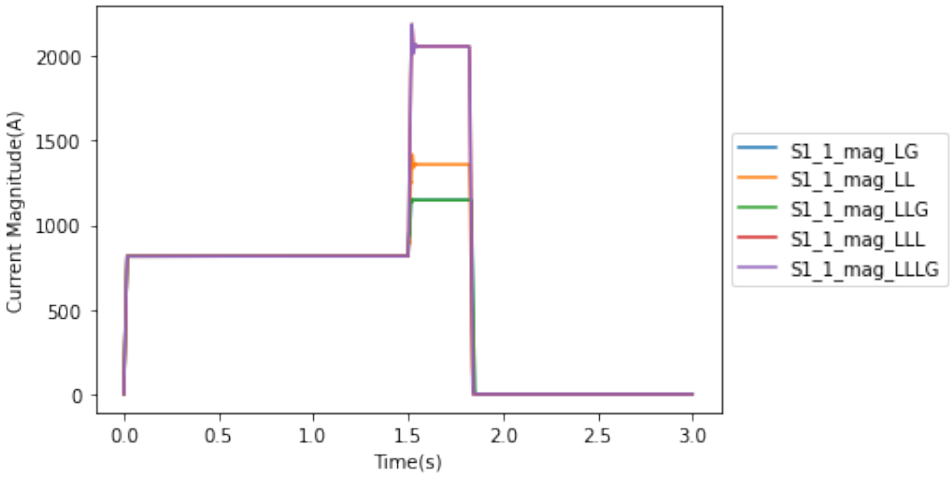

(**a**) Current source S_{1_1} magnitude

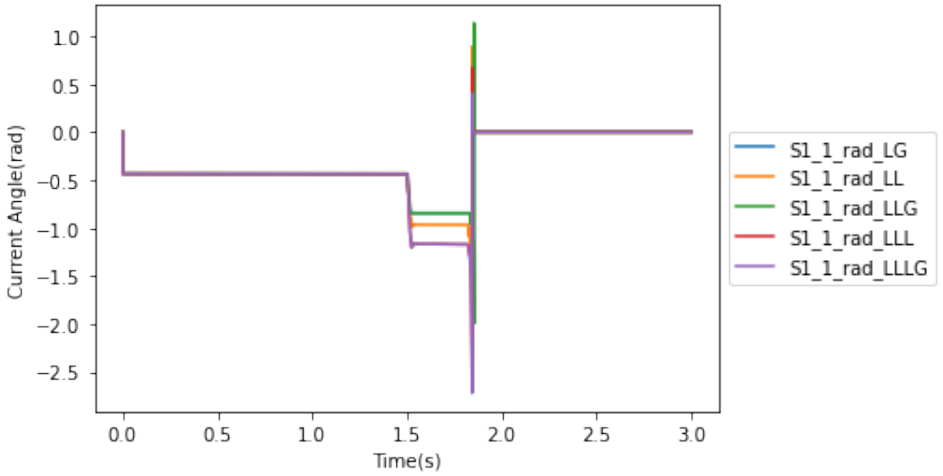

(**b**) Current source S_{1_1} angle

Figure 3.20: Backup protection current sources 1 connected to bus 1

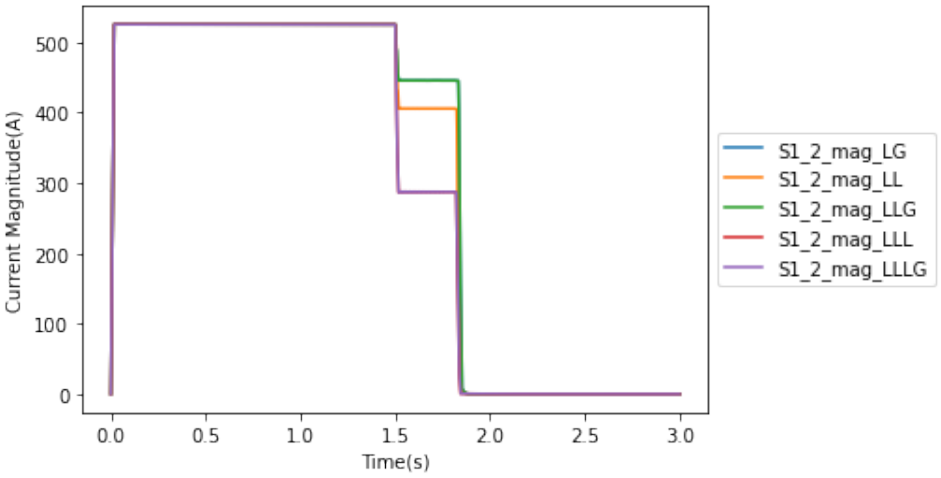

(**a**) Current source S_{1_2} magnitude

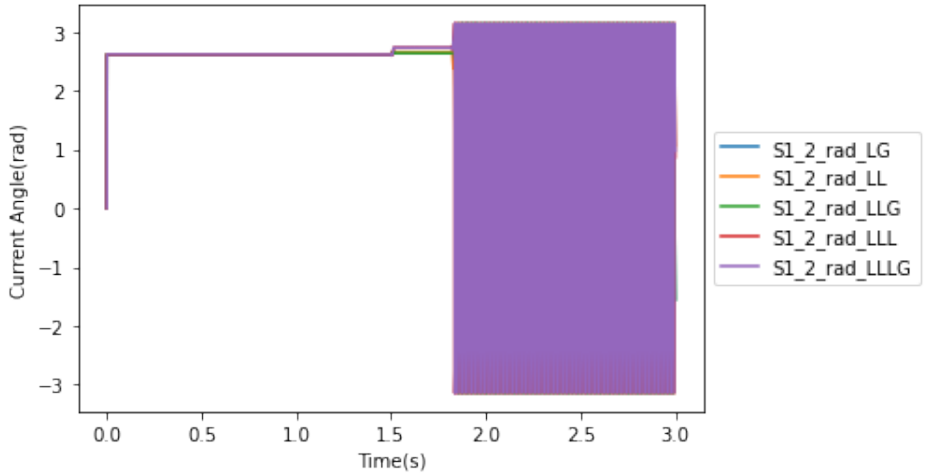

(**b**) Current source S_{1_2} angle

Figure 3.21: Backup protection current sources 2 connected to bus 1

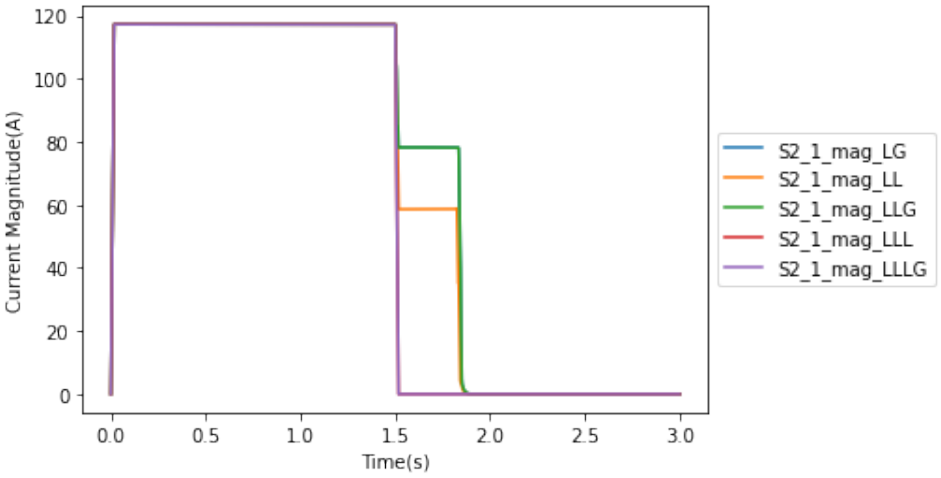

(**a**) Current source S_{2_1} magnitude

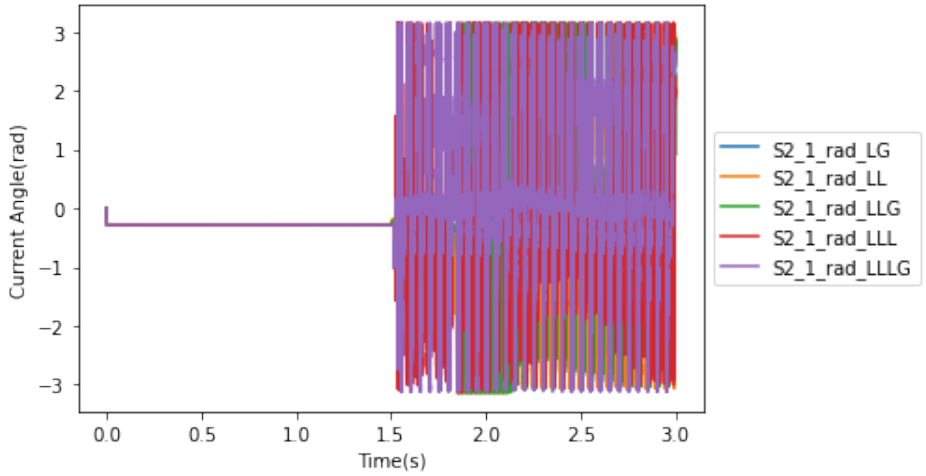

(**b**) Current source S_{2_1} angle

Figure 3.22: Backup protection current sources 1 connected to bus 2

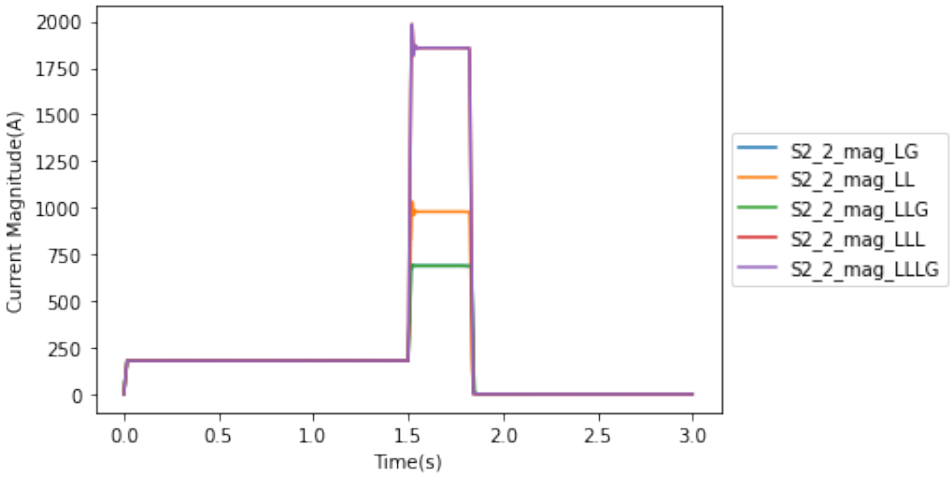

(**a**) Current source S_{2_2} magnitude

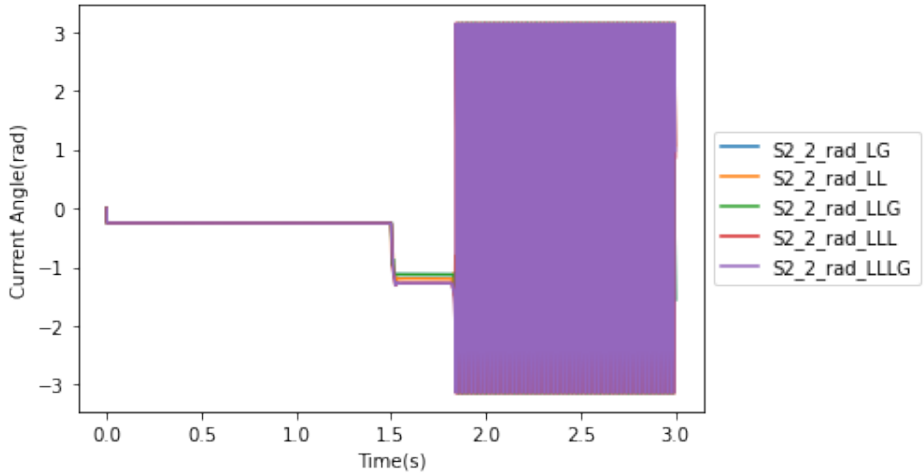

(**b**) Current source S_{2_2} angle

Figure 3.23: Backup protection current sources 2 connected to bus 2

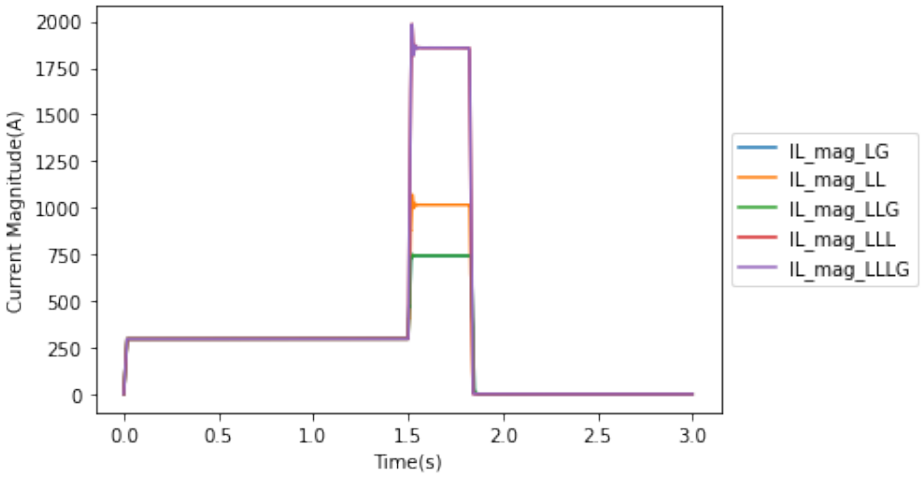

(**a**) Line current I_L magnitude

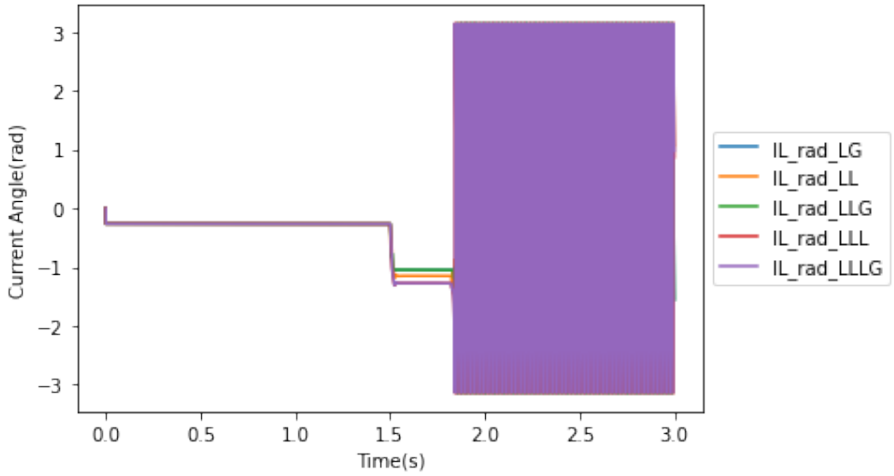

(**b**) Line current I_L angle

Figure 3.24: Backup Protection Line Current of Distribution Feeder Protection Circuit

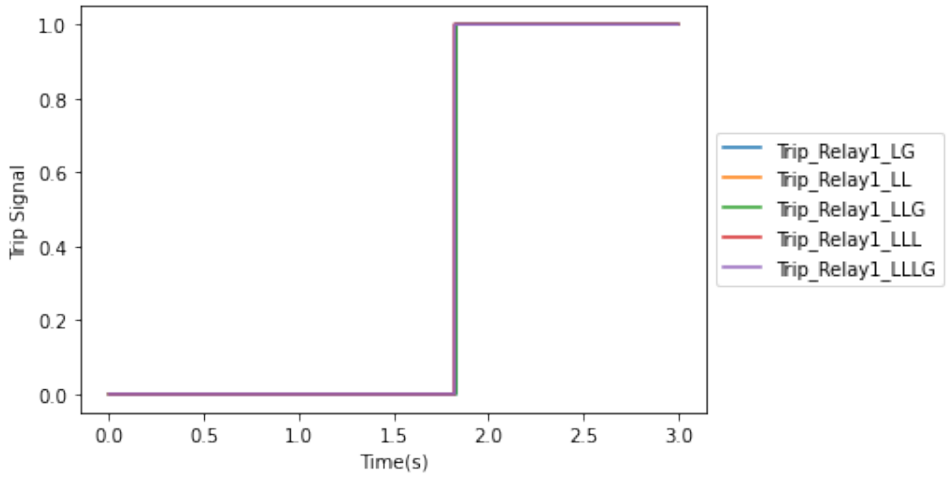

(**a**) R_1 tripping signal

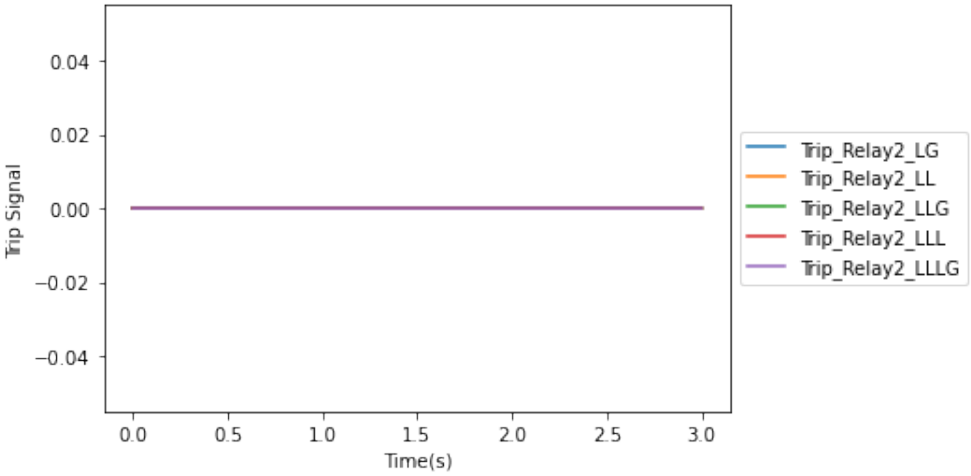

(**b**) R_2 tripping signal

Figure 3.25: Backup Protection Tripping Signal of Distribution Feeder Protection Circuit

3.4.2 Distribution Feeder Protection with DERs

The diagram of the distribution feeder protection circuit with DERs is shown in Fig. 3.26. In this diagram, a SPV is connected to bus 1 named as S_{1_3}. The EMTP simulation diagram of Fig. 3.26 is shown in Fig. 3.27.

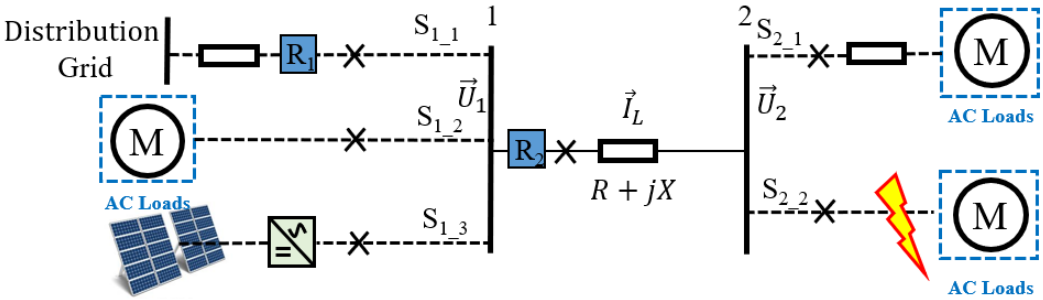

Figure 3.26: Distribution Feeder Protection with DERs

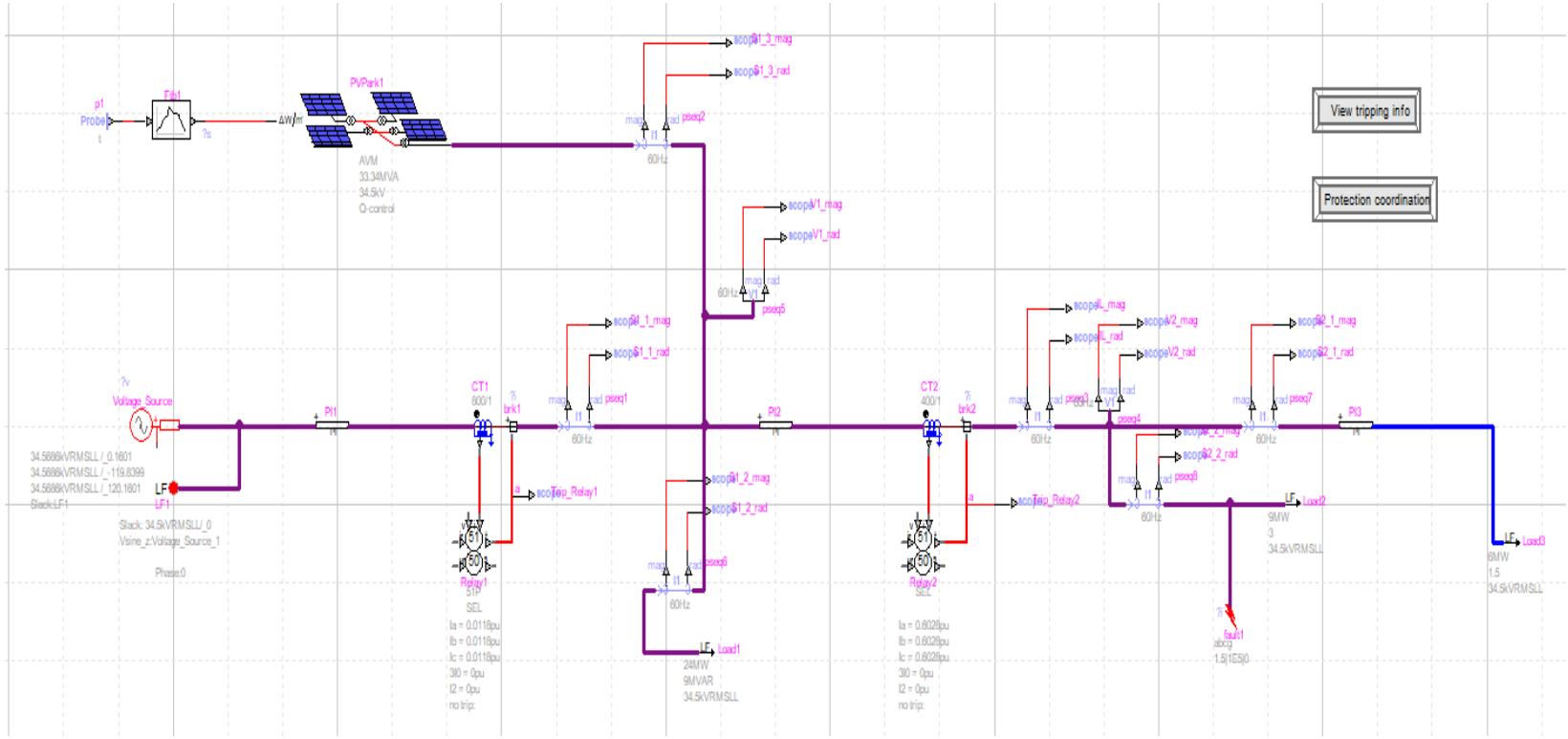

Figure 3.27: Distribution Feeder Protection Circuit with DERs in EMTP

In this simulation, the SPV system consists of a set of 5 sub-panels. Each of the sub-panels has a rated power of 1.67 MVA. The total rated power is 8.33 MVA. It takes 0.4 second for the DERs to be initialized. The simulation result in this case is shown as follows.

Primary Protection

The voltage magnitude and angle of both buses are shown in Fig. 3.28 and 3.29. The current magnitude and angle of each source are shown in Fig. 3.30, 3.31, 3.32, 3.33 and 3.34. The line current I_L is shown in Fig. 3.35. The tripping signal generated by both protection relays are shown in Fig. 3.36.

It is evident from the below figures that, with 5 solar panels injection of DERs into bus 1, the primary protection R_2 trips for all types of faults as well. The tripping time for all types of faults is between 0.2 and 0.3 seconds. This time is slightly faster than the tripping time in the distribution feeder protection circuit without DERs. This is because of the increased contribution of DERs to the fault current, thus accelerating the tripping time of R_2. R_1 does not trip in this case as R_2 is enabled and it will trip ahead of R_1.

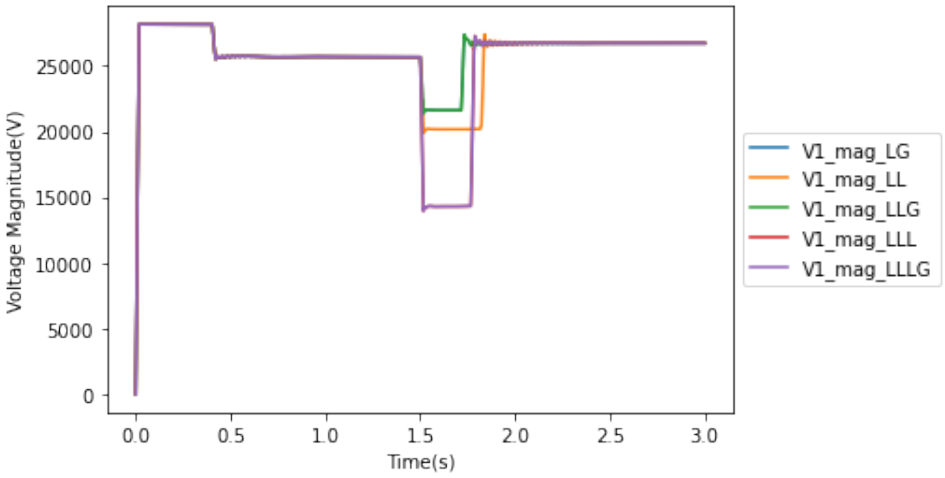

(**a**) Voltage V_1 magnitude

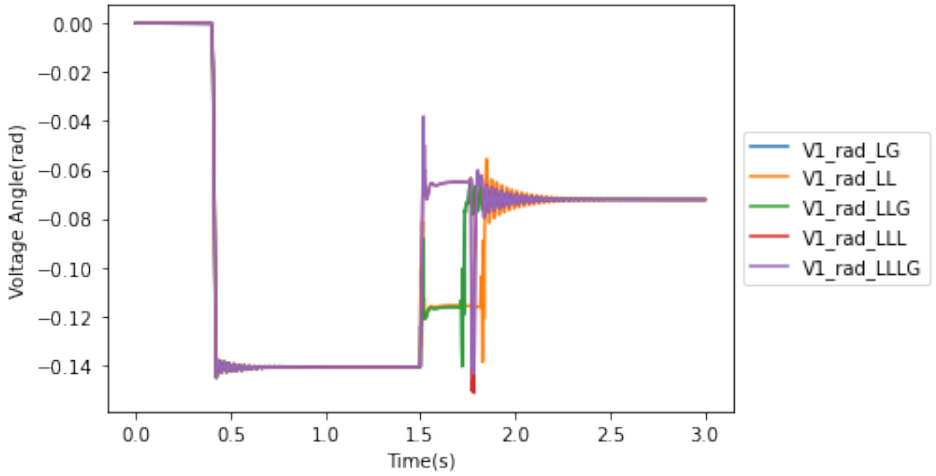

(**b**) Voltage V_1 angle

Figure 3.28: Primary protection voltage on bus 1 of distribution feeder protection circuit with DERs

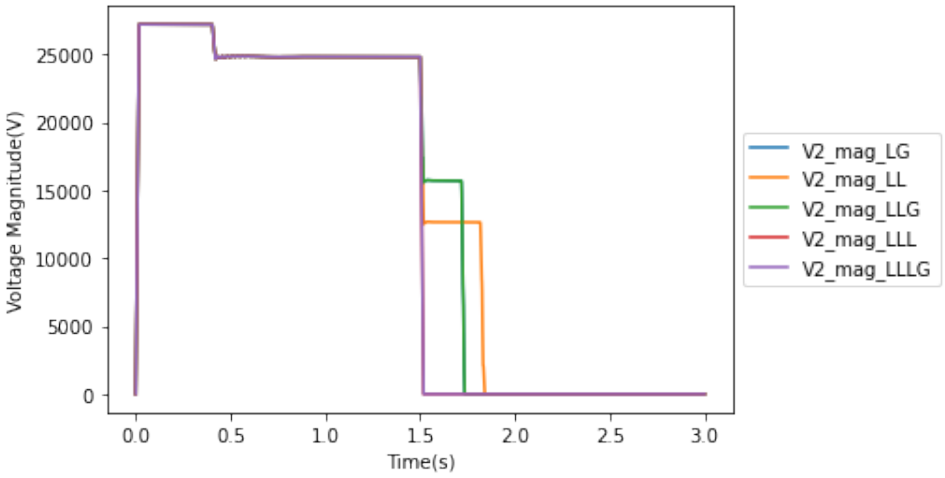

(**a**) Voltage V_2 magnitude

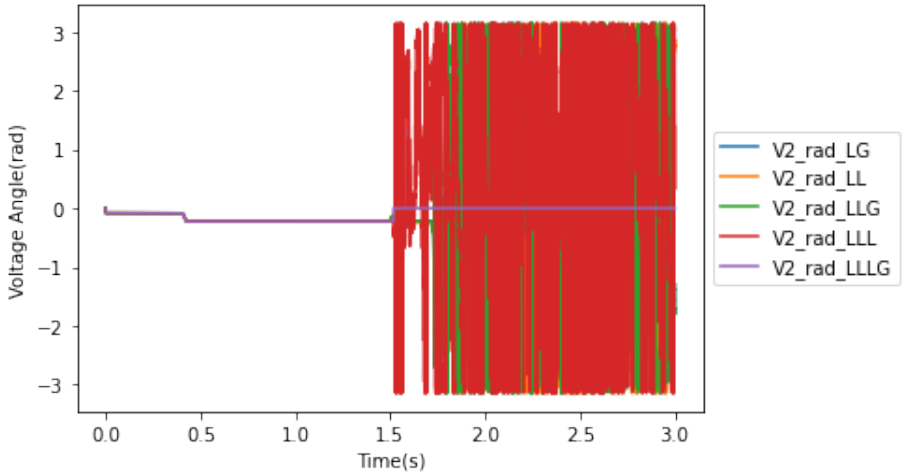

(**b**) Voltage V_2 angle

Figure 3.29: Primary protection voltage on bus 2 of distribution feeder protection circuit with DERs

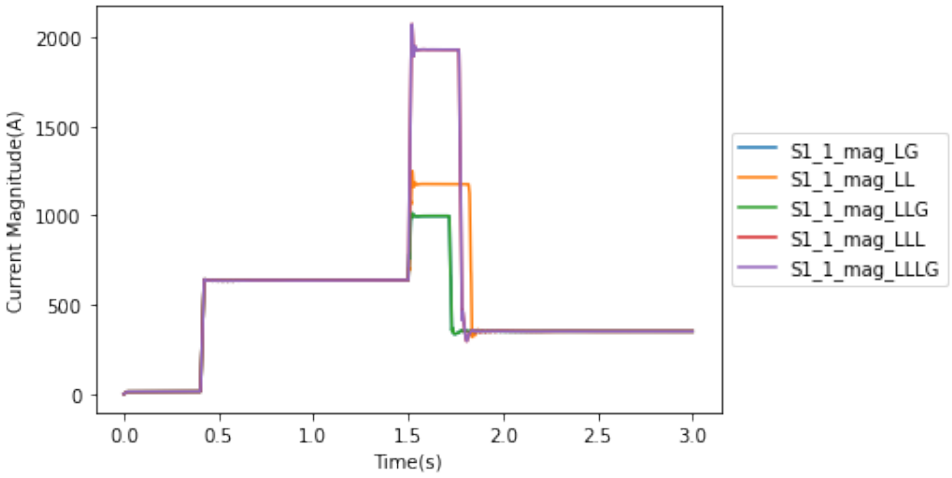

(**a**) Current source S_{1_1} magnitude

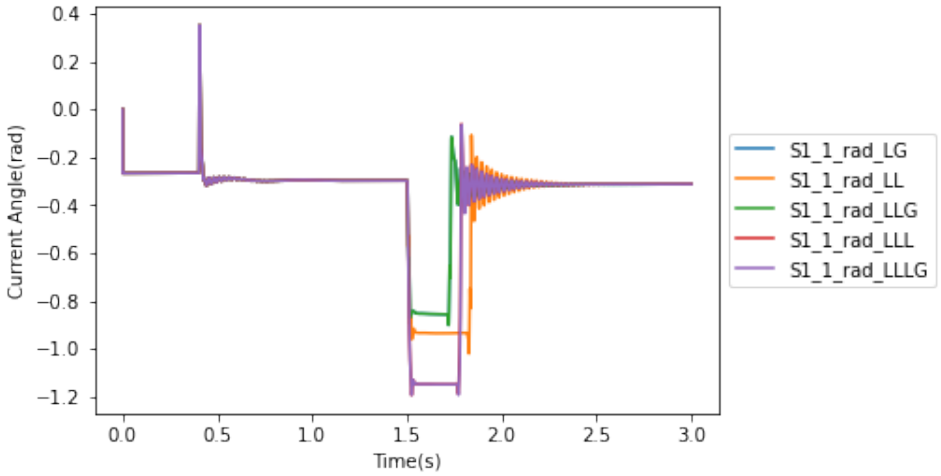

(**b**) Current source S_{1_1} angle

Figure 3.30: Primary protection current source 1 on bus 1 of distribution feeder protection circuit with DERs

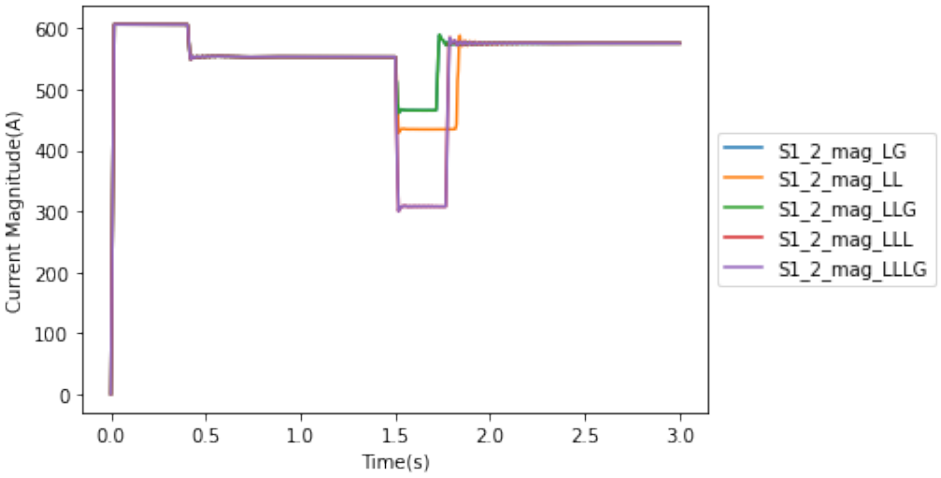

(**a**) Current source S_{1_2} magnitude

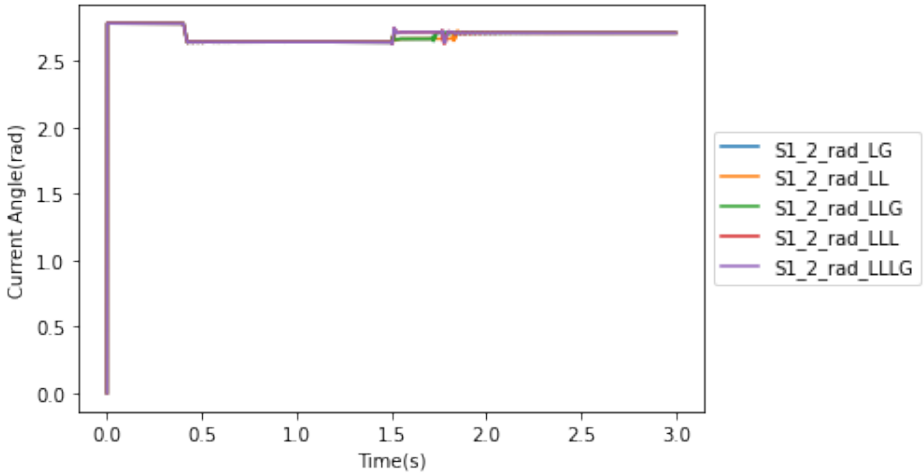

(**b**) Current source S_{1_2} angle

Figure 3.31: Primary protection current source 2 on bus 1 of distribution feeder protection circuit with DERs

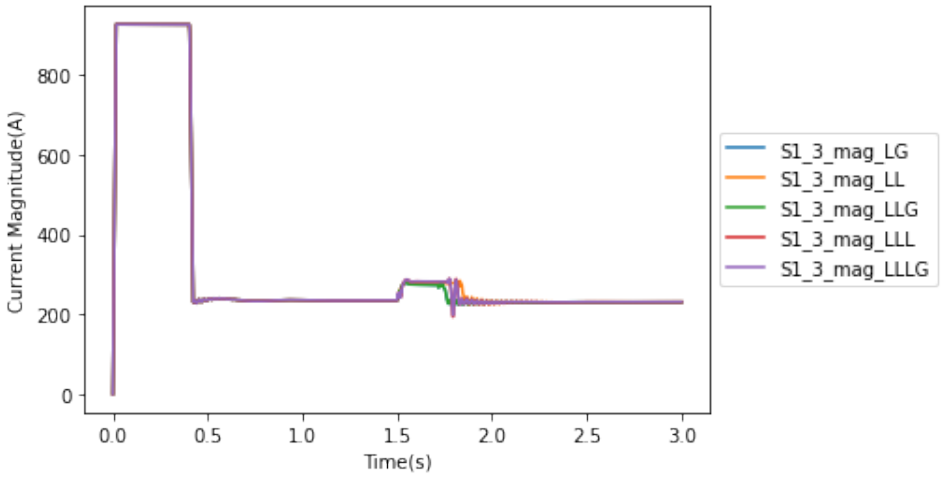

(**a**) Current source S_{1_3} magnitude

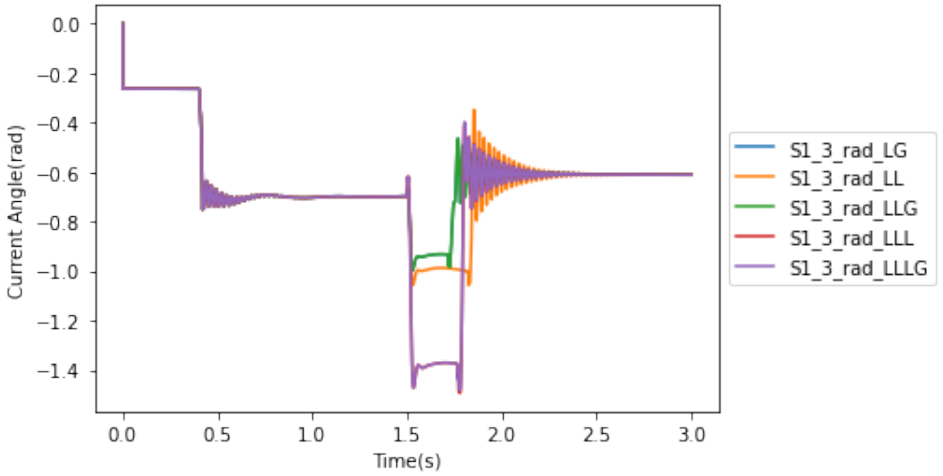

(**b**) Current source S_{1_3} angle

Figure 3.32: Primary protection current source 3 on bus 1 of distribution feeder protection circuit with DERs

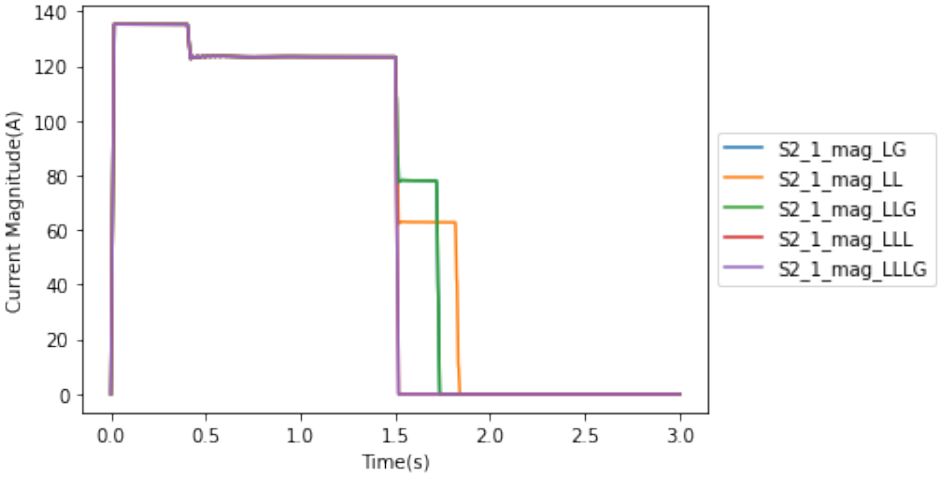

(**a**) Current source S_{2_1} magnitude

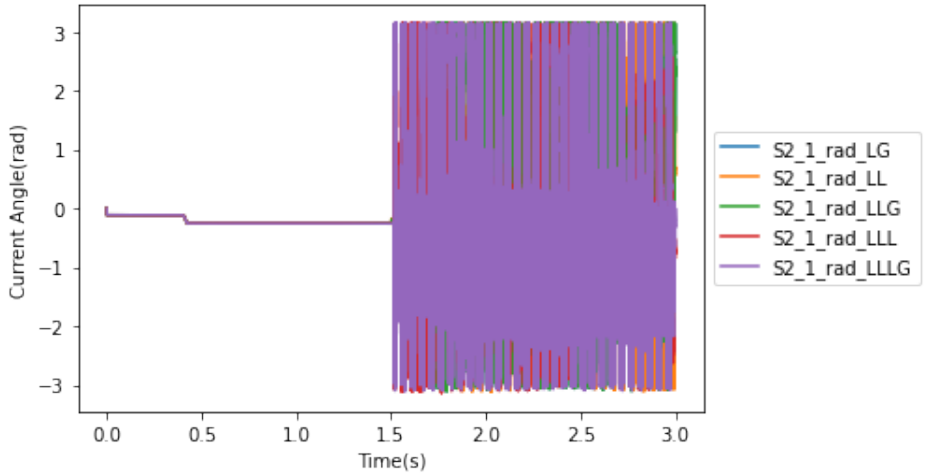

(**b**) Current source S_{2_1} angle

Figure 3.33: Primary protection current source 1 on bus 2 of distribution feeder protection circuit with DERs

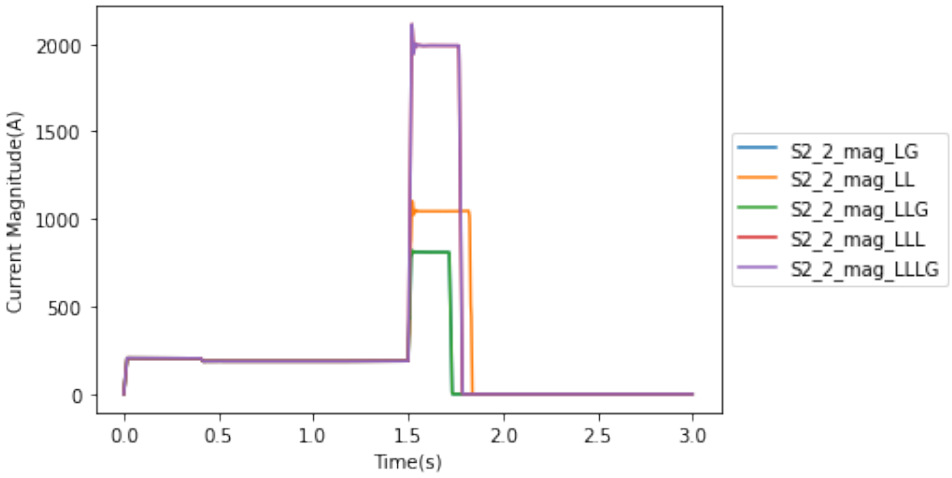

(**a**) Current source S_{2_2} magnitude

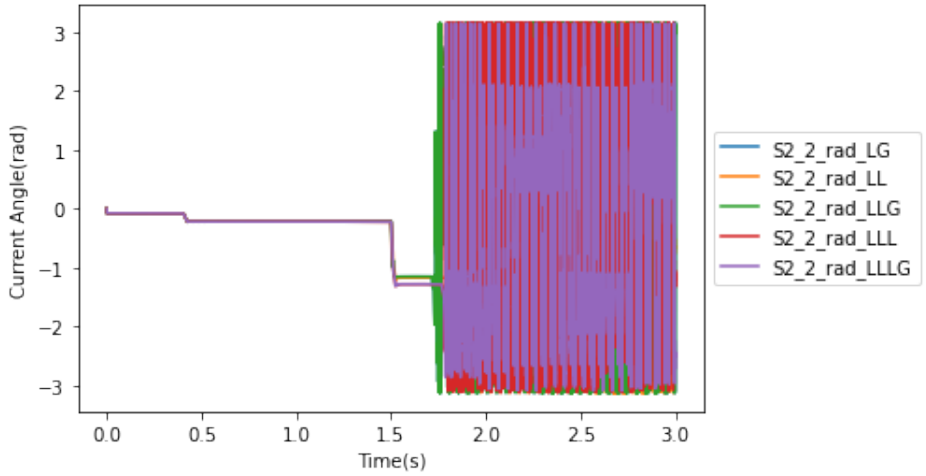

(**b**) Current source S_{2_2} angle

Figure 3.34: Primary protection current source 2 on bus 2 of distribution feeder protection circuit with DERs

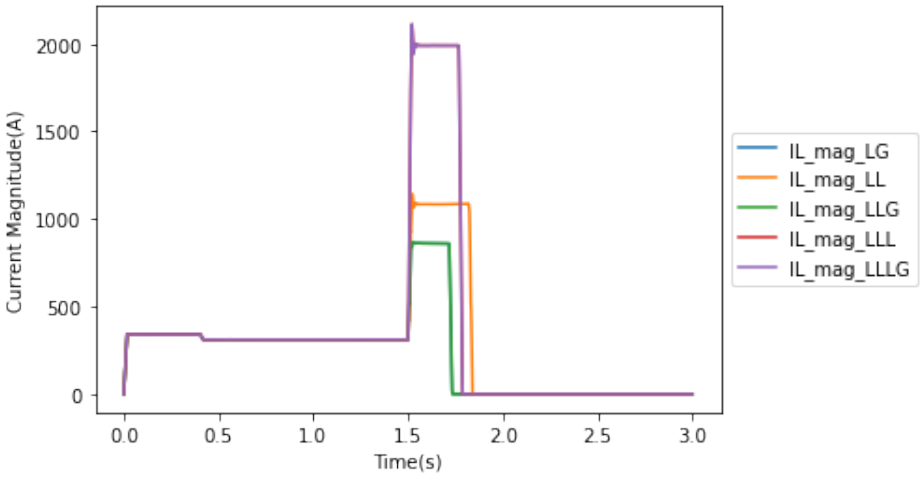

(**a**) Line current IL magnitude

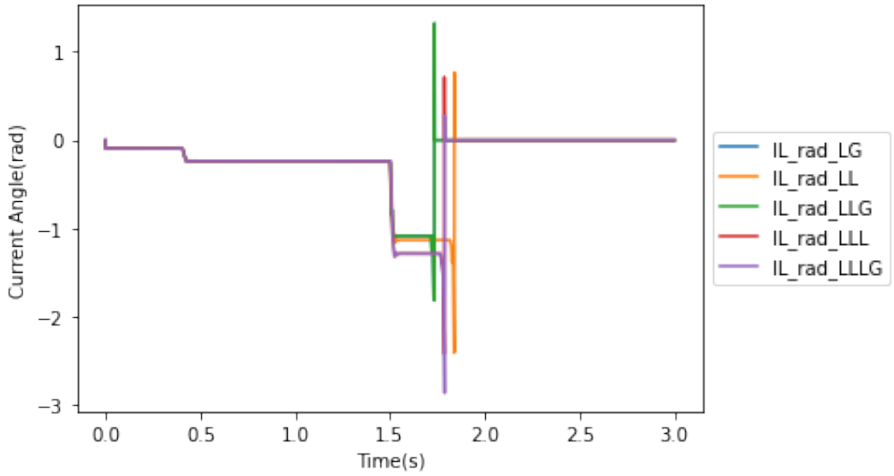

(**b**) Line current IL angle

Figure 3.35: Primary protection line current of distribution feeder protection circuit with DERs

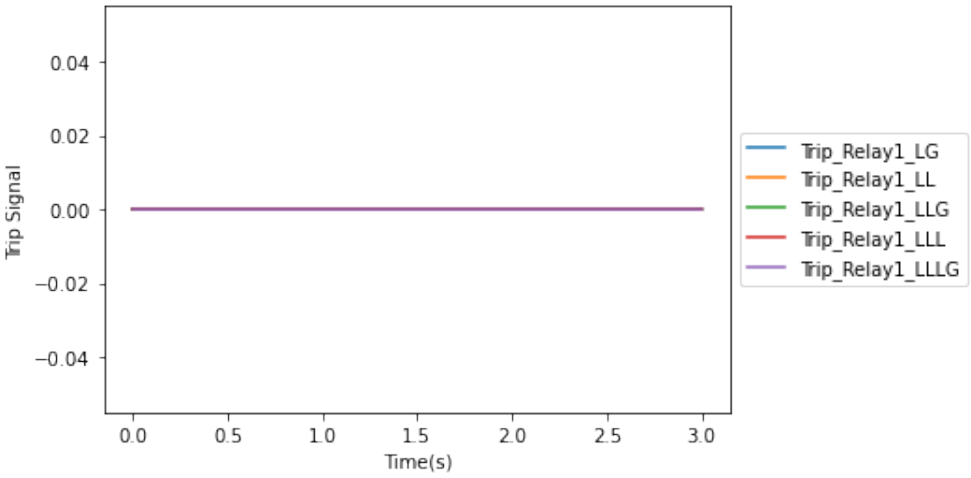

(**a**) Relay R_1 tripping signal

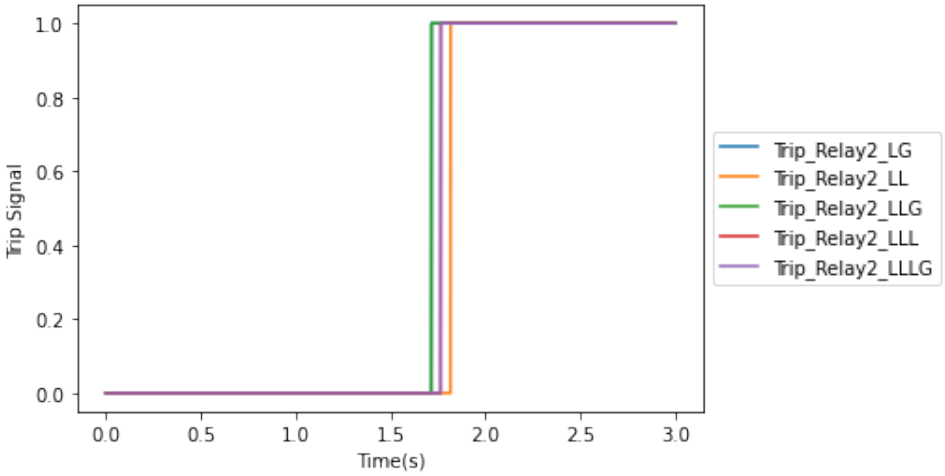

(**b**) Relay R_2 tripping signal

Figure 3.36: Primary Protection Tripping Signal of Distribution Feeder Protection Circuit with DERs

Backup Protection

Most settings in the backup protection are similar to the primary protection, except that the R_2 relay is disabled. Ideally, R_1 should trip when a fault happens at 1.5 seconds.

The voltage magnitude and angle of both buses are shown in Fig. 3.37 and 3.38. The current magnitude and angle of each source are shown in Fig. 3.39, 3.40 ,3.41, 3.42 and 3.43. The line current I_L is shown in Fig. 3.44. The tripping signal generated by both relays are shown in Fig. 3.45.

It can be observed from the below figures that, when the primary protection is disabled again, R_2 will not pick up. It is expected that R_1 will pick up and trip for the fault downstream. However, the tripping signal of R_1 is zero. The fault will never be cleared automatically in this case, because the injection of the DER causes the blinding of the upstream backup protection.

Since the fault is not cleared between 1.5 to 3 seconds, the collected measurements can be used to show the impact of the fault. Bus 1 is connected to the infinite bus, thus V_1 magnitude is reduced after the fault. LLLG is the most severe type of fault thus it causes the most significant voltage drop. Not all of the V_2 magnitude are zero after fault. This is because of the use of positive sequence voltage measurement. For those unsymmetrical faults, there are at least one phase that is not short circuited. In this case, the V_2 magnitude will not be zero based on the voltage form of Eq. (3.6). The current magnitude of infinite bus S_{1_1} and DER S_{1_3} are also worthy of discussion. S_{1_3} only increases to 1.2 times its original magnitude whereas S_{1_1} increases to 3 times its original value. Thus it is hard to distinguish the fault current by only measuring the contribution of the DER as the fault signature is not significant. Moreover, if the penetration

rate of the DER keeps increasing, the signature of the fault current coming from the infinite bus will no longer be a significant value.

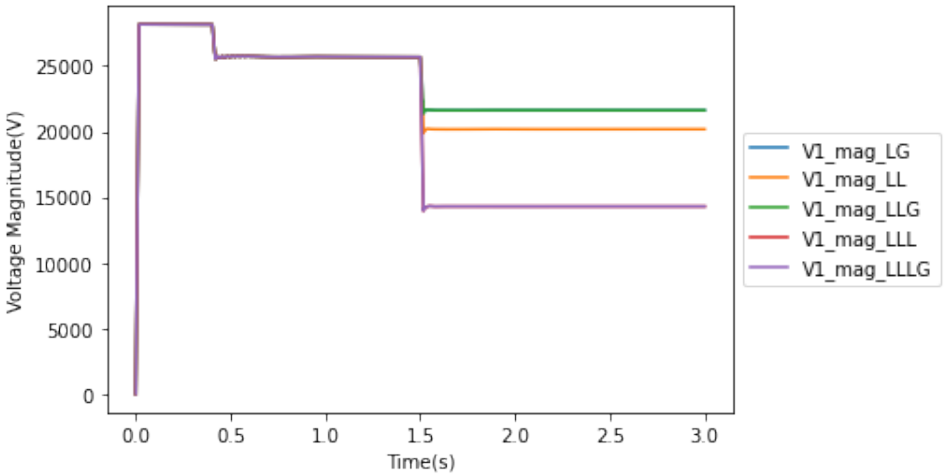

(**a**) Voltage V1 magnitude

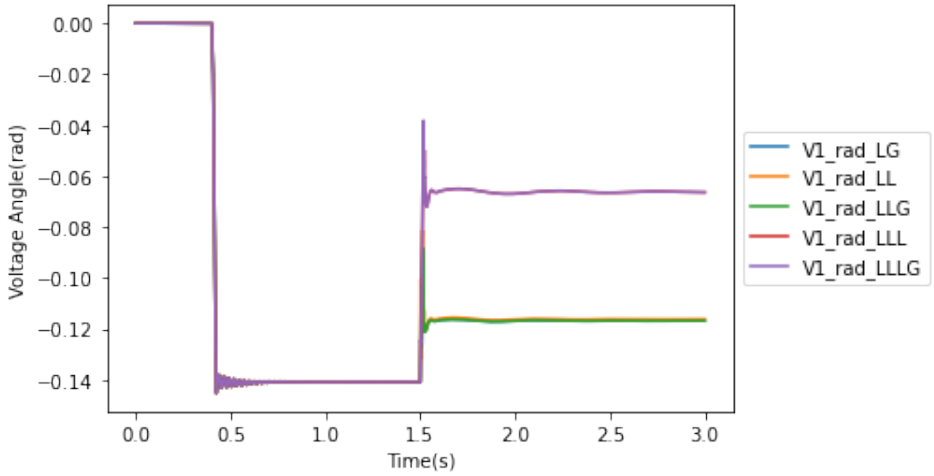

(**b**) Voltage V1 angle

Figure 3.37: Backup protection voltage on bus 1 of distribution feeder protection circuit with DER

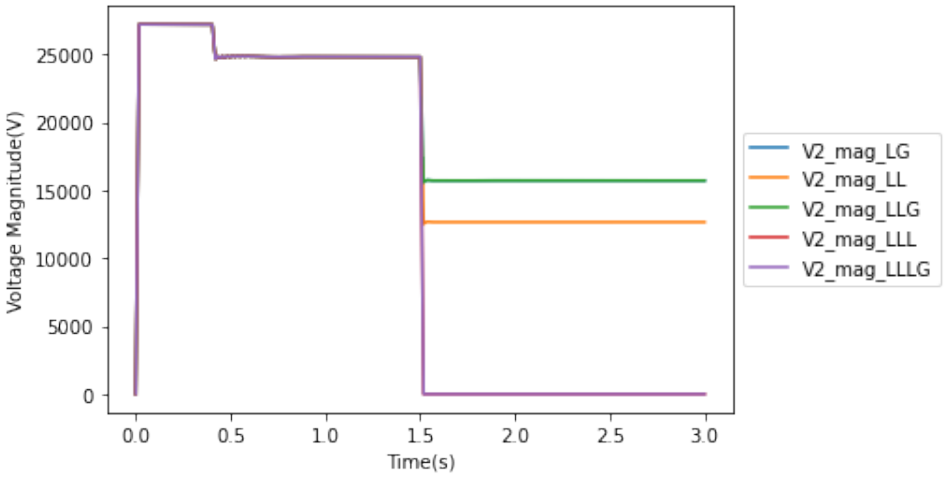

(**a**) Voltage V2 magnitude

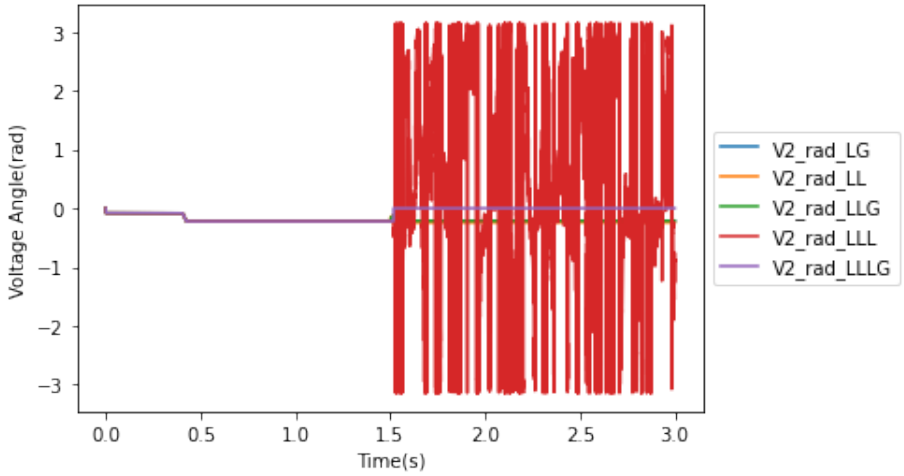

(**b**) Voltage V2 angle

Figure 3.38: Backup protection voltage on bus 2 of distribution feeder protection circuit with DER

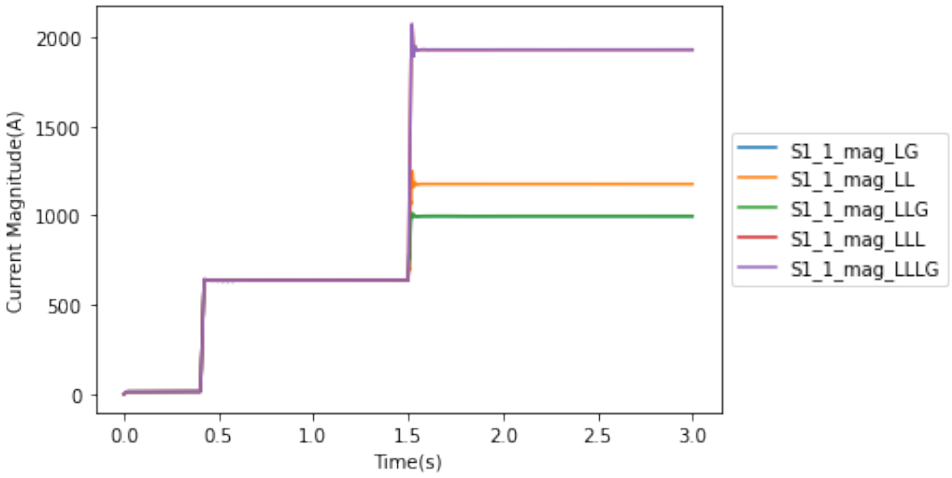

(**a**) Current source S_{1_1} magnitude

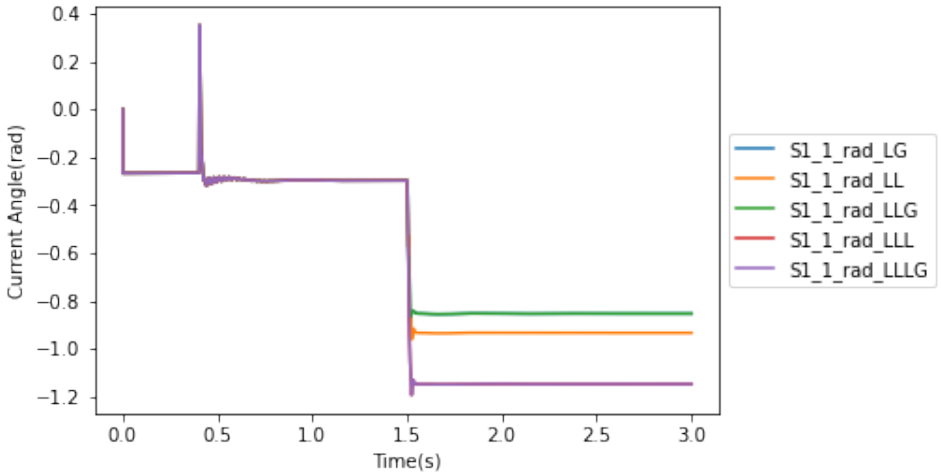

(**b**) Current source S_{1_1} angle

Figure 3.39: Backup protection current source 1 on bus 1 of distribution feeder protection circuit with DERs

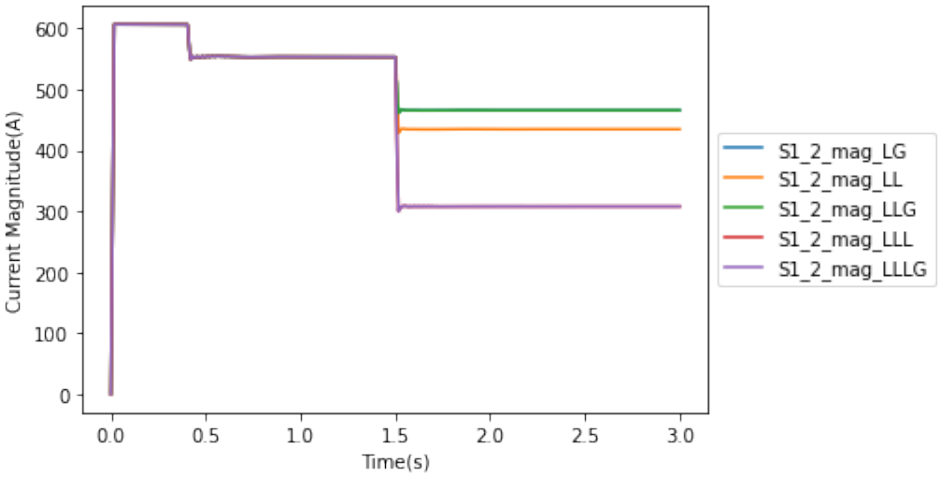

(**a**) Current source S_{1_2} magnitude

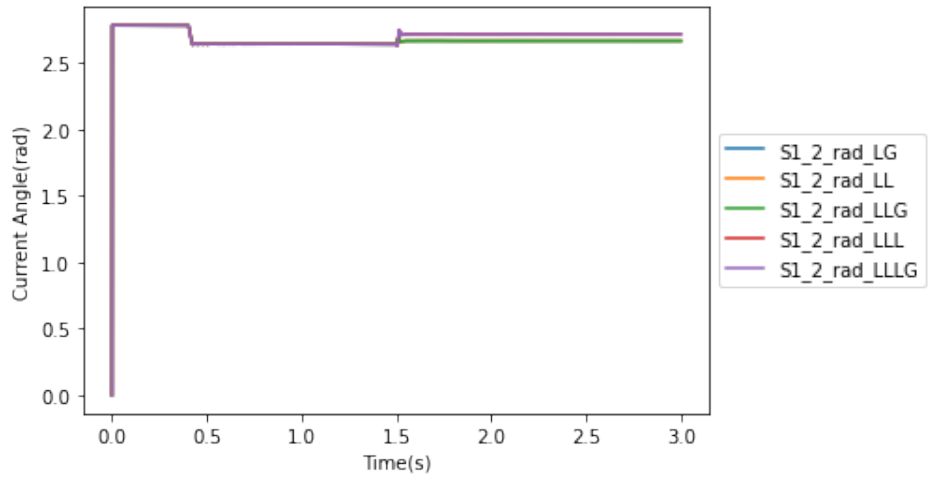

(**b**) Current source S_{1_2} angle

Figure 3.40: Backup protection current source 2 on bus 1 of distribution feeder protection circuit with DERs

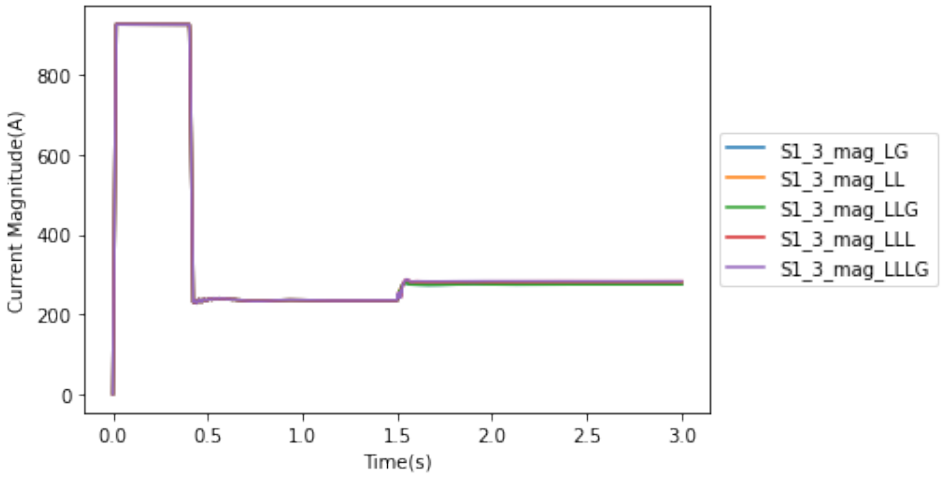

(**a**) Current source S_{1_3} magnitude

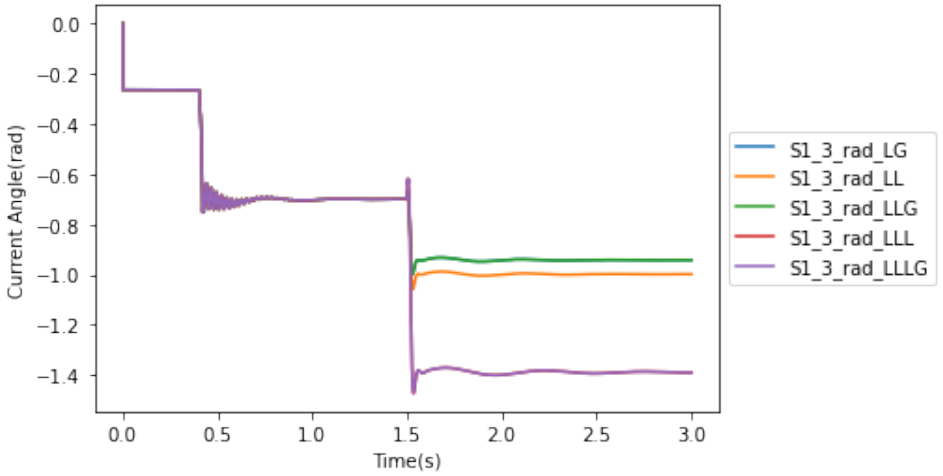

(**b**) Current source S_{1_3} angle

Figure 3.41: Backup protection current source 3 on bus 1 of distribution feeder protection circuit with DERs

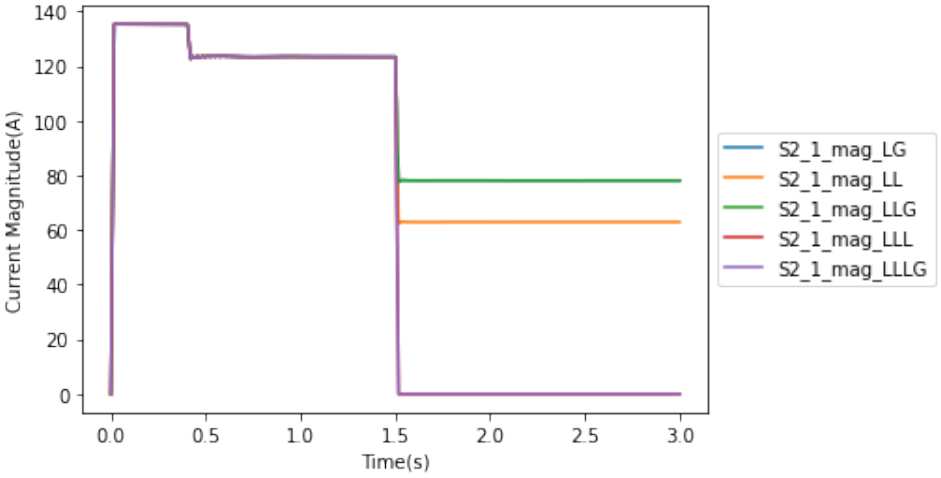

(**a**) Current source S_{2_1} magnitude

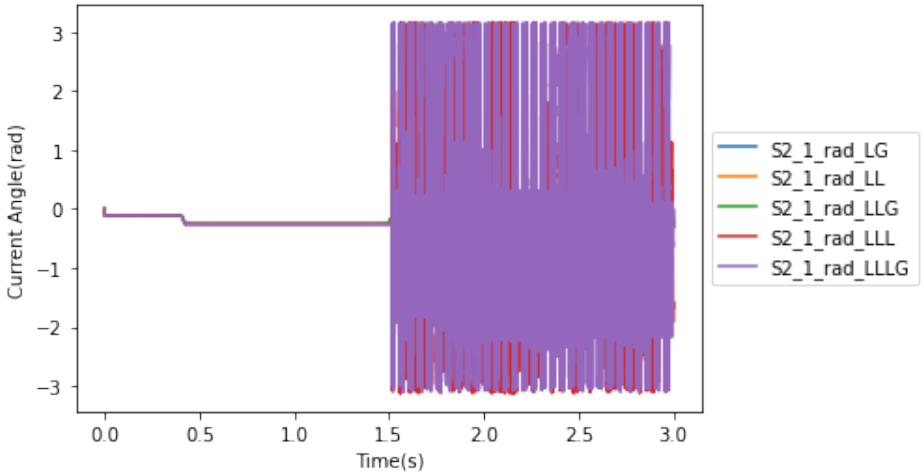

(**b**) Current source S_{2_1} angle

Figure 3.42: Backup protection current source 1 on bus 2 of distribution feeder protection circuit with DERs

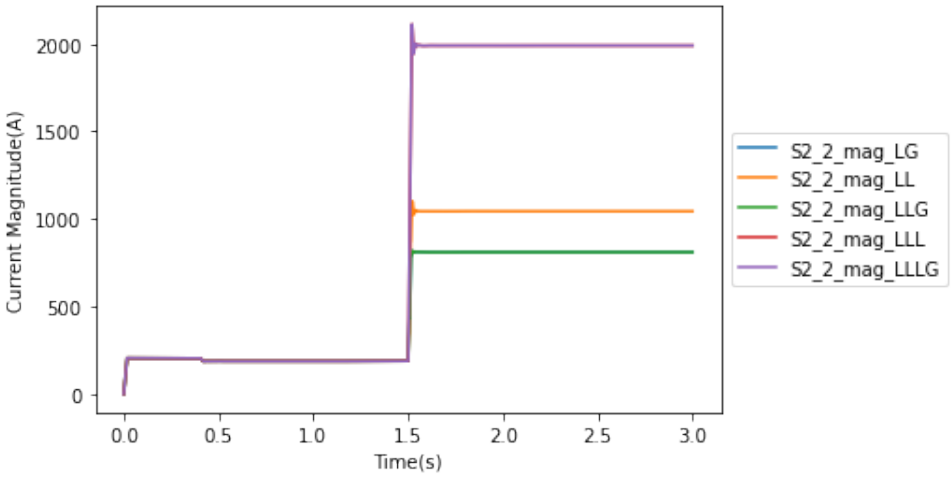

(**a**) Current source S_{2_2} magnitude

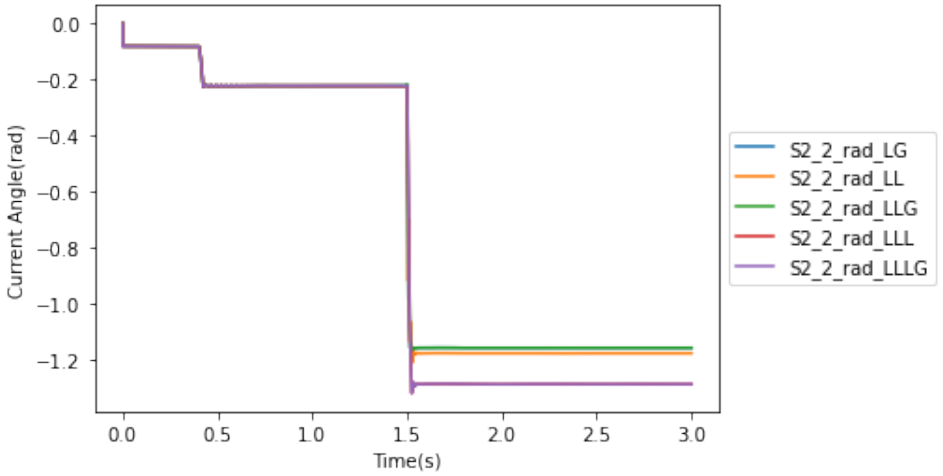

(**b**) Current source S_{2_2} angle

Figure 3.43: Backup protection current source 2 on bus 2 of distribution feeder protection circuit with DERs

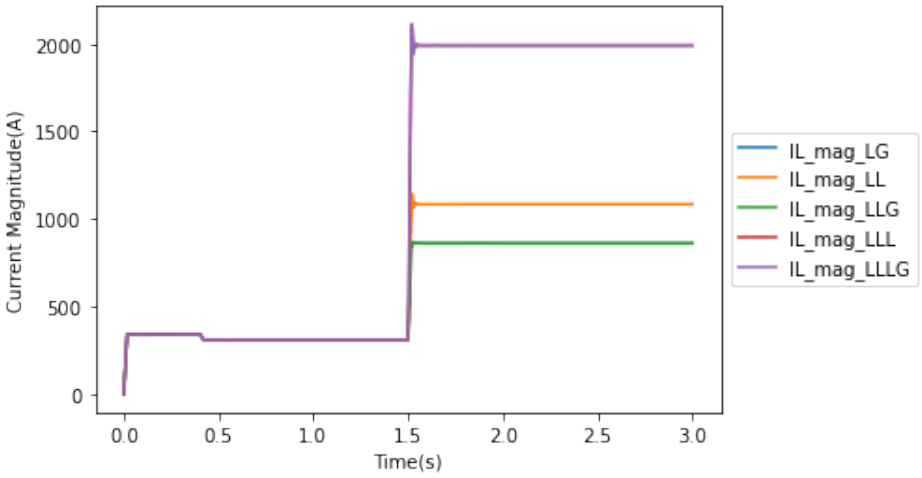

(**a**) Line current I_L magnitude

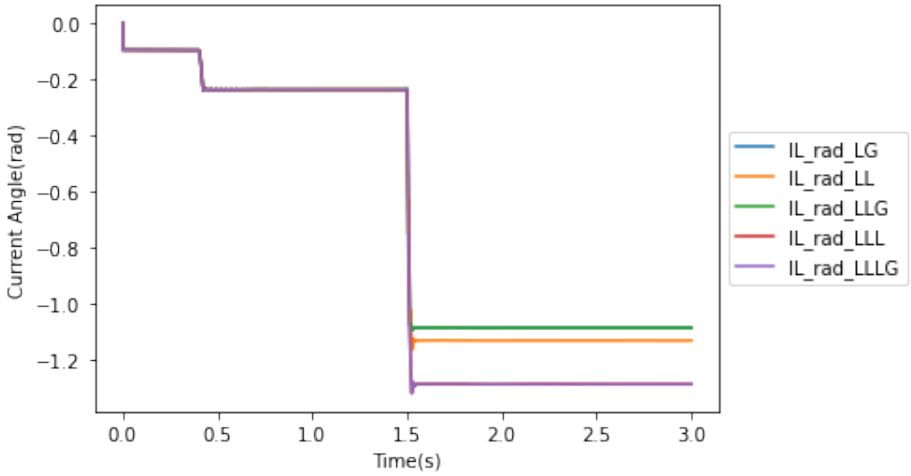

(**b**) Line current I_L angle

Figure 3.44: Backup Protection Line Current of Distribution Feeder Protection Circuit with DERs

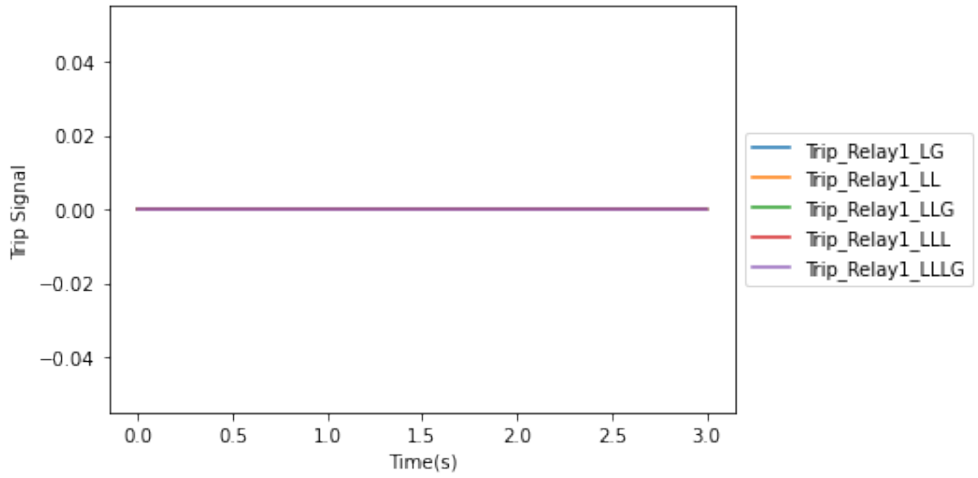

(**a**) Relay R_1 tripping signal

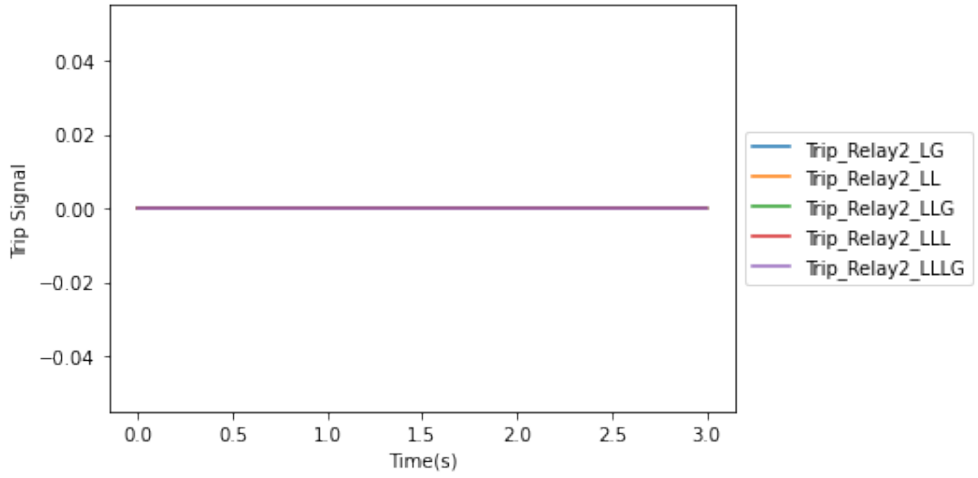

(**b**) Relay R_2 tripping signal

Figure 3.45: Backup Protection Tripping Signal of Distribution Feeder Protection Circuit with DERs

3.5 Conclusion

For most cases, when the primary relay fails to trip, the back up relay has the potential of failing to pickup or trip in advance to stay in coordination with downstream protection. What is expected is both relays pickup at the same time

and the trip operating time is based on their IDMT curves.

A possible improvement is sought that if the backup relay can get the fault information of the primary relay and operate correctly, the aforementioned malfunctioned relay problems will no longer exist. However, even if the backup relay can get the fault information of the primary relay, it does not know how to use this information to operate properly. Moreover, the backup relay will not pickup until receiving the fault information of the primary relay. The grading margin that caused by the delaying of breaker mechanism operating time should also be considered for the backup relay to trip. This process will greatly reduce the speed of operation.

Chapter 4

Theory of Current Tracing Analytics

4.1 Introduction

It was demonstrated in the previous chapter that increasing penetration of renewable energy has led to some serious protection coordination problems which do not ordinarily occur in conventional distribution grids with low renewable energy penetration. One of the key problems as mentioned before is the rising amount of distributed and intermittent renewable energy that can disrupt the existing protection coordination scheme. One approach to dealing with these issues is to examine the network topology and the need to mathematically resolve them in real time as a basis for new protection relaying algorithms.

The traditional distribution grids are designed for single direction power flow from the substation to the customers. The renewable energy at the customer end can now generate power that is consumed by the customer or feedback excess power to the rest of the distribution feeder. In a very high penetration scenario,

the back feed may affect transmission level power flows. This raises new challenges to grid modeling methods in practical problems of state estimation and feeder protection, where the impacts of excess power flow have to be considered.

Many grid modeling methods have been proposed previously. Some of the modeling methods target different types of power grids. In [55, 56], the author proposed averaged models for modular multilevel converter for high voltage direct current systems. In [57], the author took advantage of the public map data for the generation of model grids in all voltage levels of the distribution grid. A port-Hamiltonian based dynamic power system model is established in [58], which accounts for all the key elements of power system, including the grid modeling.

Most of the grid modeling methods are designed for particular parts of the power grid, including the cyber-physical power systems framework modeling [59, 60], topology modeling [61, 62], load flow modeling [63, 64], traveling wave modeling [65]. Almost all of these methods are based on the existing physical infrastructure of power system in which currents from different power sources are congested to one end of the single power line and flowing towards the other.

To solve the aforementioned practical problems, a more detailed grid model has been suggested, which not only gives the overall picture of the power grid, but also has sufficient details of the current flows from each individual renewable energy source connected to the grid.

Inspired by Dr. Yu's paper's of transmission line dissection [66], the author of this thesis modifies and expands upon this technique of electrical decomposition of networks for a generalized current tracing method for distribution grids. Instead of using the traditional grid model of currents that are congested on a single power line, the power line following the fundamental electrical and physical principles is decomposed such that currents from each individual power source can be viewed

as virtually flowing through the decomposed power lines. When all the lines in the power grid are decomposed in this manner, it becomes possible to trace the currents flowing from different renewable energy sources to different loads. By doing so, this technique can lend itself to better fault current flow identification for improved protection system responses.

4.2 Formulation of Multiple Sources to Grid Current Tracing

4.2.1 Single Distribution System Feeder Line Example

Consider the single power distribution line case where multiple renewable energy and loads are connected to bus 1 with the other end connecting to the power distribution grid as shown in Fig. 4.1.

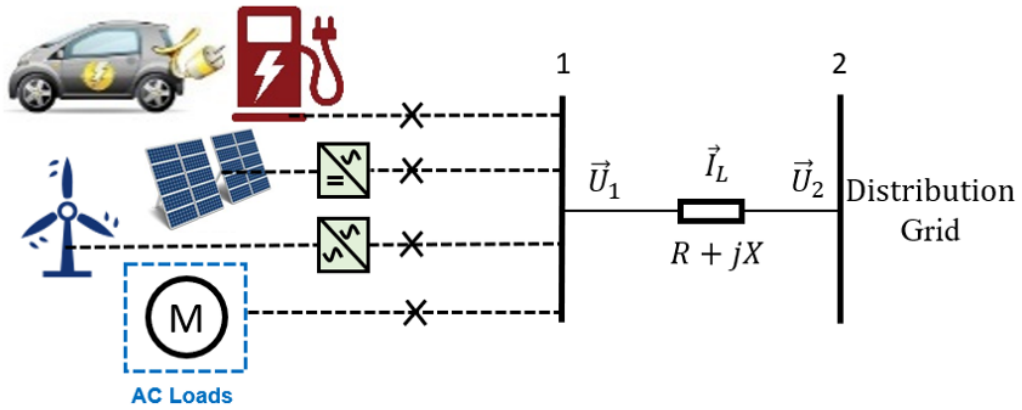

Figure 4.1: Single power distribution line

The currents $\vec{I}_L$ flowing towards either bus 1 or bus 2 depend on the load and power generation on bus 1. $\vec{U}_1$ and $\vec{U}_2$ are the voltages on bus 1 and bus 2 respectively. Generally, the currents in a distribution grid will flow from the

substation transformer to customers, in this case, from bus 2 to bus 1. The bidirectional power flow appears when the load on bus 1 cannot consume as much power as generated at the same time. The excess power must flow from bus 1 towards bus 2. The currents will also flow from bus 1 to bus 2. Moreover, it is necessary to know how much each current source contributes to the $\vec{I}_L$, for the purpose of the protection relay coordination during a fault.

4.2.2 Multiple Equivalent Current Source Model

Without loss of generality, it is assumed that the impedance between bus 1 and bus 2 is

$$Z = R + jX, \tag{4.1}$$

where $R > 0$ and $X > 0$ are the resistance and reactance of the power line respectively.

The impedance angle is θ and the voltage difference angle of $\vec{U}_1$ and $\vec{U}_2$ is ψ. The current $\vec{I}_L$ that is flowing through the power line is

$$\vec{I}_L = I_L e^{j(\psi-\theta)}, \tag{4.2}$$

where $I_L > 0$ is the magnitude of $\vec{I}_L$. The i^{th} current source connects to bus 1 can be written as,

$$\vec{I}_{Li} = I_{Li} e^{j\phi_i}, \tag{4.3}$$

where ϕ_i is the phase angle of the i^{th} current source, and $I_{Li} > 0$ is the magnitude of $\vec{I}_{Li}$. These currents can be related through Kirchhoff's current law as,

$$\vec{I}_L = \sum I_{Li} e^{j\phi_i}. \tag{4.4}$$

4.2.3 Equivalent Circuit

The single power line can be expressed with an impedance as shown in Fig. 4.1. Its equivalent circuit as shown in Fig. 4.2 has the same property as the original one, i.e., the total amount of current and power that flows from bus 1 to bus 2 is the same.

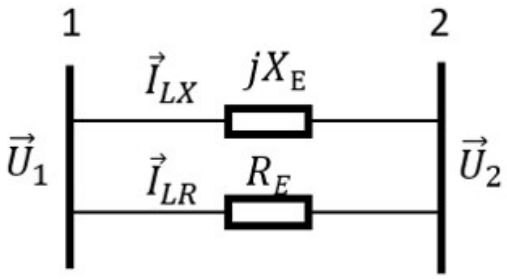

Figure 4.2: Active-reactive current equivalent circuit

The equivalent circuit consist of two parallel connected equivalent resistance and reactance. The equivalent resistance and reactance in Fig. 4.2 can be expressed as

$$R_E = \frac{R^2 + X^2}{R}, \tag{4.5}$$

$$X_E = \frac{R^2 + X^2}{X}, \tag{4.6}$$

where R_E and X_E are the equivalent resistance and reactance respectively which are both positive. Obviously, the equivalent circuit has the same resistance of the original one,

$$Z = \frac{1}{\frac{1}{R_E} + \frac{1}{jX_E}} \tag{4.7}$$

4.2.4 Active and Reactive Current

In Fig. 4.2, the equivalent circuit splits the current into two parts. The current that flows through the resistance is defined as active current, and the reactive current is defined as the current flowing through the reactance. This is in contrast to Fig. 4.1 in which the active and reactive current are flowing through the same line. In Fig. 4.2, the two types of currents are virtually flowing through two parallel connected virtual power lines.

The active current $\vec{I}_{LR}$ in $\vec{I}_L$ is in phase with the applied voltage $\vec{U}_1 - \vec{U}_2$ on the single power line as there is no phase shift on the equivalent resistance,

$$\vec{I}_{LR} = I_{LR} e^{j\psi}, \tag{4.8}$$

$$I_{LR} = I_L cos(\theta), \tag{4.9}$$

where I_{LR} is the magnitude of the active current $\vec{I}_{LR}$.

The reactive current $\vec{I}_{LX}$ in $\vec{I}_L$ is 90 degree phase shifted from the active current as follows,

$$\vec{I}_{LX} = I_{LX} e^{j(\psi - \frac{\pi}{2})}, \tag{4.10}$$

$$I_{LX} = I_L sin(\theta), \tag{4.11}$$

where I_{LX} is the magnitude of the reactive current $\vec{I}_{LX}$.

The sum of active and reactive current has to be equal to the total power line current,

$$\vec{I}_L = \vec{I}_{LR} + \vec{I}_{LX}. \tag{4.12}$$

The relationship between $\vec{I}_L$, $\vec{I}_X$ and $\vec{I}_R$ is shown in Fig.4.3.

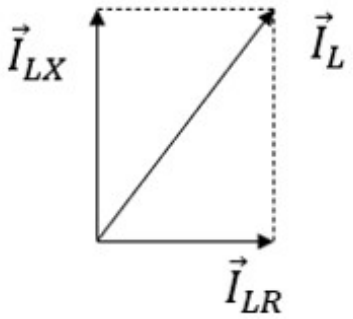

Figure 4.3: Active and reactive current

4.2.5 Current Tracing

All the current sources connected on bus 1 should follow the same rule,

$$\vec{I}_{Li} = \vec{I}_{LRi} + \vec{I}_{LXi} = I_{LRi}e^{j\psi} + I_{LXi}e^{j(\psi-\frac{\pi}{2})}, \tag{4.13}$$

where $\vec{I}_{Li}$ is the current of the i^{th} current source on the power line, and

$$I_{LRi} = I_{Li}cos(\psi - \phi_i), \tag{4.14}$$

$$I_{LXi} = I_{Li}sin(\psi - \phi_i), \tag{4.15}$$

are the magnitude of the active and reactive current of $\vec{I}_{Li}$ respectively. The sets of the active and reactive current magnitudes, I_{LRi} and I_{LXi}, are defined as Ω_{RM} and Ω_{XM} such that,

$$\Omega_{RM} = \{I_{LRi}|0 < i \leq Number\ of\ Current\ Sources\} \tag{4.16}$$

$$\Omega_{XM} = \{I_{LXi}|0 < i \leq Number\ of\ Current\ Sources\} \tag{4.17}$$

where M represents that both sets are the current magnitude sets.

From Kirchhoff's current law, the sum of the active and reactive current from

each current source should be equal to the total active and reactive current on the power line respectively as shown in Eq. (4.8) and (4.10),

$$\sum_{I_{LRi}>0}(\vec{I}_{LRi}) + \sum_{I_{LRi}<0}(\vec{I}_{LRi}) = \sum(\vec{I}_{LRi}) = \vec{I}_{LR}, \tag{4.18}$$

$$\sum_{I_{LXi}>0}(\vec{I}_{LXi}) + \sum_{I_{LXi}<0}(\vec{I}_{LXi}) = \sum(\vec{I}_{LXi}) = \vec{I}_{LX}, \tag{4.19}$$

where each of the two sums also constitutes of two parts as shown on the left hand side of Eq. (4.18) and (4.19), and $\sum_{I_{LRi}>0}(\vec{I}_{LRi})$ and $\sum_{I_{LRi}<0}(\vec{I}_{LRi})$ represents the positive and negative part of the active current on the power line respectively, $\sum_{I_{LXi}>0}(\vec{I}_{LXi})$ and $\sum_{I_{LXi}<0}(\vec{I}_{LXi})$ represents the positive and negative part of reactive current on the power line respectively. The two parts are classified by whether the magnitude is positive or negative as shown in Eq. (4.14) and (4.15).

Both $\sum_{I_{LRi}>0}(\vec{I}_{LRi})$ and $\sum_{I_{LXi}>0}(\vec{I}_{LXi})$ will be responsible for supplying the load as well as feeding excess current from one current source to the others.

The relationship of the currents is shown in Fig. 4.4.

In Fig. 4.4, R_E and jX_E are the two axes that stands for the equivalent resistance and reactance as shown in Eq. (4.5) and (4.6). The power line current $\vec{I}_L$ can be projected to the R_E and jX_E axes, known as $\vec{I}_{LR}$ and $\vec{I}_{LX}$. The power line current $\vec{I}_L$ is consisted of four current sources: $\vec{I}_1$, $\vec{I}_2$, $\vec{I}_3$ and $\vec{I}_4$. Each of them can be projected to the R_E and jX_E axes, known as $\vec{I}_{LRi}$ and $\vec{I}_{LXi}$. If $\vec{I}_{LRi}$ and $\vec{I}_{LXi}$ are pointed to the same direction of $\vec{I}_{LR}$ and $\vec{I}_{LX}$, they are considered as positive current sources that are providing active or reactive current to $\vec{I}_L$. As mentioned in Eq. (4.18) and (4.19), they will be responsible for supplying the load as well as feeding excess current from one current source to the others. However, this excess current value should be quantified such that the detailed contribution

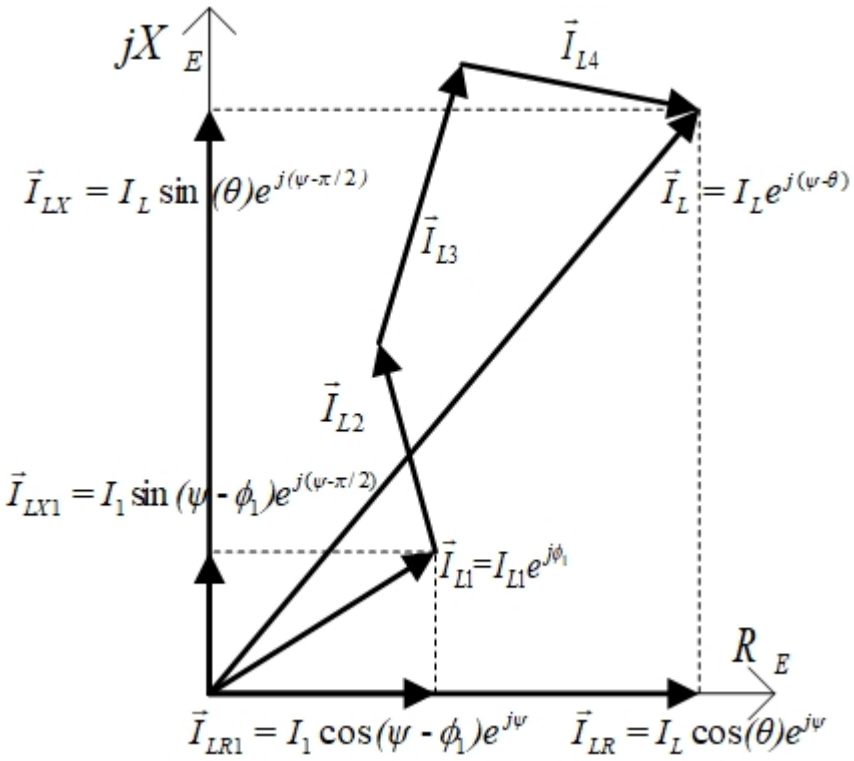

Figure 4.4: Relationship of currents

from each current source to the power distribution line will be available for further analysis.

4.2.6 Current Tracing on Distribution Power Line

Only the positive current source can contribute excess current to the other ones. If the two current sources are connected through a power line, it is necessary to quantify the excess current that flows through the power line. The j^{th} positive current source that flows through the line is

$$\vec{I}_{LRjP} = I_{LRjP} e^{j\psi}, \tag{4.20}$$

$$\vec{I}_{LXjP} = I_{LXjP} e^{j(\psi - \frac{\pi}{2})}, \tag{4.21}$$

where $\vec{I}_{LRjP}$ is positive part of the j^{th} active current source flowing through the power line with magnitude of I_{LRjP}, $\vec{I}_{LXjP}$ is positive part of the j^{th} reactive current source flowing through the power line with magnitude of I_{LXjP}.
The magnitude of the positive part of the j^{th} active and reactive current depends on its proportion in the overall active and reactive current flowing towards the power distribution network,

$$I_{LRjP} = \frac{I_{LR} I_{LRj}}{\sum\limits_{I_{LRi}>0} (I_{LRi})}, \tag{4.22}$$

$$I_{LXjP} = \frac{I_{LX} I_{LXj}}{\sum\limits_{I_{LXi}>0} (I_{LXi})}. \tag{4.23}$$

Therefore, the distribution power grid model where each of the currents are independent from each other can be shown in Fig. 4.5.

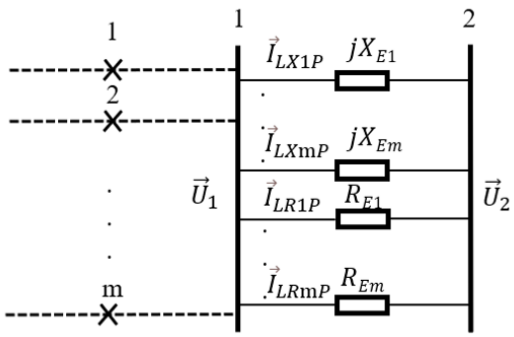

Figure 4.5: Multiple current sources tracing equivalent circuit

In Fig. 4.5, the sub resistance and reactance can be written as,

$$R_{Ej} = \frac{\sum\limits_{I_{LRi}>0} (I_{LRi})}{I_{LRj}} R_E, \tag{4.24}$$

$$X_{Ej} = \frac{\sum\limits_{I_{LXi}>0} (I_{LXi})}{I_{LRj}} R_E, \tag{4.25}$$

where R_{Ej} and X_{Ej} stand for the positive resistance and reactance of j^{th} parallel connected virtual branch as shown in Fig. 4.5. It is an equivalent circuit representation of Fig. 4.2 as given by

$$\sum \frac{1}{R_{Ej}} = \sum \frac{I_{LRj}}{R_E \sum\limits_{I_{LRi}>0} I_{LRi}} = \frac{1}{R_E}, \tag{4.26}$$

$$\sum \frac{1}{X_{Ej}} = \sum \frac{I_{LXj}}{X_E \sum\limits_{I_{LXi}>0} I_{LXi}} = \frac{1}{X_E}. \tag{4.27}$$

Therefore, the virtual parallel connected power lines have the same impedance as that of Eq. (4.1). This proves the correctness of the proposed theory that it will not violate any physical and electrical principles.

4.2.7 Equivalent Circuit of Impedance Lines

With the information expressed in Eq. (4.24-4.27), an equivalent can be established with the virtual parallel connected lines. Each of these power lines has a virtual impedance of R_{Ej} or X_{Ej}. By combining R_{Ej} and X_{Ej}, the virtual impedance line is defined as $\frac{1}{Z_{Ej}}$ such that,

$$\frac{1}{Z_{Ej}} = \frac{1}{R_{Ej}} + \frac{1}{X_{Ej}}. \tag{4.28}$$

Then the virtual current that is flowing through $\frac{1}{Z_{Ej}}$ is,

$$\vec{I}_{LZjP} = \vec{I}_{LRjP} + \vec{I}_{LXjP}. \tag{4.29}$$

where $\vec{I}_{LZjP}$ is defined as the decomposed current that flows from the j^{th} current source to the power distribution line. The equivalent circuit could be represented

as shown in Fig.4.6,

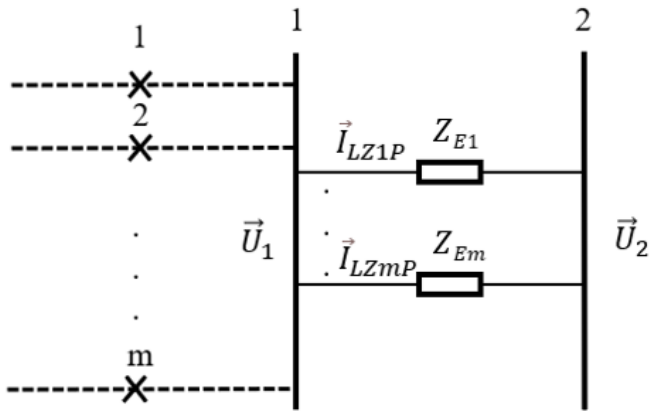

Figure 4.6: Equivalent circuit of impedance lines

With the information of the equivalent circuit of impedance lines, the values of decomposed currents can be quantified. The detailed current contribution from each current source to the power line is now available.

4.2.8 Alternative Situations

It is assumed in Eq. (4.1) that $R > 0$ and $X > 0$, but the developed current tracing model also works for the $R > 0$ and $X < 0$ situation. In this case, all of the $\psi - \frac{\pi}{2}$ terms in the equations become $\psi + \frac{\pi}{2}$. To facilitate analysis, only the $R > 0$ and $X > 0$ situation is considered in the rest of the thesis.

It is also assumed that the current is flowing from bus 1 to bus 2, in which the current magnitudes in Eq. (4.22) and (4.23) are positive. Alternatively, the current magnitudes in Eq. (4.22) and (4.23) are negative if the curernt is flowing from bus 2 to bus 1. Notice that the current tracing equation derived in Subsection 4.2.6 is also suitable for the situation where bus 1 is connecting to the distribution grid while bus 2 is connecting to multiple current sources no matter which direction the current is flowing on the power line.

4.3 Formulation of Multiple Sources to Multiple Sources on Single Distribution Line

In Fig. 4.1, only the current from multiple current sources to a single current source on the power distribution line is decomposed. In reality, DERs could connect on both sides of the power line, as shown in Fig. 4.7. Moreover, bus 2 is connecting to the distribution grid. Therefore, it is necessary to decompose the current from multiple current sources to multiple current sources such that the decomposed current between each current sources can be derived.

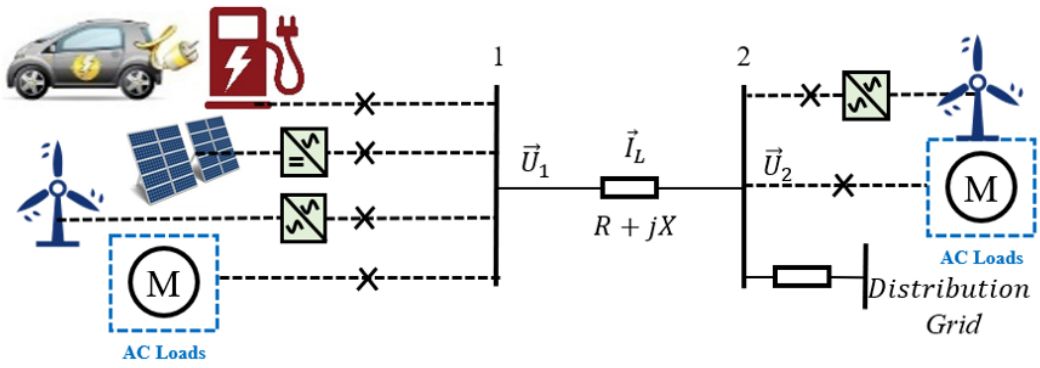

Figure 4.7: Multiple sources to multiple sources on single distribution line

4.3.1 Current Tracing of Multiple Sources to Multiple Sources

Here, it is assumed that there are m current sources connected to bus 1 and n current sources connected to bus 2. All m current sources attached to bus 1 are already decomposed as shown in Eq. (4.22), (4.23) and (4.29). Defining the set of decomposed currents on the power line from bus 1 that connect m current

sources as

$$\Omega R_{in} = \{\vec{I}_{1LRi} | 0 \leq i \leq m\}, \tag{4.30}$$

$$\Omega X_{in} = \{\vec{I}_{1LXi} | 0 \leq i \leq m\}, \tag{4.31}$$

where $\vec{I}_{1LRi}$ and $\vec{I}_{1LXi}$ stands for the i^{th} active and reactive current on the power line from bus 1 that connects m current source respectively, ΩR_{in} and ΩX_{in} are the two sets of the above active and reactive current.

Similarly, the set of decomposed currents on the power line from bus 2 that connect n current source is defined as

$$\Omega R_{out} = \{\vec{I}_{2LRj} | 0 \leq j \leq n\}, \tag{4.32}$$

$$\Omega X_{out} = \{\vec{I}_{2LXj} | 0 \leq j \leq n\} \tag{4.33}$$

where $\vec{I}_{2LRj}$ and $\vec{I}_{2LXj}$ stands for the j^{th} active and reactive current on the power line from bus 2 that connect n current sources respectively, ΩR_{out} and ΩX_{out} are the two sets of the above active and reactive current.

Given the situation that the voltage difference between the two buses should be the same, no matter how the form of the equivalent circuit changes, a mapping from the set of decomposed current ΩR_{in} and ΩX_{in} to ΩR_{out} and ΩX_{out} are

established such that,

$$\vec{I}_{i'jLR} = I_{i'jLR} \times e^{j\psi}, \tag{4.34}$$

$$I_{i'jLR} = \frac{I_{1LRi}}{I_{LR}} \times I_{2LRj}, \tag{4.35}$$

$$\vec{I}_{i'jLX} = I_{i'jLX} \times e^{j(\psi-\pi/2)}, \tag{4.36}$$

$$I_{i'jLX} = \frac{I_{1LXi}}{I_{LR}} \times I_{2LXj}, \tag{4.37}$$

where $\vec{I}_{i'jLR}$ stands for the active current flowing from current source $I_{1LRi} \in \Omega R_{in}$ to $I_{2LRj} \in \Omega R_{out}$. Similarly, $\vec{I}_{i'jLX}$ stands for the reactive current flowing from current source $I_{1LXi} \in \Omega X_{in}$ to $I_{2LXj} \in \Omega X_{out}$.

Therefore, the decomposed current that flows from the i^{th} current source connected to bus 1 to the j^{th} current source connected to bus 2 can be written as

$$\vec{I}_{i'jL} = \vec{I}_{i'jLR} + \vec{I}_{i'jLX}. \tag{4.38}$$

The combination of active and reactive current is defined as Ω such that,

$$\Omega_{in\_out} = \Omega R_{in\_out} + \Omega X_{in\_out}, \tag{4.39}$$

where $\Omega_{in\_out} = \{\vec{I}_{i'jL} \,|\, 0 \leq i \leq m,\, 0 \leq j \leq n\}$,
$\Omega R_{in\_out} = \{\vec{I}_{i'jLR} \,|\, 0 \leq i \leq m,\, 0 \leq j \leq n\}$,
$\Omega X_{in\_out} = \{\vec{I}_{i'jLX} \,|\, 0 \leq i \leq m,\, 0 \leq j \leq n\}$.

The mapping of a single decomposed current from the i^{th} current source connected to bus 1 to the j^{th} current source that connects to bus 2 can be defined as,

$$\Omega_{in\_out\_i\_j} = \vec{I}_{i'jL}, \tag{4.40}$$

where $\Omega_{in\_out\_i\_j} \in \Omega_{in\_out}$. Therefore, the magnitude and angle of $\Omega_{in\_out\_i\_j}$ can be represented as $\Omega_{in\_out\_mag\_i\_j}$ and $\Omega_{in\_out\_rad\_i\_j}$ respectively.

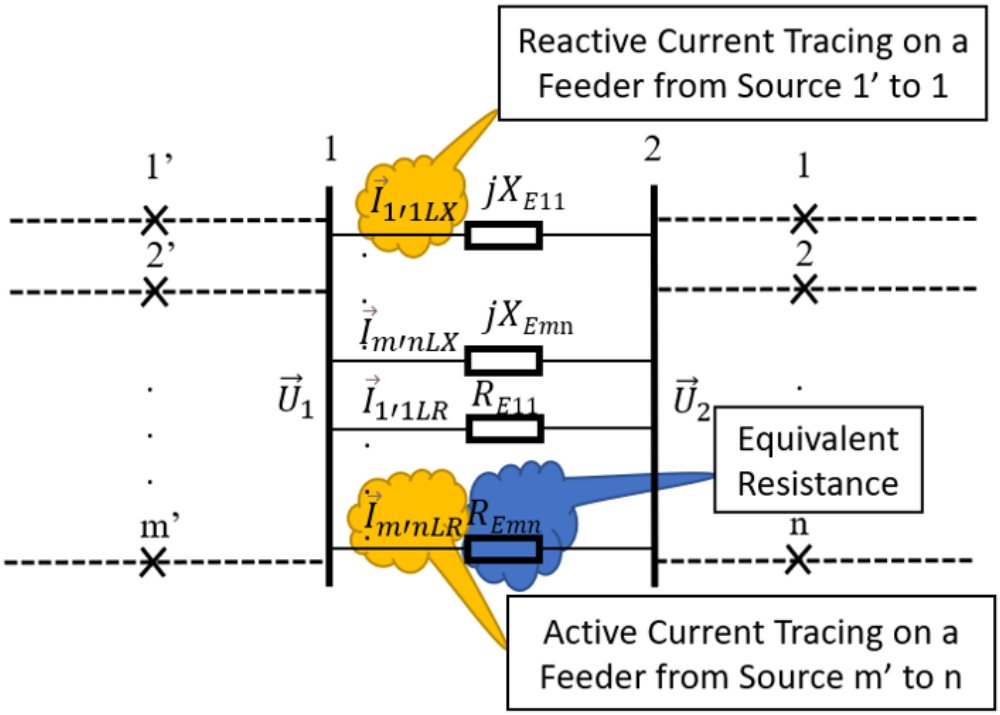

Figure 4.8: Equivalent circuit of multiple sources to multiple sources on single distribution line

The equivalent circuit is shown in Fig. 4.8. The equivalent resistance and reactance is

$$R_{Ei'j} = \frac{I_{LR} R_E}{I_{i'jLR}}, \tag{4.41}$$

$$X_{Ei'j} = \frac{I_{LX} X_E}{I_{i'jLX}}, \tag{4.42}$$

considering the voltage on bus 1 and bus 2 of the equivalent circuit is the same as the original one shown in Fig. 4.1.

Its equivalent circuit of impedance lines could be represented as shown in Fig.

4.9,

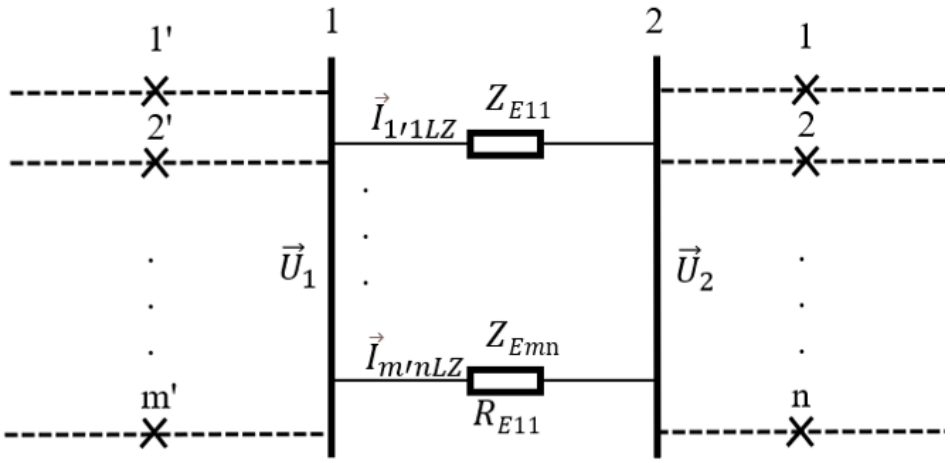

Figure 4.9: Equivalent circuit of multiple sources to multiple sources impedance lines on single distribution line

where

$$Z_{Ei'j} = \frac{1}{\frac{1}{R_{Ei'j}} + \frac{1}{jX_{Ei'j}}}. \tag{4.43}$$

The impedance line $Z_{Ei'j}$ represents the connection between two current sources that connect to different buses. If both of the two current sources are loads, or provide positive active and reactive current to the power line, this value does not exist. This is shown with simulations in the following section.

4.4 A Simulation of Current Tracing for a Small Distribution Line with Multiple Sources

4.4.1 Simulated Test System

In the following a simulation of the current tracing decomposition is carried out on a single distribution line system as shown in Fig. 4.7. The parameters of

the system are $Z = 0.005 + 0.0350j$. $\vec{U}_1 = 1$, $\vec{U}_2 = 0.9662 - 0.0298j$, $\vec{I}_L = 0.9710 - 0.8276i$, $m = 4$ and $n = 3$. The per-unit system is used through out this section. The current sources on both side of line are listed in Table 4.1.

Table 4.1: The Current Sources

Bus	**Current Source**	**Current**	
		Mag/pu	**Phase**/°
1	1'	1.5377	-20.2050
	2'	1.8339	160.6715
	3'	2.2588	-50.7172
	4'	0.8622	101.4889
2	1'	1.1049	68.0750
	2'	1.3918	-50.6532
	3'	0.8411	-112.6568

From Eq. (4.5) and (4.6), the equivalent resistance and reactance in Fig. 4.2 is $R_E = 0.2500\ pu$, $X_E = 0.0357\ pu$.

4.4.2 Results of Multiple Sources to Grid Current Tracing

The decomposed current in Eq. (4.13) that is flowing between bus 1 and bus 2 in the equivalent circuit is listed in Table 4.2. In Table 4.2, the positive elements indicate an absorption of power whereas negative elements represents generating power. Only currents with positive magnitude can contribute to the current flowing through the distribution line. The results of current tracing on the distribution line described by Eq. (4.20-4.21) are shown in Table 4.3.

In Table 4.3, a value of 0 means the corresponding current source does not contribute to the current on the distribution line. The phase angle of currents with positive magnitude in Table 4.3 are the same to that of Table 4.2. This proves that in Eq. (4.20-4.21), the angle of the currents are the same to that of

Table 4.2: Results of Current Tracing of Eq. (4.13)

Bus	**Current Source**	**Active Current**		**Reactive Current**	
		Mag/pu	**Phase**/°	**Mag**/pu	**Phase**/°
1	1'	0.7306	41.4284	1.3531	-48.5716
	2'	-0.8959	41.4284	-1.6002	-48.5716
	3'	-0.0846	41.4284	2.2572	-48.5716
	4'	0.4303	41.4284	-0.7471	-48.5716
2	1	0.9875	41.4284	-0.4955	-48.5716
	2	-0.0506	41.4284	1.13909	-48.5716
	3	-0.7565	41.4284	0.03676	-48.5716

Table 4.3: Results of Current Tracing of Eq. (4.20-4.21)

Bus	**Current Source**	**Active Current**		**Reactive Current**	
		Mag/pu	**Phase**/°	**Mag**/pu	**Phase**/°
1	1'	0.1135	41.4284	0.4734	-48.5716
	2'	0	0	0	0
	3'	0	0	0.7897	-48.5716
	4'	0.0669	41.4284	0	0
2	1	0.1804	41.4284	0	0
	2	0	0	0.9990	-48.5716
	3	0	0	0.2640	-48.5716

Eq. (4.13).

The results of the equivalent circuit parameter described by Eq. (4.26-4.28) is shown in Table 4.4.

Table 4.4: Equivalent Circuit Parameter of Eq. (4.26-4.28)

Bus	**Current Source**	**Sub-resistance**	**Sub-reactance**	**Impedance**
		pu	pu	pu
1	1'	0.3972	0.0953	0.0216+0.0901i
	2'	∞	∞	∞
	3'	∞	0.0571	0.0571i
	4'	0.6744	∞	0.6744
2	1	0.2500	∞	0.2500
	2	∞	0.0452	0.0452i
	3	∞	0.1708	0.1708i

These infinity parameters mean there is no sub resistance or reactance from the corresponding current sources to the other end of the line.

4.4.3 Results of Multiple Source to Multiple Source Current Tracing

The results of multiple sources to multiple sources current tracing on the power line calculated by Eq. (4.34-4.35), (4.36-4.37) and (4.38) are shown in Table 4.5, 4.6 and 4.7, respectively.

In Table 4.5-4.7, zero magnitude and angle stand for no current can be decomposed between the two corresponding current sources. It is noteworthy that some of the current sources only receive or contribute active current. For example, the decomposed current between current source 4', and current source 1. Some of the current sources only receive or contribute reactive current, for example, the decomposed current between current source 1' and current source 2. The sum of

Table 4.5: Multiple Sources to Multiple Sources Active Current Tracing on the Power Line

Current Source	**1**		**2**		3	
	Mag/pu	Phase/°	Mag/pu	Phase/°	Mag/pu	Phase/°
1'	0.1135	41.4284	0	0	0	0
2'	0	0	0	0	0	0
3'	0	0	0	0	0	0
4'	0.0669	41.4284	0	0	0	0

Table 4.6: Multiple Sources to Multiple Sources Reactive Current Tracing on the Power Line

Current Source	**1**		**2**		**3**	
	Mag/pu	Phase/°	Mag/pu	Phase/°	Mag/pu	Phase/°
1'	0	0	0.3744	-48.5716	0.0989	-48.5716
2'	0	0	0	0	0	0
3'	0	0	0.6246	-48.5716	0.1651	-48.5716
4'	0	0	0	0	0	0

Table 4.7: Multiple Sources to Multiple Sources Current Tracing on the Power Line

Current Source	**1**		**2**		**3**	
	Mag/pu	Phase/°	Mag/pu	Phase/°	Mag/pu	Phase/°
1'	0.1135	41.4284	0.3744	-48.5716	0.0989	-48.5716
2'	0	0	0	0	0	0
3'	0	0	0.6246	-48.5716	0.1651	-48.5716
4'	0.0669	41.4284	0	0	0	0

all of the decomposed currents in Table 4.7 is equal to the line current $\vec{I}_L$. This proves the effectiveness of the proposed current tracing method such that it does not violate any physical or electrical laws.

The results of multiple sources to multiple sources equivalent resistance, reactance and impedance on the power line calculated by Eq. (4.41), (4.42) and

(4.43) are shown in Table 4.8, 4.9 and 4.10, respectively.

Table 4.8: Multiple Sources to Multiple Sources Equivalent Resistance on the Power Line

Current Source	**1**	**2**	**3**
	pu	pu	pu
1'	0.3972	∞	∞
2'	∞	∞	∞
3'	∞	∞	∞
4'	0.6744	∞	∞

Table 4.9: Multiple Sources to Multiple Sources Equivalent Reactance on the Power Line

Current Source	**1**	**2**	**3**
	pu	pu	pu
1'	∞	0.1205	0.4559
2'	∞	∞	∞
3'	∞	0.0722	0.2733
4'	∞	∞	∞

Table 4.10: Multiple Sources to Multiple Sources Equivalent Impedance on the Power Line

Current Source	**1**	**2**	**3**
	pu	pu	pu
1'	0.3972	0.1205j	0.4559j
2'	∞	∞	∞
3'	∞	0.0722j	0.2733j
4'	0.6744	∞	∞

In Table 4.8-4.10, the "∞ " stands for no equivalent resistance, reactance or impedance exists between the two current sources. In this case, the decomposed current between the two current sources is zero. The decomposed currents shown

in Table 4.7 multiplied by the corresponding impedance in Table 4.10 are exactly equal to the voltage difference between bus 1 and bus 2. This also proves the effectiveness of the proposed current tracing method such that it does not violate any physical or electrical laws.

4.5 Conclusion

In this chapter, a current tracing method is proposed to model the distribution grid. Unlike the traditional grid model where currents are congested on the bus and flowing through the power line, an equivalent circuit model is developed, where currents are flowing through several parallel connected lines. The equivalent circuit provides a detailed current flowing route from each current source to each load on the power line, regardless of the bidirectional power flow. The developed model has sufficient detailed information which could potentially be exploited for enhanced sensitivity in power system protection as explored in the following chapters.

Chapter 5

Fault Current Tracing for Primary Protection

5.1 Introduction

To address the aforementioned practical problems such as relay sensitivity and blinding of protection issues, a current tracing model was proposed in the previous chapter. This method has enhanced circuit information of the current flows on the power line from each of the individual current source connected to the grid. With this more detailed current flow information, the contribution of each individual current source to the fault current can be clearly identified. This chapter will demonstrate the application of this technique in improving dependability and sensitivity of the primary protection considering multiple DERs in a distribution feeder.

Thus, the main objectives of this chapter are as follows. First, it will be shown, for the first time, how the accuracy of implementing artificial intelligence (AI) algorithms on such a detailed grid model can be improved. Specifically, imple-

menting the support vector machine (SVM) algorithm on the proposed current tracing model is explored. Second, in addition to using fault current flows as the only input feature, the decomposed current information to expand the dimension of the feature space is explored. Finally, the performance of the combination of current tracing method with the SVM is demonstrated in the practical scenario of fault identification with DERs operating in distribution grids. Specifically, this work shows how applying this hybrid method can improve sensitivity in detecting very low level faults.

5.2 Support Vector Machine and Current Tracing Kernel

5.2.1 Binary Classification Problem Formation

Given a set of power line current measurements $Z = \{z_i, i = 1...n\}$, $z_i \in \mathbb{R}^m$ that may or may not contain fault current and the set of labels $Y = \{y_i, i = 1...n\}$, $y_i \in \{0, 1\}$, m stands for the dimension of the measurement, and n is the number of observations. The fault current identification problem can be modeled as a binary classification problem by establishing the connection between the above two sets such that

$$y_i = \begin{cases} -1, \\ 1 \end{cases} \tag{5.1}$$

$y_i = 1$ indicates that the i^{th} current measurement is fault current, or, alternatively, there are no fault currents for $y_i = -1$.

5.2.2 Support Vector Classifiers

The general idea of binary classification is to use input data to classify faults or abnormal conditions from normal ones by generating an optimal hyper-plane. In a p dimensional space, a hyper-plane is a flat affine subspace of hyper-plane dimension $p-1$. The hyper-plane in 2-D space is a line as shown in Fig. 5.1

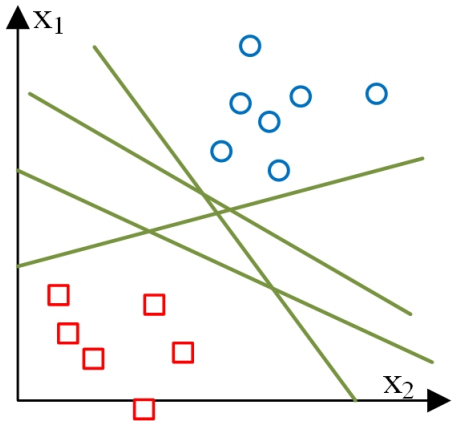

Figure 5.1: Hyper-plane

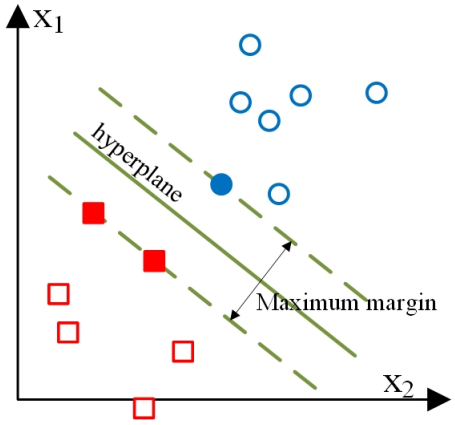

Figure 5.2: Maximum Margin

Figure 5.3: SVM hyper-plane and its maximum margin

For a p dimensional space, a hyper-plane is defined by the equation

$$\omega Z + \omega_0 = 0, \tag{5.2}$$

for parameters $\omega = [\omega_0, \omega_1, ...\omega_p]^T$ and ω_0. A separating hyper-plane has the property that

$$y_i(\omega^T z_i + \omega_0) > 0. \tag{5.3}$$

In a linearly separable classification problem, there exists an infinite number of hyper-planes as shown in Fig. 5.1. The objective is to find the maximal margin hyper-plane that has the greatest minimum distance between the training observations and the hyper-plane. The maximum margin hyper-plane is shown in Fig. 5.2.

The two rectangles and the circle that lie on the dashed lines in Fig. 5.2 are defined as the support vectors. The two dashed lines are defined as the positive and negative hyper-plane respectively such that

$$\omega_0 + \omega^T Z_P = 1, \tag{5.4}$$

$$\omega_0 + \omega^T Z_N = -1, \tag{5.5}$$

where Z_P is the subset of Z whose labels are positive, i.e. $y = 1$, alternatively, Z_N represents the negative subset of Z.

Subtracting Eq. (5.4) from Eq. (5.5) yields

$$\omega^T(Z_P - Z_N) = 2. \tag{5.6}$$

Eq. (5.6) can be normalized by the two-norm of ω as

$$||\omega|| = \sqrt{\sum_{j=1}^{p} \omega_j^2}. \tag{5.7}$$

Therefore, Eq. (5.6) is rewritten as

$$\frac{\omega^T(Z_P - Z_N)}{||\omega||} = \frac{2}{||\omega||}. \tag{5.8}$$

The left side of Eq. (5.8) is the distance or margin between the positive and negative hyper-plane. Therefore, the objective function of SVM is to find the maximum value of $\frac{2}{||\omega||}$ or the minimum value of $\frac{1}{2}||\omega||$ which is subject to the constraint that the samples are classified correctly. With the positive and negative hyper-plane, the constraint could further be written as

$$y_i(\omega z_i + \omega_0) \geq 1. \tag{5.9}$$

To relax the constraint, a slack variable ξ_i is introduced resulting in

$$\omega_0 + \omega^T z_i \geq 1 - \xi_i \ \textit{if}\ y_i = 1, \tag{5.10}$$

$$\omega_0 + \omega^T z_i \leq \xi_i - 1 \ \textit{if}\ y_i = -1. \tag{5.11}$$

The classification problem is reformatted into the optimization problem in [67]. The objective function can be defined as

$$\texttt{min}\ \frac{1}{2}||\omega||^2 + C\sum_{i=1}^{m}\xi_i, \tag{5.12}$$

where C is used to control the penalty of misclassification, such that a smaller value of C corresponds to less strictness of misclassification errors.

5.2.3 Support Vector Machines

As an extension of the support vector classifier, SVM is established by enlarging the feature space using kernel. Kernel is a function that is used to quantify the similarity of two observations. It generally transforms the training set of data into a higher number of dimension spaces. There are many ways to define the kernel function. For example, a linear Kernel is defined as the inner product of two observations [67]:

$$K(z_i, z_{i'}) = \sum_{j=1}^{m} z_{i,j} z_{i',j}, \tag{5.13}$$

where z_i and $z_{i'}$ are the two observations, and $z_{i,j}$ and $z_{i',j}$ are the observations on jth dimension. Sometimes, faults and normal conditions are non-separable using the linear kernel function. In these cases, the non-linear kernel can be used such that the non-separable binary classification problem can become separable in a higher dimension space. Some commonly used non-linear kernels are [67]

- Polynomial kernel: $K(z_i, z_{i'}) = (1 + \sum_{j=1}^{m} z_{i,j} z_{i',j})^d$
- Radial kernel: $K(z_i, z_{i'}) = exp(-\gamma \sum_{m}^{j=1} (x_{i,j} - x_{i',j})^2)$

where γ and d are positive constants and r is a constant.

5.2.4 Proposed Current Tracing Kernel

In [68], the author applied principle component analysis to select the features with the highest information content to identify faults. This study concluded that the top three features for fault identification were reactive power, real power, and angle of voltage. Interestingly, current was not one of them. The author concluded that with all three of the selected features, the accuracy of identification is almost

96%. With all of the six features, i.e., the above features plus magnitude and angle of current and magnitude of voltage, the accuracy of identification is no more than 97%. Most feeder protection relays in the distribution system only operate based on current information and therefore practically is the most appropriate quantity to expand upon. The other quantities require more instrumentation and cost to measure voltage and current in each phase.

In the proposed approach, decomposed current is used as the only feature to identify the fault current. Without current tracing, the feature space consists of only the line current magnitude and angle.

Based on Equations (4.20)–(4.23), the line current can be decomposed into several decomposed currents flowing through virtual impedance lines as shown earlier in Fig. 4.6. The feature space of line currents can be enlarged by using the decomposed currents:

$$K(I_L, e^{j(\psi-\theta)}) = \vec{I}_{LRjP} + \vec{I}_{LXjP}, \tag{5.14}$$

where K represents the positive part of the linear mapping from power line current to the decomposed current as shown in Eq. 4.30-4.33. Unlike the polynomial kernel and the radial kernel, when the current tracing kernel is used, the feature space of the fault current becomes more clear. That is, it provides the detailed contribution of fault current from each current source to the power line.

5.3 SVM Simulation Results

5.3.1 Current Tracing Kernel Results

In this simulation, the proposed current tracing kernel is applied to the same single line system as that of Fig. 4.7. Both sides of the single line have a group of DERs and loads, and bus 2 is connected directly to the external distribution grid. All of the loads are of a constant power type, and the DERs are static generators. The parameters are given in the format of active and reactive power which is different from Chapter 4.

The current sources parameters are listed in Table 5.1. DERs that connect to bus 1 cannot support the AC loads attached to bus 1 so that the currents flow from bus 2 to bus 1, which is opposite from the case shown in a companion paper [69]. Bus 2 is selected as the reference bus and the single power line is 20 km long with a series impedance of 0.121 + j0.107 Ω/km.

Table 5.1: The current source parameters.

Bus	**Current Source**	**Power**	
		Active/MW	**Reactive/MVar**
1	1'	-20	-10
	2'	-20	-5
	3'	30	15
	4'	20	5
2	1	-20	-10
	2	40	15
	3	30.872544	10.771589

In Table 5.1, the positive elements indicate an absorption of power whereas negative elements represents generating power. The third current source attached to bus 2 is the external grid and is calculated by the power flow. Equations (4.20)

and (4.21) are applied to find the decomposed current on the power line from each bus as shown in Table 5.2. All of the decomposed currents are listed in per unit value. The decomposed current magnitude and phase in radians are selected as the kernel for fault current identification.

Table 5.2: Current tracing results with Equations (4.20)–(4.23).

Bus	**Current Source**	**Active Current**		**Reactive Current**	
		Mag	**Phase/°**	**Mag**	**Phase/°**
1	1'	0	0	0	0
	2'	0	0	0	0
	3'	5.3677	13.5251	5.6267	−76.4749
	4'	3.8535	13.5251	2.5276	−76.4749
2	1	0	0	0	0
	2	3.5366	13.5251	3.6588	−76.4749
	3	5.6847	13.5251	4.4955	−76.4749

In Table 5.2, a zero value indicates that the corresponding current source does not contribute to the current on the power line. It can be observed that the zero value occurs at bus 1; Current Sources 1 and 2; and bus 2, Current Source 1. This does not violate common sense as these are all labeled as loads that are consuming active and reactive power and do not contribute to the power line current. Moreover, all of the decomposed active currents have the same phase angle regardless of how the power is flowed from bus 1 or bus 2 in either direction. The same rationale applies to the reactive currents. This is also consistent with the fact that the voltages applied on the buses do not change when the current is decomposed into its decomposed components. The reactive current is 90 degrees out of phase from the active current, which complies with Equations (4.20) and (4.21).

It is observed that, if all of the decomposed currents from the same bus are

summed, the result is equivalent to the total power line current. This proves the equivalence of the current tracing theory as the decomposed current will not lose or generate new currents in addition to the line current.

5.3.2 SVM Results

In distribution systems with DERs, the fault current can be very small, as inverter-based DERs can only produce exceptionally small fault current contributions due to inverter current limiting action. Moreover, injected currents on different loads are continuously fluctuating in the normal condition. To obtain representative currents in the single line system, sample noises are injected to the specified load powers in Table 5.1 and the power flow is recalculated to obtain the decomposed current. This process is then repeated to obtain the load profile and a continuous currents curve. The injected noise follows the normal distribution such that,

$$X \sim N(\mu, \sigma^2), \tag{5.15}$$

where X represents active or reactive power sample noises; μ represents the average of the sample noises, which is set to 0; and σ stands for the standard deviation, which is set to 0.1. All of the sample noises are independent from each other. The sample noises were injected cumulatively to the loads such that the kth point on the load profile is

$$P_k = P + \sum_{i=1}^{k} X p_i, \tag{5.16}$$

$$Q_k = Q + \sum_{i=1}^{k} X q_i, \tag{5.17}$$

where P_k and Q_k represent the active and reactive power of the kth point of the load profile, respectively; P and Q represent the given active and reactive power (Table 5.1); and Xp_i and Xq_i stand for the ith active or reactive power sample noises, respectively.

This process is repeated 500 times, and all of the parameters that are used for current tracing and SVM training purposes are recorded. In addition to sample noises, a small fault is also injected by increasing the active power consumption of bus 1, with current source 3 increased by 10% and the reactive power decreased by 10% of the same current source. Again, the process is repeated 500 times, and all parameters are recorded. Only the decomposed current on the power line from bus 2 side is used as the current tracing kernel; however, it is the same as if the decomposed current from bus 1 side was used as the current tracing kernel, as in the authored conference paper [69]. The first 500 parameters are taken as normal condition, i.e., $y_i = -1$, and the last 500 parameters are considered as fault condition, i.e., $y_i = 1$. The hyper-parameter C is set to be 1. This is selected by the grid search method: comparing the performance of the SVM method with different hyper-parameter from the list: $[0.01, 0.1, 1, 10]$. Only the one that has the best performance is used. The performance is evaluated by the confusion matrix which will be introduced shortly.

Seventy percent of the parameters are randomly selected as the training data, and the remaining 30% are taken as the testing data. In this work, the non-waveform phasor current information is used for the fault identification problem. Other alternative measurement data have been considered in other research, such as exploiting sub-cycle waveform distortion features in pattern recognition algorithms as a part of the identification process [70, 71].

The confusion matrix is used to represent the testing results as defined in [72].

The f-score, recall, and precision parameters are used to evaluate the performance of fault current identification based on the confusion matrix such that,

$$prec = \frac{tp}{tp + fp}, \tag{5.18}$$

$$rec = \frac{tp}{tp + fn}, \tag{5.19}$$

$$fs = 2\frac{prec * rec}{prec + rec}, \tag{5.20}$$

where *tp*, *fp*, *tn*, and *fn* represent true positive, false positive, true negative, and false negative, respectively.

To show the advantage of using the current tracing kernel, the fault current identification results using different feature spaces is compared. First, only the power line current $\vec{I}_L$ is used as the feature space. Then, the polynomial kernel, radial kernel, and current tracing kernel are added as the expanded feature space. All of the confusion matrices are calculated based on the same training and testing data. The confusion matrices and the performance based on the confusion matrices are shown in Tables 5.3 and 5.4, respectively.

Table 5.3: Confusion matrix using different feature spaces.

Feature Space		**Fault**	**Normal**
No Kernel	Predict Fault	tp = 90	fp = 61
	Predict Normal	fn = 13	tn = 136
Polynomial Kernel	Predict Fault	tp = 100	fp = 51
	Predict Normal	fn = 19	tn = 130
Radial Kernel	Predict Fault	tp = 95	fp = 56
	Predict Normal	fn = 16	tn = 133
Current Tracing Kernel	Predict Fault	tp = 145	fp = 6
	Predict Normal	fn = 0	tn = 149

It is clearly seen that among all the feature spaces used, the current tracing

Table 5.4: Performance using different feature spaces.

Feature Space	**Precision**	**Recall**	**f1-Score**
No Kernel	0.596	0.874	0.709
Polynomial Kernel	0.662	0.840	0.74
Radial Kernel	0.629	0.856	0.725
Current Tracing Kernel	0.96	1	0.98

kernel has the best performance. All three performance parameters are significantly higher than the other feature spaces that were used. The recall value equals 1, which indicates that when there is a fault current on the power line, the SVM method using current tracing kernel will definitely detect it. In addition, the polynomial kernel and radial kernel have a better performance than if only $\vec{I}_L$ is used as feature space. However, the performance parameters do not increase significantly. When compared with the results shown in [68], which have 97% overall accuracy, the overall current tracing kernel result in this paper has improved, i.e., an f1-score value of 98%. This indicates that the current tracing kernel can slightly improve the sensitivity and dependability of the primary protection.

5.4 EMTP-MATLAB Simulation Results and Discussion

The result is further validated in the EMTP simulation platform. The simulation circuit is the same as shown earlier in Fig. 3.27. If the fault happens at the same location, the primary protection is R_2 with R_1 as the backup protection. In this case, the fault current could be identified by tracing the fault current contribution of current source S_{1_1}, S_{1_2} and S_{1_3} on the left hand side or S_{2_1} and S_{2_2} on

the right hand side. Only the result of current tracing from the left hand side is shown as an example here.

The current tracing method is first implemented in a MATLAB Simulink platform. The diagram of the Simulink platform is shown in Fig. 5.4.

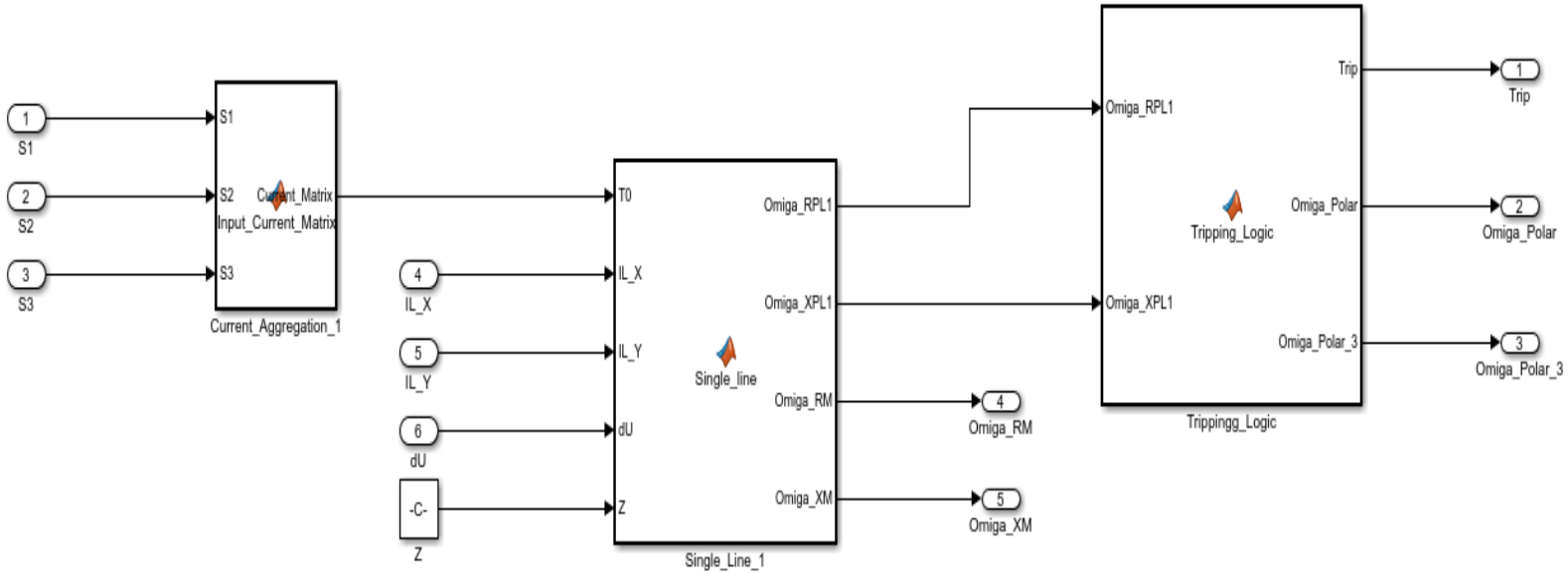

Figure 5.4: MATLAB Simulink platform for primary protection

The platform consists of three blocks. The current aggregation block is used to aggregate the collected polar phasor data of each current source and convert it into the rectangular form in real time. The output of these two blocks are the aggregated real time currents.

The single line block is used for the multiple sources to grid current tracing. It takes in the real time currents from the current aggregation block, the voltages and the constant value of the line impedance. The output of this block is the decomposed currents from Eq. (4.20-4.21).

In the tripping logic block, a threshold based tripping logic is used. This block takes in the decomposed current from the single line block. Once the decomposed current is beyond a given percentage of the rated decomposed current, the trip signal will be activated. Thus one of the outputs of this block is the tripping signal. In addition, the sum of the decomposed currents from the single line block is also included as the output of this block. This can be used to verify if it is equal to the line current $\vec{I}_L$ and prove the correctness of the algorithm.

Due to the availability of the fault current data, a threshold based tripping logic is used in the tripping logic block. The threshold is set to be 1.5 times of the rated decomposed current. The tripping time is set to be instantaneous for the simulation, but it could be adjusted based on the IDMT curve of the decomposed currents. Therefore, once the decomposed current is above the threshold, the tripping logic block will send a trip signal immediately.

The MATLAB-Simulink platform is integrated using the C++ compiler and a DLL file is generated. The DLL file can be imported into the EMTP's Simulink DLL interface which can be used to customized the algorithm for power system protection. Thus, an integrated EMTP-MATLAB simulation platform is generated as shown in Fig. 5.5.

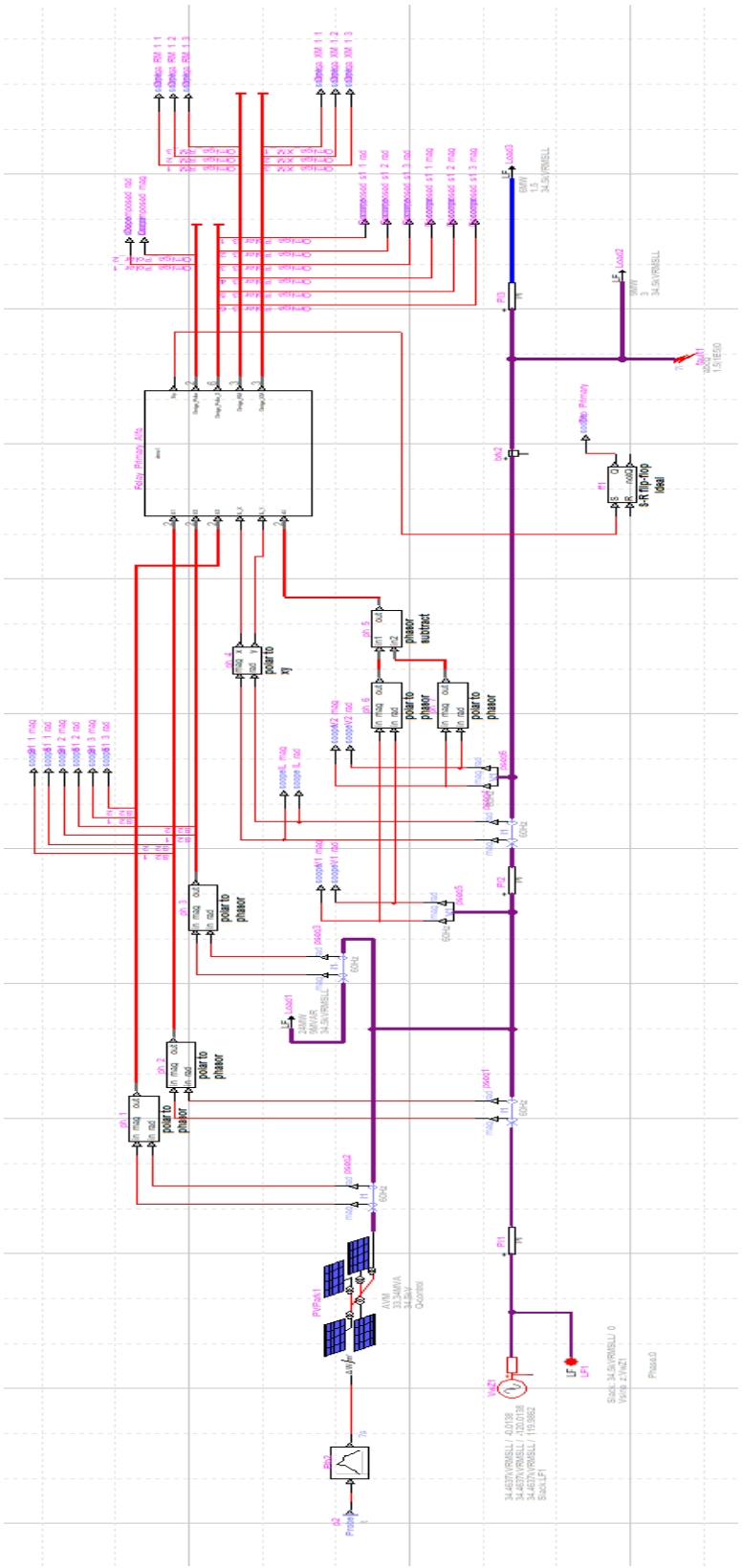

Figure 5.5: EMTP-MATLAB primary protection

It can be observed that the EMTP-MATLAB primary protection interface takes in the positive sequence value of current sources, voltage angle and the line current. The current measurements of each current sources have to follow the principle such that the positive pole of the current meter that connects to the same bus are always pointing towards the same direction: either from current sources to the bus or the opposite. The trip signal goes into a "set reset latch flip flop" block. This is to guarantee that the once the trip signal goes from -1 to 1, the output of the flip-flop will maintain its value to 1. Thus the trip signal will keep the breaker open. However, in order to observe the fault current and its related impacts, the trip signal is set to be observed in a scope, but not connected to the breaker.

In the following sections, the EMTP-MATLAB primary protection interface using the developed current tracing analytics is evaluated based on the fault type under different levels of DERs penetration. All of the measured values are positive sequence values. The DER injection or penetration level is set to increase from 5 panels to 20 panels using 5 panels increments each time. Each panel has a rated power of 1.67 MVA. The rest of the simulation settings are almost the same to that of Section 3.4.2. The total simulation time is 3 seconds with a time step of 10^{-5} second. A fault is programmed to occur at 1.5 seconds. The fault is controlled by the EMTP fault block which can generate all types of resistive faults. For example, when the switch between phase A and ground is closed at 1.5 seconds, a LG fault happens.

5.4.1 LG Fault Results and Explanation

The voltage magnitude and angle of both buses are shown in Fig. 5.6 and 5.7.

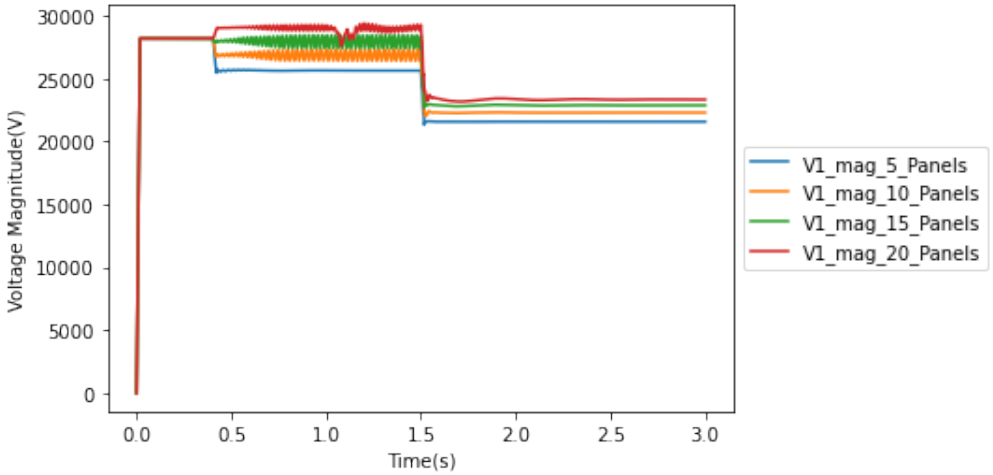

(**a**) Voltage V1 magnitude

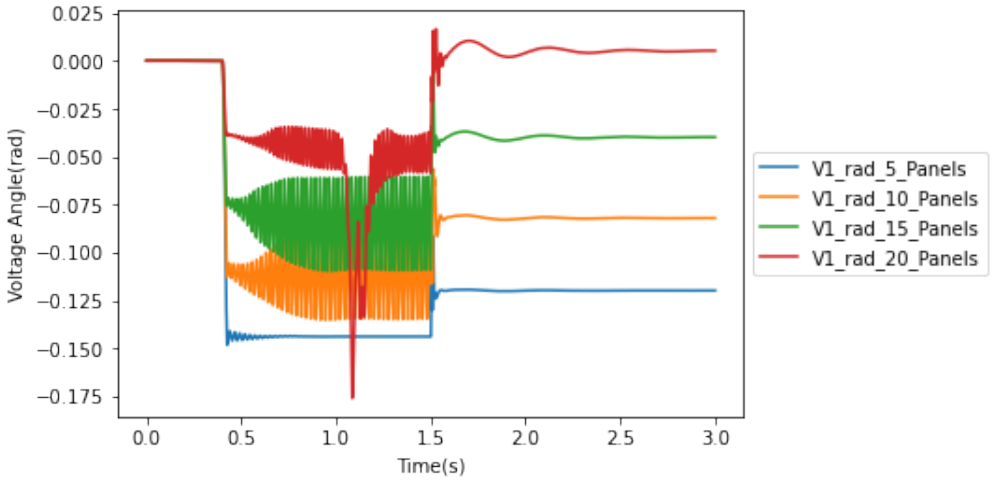

(**b**) Voltage V1 angle

Figure 5.6: Primary protection voltage on bus 1 of distribution feeder protection circuit with LG fault under different level of DER penetration

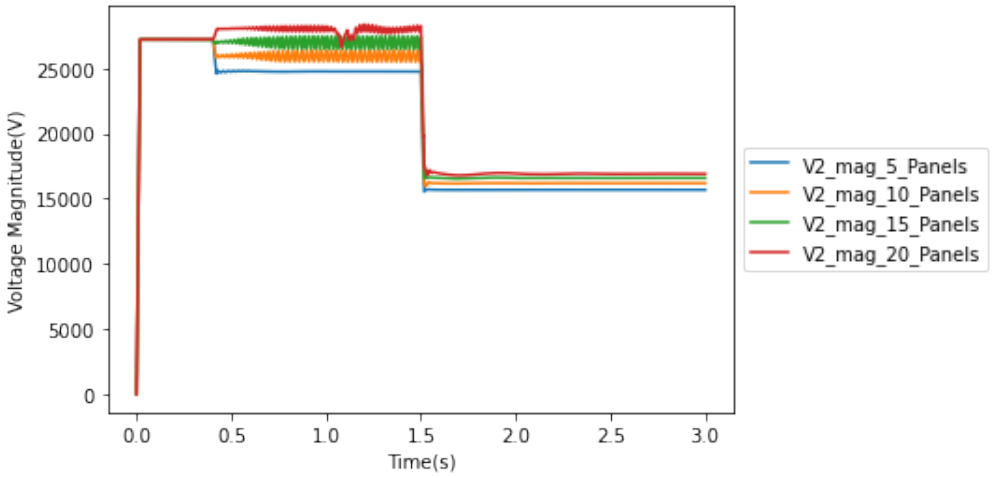

(**a**) Voltage V2 magnitude

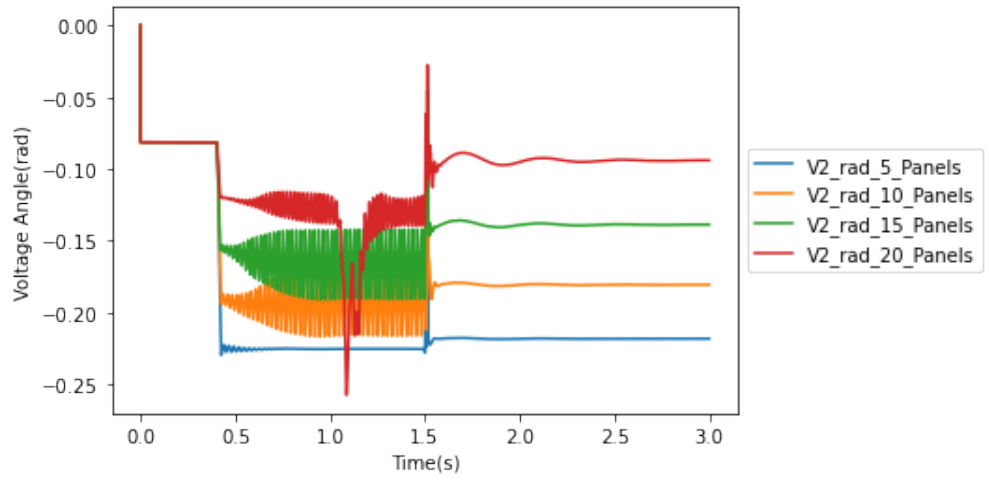

(**b**) Voltage V2 angle

Figure 5.7: Primary protection voltage on bus 2 of distribution feeder protection circuit with LG fault under different level of DER penetration

It takes 0.4 second for the DERs to be initialized. Voltage magnitude on both side drops significantly due to the fault. The current magnitude and angle of each sources that connects to bus 1 are shown in Fig. 5.8, 5.9 and 5.10.

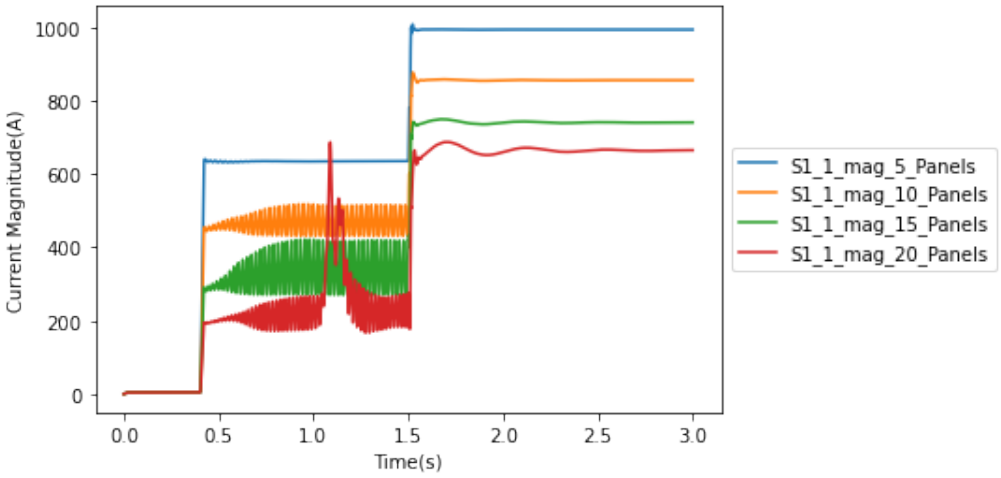

(**a**) Current source S_{1_1} magnitude

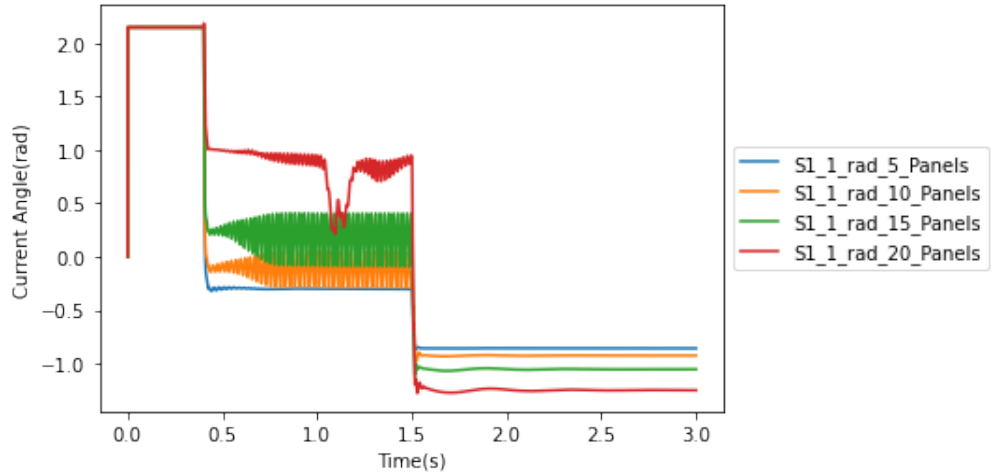

(**b**) Current source S_{1_1} angle

Figure 5.8: Primary protection current source 1 on bus 1 of distribution feeder protection circuit with LG fault under different level of DER penetration

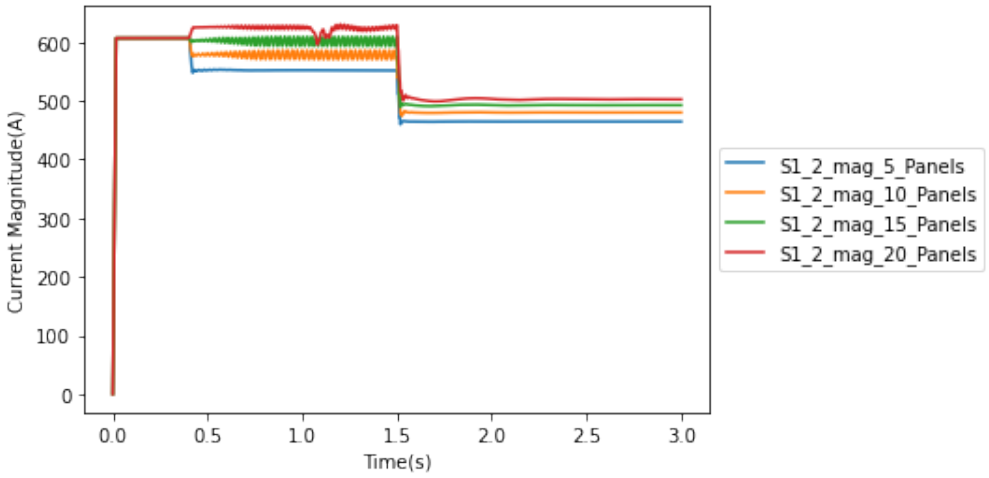

(**a**) Current source S_{1_2} magnitude

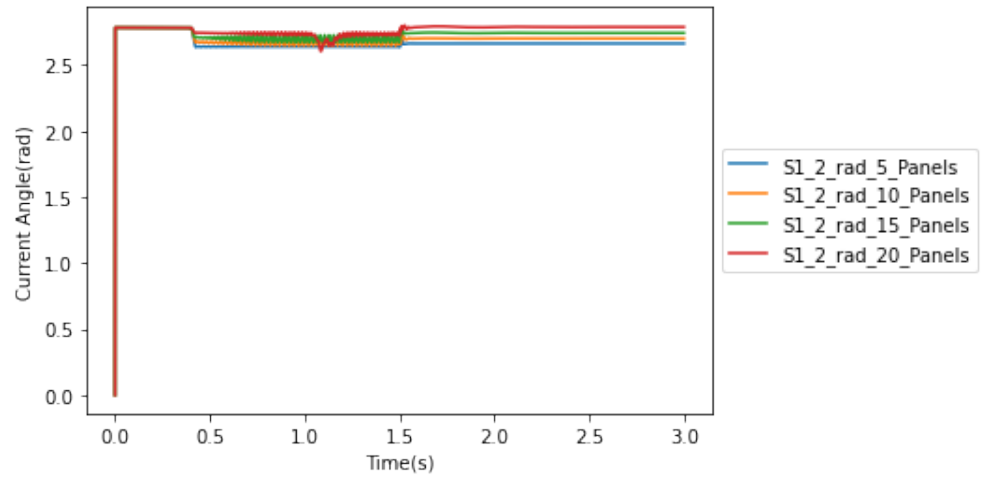

(**b**) Current source S_{1_2} angle

Figure 5.9: Primary protection current source 2 on bus 1 of distribution feeder protection circuit with LG fault under different level of DER penetration

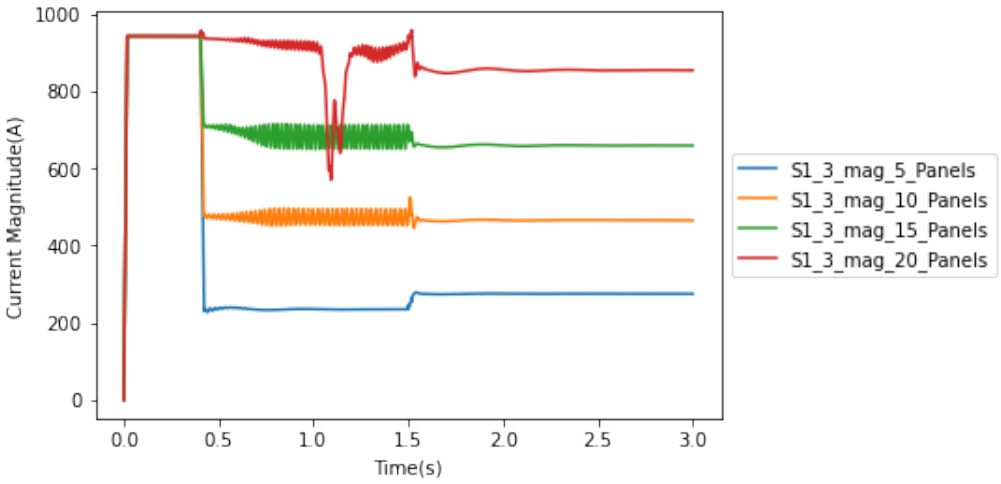

(**a**) Current source S_{1_3} magnitude

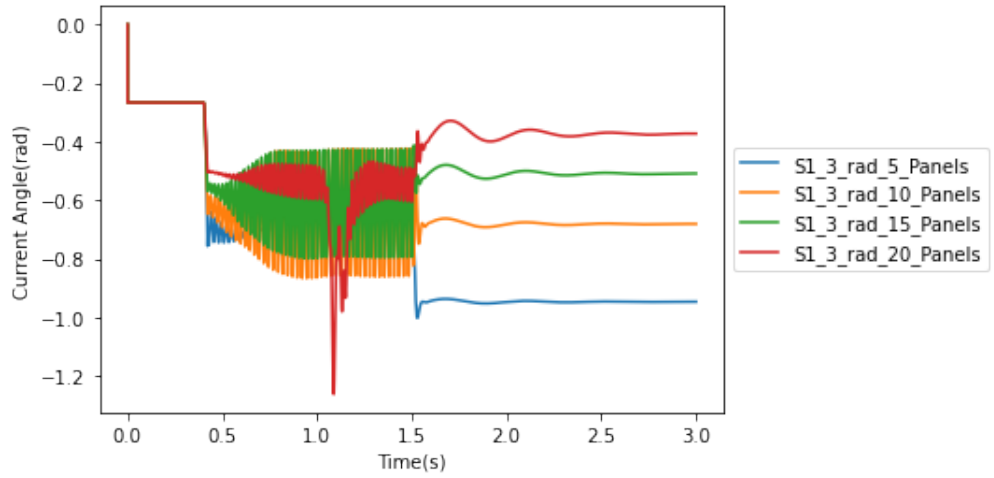

(**b**) Current source S_{1_3} angle

Figure 5.10: Primary protection current source 3 on bus 1 of distribution feeder protection circuit with LG fault under different level of DER penetration

It can be observed that the DER current magnitude S_{1_3} increases while the DER penetration rate increases before and after the fault happens at 1.5 seconds. However, the magnitude of fault from all penetration levels of DER does not change very much at 1.5 seconds. The current magnitude from infinite bus S_{1_1} and load S_{1_2} increase and decrease, respectively.

The current sets in Eq. (4.14) and (4.15) are shown in Fig. 5.11, 5.12 and 5.13. In these figures, I_{LR1}, I_{LR2} and I_{LR3} belong to Ω_{RM} and I_{LX1}, I_{LX2} and I_{LX3} belong to Ω_{XM}.

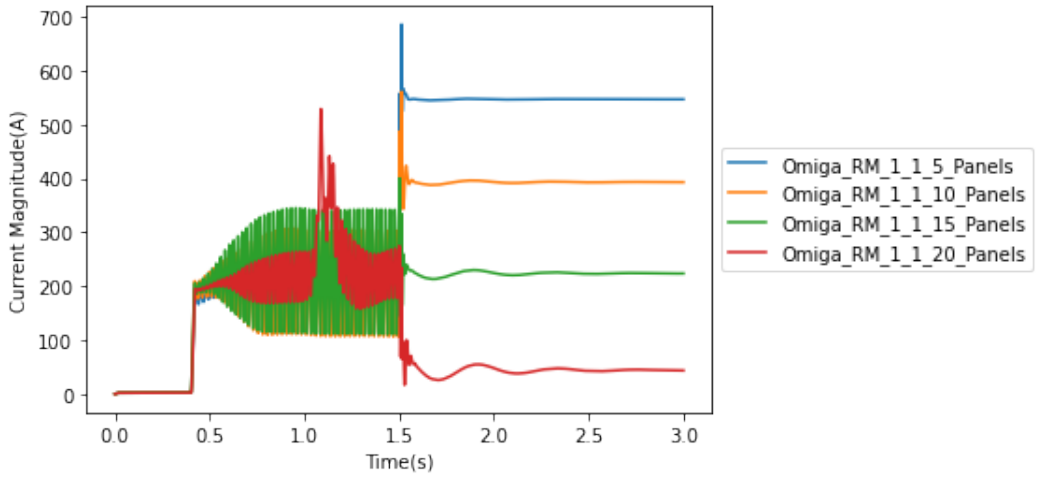

(**a**) Active current I_{LR1}

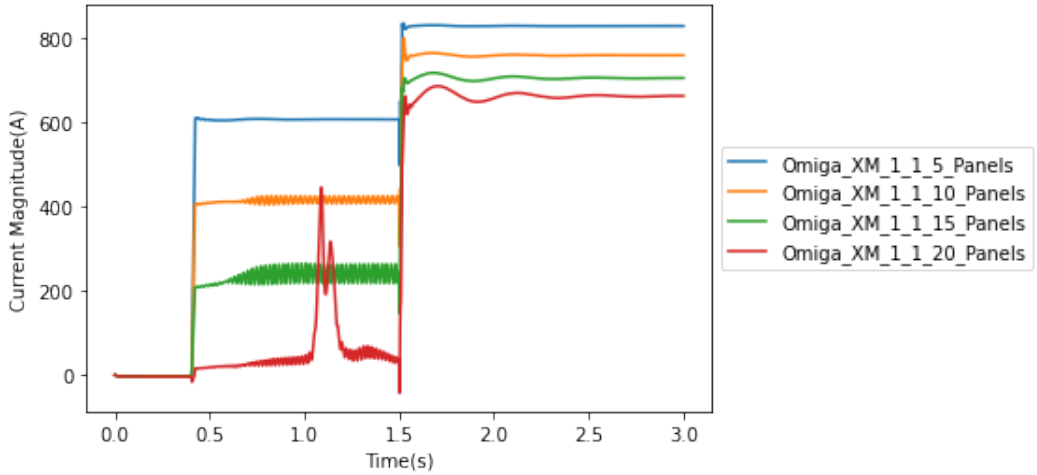

(**b**) Reactive current I_{LX1}

Figure 5.11: Active and reactive currents from current source 1 on bus 1 to the power line with LG fault under different level of DER penetration

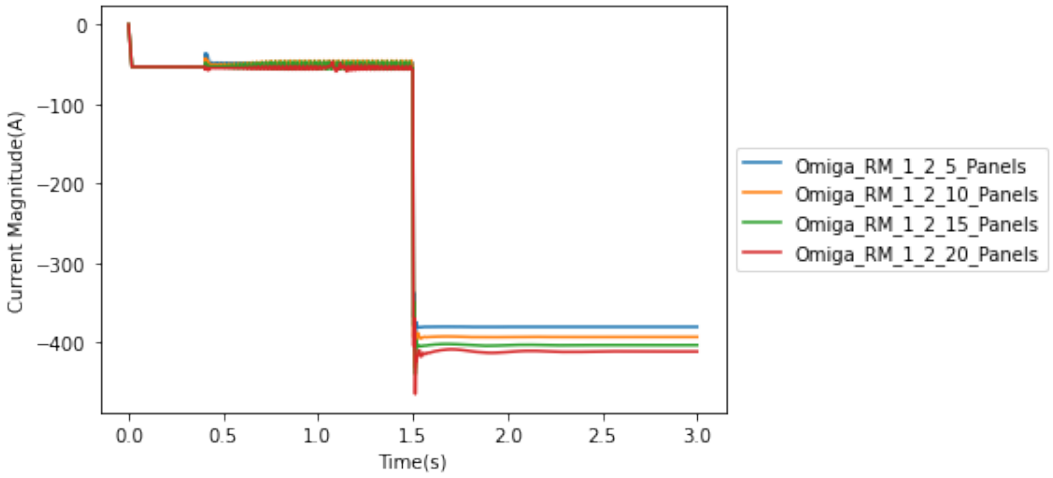

(**a**) Active current I_{LR2}

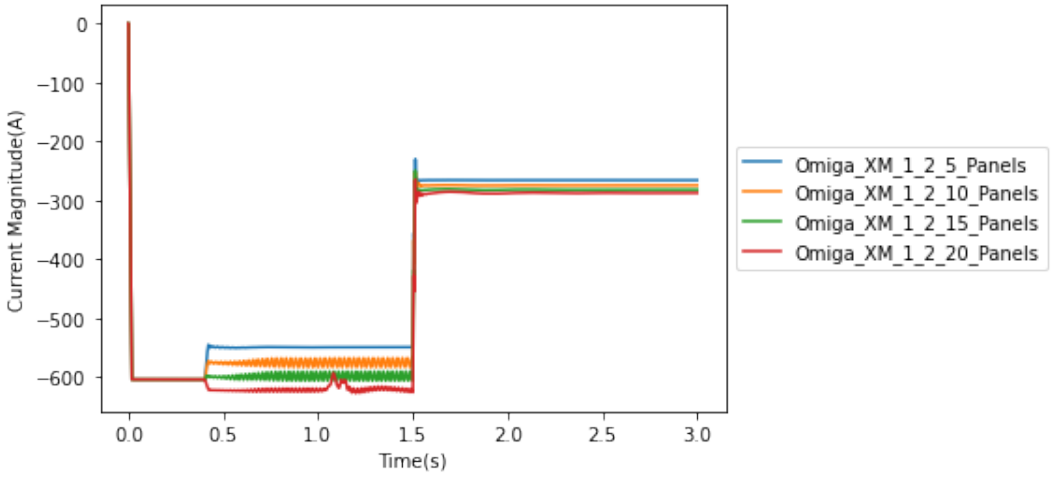

(**b**) Reactive current I_{LX2}

Figure 5.12: Active and reactive currents from current source 2 on bus 1 to the power line with LG fault under different level of DER penetration

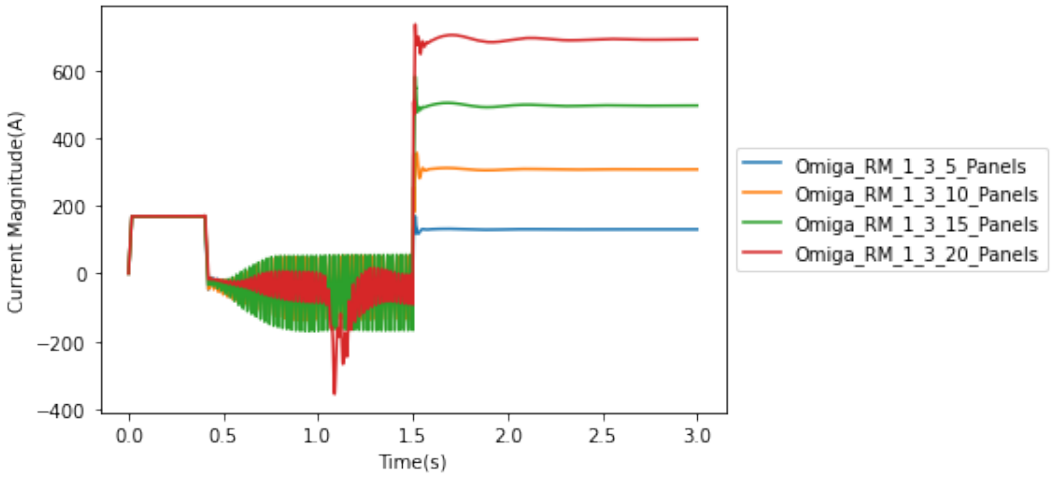

(**a**) Active current I_{LR3}

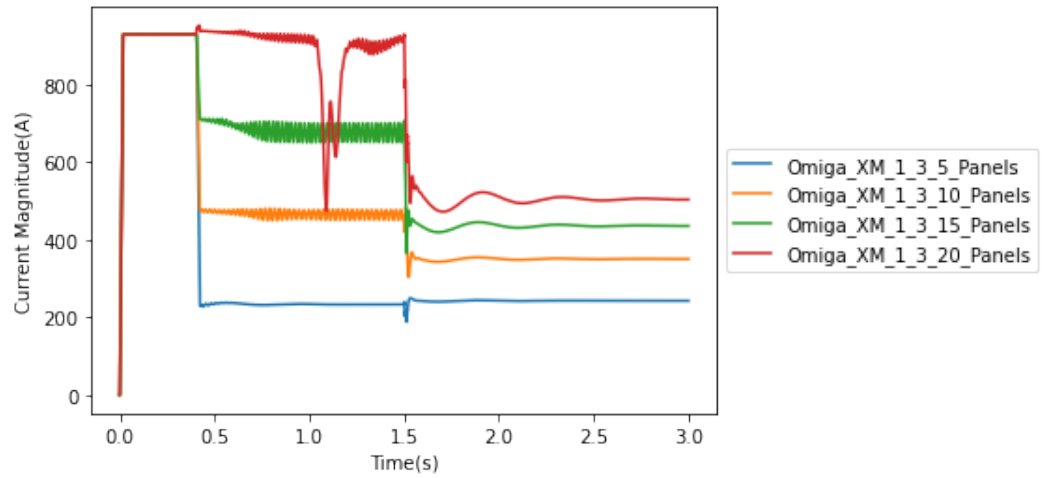

(**b**) Reactive current I_{LX3}

Figure 5.13: Active and reactive currents from current source 3 on bus 1 to the power line with LG fault under different level of DER penetration

It can be observed from the above figures that in active current magnitude set Ω_{RM}, the decomposed current I_{LR2} is also the only magnitude that is negative. The decomposed current I_{LX2} is the only magnitude that is negative in reactive current magnitude set Ω_{XM}. Thus current source S_{1_2} does not contribute to the line current I_L. This is obvious since S_{1_2} is an AC load. It can also be observed that the DER decomposed current magnitude I_{LR3} is increasing while

the penetration level of DER is varied after the fault happens. This demonstrates the key advantage of applying the current tracing method in protection relays in that the decomposed fault current signature is more significant compared to the regular fault current measurement where the contribution of DERs does not have any significant effect.

The magnitude and angle of decomposed current from each individual current source to the distribution line are shown in Fig. 5.14, 5.15 and 5.16.

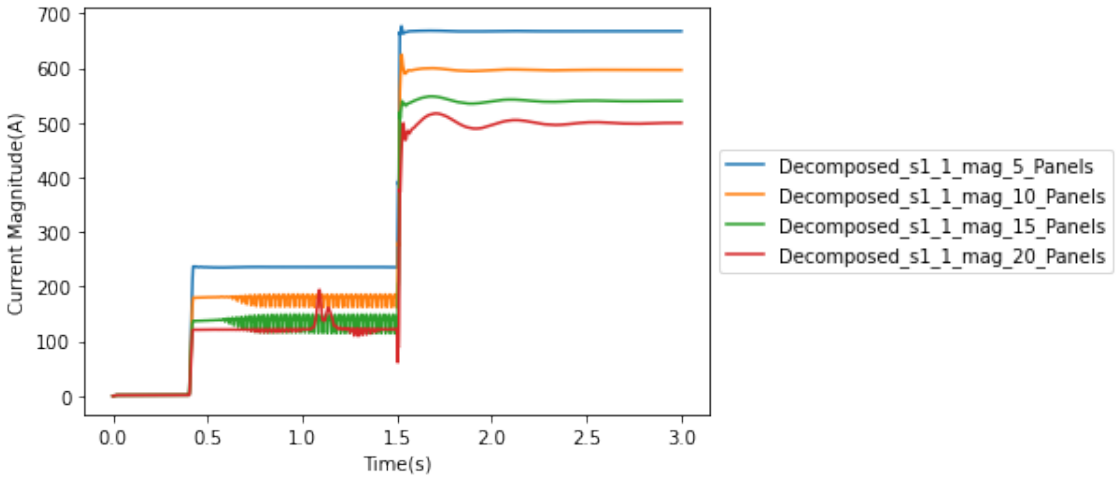

(**a**) Magnitude of decomposed current from S_{1_1}

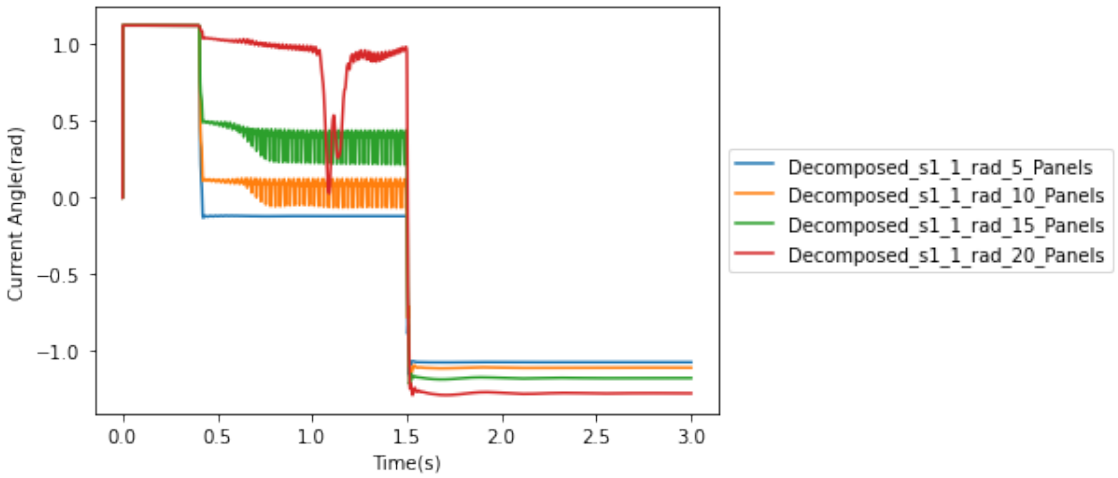

(**b**) Angle of decomposed current from S_{1_1}

Figure 5.14: Decomposed current from current source 1 on bus 1 to the power line with LG fault under different levels of DER penetration

According to Eq. (4.20) and (4.21), the negative currents in Fig. 5.15 are zero. Thus, the decomposed current magnitude and angle from S_{1_2} is zero. It also can be observed that the magnitude of decomposed current from S_{1_3} increases significantly when a fault occurs. This means that the method can clearly identify the fault current contribution from DERs compared to the current measurements where the fault current contribution from DERs are non-distinguishable before

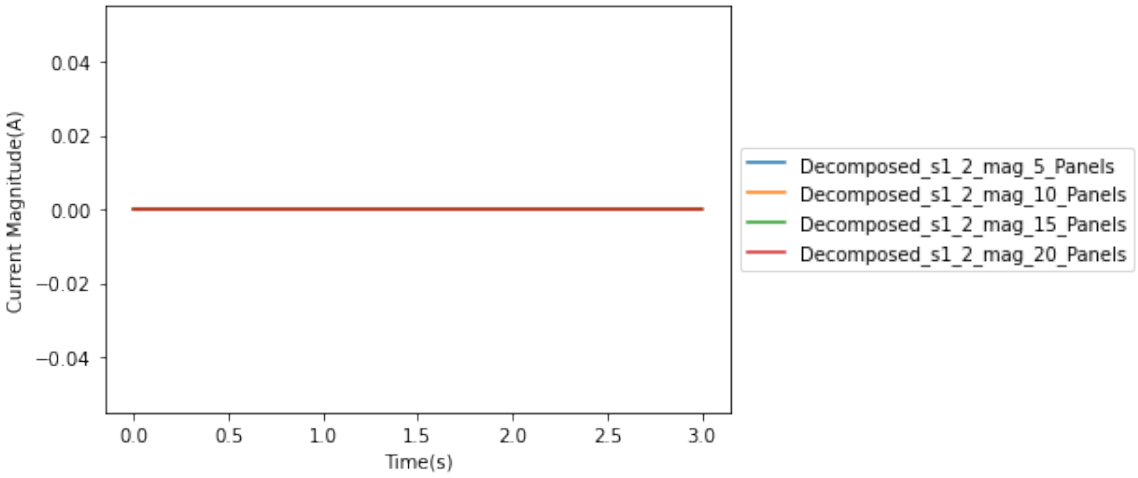

(**a**) Magnitude of decomposed current from S_{1_2}

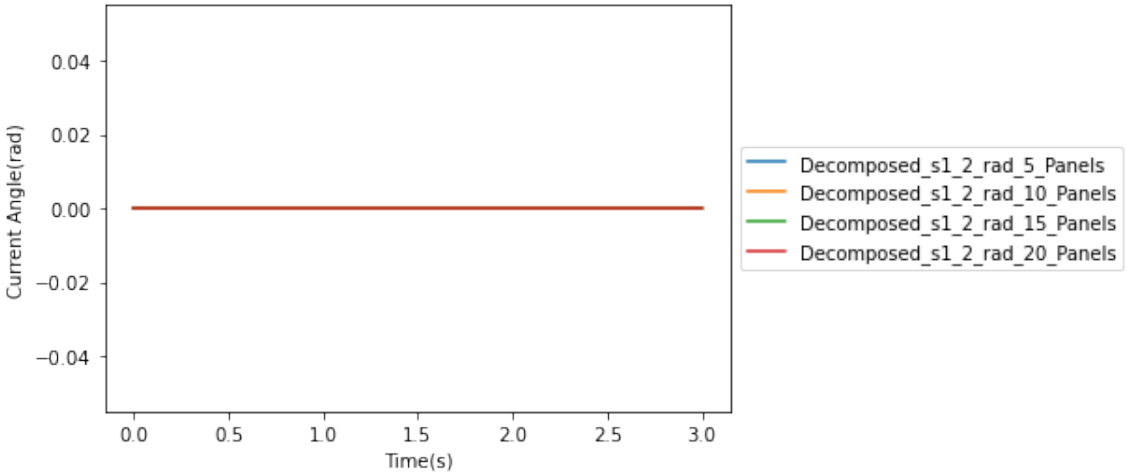

(**b**) Angle of decomposed current from S_{1_2}

Figure 5.15: Decomposed current from current source 2 on bus 1 to the power line with LG fault under different levels of DER penetration

and after the fault.

Moreover, the magnitude of decomposed current from S_{1_1} are more than doubled after faults for each level of DERs penetration. Compared to the measured current increments where the magnitude is doubled, the decomposed current magnitude is more suitable to be the fault current identification signature. Therefore, using the decomposed current instead of the measured current for the primary

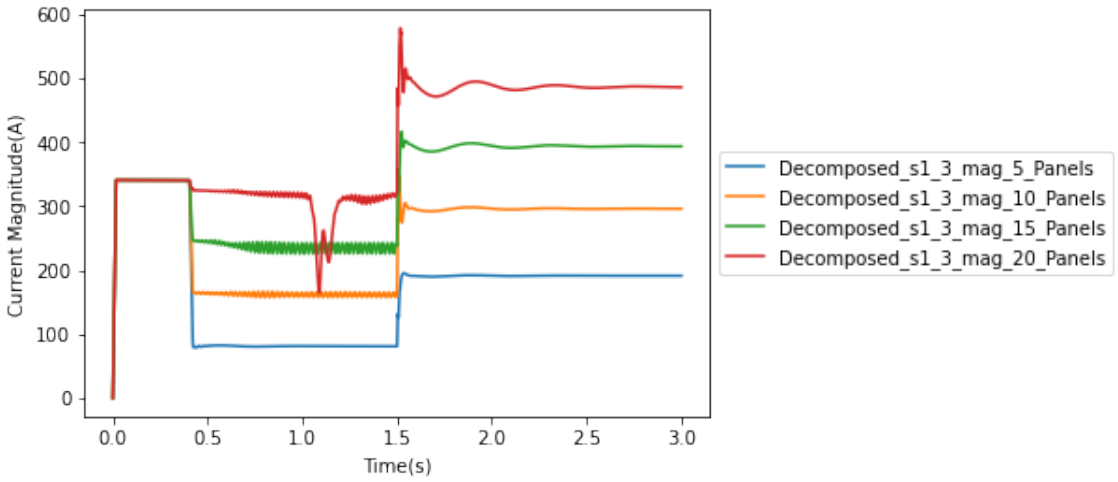

(**a**) Magnitude of decomposed current from S_{1_3}

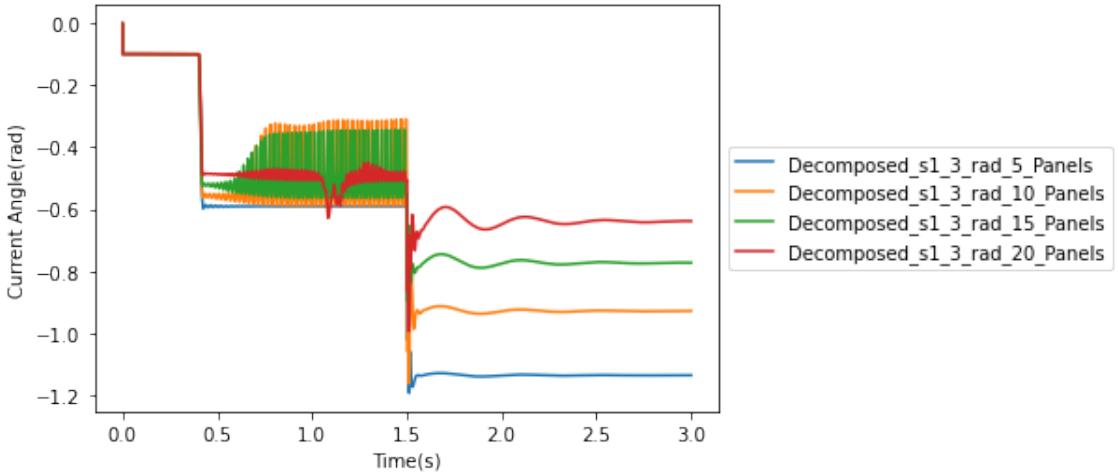

(**b**) Angle of decomposed current from S_{1_3}

Figure 5.16: Decomposed current from current source 3 on bus 1 to the power line with LG fault under different levels of DER penetration

protection can significantly increase the sensitivity of the over current relay.

The line current I_L and the current sum after decomposition are shown in Fig. 5.17. It can be observed that both magnitude and the angle of line current I_L and the current sum after decomposition under different levels of penetration rate are overlapped with each other. This proves the correctness of this method as no physical or electrical laws are broken.

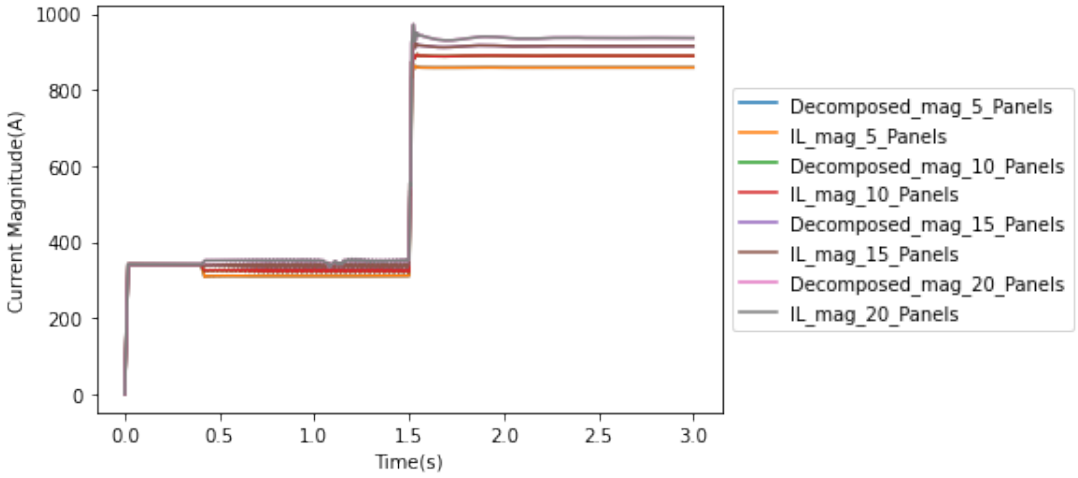

(**a**) Magnitude of I_L and the sum of decomposed current

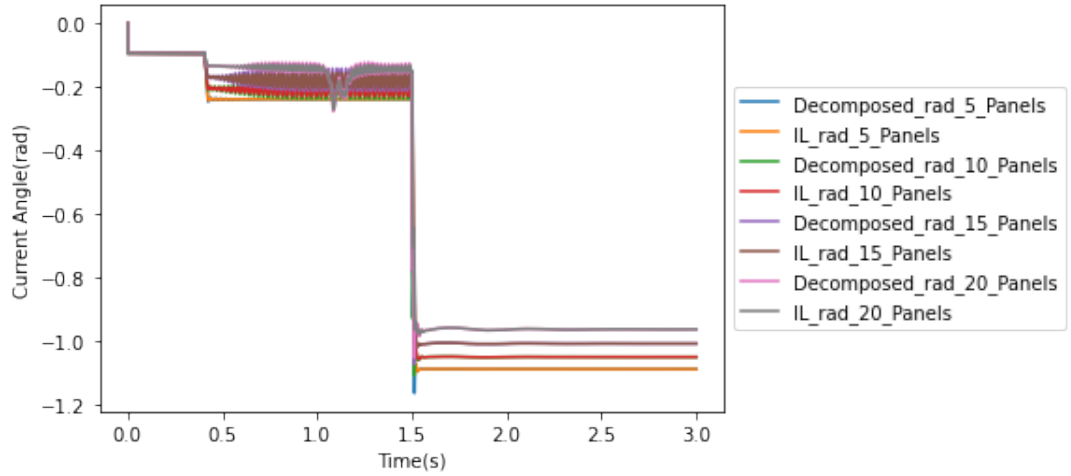

(**b**) Angle of I_L and the sum of decomposed current

Figure 5.17: Comparison between I_L and the sum of decomposed current of primary protection with LG fault under different levels of DER penetration rate

The trip signals are shown in Fig. 5.18. The EMTP-MATLAB primary protection interface trips for all levels of DER penetration as expected.

More supporting simulation results, such as LL, LLG, LLL and LLLG faults under different levels of DER penetration, are presented in the Appendix B.

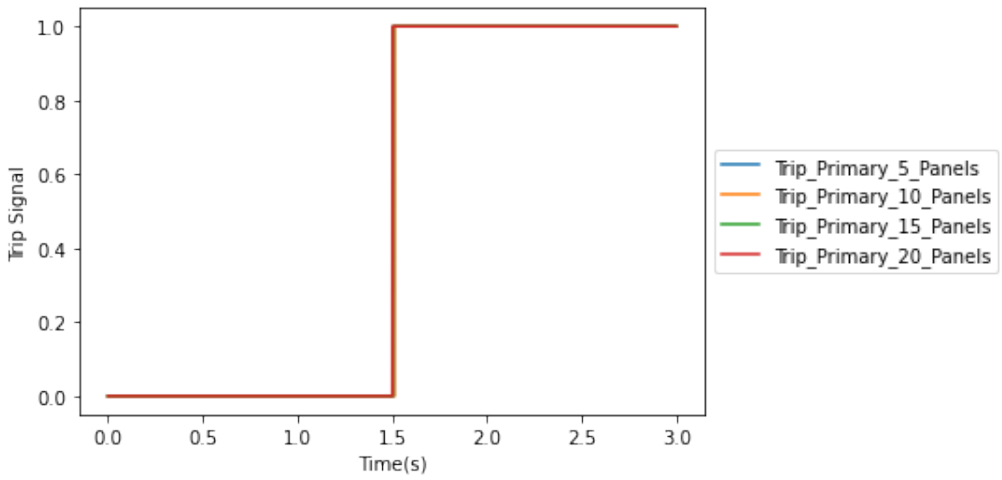

Figure 5.18: EMTP-MATLAB primary protection interface trip signal

5.5 Conclusion

In this chapter, the current tracing method is applied to a realistic simulation of a distribution feeder with DERs for the purpose of demonstrating a new protection relaying approach for the primary protection. The decomposed current provides sufficient details and sensitivity for identifying faults and abnormal conditions in the distribution feeder. With these details, the feature space of the power line current is enlarged through the "current tracing kernel". That is, the decomposed current is used along with the power line current as the expanded feature space to identify the fault current which is a departure from existing methods. In addition, the results proved and demonstrated the proposed method on a single power line distribution system, and the SVM method's performance is evaluated and compared by using different kernel methods. The results indicate that with the benefits of the proposed current tracing kernel, the SVM method is enhanced with more sensitivity and dependability to very low level faults compared to the commonly used kernels such as polynomial kernel and radial kernel.

Moreover, the multiple sources to power line current tracing method is realized

through the MATLAB-Simulink integrated simulation package. For the first time, the results show that both the magnitude of the decomposed current from DER and infinite bus are increased significantly compared to the measured current magnitude that is ordinarily used in protection relaying. The main contribution is that the proposed method provides a new set of features that can be decomposed and exploited for added sensitivity in primary protection relaying schemes in distribution feeders. Furthermore, the new approach makes use of existing sensing and metering infrastructure that is already available to conventional protection relays.

Chapter 6

Fault Current Tracing for Backup Protection

6.1 Introduction

In the previous chapters, the current tracing method is proven to be effective for increasing the dependability and sensitivity of the primary protection. In a protection scheme, coordination must be maintained such that the when the primary protection fails to pick up, the backup protection has to be sensitive enough to see faults for an adjacent or more zones, which can be challenging if the fault current is lower. Failing to react to the fault that is not isolated by the primary protection can cause severe problems. When the fault is not removed in time, a LG fault could become a three phase LLLG fault. In an extreme situation, if all of the backup protection relays fails to trip, it will lead to a cascading failure from a local distribution feeder to the entire substation.

On the other end of the spectrum, bidirectional power flow will lead to the malfunction of the existing backup protection scheme in distribution networks

that are designed for single direction power flow from the substation to the loads.

Chapter 3 has already introduced the impact of DERs to distribution network backup protection. The issue caused by the injection of DERs to distribution network is that it will reduce the sensitivity of the upper stream relay to the fault current, causing increased relay operating time delays, or, in a worst case not, not reacting at all to the downstream faults if the primary protection fails.

A good relay backup protection scheme should consider the impact caused by the injection of DERs, including the bidirectional flow and the lower sensitivity of the protection system. Using adaptive schemes have been proposed to overcome this, but are not immune to the issues discussed. Therefore, this chapter is mainly focusing on exploring the implementation of current tracing method to solve aforementioned problems in distribution networks.

6.2 Fault Current Tracing for Backup Protection

The system diagram of the distribution circuit that is being simulated for demonstrating backup protection performance is shown in Fig. 6.1.

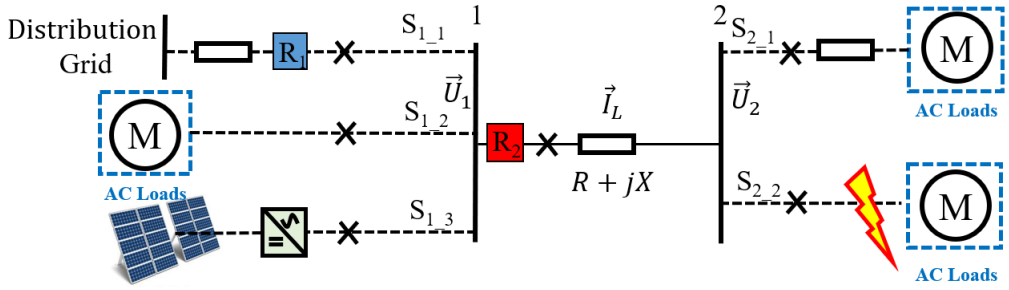

Figure 6.1: Distribution Feeder Protection with DERs while R_2 is disabled

In Fig. 6.1, relay R_2 is disabled such that it will not pickup when a fault happens in its zone downstream. Thus it is intentionally marked as red in the diagram. Based on Eq. (4.34) and Eq. (4.36), a decomposed current can be derived from current source S_{1_1} to S_{2_2}. This decomposed current describes the amount of fault current contribution from distribution grid to the fault current. Thus this backup protection issue can be converted to a primary protection issue using the decomposed current as a substitute of the measured current. R_1 and R_2 can also be coordinated through this decomposed current using the IDMT curve.

6.3 EMTP-MATLAB Simulation Results and Analysis

Based on Eq. (4.20 - 4.21), Eq. (4.34) and Eq. (4.36), the current tracing algorithm for backup protection is implemented in a MATLAB Simulink platform. The diagram is shown in Fig. 6.2, which consists of seven blocks.

The two current aggregation and single line blocks are the same control blocks that were implemented in Chapter 5 primary protection results

The current verification block is used to verify the current tracing results from each single line block and make sure the result is correct. This is realized by comparing the sum of the decomposed currents from the two single line block. Theoretically, they should equal to the line current $\vec{I_L}$.

The single line dissection block is the multiple sources to multiple sources current tracing block. This block takes in the output decomposed currents from the two single line blocks. The output of this block are the multiple sources to

multiple sources current tracing results including the decomposed currents. Only the decomposed current are used for the tripping logic block.

The tripping logic block is almost the same control block that was implemented in Chapter 6 primary protection results, except that it takes in the decomposed current from the single line dissection block.

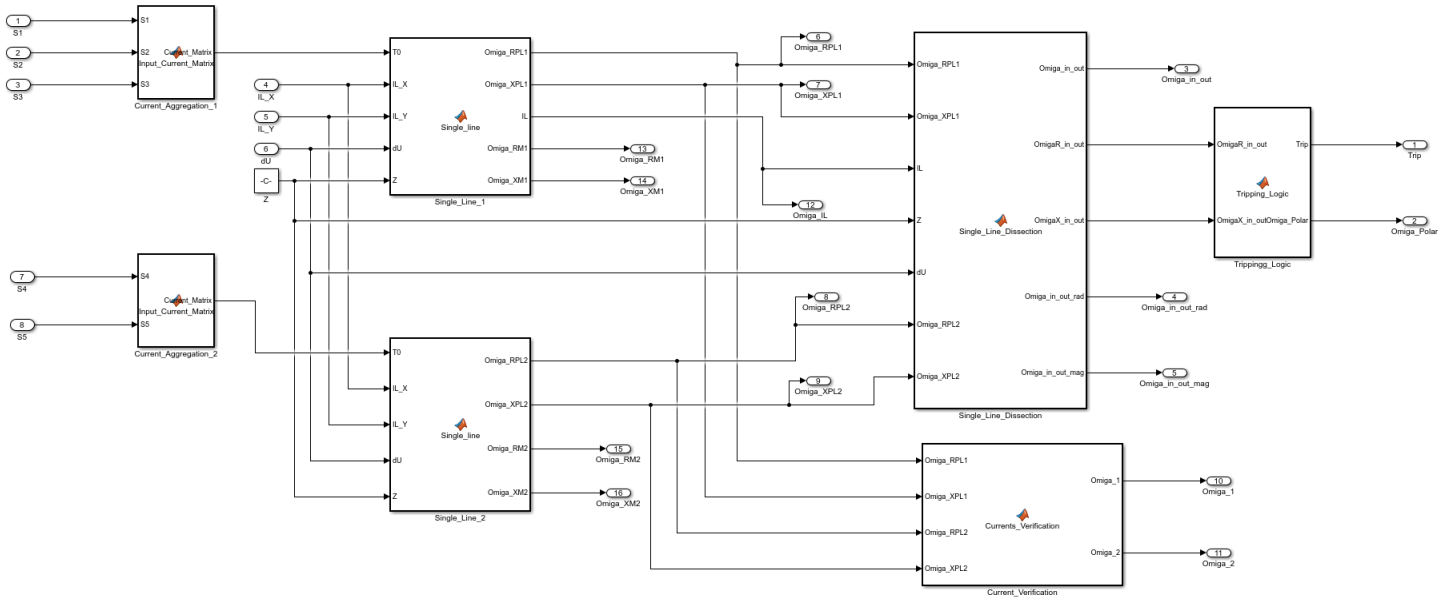

Figure 6.2: Matlab simulation for multiple sources to multiple sources current tracing

The EMTP-MATLAB simulation is shown in Fig. 6.3.

In Fig. 6.3, the trip signal is connected to a "set reset latch flip flop" block which is the same to Fig. 5.5. The "set reset latch flip flop" block is also not connected to the breaker, so that the fault current can be observed.

The EMTP-MATLAB backup protection interface is evaluated based on the fault type under different levels of DERs penetration. All of the measured values are positive sequence value.

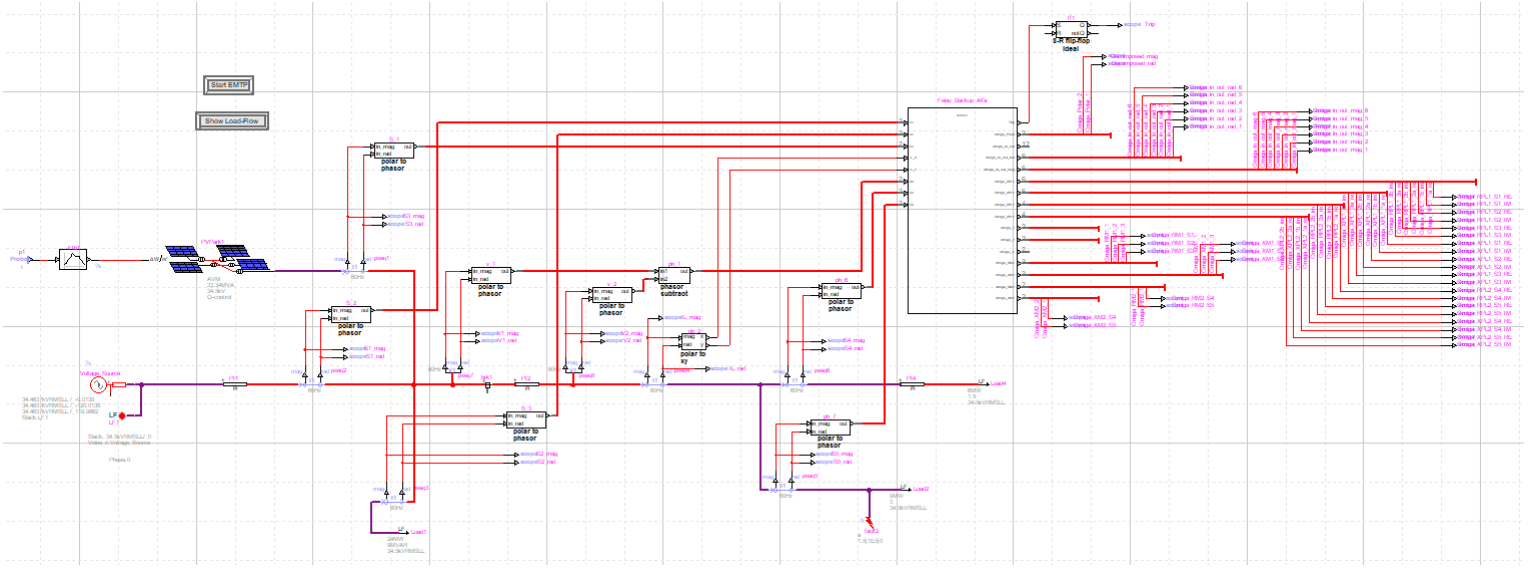

Figure 6.3: EMTP-MATLAB backup protection interface

6.3.1 LG Fault Results and Discussion

The decomposed currents from each individual current source on bus 1 to each individual current source on bus 2 are shown in Fig. 6.4-6.9. The measurement voltage and current information are neglected here as they are the same to that of Chapter 5.

It can be observed from Fig. 6.4, the current magnitude $\Omega_{in\_out\_mag\_1\_1}$ from distribution grid to current source 1 that is connected to bus 2 decreases when the number of SPV increases. Oppositely, in Fig. 6.6, the current magnitude $\Omega_{in\_out\_mag\_3\_1}$ from SPV to current source S_{2_1} increases when the number of SPV increases. This is obvious as the total power consumption of the loads is not changing, and more numbers of SPV will lead to less power consumption from the distribution feeder. When a fault occurs at 1.5 seconds, both $\Omega_{in\_out\_mag\_1\_1}$ and $\Omega_{in\_out\_mag\_3\_1}$ decreases as current source 1 that is connected to bus 2 does not have any fault on it. As a load, current source S_{1_2} does not contribute any current to the other current sources, thus $\Omega_{in\_out\_mag\_2\_1}$ is always 0.

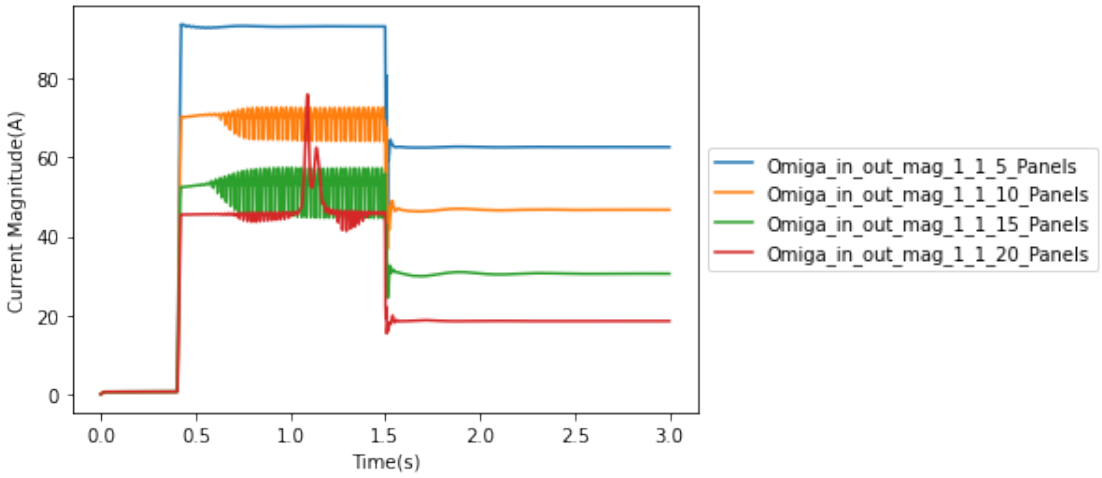

(**a**) Magnitude of $\Omega\_in\_out\_mag\_1\_1$

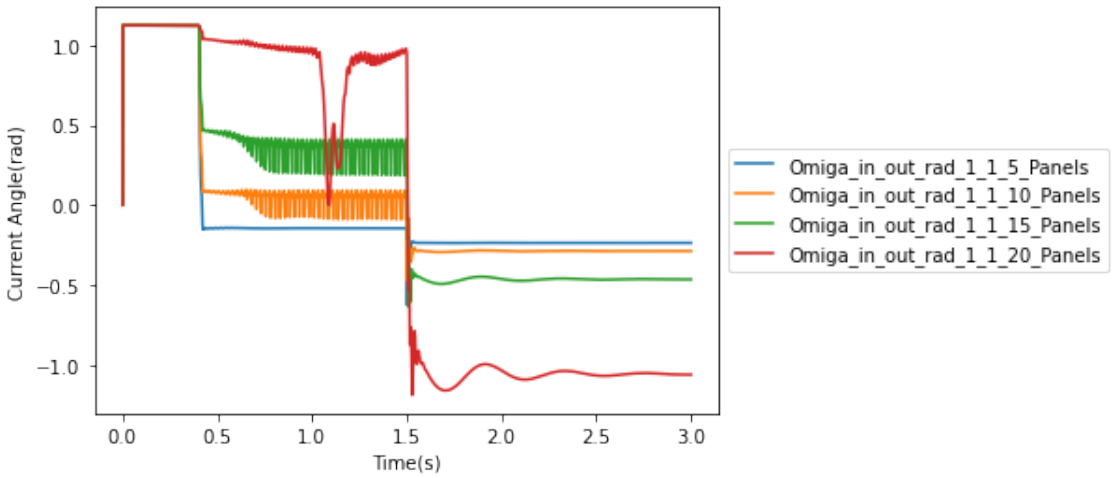

(**b**) Angle of $\Omega\_in\_out\_rad\_1\_1$

Figure 6.4: Decomposed current between current source 1 on bus 1 to current source 1 on bus 2 with LG fault under different level of DER penetration rate

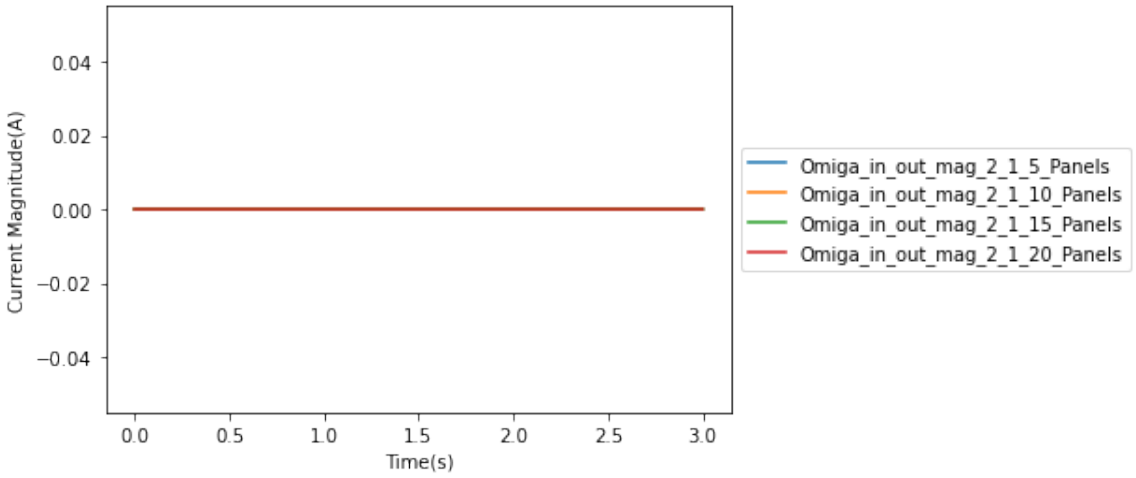

(**a**) Magnitude of $\Omega\_in\_out\_mag\_2\_1$

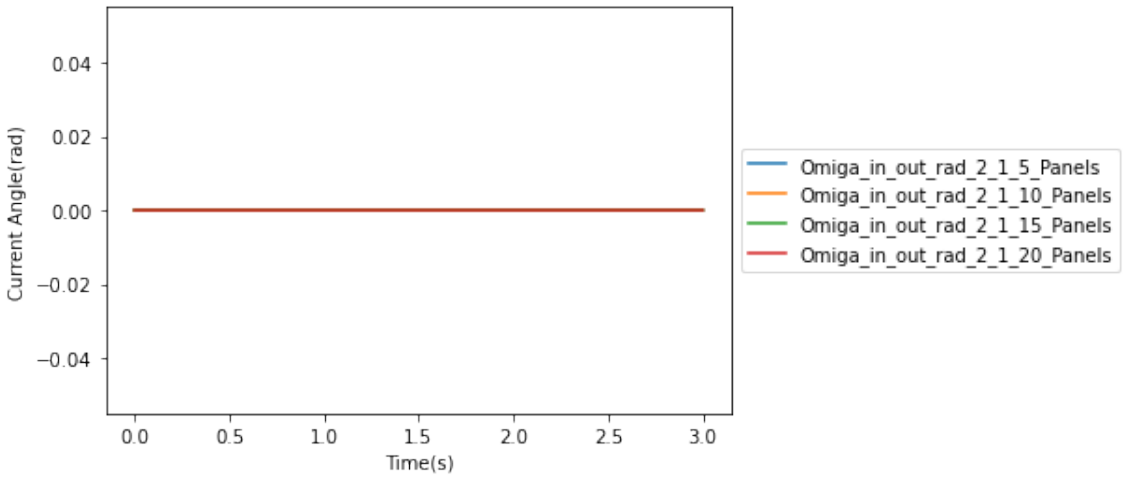

(**b**) Angle of $\Omega\_in\_out\_rad\_2\_1$

Figure 6.5: Decomposed current between current source 2 on bus 1 to current source 1 on bus 2 with LG fault under different level of DER penetration rate

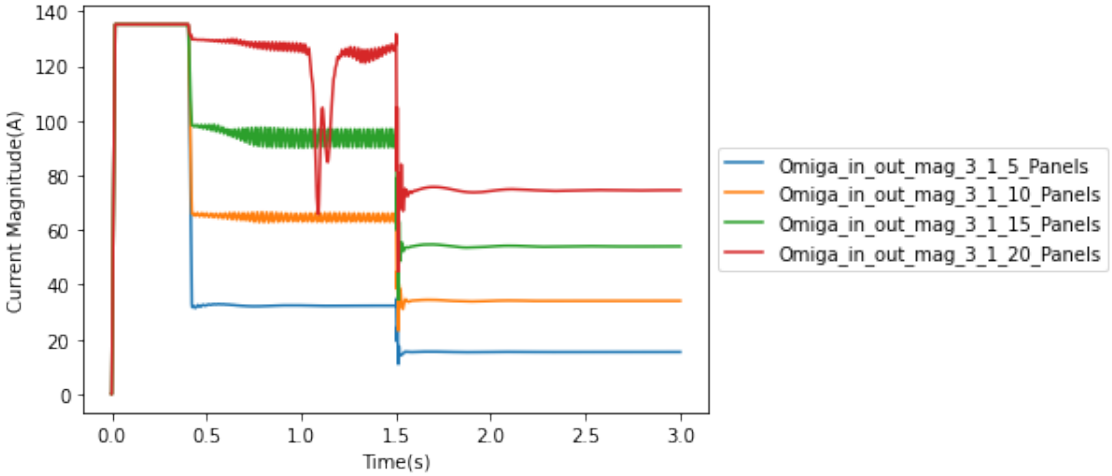

(**a**) Magnitude of Ω_*in*_*out*_*mag*_3_1

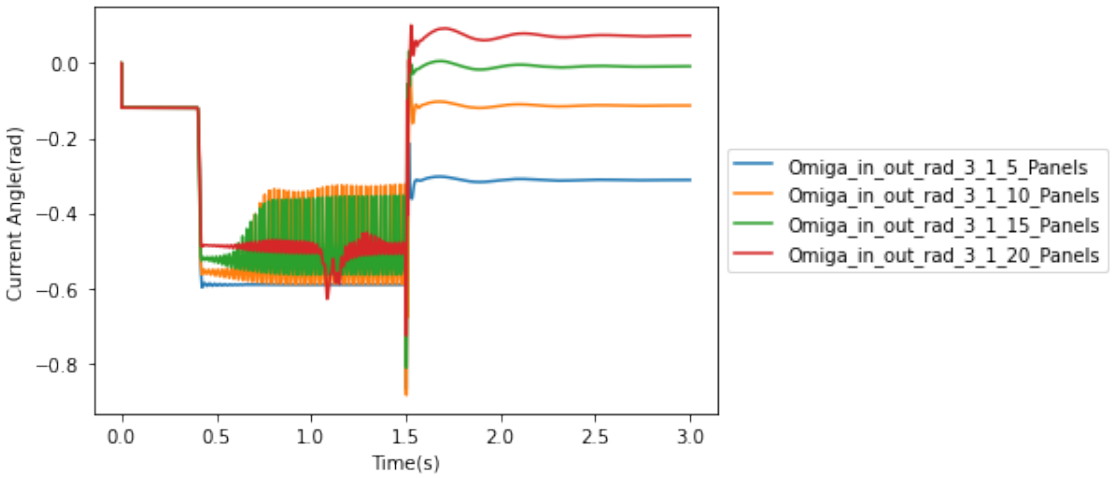

(**b**) Angle of Ω_*in*_*out*_*rad*_3_1

Figure 6.6: Decomposed current between current source 3 on bus 1 to current source 1 on bus 2 with LG fault under different level of DER penetration rate

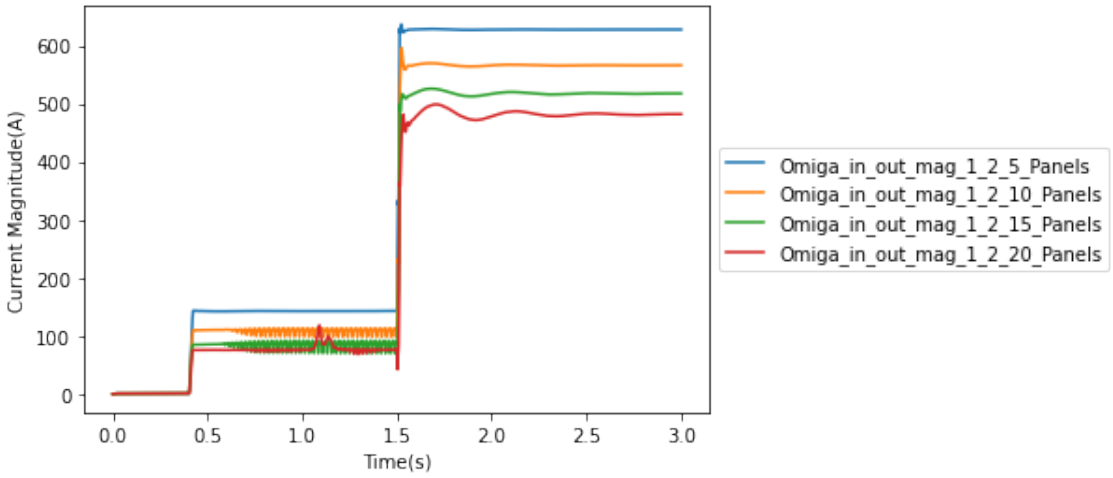

(**a**) Magnitude of $\Omega\_in\_out\_mag\_1\_2$

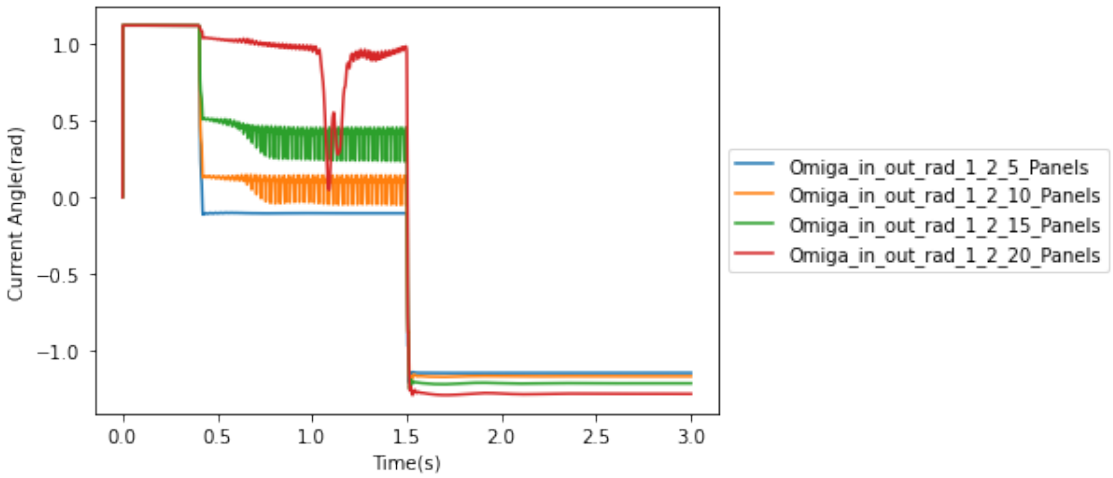

(**b**) Angle of $\Omega\_in\_out\_rad\_1\_2$

Figure 6.7: Decomposed current between current source 1 on bus 1 to current source 2 on bus 2 with LG fault under different level of DER penetration rate

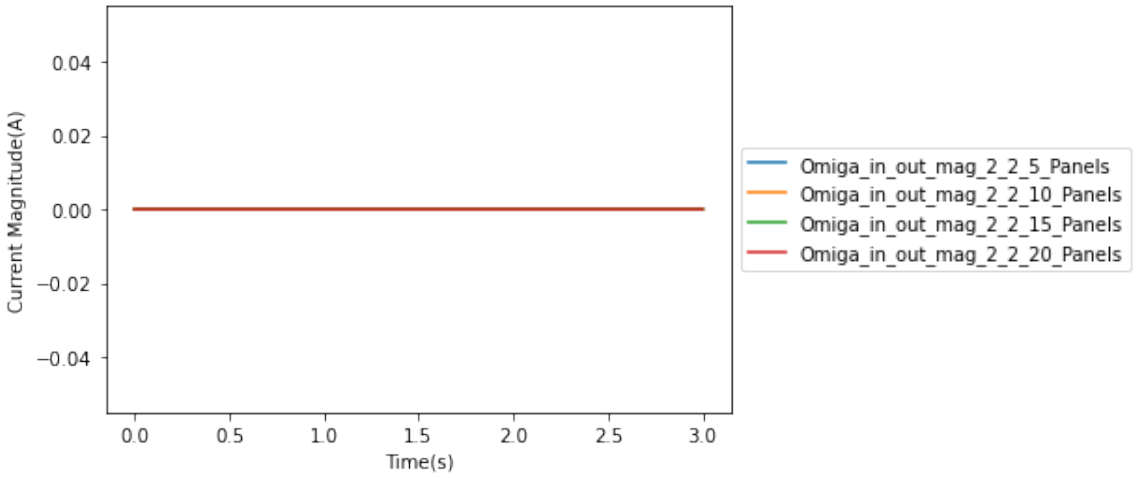

(**a**) Magnitude of $\Omega\_in\_out\_mag\_2\_2$

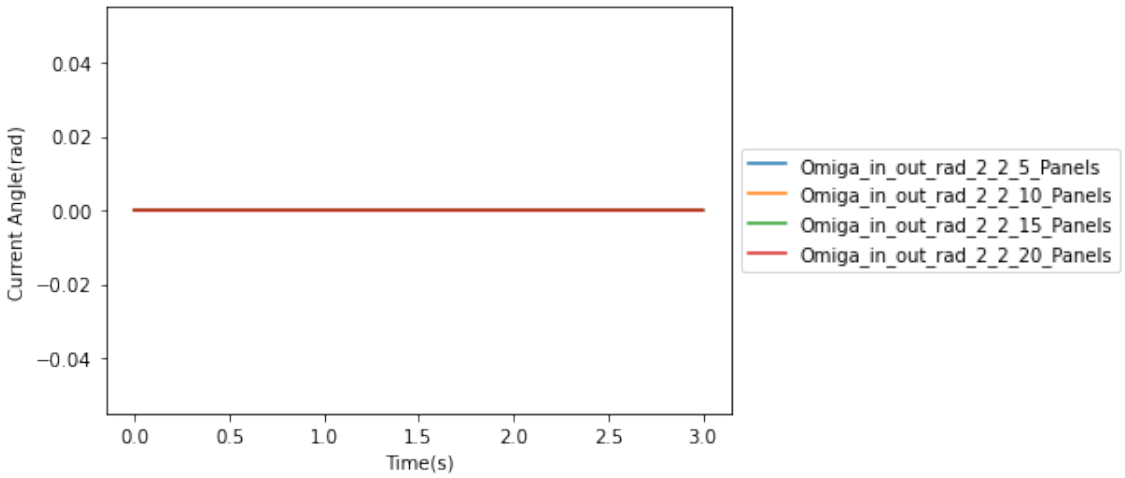

(**b**) Angle of $\Omega\_in\_out\_rad\_2\_2$

Figure 6.8: Decomposed current between current source 2 on bus 1 to current source 2 on bus 2 with LG fault under different level of DER penetration rate

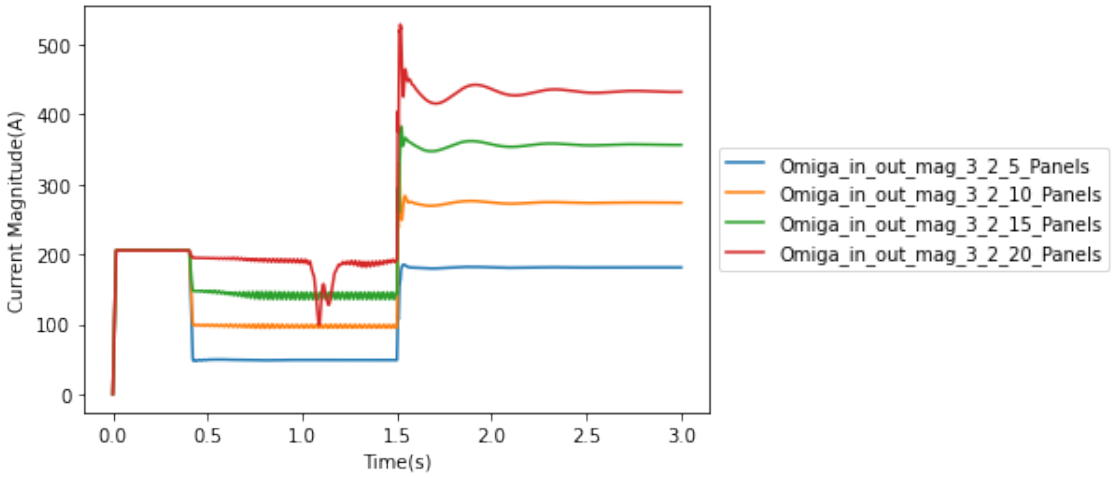

(**a**) Magnitude of $\Omega\_in\_out\_mag\_3\_2$

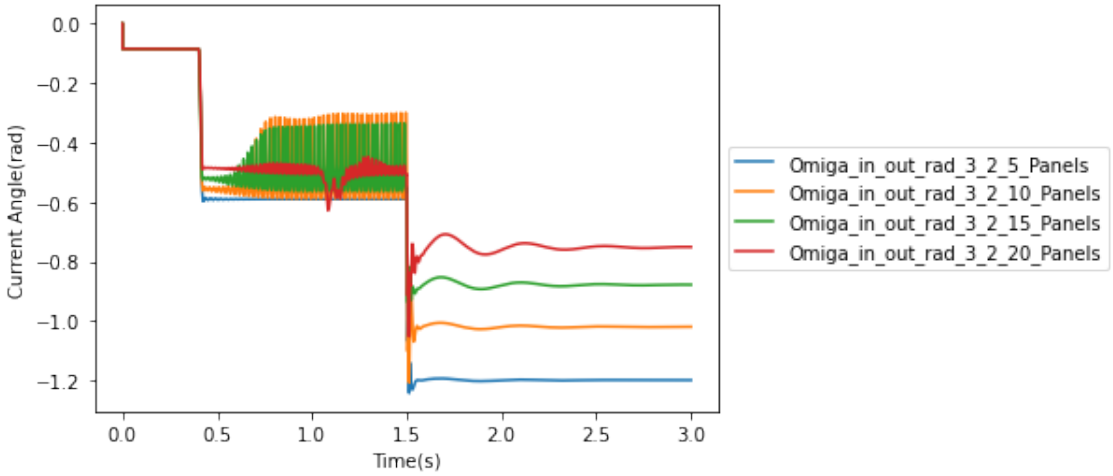

(**b**) Angle of $\Omega\_in\_out\_rad\_3\_2$

Figure 6.9: Decomposed current between current source 3 on bus 1 to current source 2 on bus 2 with LG fault under different level of DER penetration rate

In Fig. 6.7, the current magnitude $\Omega_{in\_out\_mag\_1\_2}$ from distribution grid S_{1_1} to current source S_{2_2} decreases when the number of SPV and the decomposed current $\Omega_{in\_out\_mag\_3\_2}$ increases. Similar to Fig. 6.4, this is due to the fact that total power consumption is not changing. When a LG fault is initiated at 1.5 seconds, the decomposed current $\Omega_{in\_out\_mag\_1\_2}$ increased from 80-140 A to 480-650 A, which is about five to six times its rated decomposed current. Whereas in Fig. 3.39, the measured current magnitude from current source S_{1_1} increased from 700 A to 1000 A, which is about 1.42 times its rated current. Compared to Fig. 3.39 that uses current measurement for backup protection, the decomposed current magnitude $\Omega_{in\_out\_mag\_1\_2}$ has a more significant fault current signature. Thus it greatly increases the sensitivity and dependability of the backup protection. With the significant increases of the decomposed current $\Omega_{in\_out\_mag\_1\_2}$, R_1 will be sensitive enough to see LG fault at the downstream of R_2. Thus the blinding of protection issue can be solved. In addition, R_1 and R_2 can be coordinated through the IDMT curve using the decomposed current $\Omega_{in\_out\_mag\_1\_2}$ to determine the trip time. In this simulation, relay R_1 is set to trip instantaneously. In addition, it is not needed to shift the IDMT curve compared to the adaptive relay scheme since the decomposed current received by the primary protection relay is the same to that of the backup protection relay.

Likewise, the measured current magnitude from the SPV current source S_{1_3} in Fig. 3.41 have very little change before and after fault inception at 1.5 seconds. Whereas, the decomposed current $\Omega_{in\_out\_mag\_3\_2}$ in Fig. 6.9 increases from 50-200 A to 200-430 A, which is about two times its rated decomposed current. In this case, if a new relay R_3 is placed at current source S_{1_3}, the decomposed current $\Omega_{in\_out\_mag\_3\_2}$ can be used to coordinate R_3 and R_2 without any issue of the relay blinding.

It can be observed from Fig. 6.5 and 6.8 that the magnitude and angle between two loads are always zero. This is obvious as there are no decomposed currents existing between loads.

The other angle information does not have any practical meaning in the proposed backup protection coordination scheme in this thesis. However, the angle information together with the decomposed current magnitude shown in Fig. 6.4-6.9 can be used to demonstrate that the sum of the decomposed currents between multiple current sources add up to the power line current $\vec{I}_L$, thus verifying the correctness of the algorithm. The result is shown in Fig. 6.10.

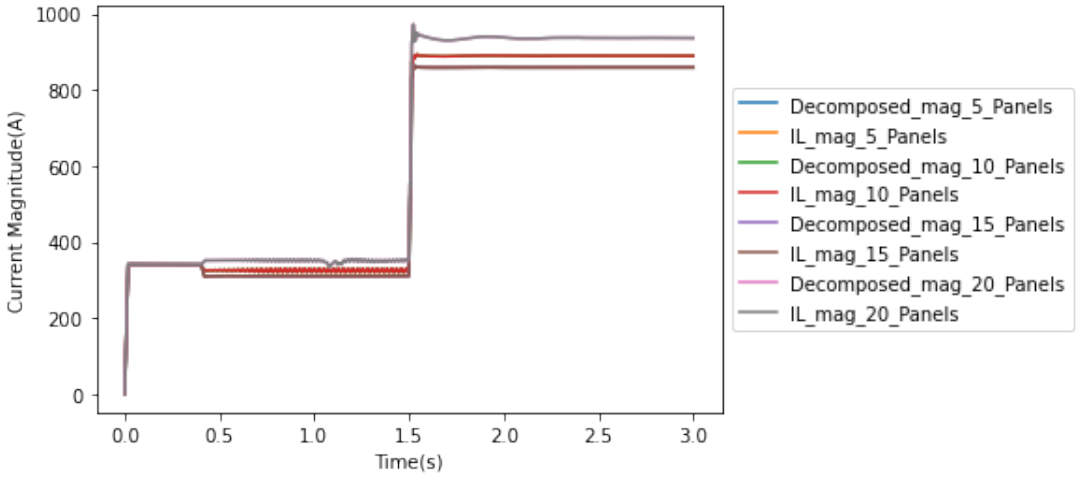

(**a**) Magnitude of I_L and the sum of the decomposed current between multiple current sources

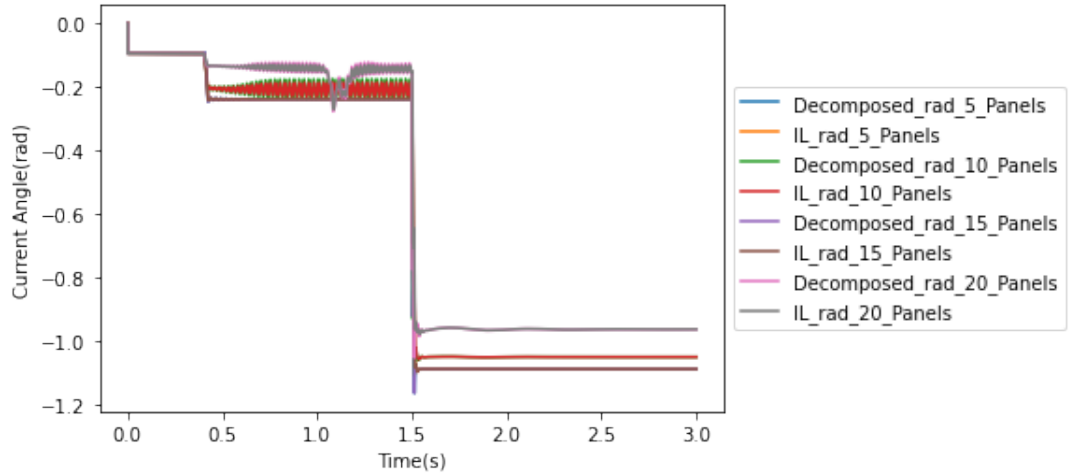

(**b**) Angle of I_L and the sum of the decomposed current between multiple current sources

Figure 6.10: Magnitude and angle of I_L and the sum of the decomposed current between multiple current sources

It is observed from Fig. 6.10 that both magnitude and the angle of the line current I_L and the sum of the decomposed current between multiple current sources under different levels of penetration of DERs are overlapped with each other. This proves that the current tracing based EMTP-MATLAB backup protection interface can be implemented in a real time protection system without violating any physical or electrical laws.

The EMTP-MATLAB backup protection interface trip signal is shown in Fig. 6.11. It can be observed that EMTP-MATLAB backup protection interface is tripped for all levels of DERs penetration instantaneously. Thus the EMTP-MATLAB backup protection interface is proved to be effective to overcome the blinding of protection.

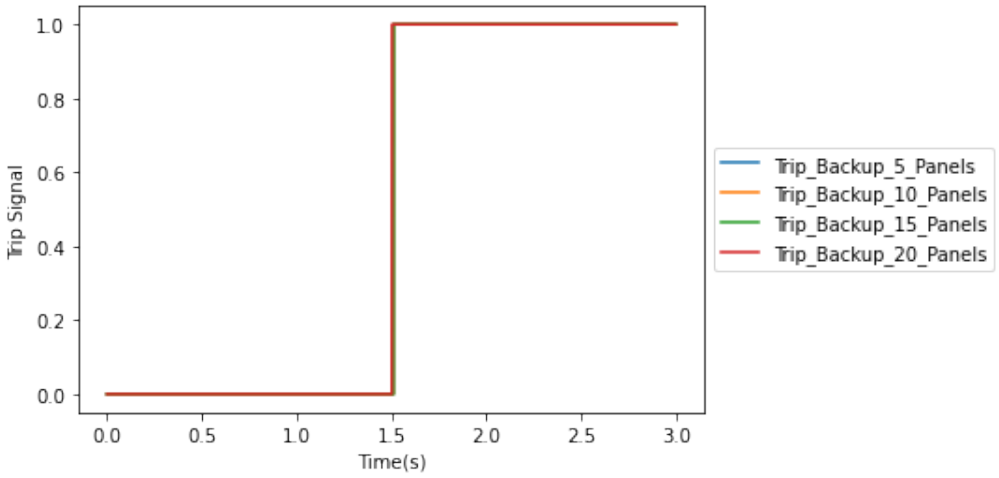

Figure 6.11: EMTP-MATLAB backup protection interface trip signal

In addition to the results that shown above, the proposed EMTP-MATLAB backup protection interface is not sensitive to the direction of the power flow. The SPV or any kinds of DERs can be installed at either side of the buses and no directional overrcurrent element is needed in the interface. Therefore, the proposed technique is suitable for the bidirectional power flow situation.

Finally, the proposed backup protection scheme has the advantage over adaptive protection schemes proposed by others where the pickup threshold is varied based on system operating conditions. Since the decomposed current has a more significant fault current signature compared to the measured currents, the tripping current thresholds can be set more simply to fixed settings. The decomposed current can easily surpass the fixed threshold when a fault occurs. It is also not necessary to consider the coordination between the backup protection relay and the backup of the backup protection relay at the same time. This is because the decomposed current is only derived between the two adjacent primary and backup protection relays.

Additional simulation results considering LL, LLG, LLL and LLLG faults

under different levels of DERs penetration rate, are listed in the Appendix C.

6.4 Conclusion

In this chapter, a backup protection scheme is proposed based on the multiple current sources to multiple current sources current tracing method. Instead of using the measured current, the proposed backup protection scheme uses the decomposed currents between each individual current source to determine the trip time from the IDMT curve. With the decomposed current, a direct virtual circuit is established from the backup relay to where the fault happens. Therefore, the backup protection coordination problem can be treated as a primary protection problem with the proposed decomposed current tracing analytics. In addition, the backup protection can also coordinate with the primary protection using the same decomposed current.

The proposed method is realized and validated through the EMTP-MATLAB simulation interface. The multiple current sources to multiple current sources current tracing method is first implemented in the MATLAB Simulink and compiled into a DLL file. The DLL file is then imported into the EMTP-MATLAB simulation interface. The blinding of protection issue in Chapter 3 is reproduced again in the simulation, but the traditional backup relay is replaced with the proposed EMTP-MATLAB simulation interface.

The simulation is run under different levels of DER injection. The simulation result shows that the proposed backup protection scheme works well under different levels of DER penetration without any complications arising from the bidirectional power flow issue. In addition, the decomposed currents have more significant fault current signatures compared to traditionally measured currents

in relays. This character makes the proposed backup protection outstanding from the traditional backup protection in regard to its higher sensitivity and dependability. Particularly, the blinding of protection issue can be solved through the proposed backup protection scheme.

When compared to the adaptive relay protection scheme that is being heavily promoted in literature, the proposed backup protection scheme has the advantage of a fixed tripping current threshold. This may be more preferable to utilities for regulation compliance that are used to protection relays with fixed pickups, and may be wary of ambiguous thresholds that may change unexpectedly. In addition, the proposed backup protection scheme does not need to consider the coordination with any adjacent relays except with the primary relay. This can greatly reduce the complexity of coordination when the system operating conditions change with DER injection and network reconfiguration.

Chapter 7

Conclusion and Future Works

7.1 Conclusion

The challenges associated with the impact of DERs to distribution network protection are addressed in this thesis with current tracing method and associated derived methods. In this thesis, a detailed description of the analytical foundation of fault current flow model is provided from a circuit principle perspective.

Unlike the traditional grid model, where current sources are congested on the bus and the power flowing through the power line, an equivalent circuit model is developed, where currents can flow through several parallel connected virtual power lines, which are electrically and physically equivalent to the widely used single power line model. Each parallel connected virtual power line is established based on the current contribution of each current source to the power line, known as the decomposed current. In addition, the contribution of currents between each individual current source is also provided in the form of parallel connected virtual power lines, which also follow electrical and physical principles. These equivalent power lines provide the possibility of relieving or eliminating the impact of DERs

to distribution network protection on the basis of only using decomposed currents as the fault signature.

The detailed foundation of current tracing method is described in Chapter 4 which is demonstrated and validated with MATLAB simulations. The theoretical derivation and simulation results show the mathematical correctness of the current tracing method, given the off-line synchronized current and voltage measurement data.

With the off-line synchronized current and voltage measurement data, a SVM based machine learning method is introduced in Chapter 5. The SVM method's performance is evaluated and compared by using the proposed current tracing kernel, polynomial kernel, and radial kernel methods. The results indicate that with the current tracing kernel, the SVM method is enhanced with more sensitivity and dependability to very low level faults compared to polynomial kernel and radial kernel. Further, EMTP-MATLAB primary protection interface is developed and for the first time, the current tracing method is implemented in power system primary protection relaying using the EMTP-MATLAB simulation platform with real time synchronized measurement data. The simulation results indicate that the decomposed currents have a more significant signature compared to measured currents when a fault happens. This also indicates that the proposed EMTP-MATLAB primary protection interface has higher sensitivity and dependability in regard to primary protection.

The power system backup protection is shown in Chapter 6. Through multiple current sources to multiple current sources current tracing, for the first time, the proposed EMTP-MATLAB backup protection interface is developed, which could identify the fault current contribution for the upstream relay. The simulation results indicate that the EMTP-MATLAB backup protection interface could

increase the sensitivity and dependability of the backup protection. The results strongly suggest that the blinding of relay issue can be completely avoided. The work is a departure from current research trends exploring adaptive relay protection schemes. The proposed EMTP-MATLAB backup protection interface has fixed tripping current thresholds and it does not need to consider the coordination with any adjacent relays except the primary relay. Therefore, less experiences and work loads are expected from the designers when implementing the proposed backup protection scheme.

7.2 Future Work

A few research directions are opened up in this thesis for future work.

In Chapter 4, the capacitance of the distribution line is neglected. Thus in the current tracing method, no capacitance information is included. In the future, the capacitance could be included, particularly for those long distribution feeders or applications in transmission lines.

The impedance of the virtual parallel connected power lines is available from the decomposed current. This could be used to develop and enhance the distance protection relay performance.

Moreover, with the decomposed current, advanced machine learning or deep learning method can be developed, not only for identifying the fault current but also for predicting the fault current. The off-line learning can also be extend to online learning.

Finally, since this method is proven to be effective on a small scale distribution network, extension of this work could be focused on the practical hardware implementation of current tracing method on a larger scale distribution network.

Appendix A

Real Time Distribution Network Topology Identification

A.1 Graph Representation of Distribution Network

Let G be a connected and directed graph such that

$$G = (\mathscr{V}, \mathscr{E}) \tag{A.1}$$

where $\mathscr{V} = \{v_1, v_2...v_n\}$ and $\mathscr{E} = \{e_1, e_2...e_m\}$ denoted as the set of vertex (or node) and edge of graph G respectively. $e_k(v_i, v_j)$ denoted as the function of edge e_k leaves source vertex v_i and entries terminal vertex v_j. $n = |\mathscr{V}|$ and $m = |\mathscr{E}|$ denoted as the number of vertexes and edges of graph G respectively.

With respect to these labelings, the incidence matrix $M = (m_{kh})$ is defined as $m \times n$ matrix, denoted as $M \in \mathbb{R}^{m \times n}$, such that

$$m_{kh} = \begin{cases} 1, & \text{if } v_h \text{ is the terminal vertex of } e_k. \\ -1, & \text{if } v_h \text{ is the source vertex of } e_k. \\ 0, & \text{otherwise.} \end{cases} \tag{A.2}$$

In this section, the distribution networks are modeled as graphs, where vertexes represent the loads and transformer of the distribution network, the edges represent the distribution lines. Any two vertices in such a distribution network are connected by exactly one path.

The Laplacian matrix, $\mathcal{L} = (l_{kh})$,$\mathcal{L} \in \mathbb{R}^{n \times n}$, is defined as

$$\mathcal{L} = M^T M \tag{A.3}$$

Mathematically, $\mathcal{L}$ can also be represented as

$$\mathcal{L} = \mathcal{D} - \mathcal{A} \tag{A.4}$$

where $\mathcal{D}$ is the degree matrix, $\mathcal{D} \in \mathbb{R}^{n \times n}$, and $\mathcal{A} = (a_{kh})$ is the adjacency matrix, $\mathcal{A} \in \mathbb{R}^{n \times n}$ of graph G.

Take the square of Eq. (A.4), the following equation could get,

$$\mathcal{L}^2 = \mathcal{D}^2 - \mathcal{A}\mathcal{D} - \mathcal{D}\mathcal{A} + \mathcal{A}^2. \tag{A.5}$$

For easy and concise description, the sign structure matrix of a matrix $\mathcal{T} = (t_{kh})$, $\mathcal{T} \in \mathbb{R}^{n \times n}$ is defined as $\mathcal{S}(\mathcal{T}) = (s_{kh}(\mathcal{T}))$ such that

$$s_{kh}(\mathcal{T}) = \begin{cases} 1, & \text{if } t_{kh} \text{ is negative,} \\ 0, & \text{otherwise.} \end{cases} \tag{A.6}$$

With respect to this labeling, the following equation could get,

$$S(\mathcal{L}^2) = S(-\mathcal{A}\mathcal{D} - \mathcal{D}\mathcal{A}). \tag{A.7}$$

Since the degree matrix of a tree is positive-definite, the following equation could get,

$$S(\mathcal{L}^2) = \mathcal{A}. \tag{A.8}$$

Therefore, the adjacency matrix could also be constructed from $\mathcal{L}^2$ matrix.

A.2 Voltage Expansion Model

Consider a distribution network of n vertices with node voltage phasor implemented on each vertex. A collection of SCADA voltage magnitude is given by

$$|U| = \{|u_1|, |u_2|, ...|u_v|, ...\} \tag{A.9}$$

where $|u_v| \in \mathbb{R}^{n \times 1}$ is the magnitude of v^{th} voltage measurement. The Taylor Series expansion of $|u_v|$ with respect to the transformer voltage magnitude $|U_N|$

is defined in [73] such that

$$|u_v| = |U_N| \cdot \mathbf{1} + \frac{1}{|U_N|}\Re(e^{j\theta} X \overline{s}_v) + \frac{d_v(|U_N|)}{|U_N|^2} \tag{A.10}$$

where $\overline{s}_v$ is the conjugate of injective power at v^{th} measurement, $\mathbf{1} \in \mathbb{R}^{n\times 1}$ such that $\mathbf{1} = \{1, 1, 1, ..., 1\}$, θ is the ratio of conductance /impedance (L/R ratio) based on the assumption of uniformed inductance/resistance ratio, X represents the impedance matrix of the network, $\frac{d_v(U_N)}{U_N^2}$ is the high order term of the Taylor Series expansion which is bonded when $|U_N|$ goes to infinite.

A.2.1 Model of Topology Estimation

By neglecting the high order terms in Eq. (A.10), a covariance matrix Λ of $|U|$ can be expressed in the following simple clean form,

$$\Lambda = E[(|u| - E|u|)(|u| - E|u|)^T] = \frac{X\Psi X}{U_N^2} \tag{A.11}$$

where Ψ is the diagonal positive-definite matrix defined as,

$$\Psi = cos\theta \cdot diag(\sigma_{pv}^2) + sin\theta \cdot diag(\sigma_{qv}^2) \tag{A.12}$$

where $diag(\sigma_{pv}^2)$ and $diag(\sigma_{qv}^2)$ are diagonal covariance matrices of active power and reactive power of each vertex respectively based on the assumption of independent injective power.

It is known that the impedance matrix X is the pseudo-inverse of admittance matrix Y. The admittance matrix could be represented as

$$Y = M^T W^{-1} M = \mathcal{L}_W \tag{A.13}$$

where $\mathcal{L}_W$ is the weighted Laplacian matrix, $W = (w_{kh})$ is the diagonal positive semi-definite matrix such that

$$w_{kh} = \begin{cases} z^{-1}(e_k), & \text{if } h = k. \\ 0, & \text{otherwise.} \end{cases} \tag{A.14}$$

where $z(e_k)$ is the impedance of edge e_k.

In order to describe the relationship between SCADA voltages and the topological structure in terms of covariance, the pseudoinverse of Λ is introduced and denoted by K, which is also known as the concentration matrix of Λ.

$$K = U_N^2 \mathcal{L}_W \Psi^\dagger \mathcal{L}_W, \tag{A.15}$$

where $\Psi^\dagger$ is the diagonal pseudoinverse of Ψ, which is positive semi-definite.

Since $\Psi^\dagger$ is a diagonal positive semi-definite matrix, W^{-1} is a diagonal positive definite matrix, U_N is a constant, the sign structure of K and $\mathcal{L}^2$ are the same. Based on Eq. (A.8), the following equation could get,

$$S(\mathcal{L}^2) = S(K) = S(U_N^2 \mathcal{L}_W \Psi^\dagger \mathcal{L}_W) = \mathcal{A}. \tag{A.16}$$

Therefore, the topology of the distribution network could be identified by locating the negative entries in the K matrix.

A.2.2 Impact Variables on System Identification

At first glance, it seems that the K matrix has the same sign structure of $\mathcal{L}^2$ matrix, however, the identification process was carried out based on the following assumptions and constrains which may restrict or even change the results of

identification if they are not well followed:

- The L/R ratio of impedance of each cable of the distribution network are assumed all the same, which is a strict constraint that hard to be reached.
- The injective power of every vertex is assumed to be independent to each other, i.e. the changing of injective power of one vertex does not affect the others, which also contradict to the case that the increasing temperature of one block causes the increasing of injective power at all vertices within the block where the injective powers are correlated.
- The high order term of $|u|$ was neglected when constructing the Λ matrix, which introduce errors in , where the sign structure of K changes, which affects directly to the identification.
- The voltage at the transformer is assumed to be a constant fundamental wave that the harmonic wave, which appears quite often in transformer, is not considered. When there are harmonics, the impedance changes while L/R ratio of each line differs dramatically.

Due to the possible impact of the assumptions used in the derivation of Eq. (A.15), it is necessary to understand K matrix and analysis the possible errors caused by violating the assumptions above. Since this chapter is mainly focus on the modeling errors, it is assumed that there are no voltage measurement errors and no harmonics in the distribution network.

A.3 Simulations of Impact of Modeling Errors

The voltage sample was collected on a 9-bus distribution network shown in Fig. A.1.

In order to avoid errors from measurement, the voltage set $|U|$ is constructed

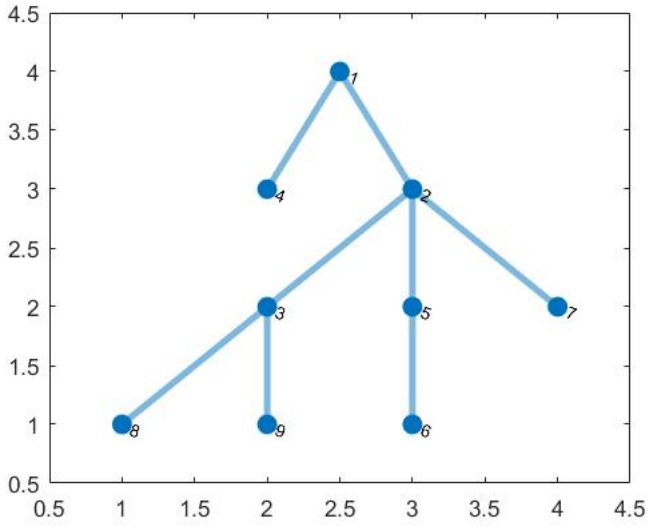

(**a**) Graph representation

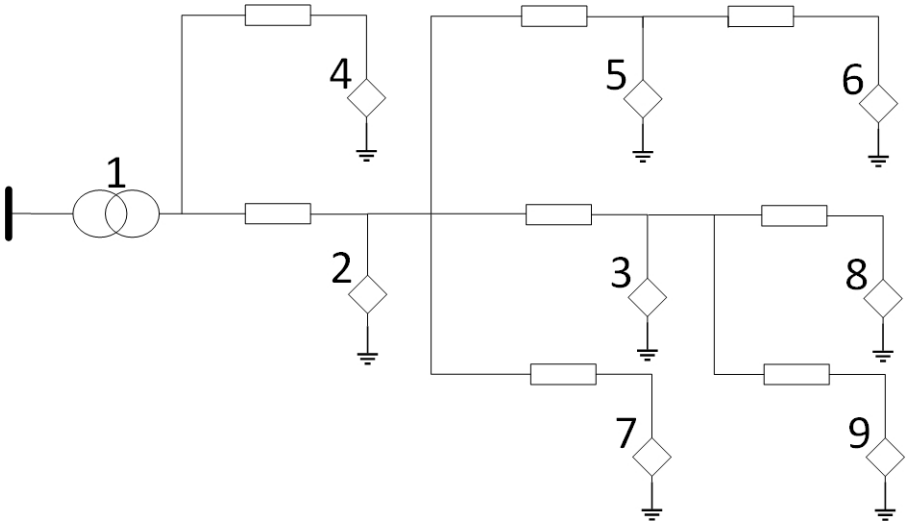

(**b**) Electric representation

Figure A.1: The original 9-bus distribution network.

by calculating the power flows. The back-forward method is used to calculate the power flow. To help us observe the modeling errors, the voltage magnitude difference between two iterations is restricted to 10^{-8} to maintain the voltage set $|U|$ as accurate as possible.

This chapter focus on the simulation of case 2 and case 4, because these two cases are more common in practice.

In case 2, the impedance of each distribution line is set to $1 + 1j$. In case 4, the impedance of distribution line is changed, which is listed in Tab. A.1, so that it violates the uniformed L/R ratio assumption. In both cases, the reactive

Table A.1: Impedance of distribution network in case 4

Vertex i	Vertex j	Resistance	Inductance
1	2	0.5	1.5
2	3	0.5	1
1	4	1	1.5
2	5	1	1.5
5	6	0.5	1
2	7	0.5	1
3	8	0.5	1
3	9	1	1

power of each vertex are set to be unchanged, the active power of each vertex are uniformly distributed from 9.9-10.1 MVA.

The correlation of the active power with different sizes of active power samples is computed. The diagonal entries of ψ is shown in Fig.A.2. The reactive power of each vertex is set to be constant. The simulation result is listed in Tab. A.2. The partial graph representation of the identification results are show in Fig. A.3,Fig. A.4 and Fig. A.5.

It can be observed that for the 30 size of sample voltage, if the L/R ratio is uniformed, the distribution network could be identified. However, if the non-uniformed L/R ratio assumption is violated, the distribution network couldn't be identified. As it was analyzed in case 4, the different result is caused by the non-symmetric error E_S.

It can also be observed that for both cases, when the sample size is increasing,

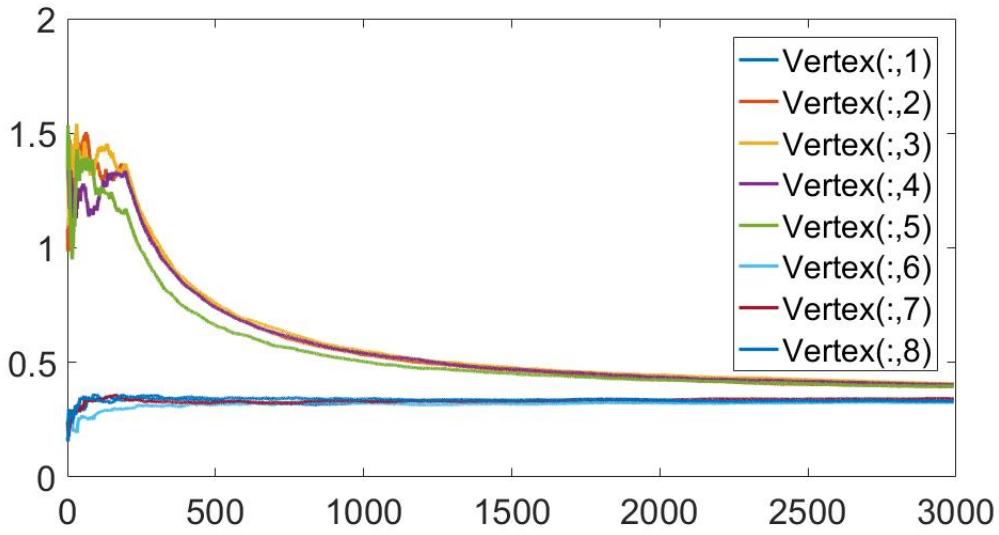

Figure A.2: The value of diagonal entries of ψ with different sizes of active power samples

Table A.2: Identification results with different voltage sample size

Sample Size	Whether Identified	
	Case 2	Case 4
9	No	No
30	No	No
70	Yes	No
100	Yes	Yes
150	Yes	Yes

the correlation error $E_{W\psi}$ is decreasing. Therefore the distribution network could be identified.

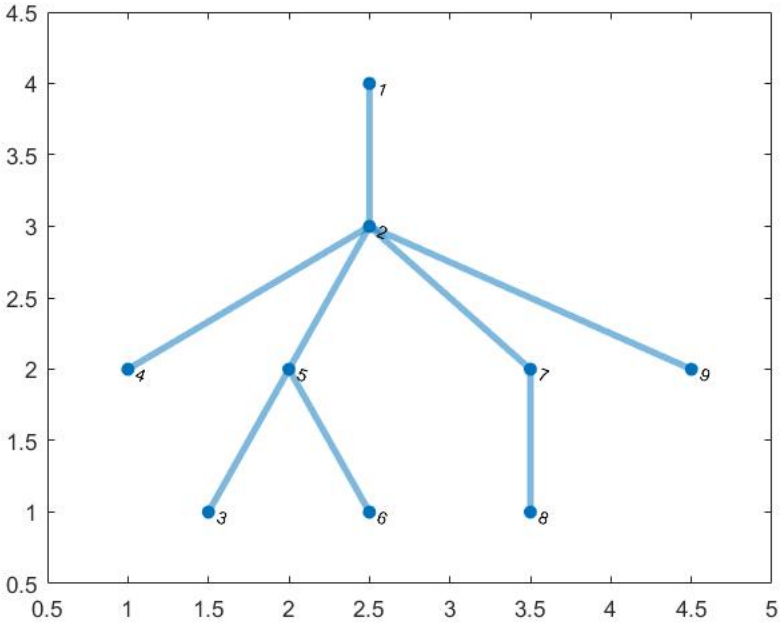

(**a**) case 2

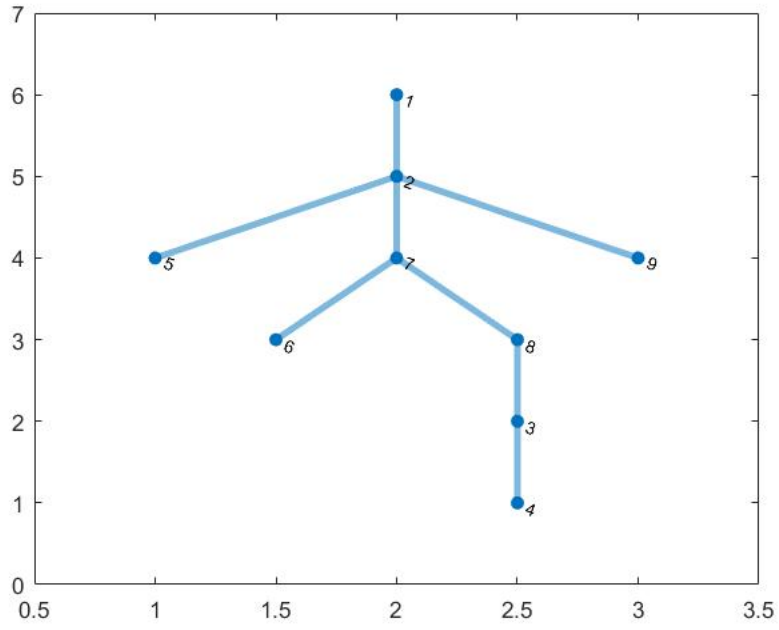

(**b**) case 4

Figure A.3: Identification result when voltage sample size is 9

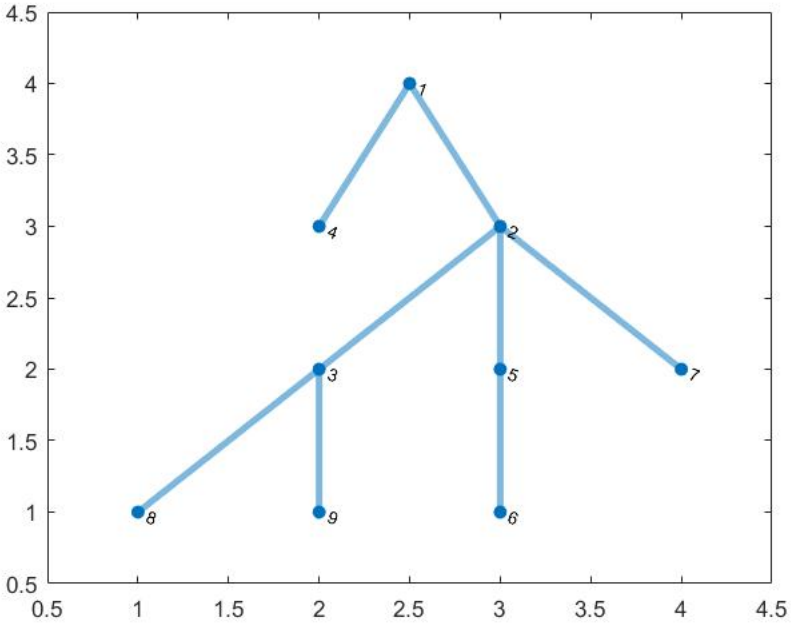

(**a**) case 2

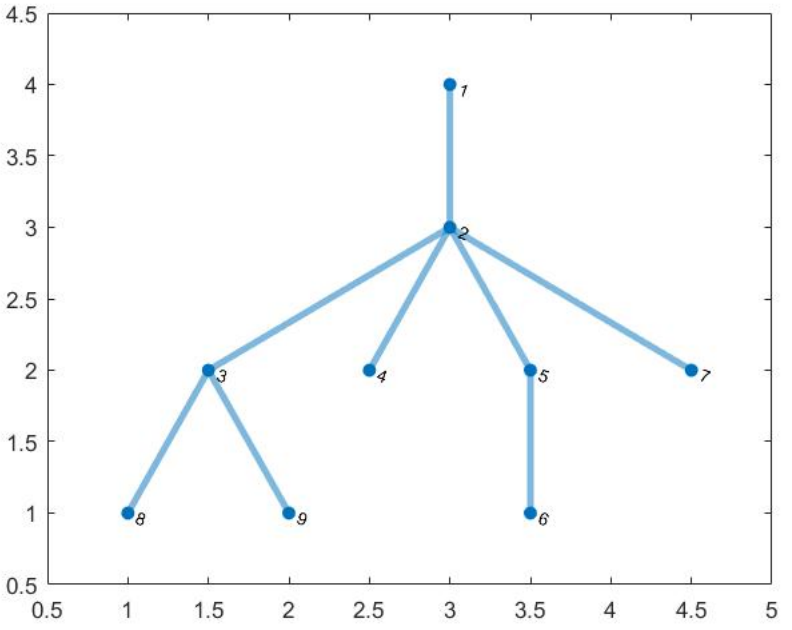

(**b**) case 4

Figure A.4: Identification result when voltage sample size is 70

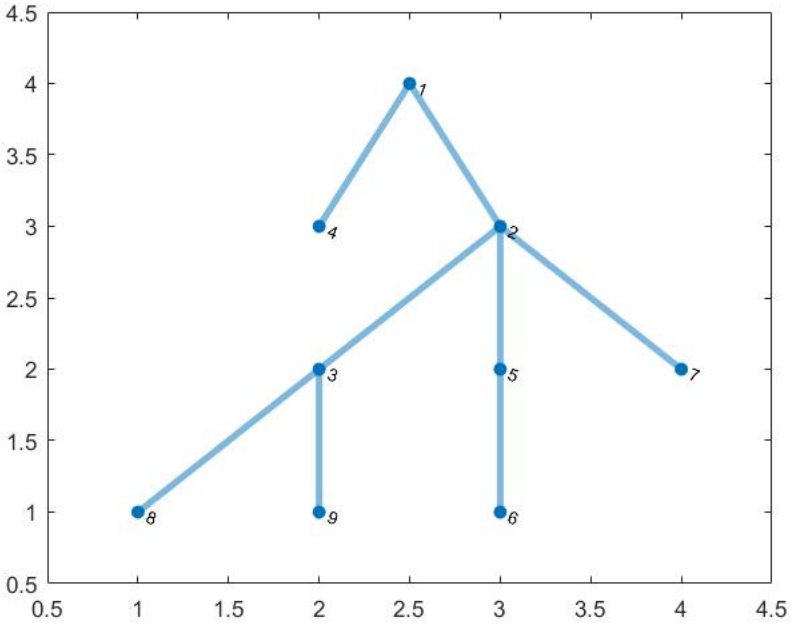

(**a**) case 2

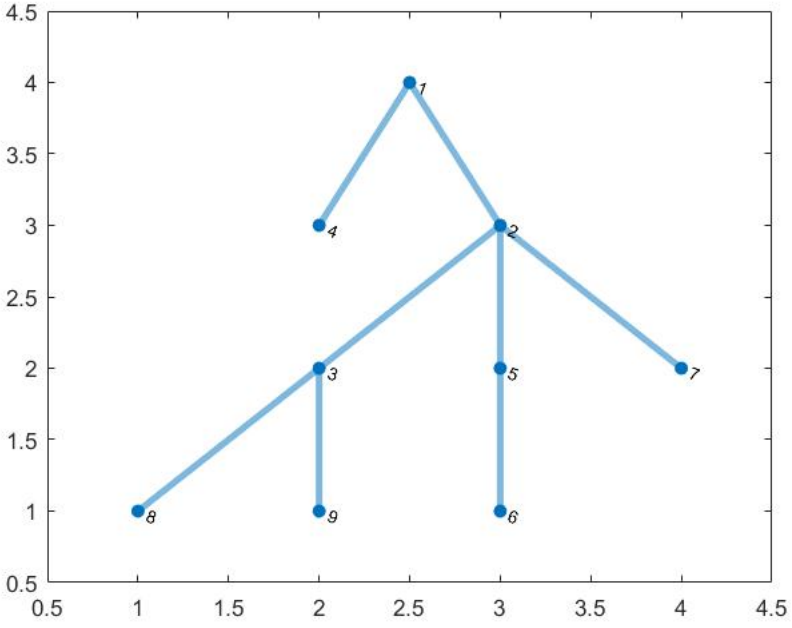

(**b**) case 4

Figure A.5: Identification result when voltage sample size is 100

A.4 Conclusion

In this chapter, the modeling errors in the topology identification of radical distribution networks are analyzed. It is shown that if the measurement of voltage is accurate enough, there are two factors that affects the result of identification: the L/R ratio and the correlation of nodal injective power. The non-uniformed L/R ratio would cause the non-symmetric error E_S and the correlation of nodal injective power would cause the correlation error $E_{W\psi}$. The impact of these two errors were discussed separately and founded two cases that are common in practice. In both cases, the error could be decreased by increasing the voltage sample size.

Appendix B

More Simulation Results of Primary Protection

B.1 LL Fault for Primary Protection

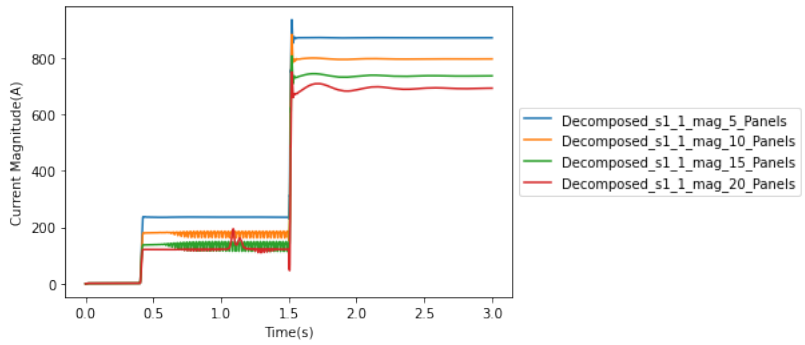

(**a**) Magnitude of decomposed current from $S1\_1$

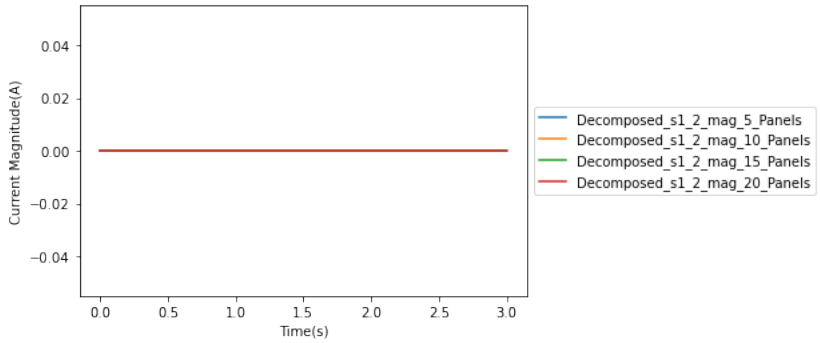

(**b**) Magnitude of decomposed current from $S1\_2$

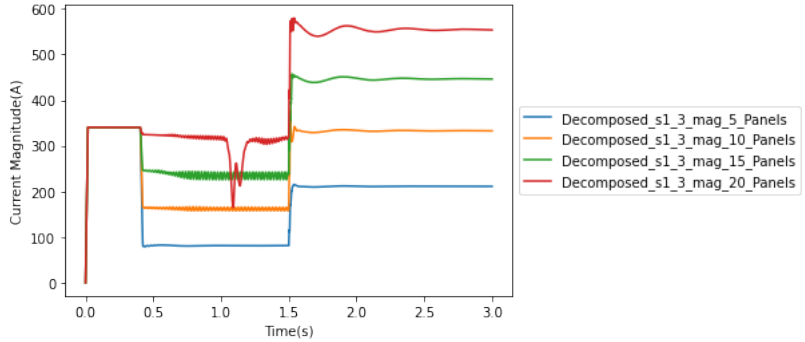

(**c**) Magnitude of decomposed current from $S1\_3$

Figure B.1: Magnitude of decomposed current from each individual current sources to the distribution line with LL fault under different level of DER penetration rate on bus 1

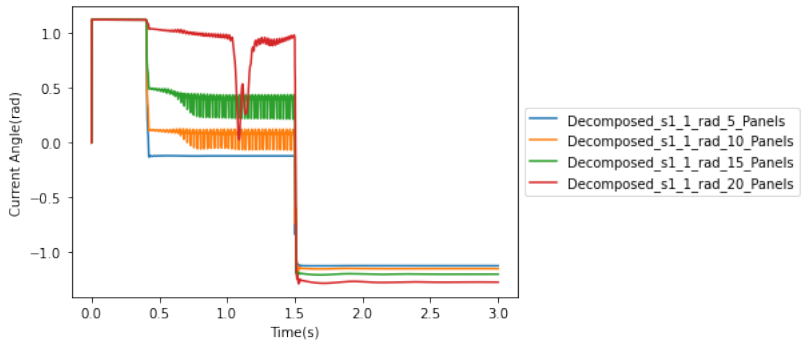

(**a**) Angle of decomposed current from $S1\_1$

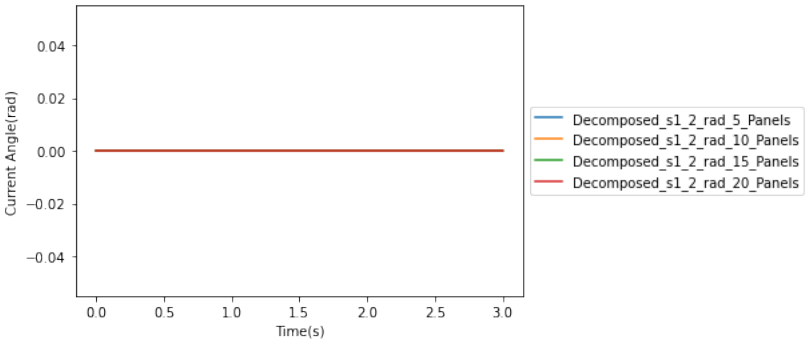

(**b**) Angle of decomposed current from $S1\_2$

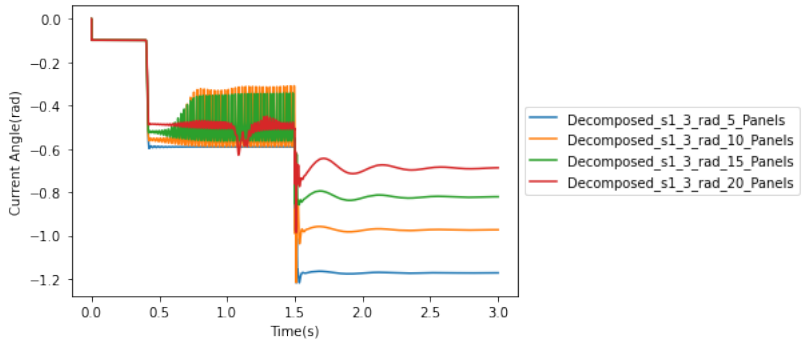

(**c**) Angle of decomposed current from $S1\_3$

Figure B.2: Angle of decomposed current from each individual current sources to the distribution line with LL fault under different level of DER penetration rate on bus 1

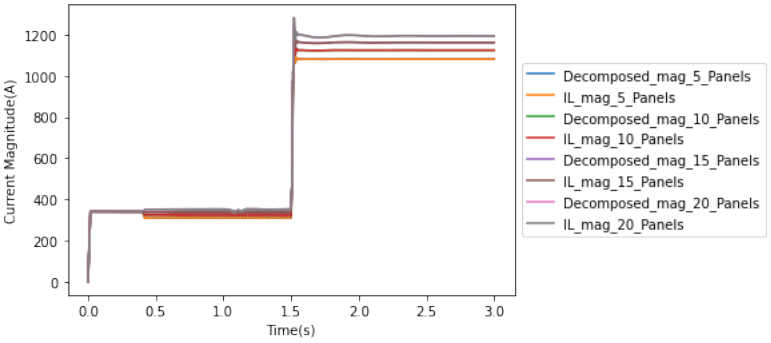

(**a**) IL and the sum of decomposed current magnitude

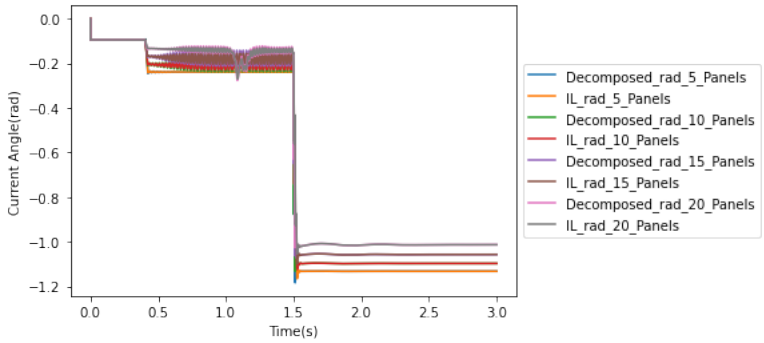

(**b**) IL and the sum of decomposed current angle

Figure B.3: Comparison between IL and the sum of decomposed current of primary protection with LL fault under different level of DER penetration rate

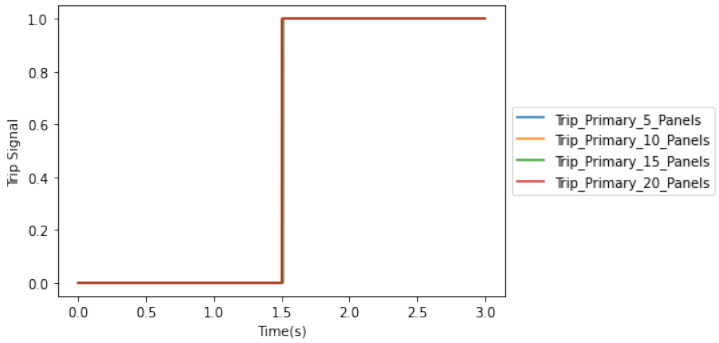

Figure B.4: EMTP-MATLAB primary protection interface trip signal

B.2 LLG Fault for Primary Protection

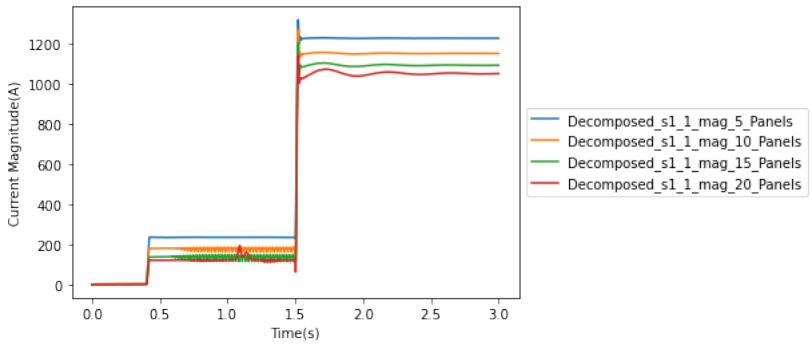

(**a**) Magnitude of decomposed current from $S1\_1$

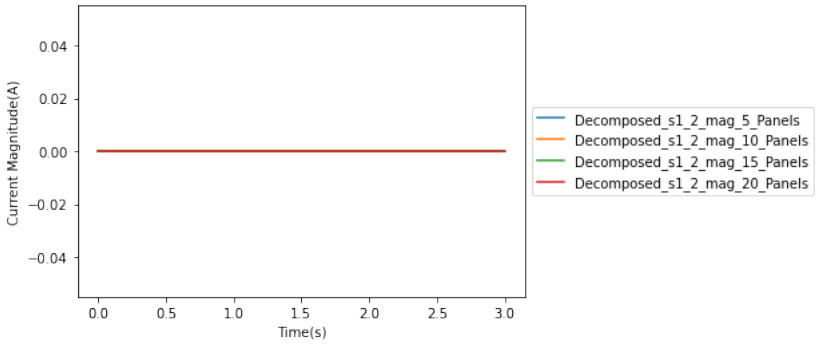

(**b**) Magnitude of decomposed current from $S1\_2$

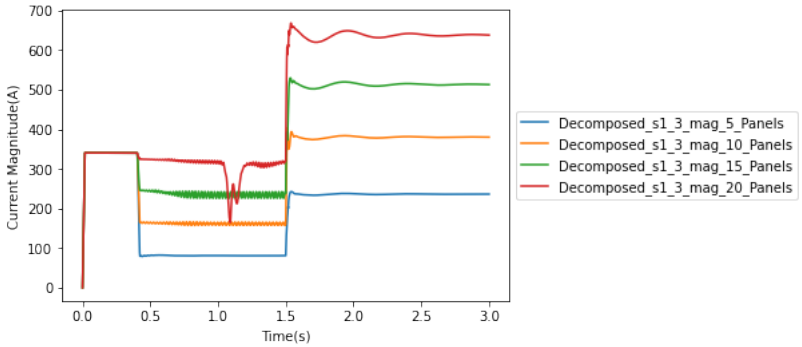

(**c**) Magnitude of decomposed current from $S1\_3$

Figure B.5: Magnitude of decomposed current from each individual current sources to the distribution line with LLG fault under different level of DER penetration rate on bus 1

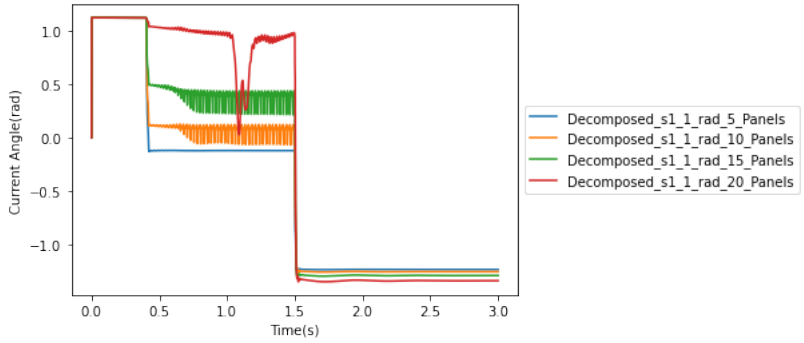

(**a**) Angle of decomposed current from $S1\_1$

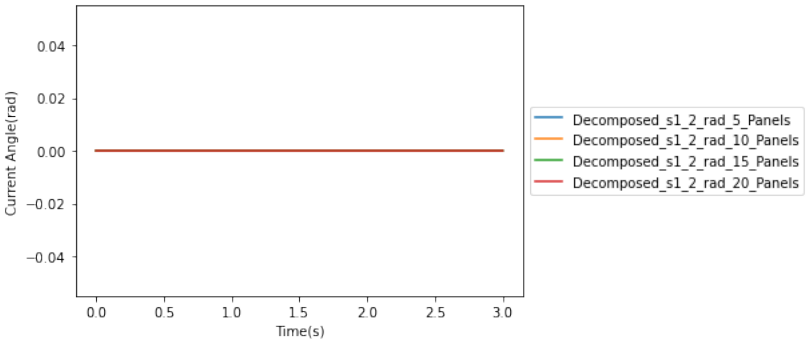

(**b**) Angle of decomposed current from $S1\_2$

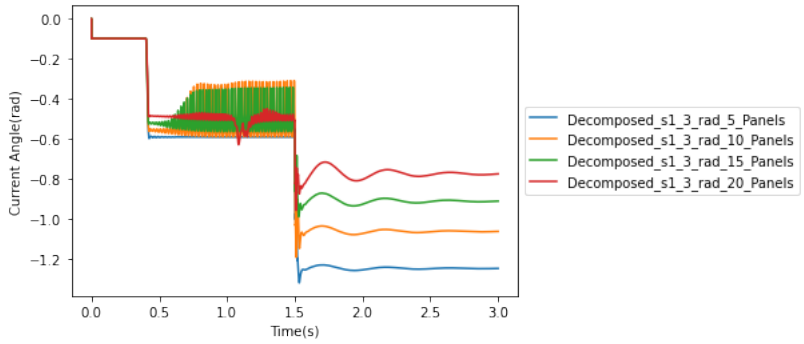

(**c**) Angle of decomposed current from $S1\_3$

Figure B.6: Angle of decomposed current from each individual current sources to the distribution line with LLG fault under different level of DER penetration rate on bus 1

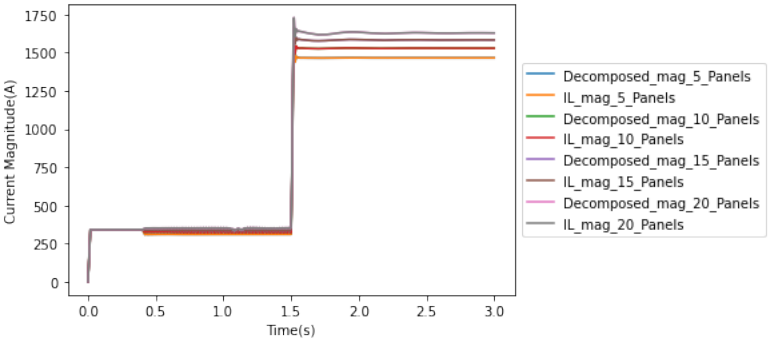

(**a**) IL and the sum of decomposed current magnitude

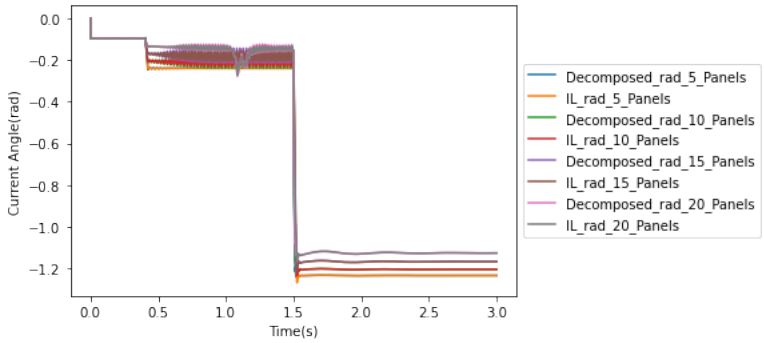

(**b**) IL and the sum of decomposed current angle

Figure B.7: Comparison between IL and the sum of decomposed current of primary protection with LLG fault under different level of DER penetration rate

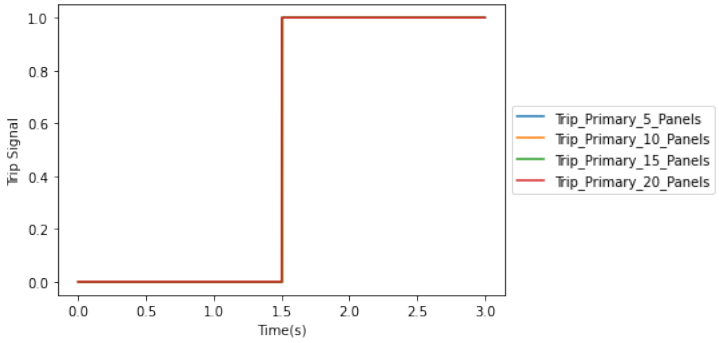

Figure B.8: EMTP-MATLAB primary protection interface trip signal

B.3 LLL Fault for Primary Protection

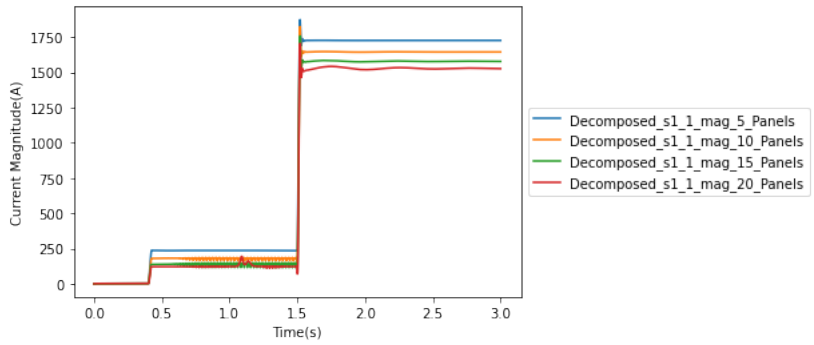

(**a**) Magnitude of decomposed current from $S1\_1$

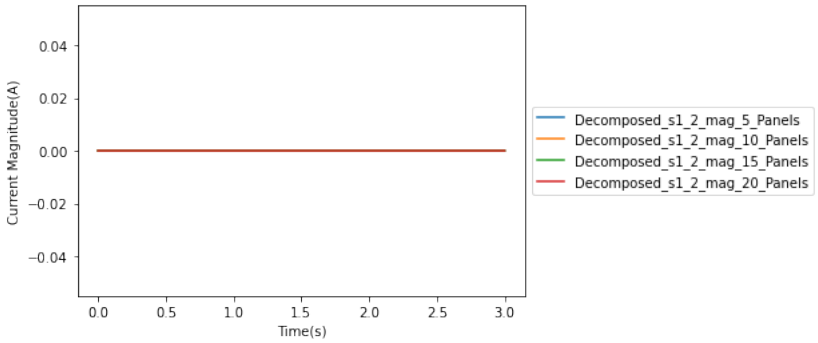

(**b**) Magnitude of decomposed current from $S1\_2$

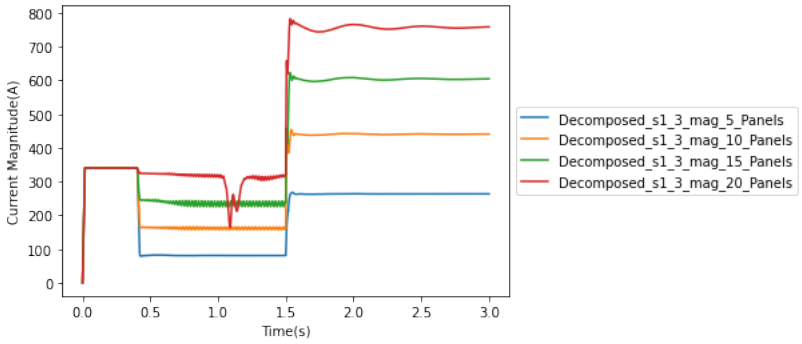

(**c**) Magnitude of decomposed current from $S1\_3$

Figure B.9: Magnitude of decomposed current from each individual current sources to the distribution line with LLL fault under different level of DER penetration rate on bus 1

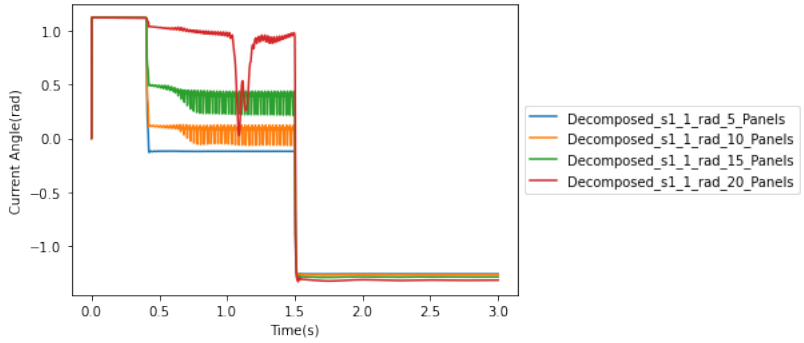

(**a**) Angle of decomposed current from $S1\_1$

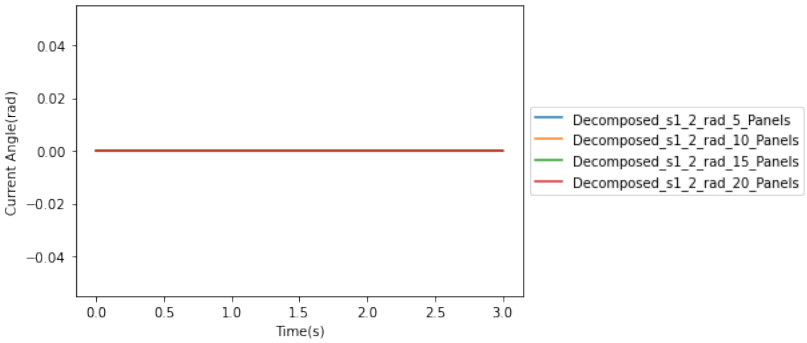

(**b**) Angle of decomposed current from $S1\_2$

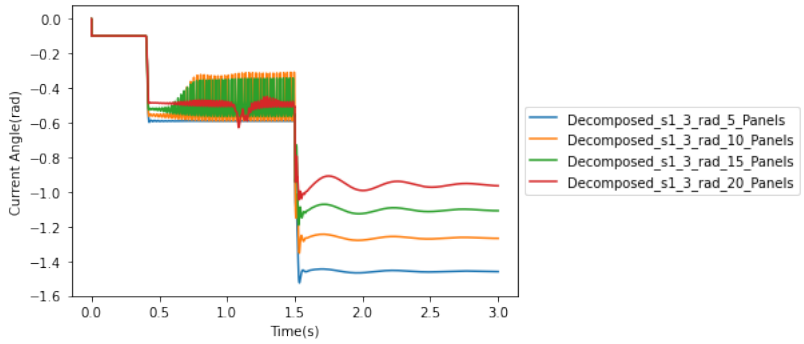

(**c**) Angle of decomposed current from $S1\_3$

Figure B.10: Angle of decomposed current from each individual current sources to the distribution line with LLL fault under different level of DER penetration rate on bus 1

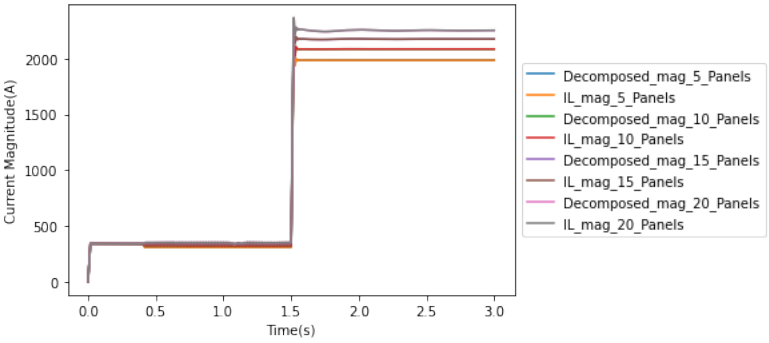

(**a**) IL and the sum of decomposed current magnitude

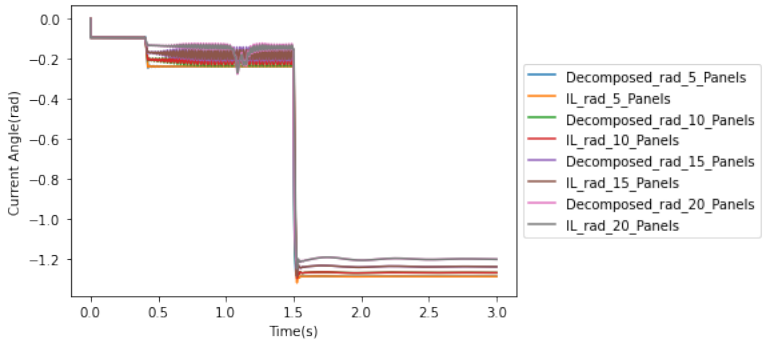

(**b**) IL and the sum of decomposed current angle

Figure B.11: Comparison between IL and the sum of decomposed current of primary protection with LLL fault under different level of DER penetration rate

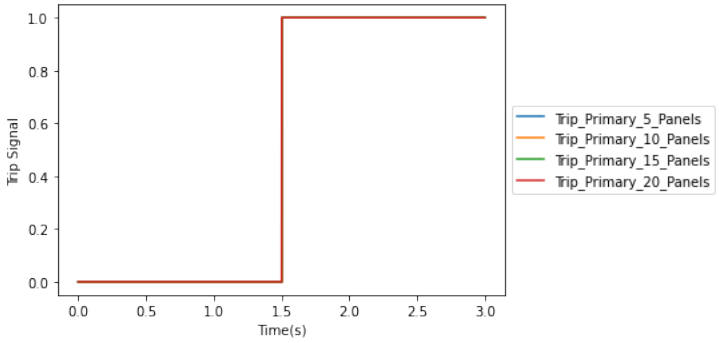

Figure B.12: EMTP-MATLAB primary protection interface trip signal

B.4 LLLG Fault for Primary Protection

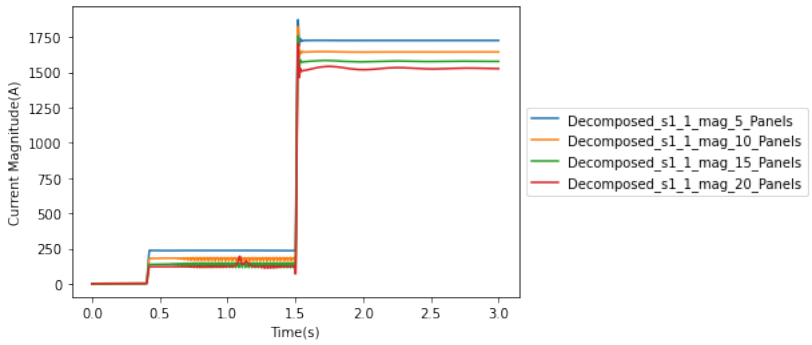

(**a**) Magnitude of decomposed current from $S1\_1$

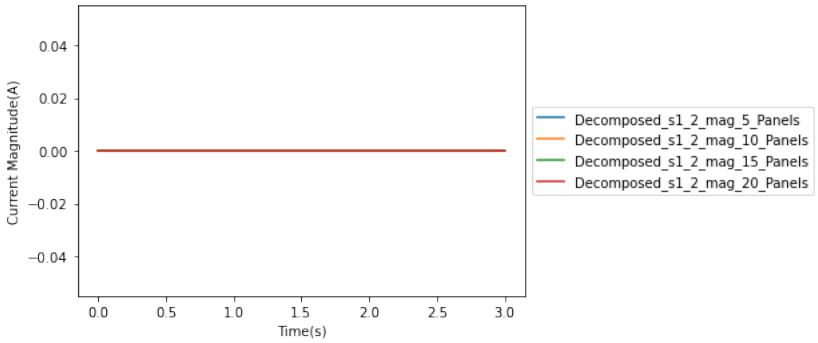

(**b**) Magnitude of decomposed current from $S1\_2$

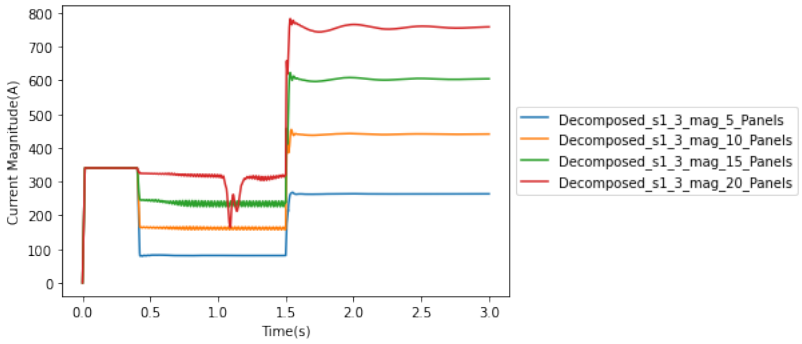

(**c**) Magnitude of decomposed current from $S1\_3$

Figure B.13: Magnitude of decomposed current from each individual current sources to the distribution line with LLLG fault under different level of DER penetration rate on bus 1

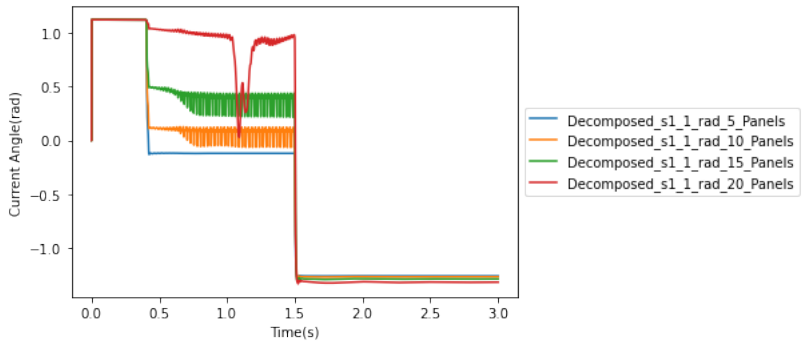

(**a**) Angle of decomposed current from $S1\_1$

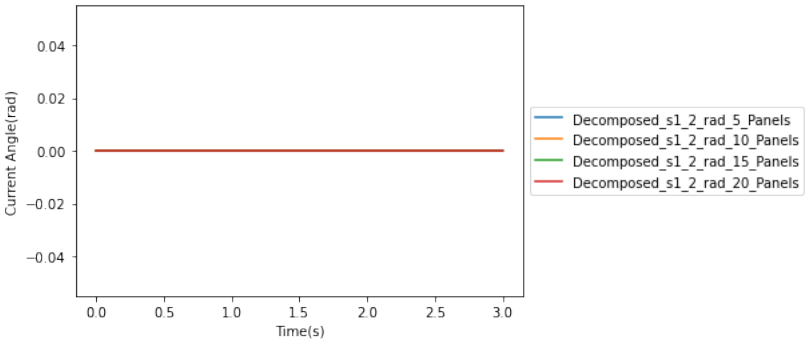

(**b**) Angle of decomposed current from $S1\_2$

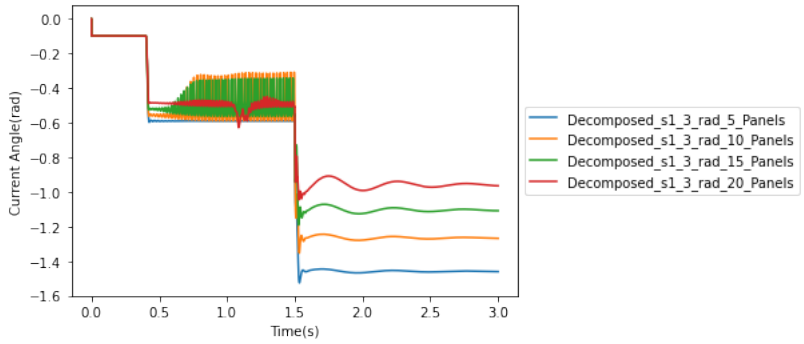

(**c**) Angle of decomposed current from $S1\_3$

Figure B.14: Angle of decomposed current from each individual current sources to the distribution line with LLLG fault under different level of DER penetration rate on bus 1

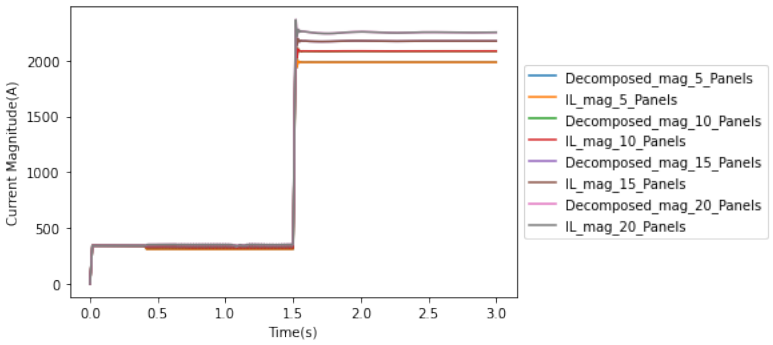

(**a**) IL and the sum of decomposed current magnitude

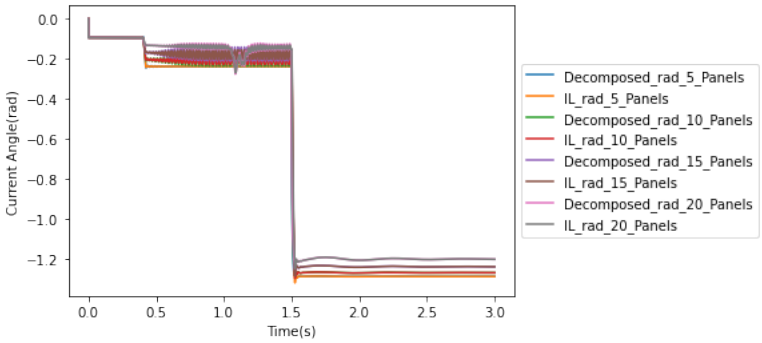

(**b**) IL and the sum of decomposed current angle

Figure B.15: Comparison between IL and the sum of decomposed current of primary protection with LLLG fault under different level of DER penetration rate

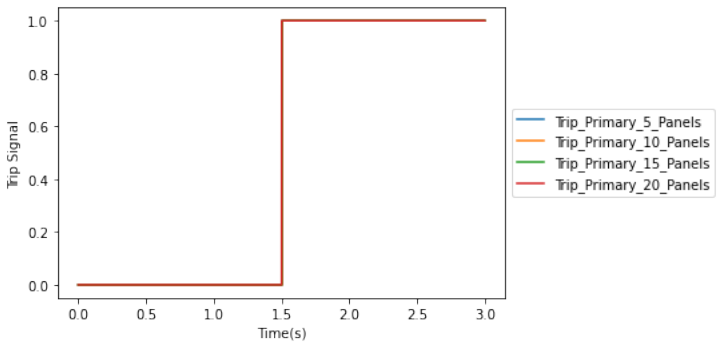

Figure B.16: EMTP-MATLAB primary protection interface trip signal

Appendix C

More Simulation Results of Backup Protection

C.1 LL Fault for Backup Protection

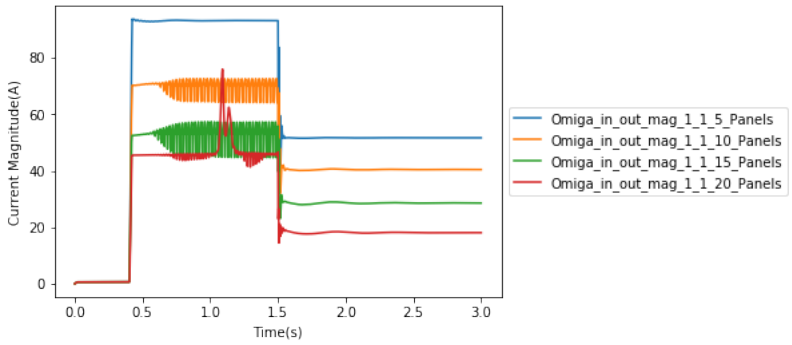

(**a**) $\Omega\_in\_out\_mag\_1\_1$

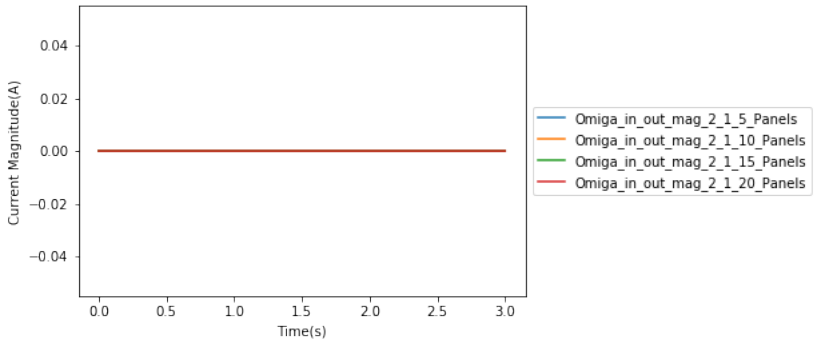

(**b**) $\Omega\_in\_out\_mag\_2\_1$

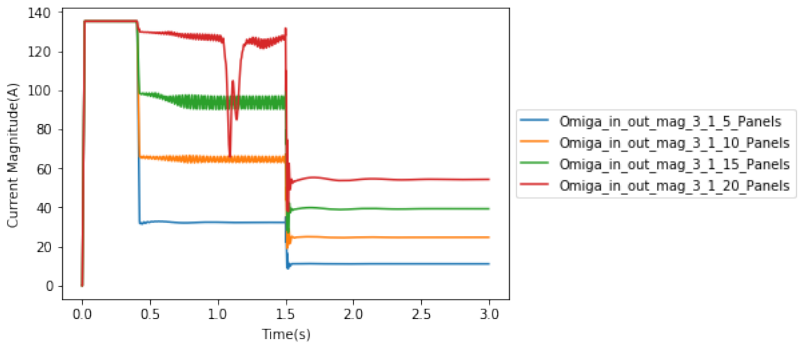

(**c**) $\Omega\_in\_out\_mag\_3\_1$

Figure C.1: Magnitude of decomposed current between current sources on bus 1 to current source 1 on bus 2 with LL fault under different level of DER penetration rate

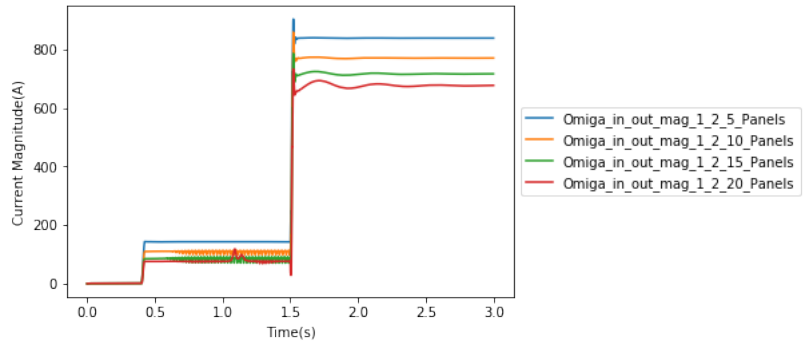

(**a**) $\Omega\_in\_out\_mag\_1\_2$

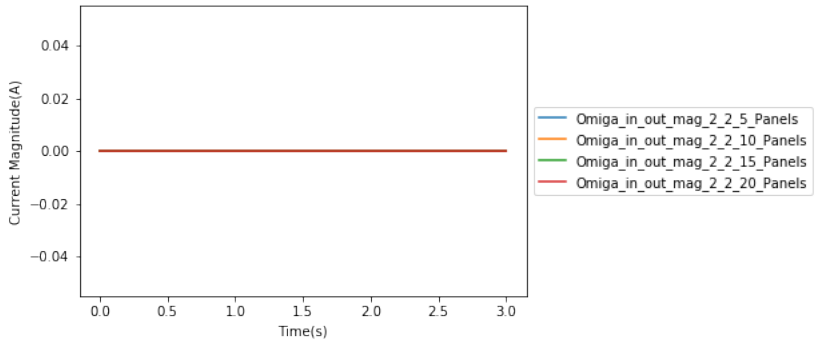

(**b**) $\Omega\_in\_out\_mag\_2\_2$

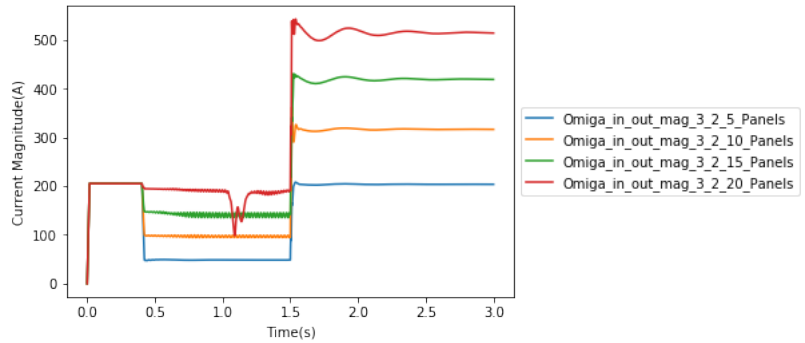

(**c**) $\Omega\_in\_out\_mag\_3\_2$

Figure C.2: Magnitude of decomposed current between current sources on bus 1 to current source 2 on bus 2 with LL fault under different level of DER penetration rate

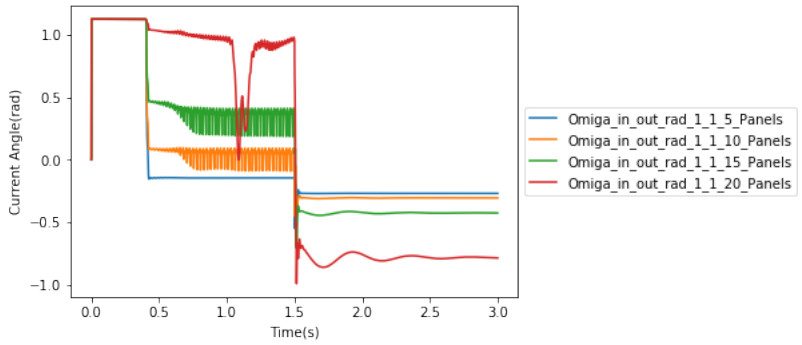

(**a**) $\Omega\_in\_out\_rad\_1\_1$

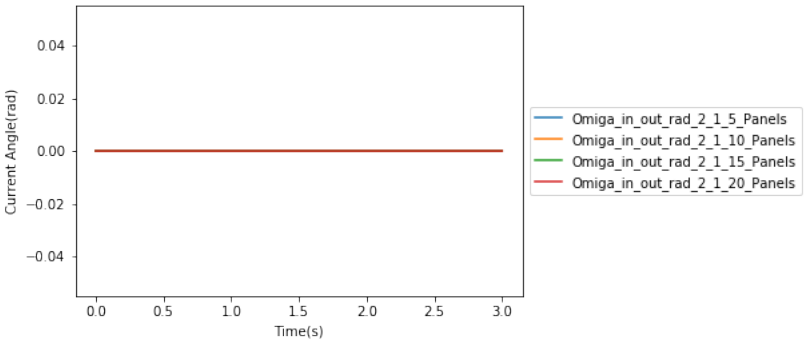

(**b**) $\Omega\_in\_out\_rad\_2\_1$

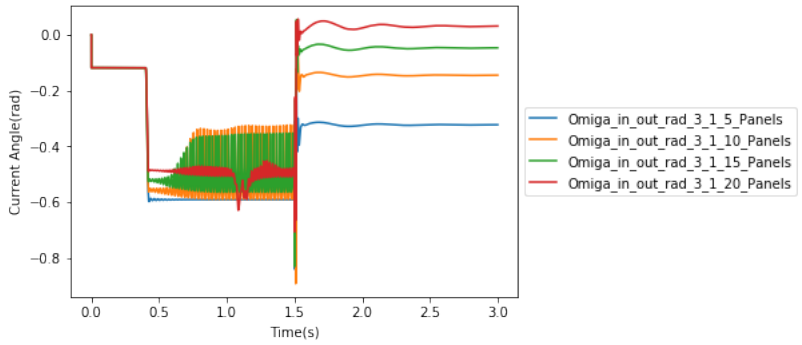

(**c**) $\Omega\_in\_out\_rad\_3\_1$

Figure C.3: Angle of decomposed current between current sources on bus 1 to current source 1 on bus 2 with LL fault under different level of DER penetration rate

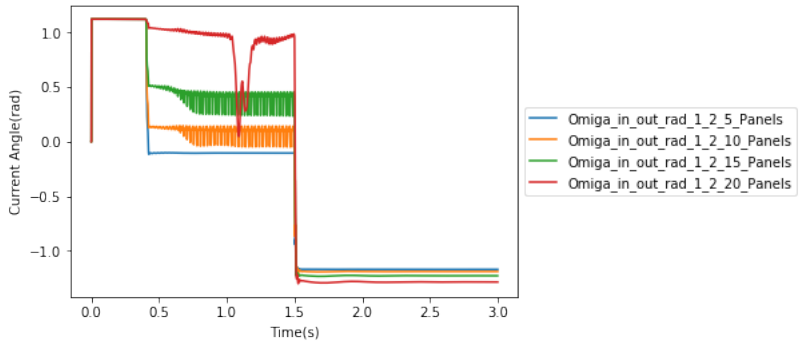

(**a**) $\Omega\_in\_out\_rad\_1\_2$

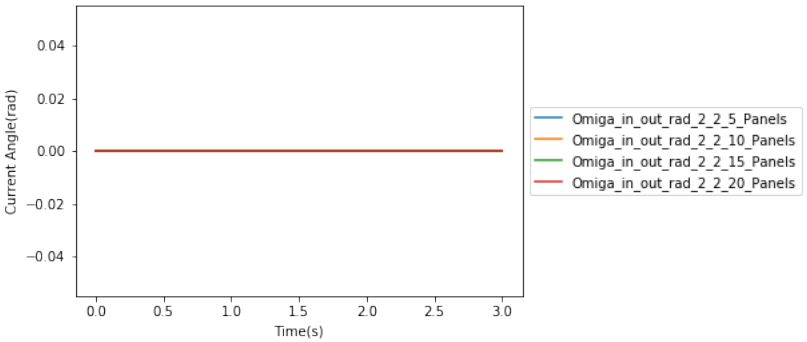

(**b**) $\Omega\_in\_out\_rad\_2\_2$

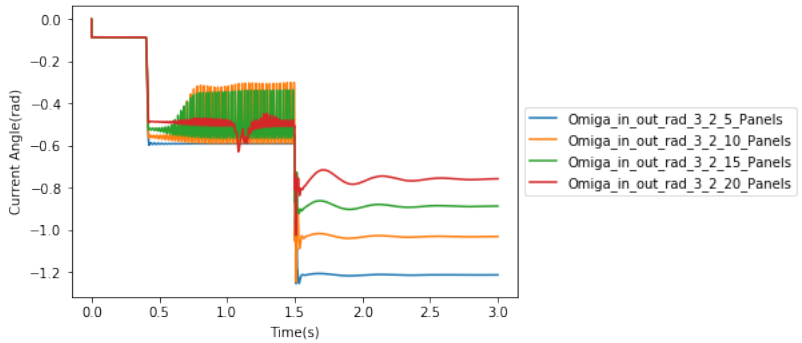

(**c**) $\Omega\_in\_out\_rad\_3\_2$

Figure C.4: Angle of decomposed current between current sources on bus 1 to current source 2 on bus 2 with LL fault under different level of DER penetration rate

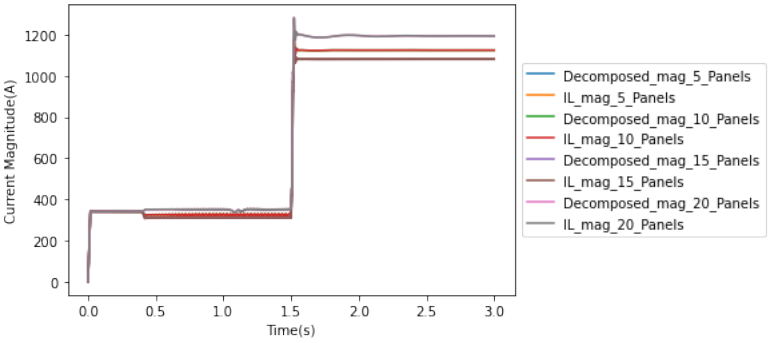

(**a**) Magnitude of I_L and the sum of the decomposed current between multiple current sources

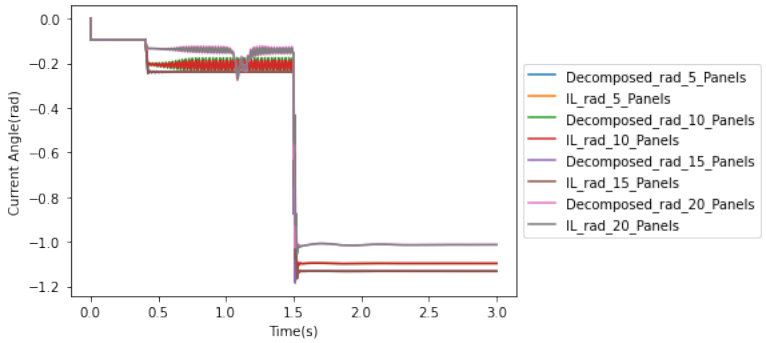

(**b**) Angle of I_L and the sum of the decomposed current between multiple current sources

Figure C.5: Magnitude and angle of I_L and the sum of the decomposed current between multiple current sources

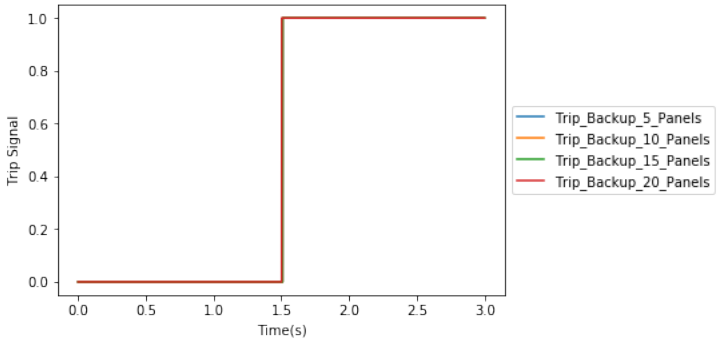

Figure C.6: EMTP-MATLAB backup protection interface trip signal

C.2 LLG Fault for Backup Protection

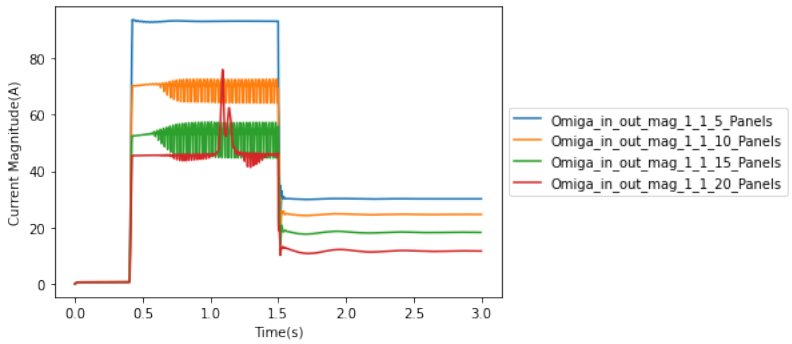

(**a**) $\Omega\_in\_out\_mag\_1\_1$

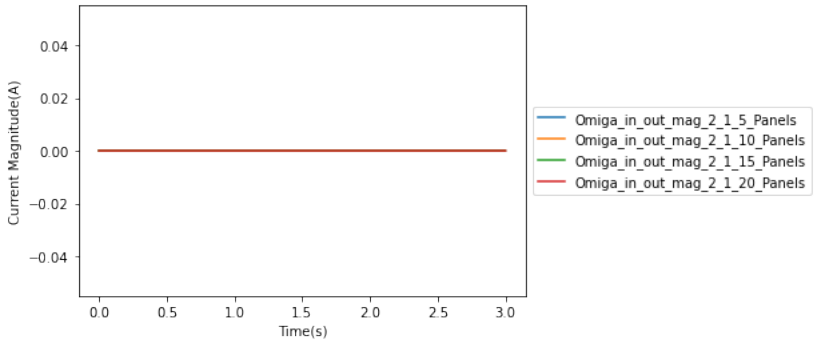

(**b**) $\Omega\_in\_out\_mag\_2\_1$

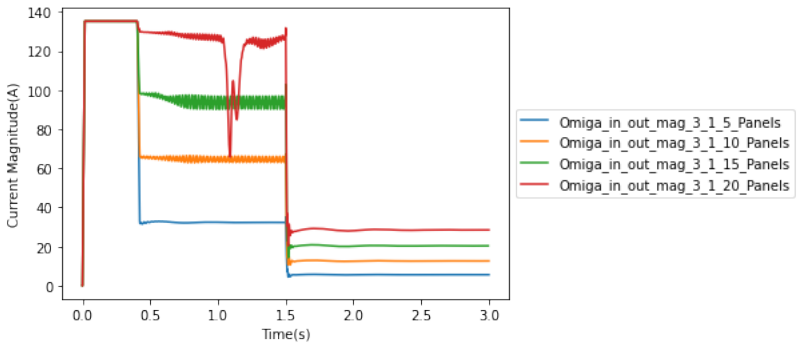

(**c**) $\Omega\_in\_out\_mag\_3\_1$

Figure C.7: Magnitude of decomposed current between current sources on bus 1 to current source 1 on bus 2 with LLG fault under different level of DER penetration rate

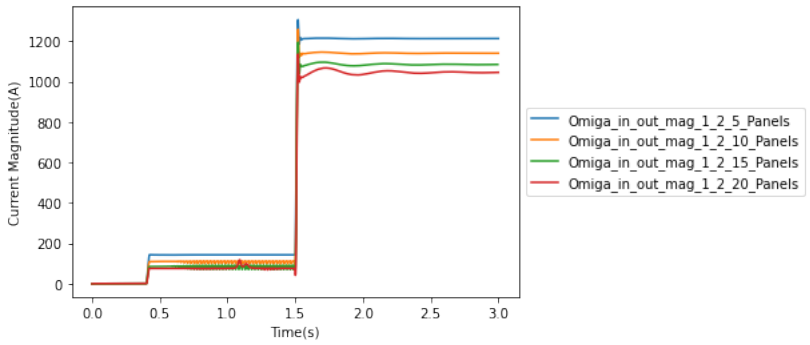

(**a**) $\Omega\_in\_out\_mag\_1\_2$

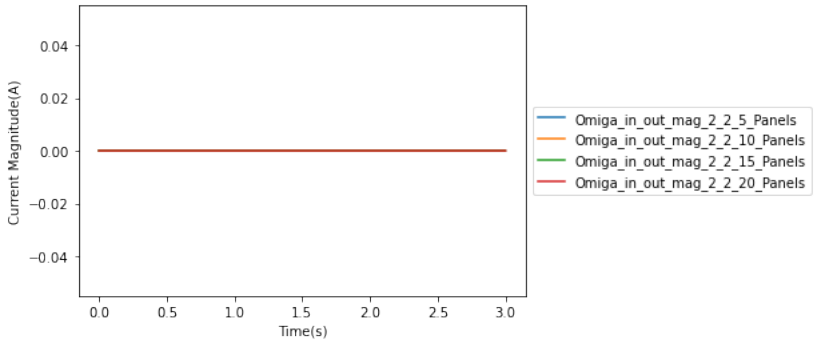

(**b**) $\Omega\_in\_out\_mag\_2\_2$

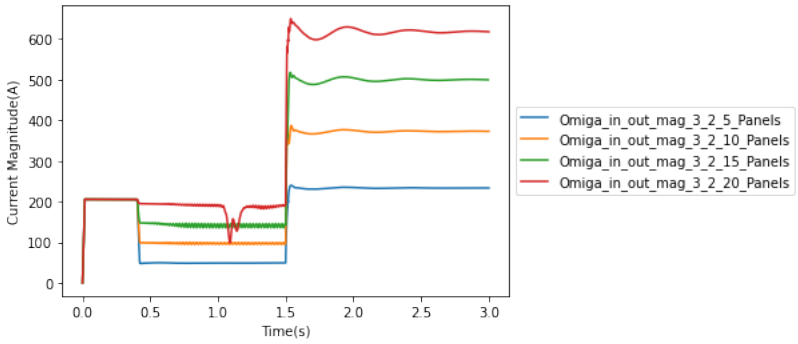

(**c**) $\Omega\_in\_out\_mag\_3\_2$

Figure C.8: Magnitude of decomposed current between current sources on bus 1 to current source 2 on bus 2 with LLG fault under different level of DER penetration rate

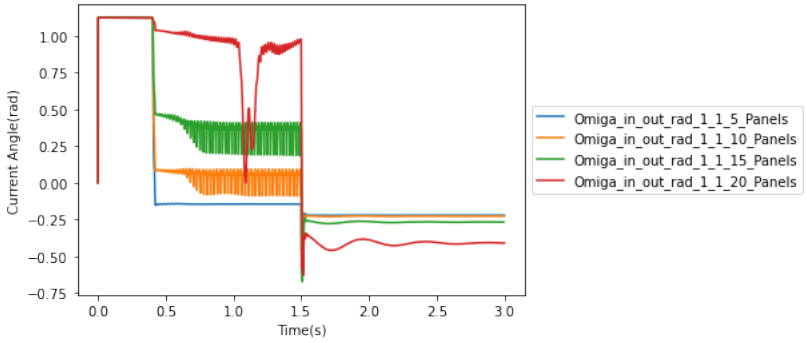

(**a**) $\Omega\_in\_out\_rad\_1\_1$

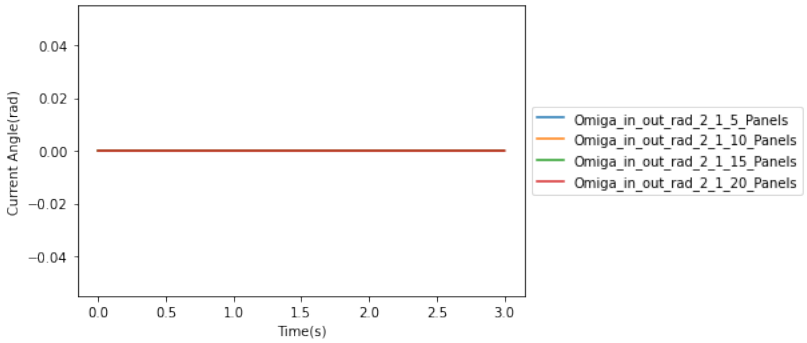

(**b**) $\Omega\_in\_out\_rad\_2\_1$

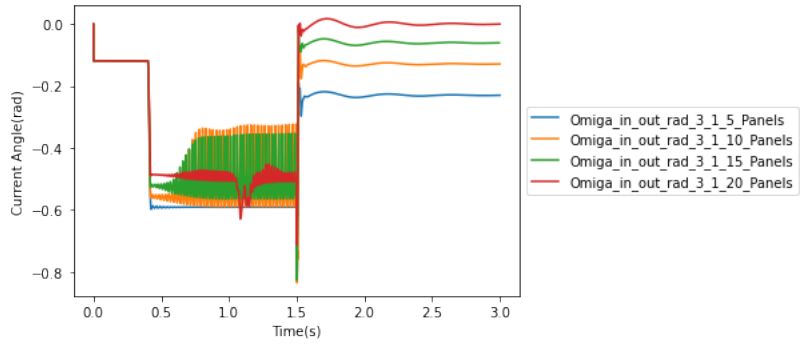

(**c**) $\Omega\_in\_out\_rad\_3\_1$

Figure C.9: Angle of decomposed current between current sources on bus 1 to current source 1 on bus 2 with LLG fault under different level of DER penetration rate

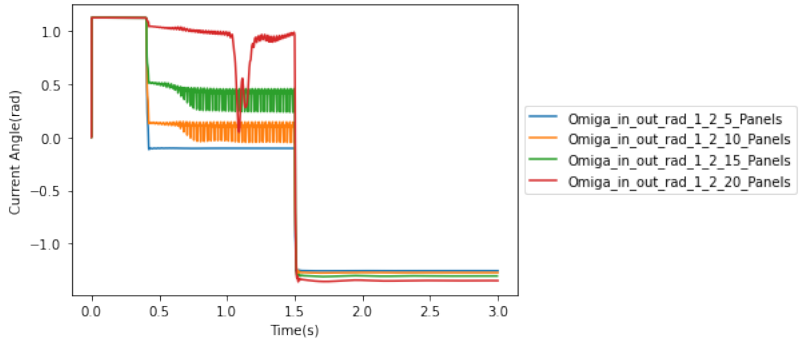

(**a**) $\Omega\_in\_out\_rad\_1\_2$

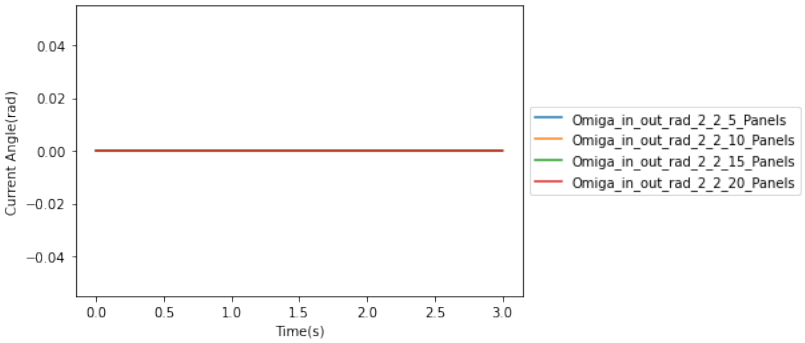

(**b**) $\Omega\_in\_out\_rad\_2\_2$

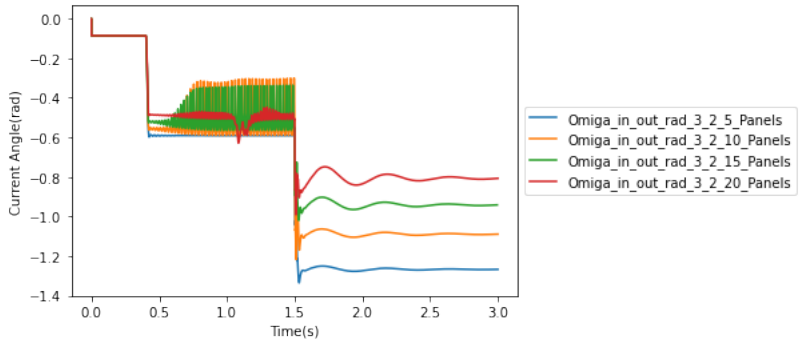

(**c**) $\Omega\_in\_out\_rad\_3\_2$

Figure C.10: Angle of decomposed current between current sources on bus 1 to current source 2 on bus 2 with LLG fault under different level of DER penetration rate

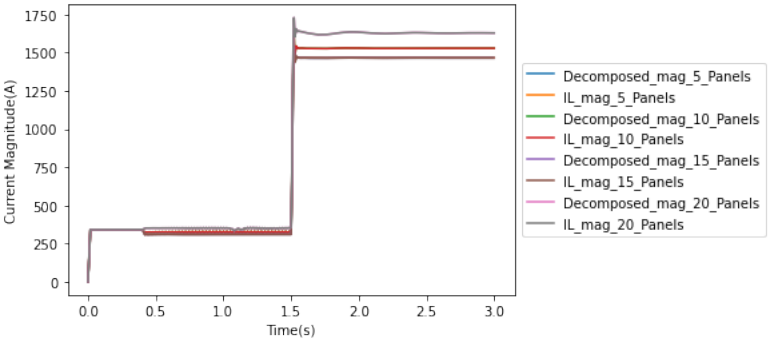

(**a**) Magnitude of I_L and the sum of the decomposed current between multiple current sources

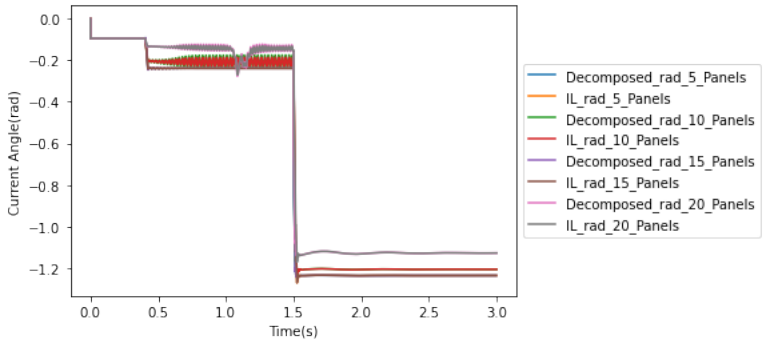

(**b**) Angle of I_L and the sum of the decomposed current between multiple current sources

Figure C.11: Magnitude and angle of I_L and the sum of the decomposed current between multiple current sources

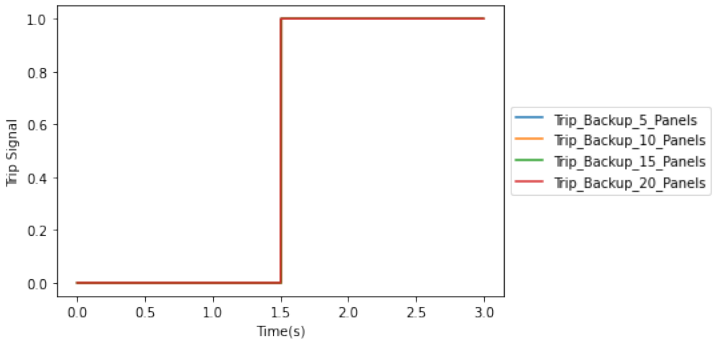

Figure C.12: EMTP-MATLAB backup protection interface trip signal

C.3 LLL Fault for Backup Protection

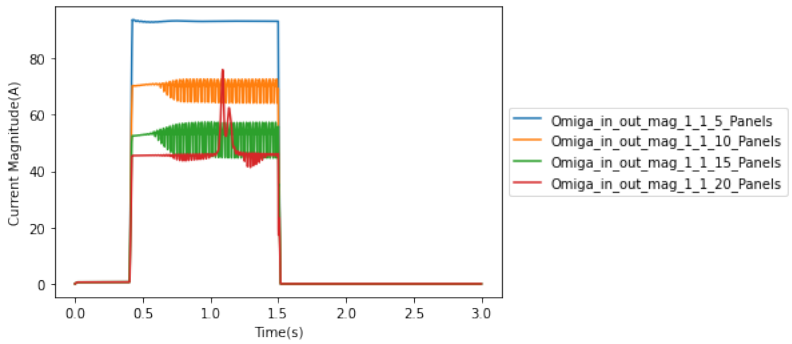

(**a**) $\Omega\_in\_out\_mag\_1\_1$

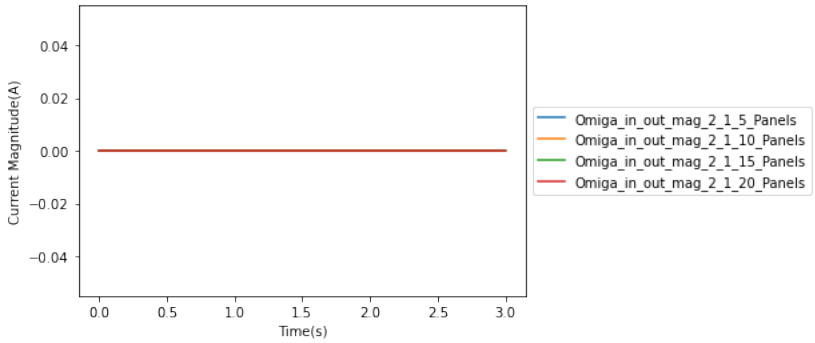

(**b**) $\Omega\_in\_out\_mag\_2\_1$

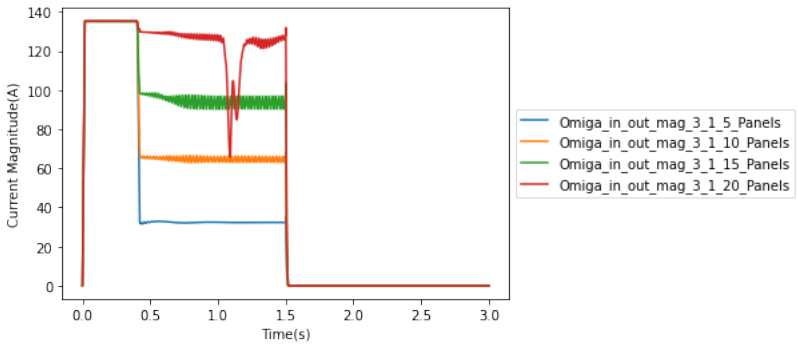

(**c**) $\Omega\_in\_out\_mag\_3\_1$

Figure C.13: Magnitude of decomposed current between current sources on bus 1 to current source 1 on bus 2 with LLL fault under different level of DER penetration rate

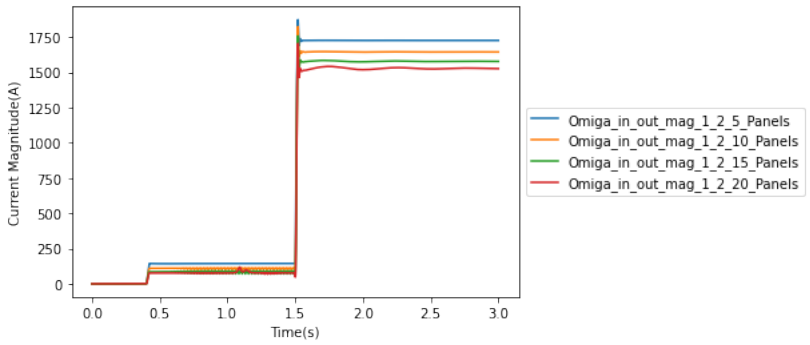

(**a**) $\Omega\_in\_out\_mag\_1\_2$

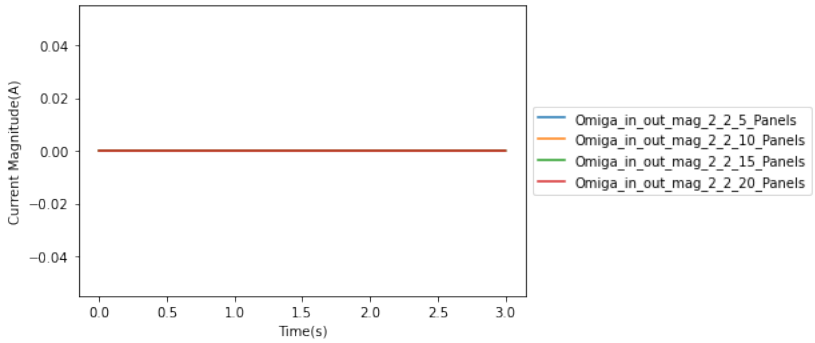

(**b**) $\Omega\_in\_out\_mag\_2\_2$

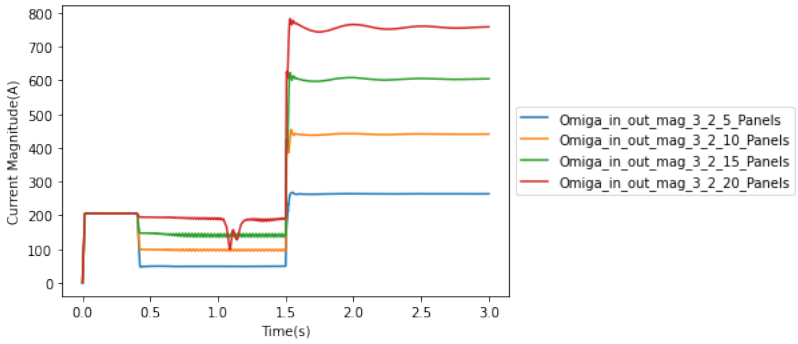

(**c**) $\Omega\_in\_out\_mag\_3\_2$

Figure C.14: Magnitude of decomposed current between current sources on bus 1 to current source 2 on bus 2 with LLL fault under different level of DER penetration rate

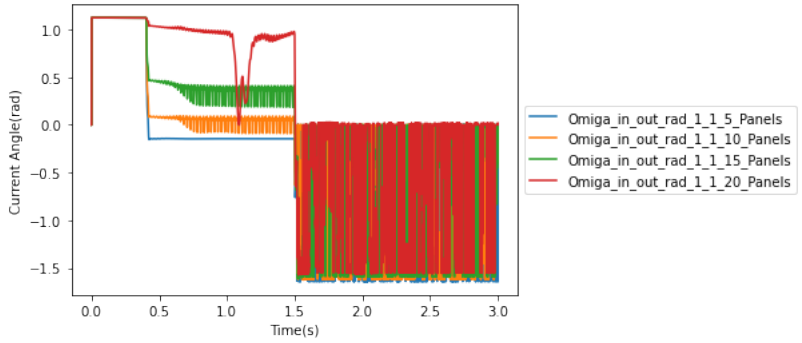

(**a**) $\Omega\_in\_out\_rad\_1\_1$

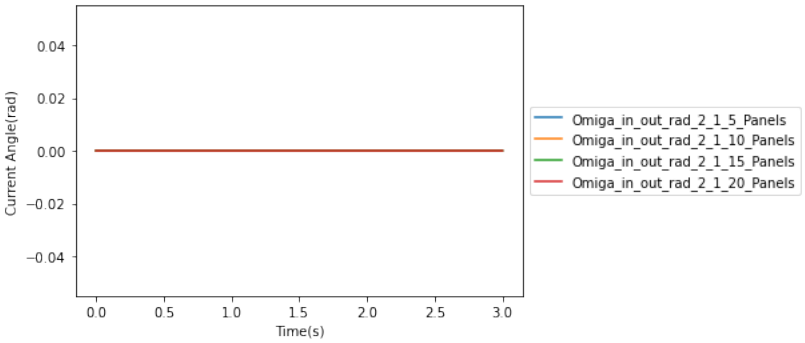

(**b**) $\Omega\_in\_out\_rad\_2\_1$

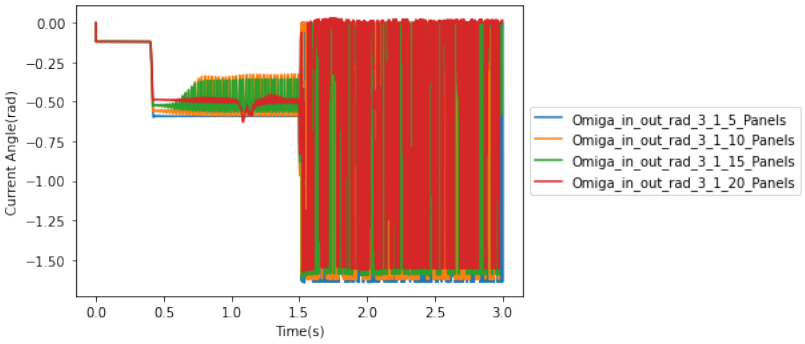

(**c**) $\Omega\_in\_out\_rad\_3\_1$

Figure C.15: Angle of decomposed current between current sources on bus 1 to current source 1 on bus 2 with LLL fault under different level of DER penetration rate

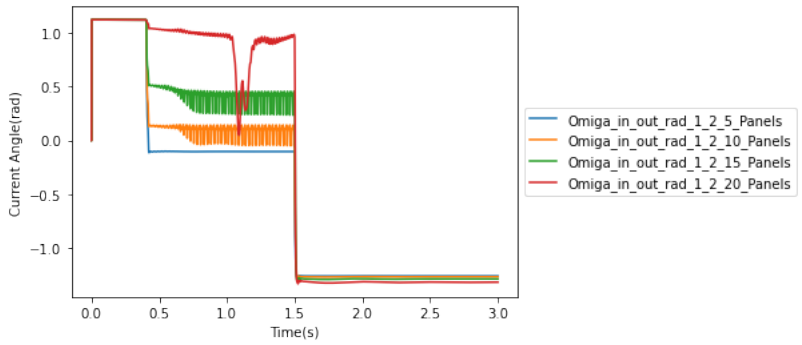

(**a**) $\Omega\_in\_out\_rad\_1\_2$

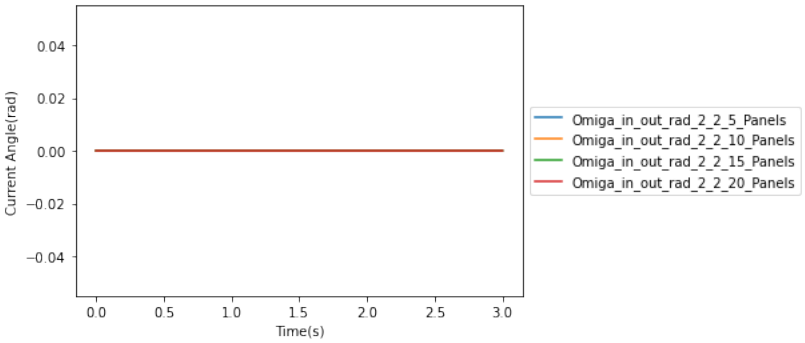

(**b**) $\Omega\_in\_out\_rad\_2\_2$

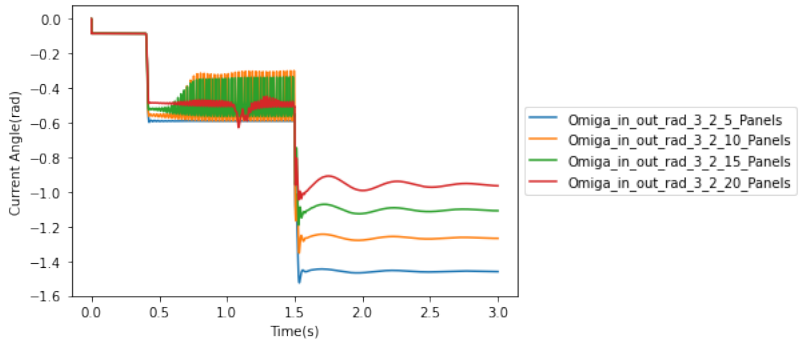

(**c**) $\Omega\_in\_out\_rad\_3\_2$

Figure C.16: Angle of decomposed current between current sources on bus 1 to current source 2 on bus 2 with LLL fault under different level of DER penetration rate

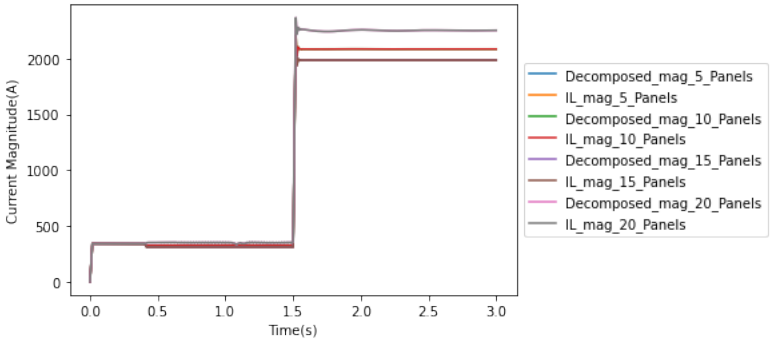

(**a**) Magnitude of I_L and the sum of the decomposed current between multiple current sources

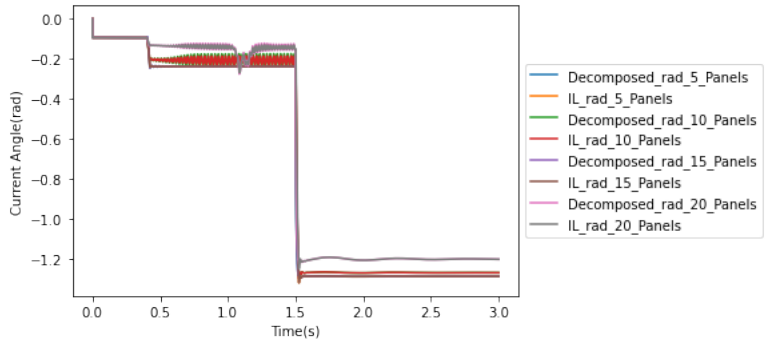

(**b**) Angle of I_L and the sum of the decomposed current between multiple current sources

Figure C.17: Magnitude and angle of I_L and the sum of the decomposed current between multiple current sources

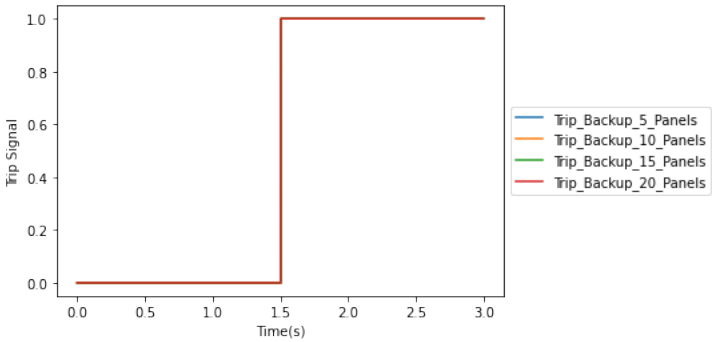

Figure C.18: EMTP-MATLAB backup protection interface trip signal

C.4 LLLG Fault for Backup Protection

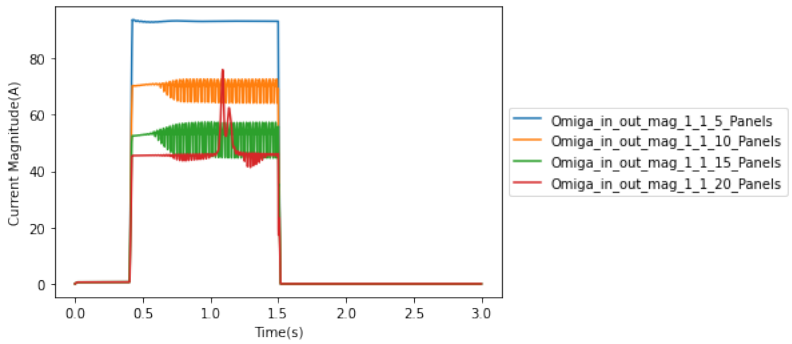

(**a**) $\Omega\_in\_out\_mag\_1\_1$

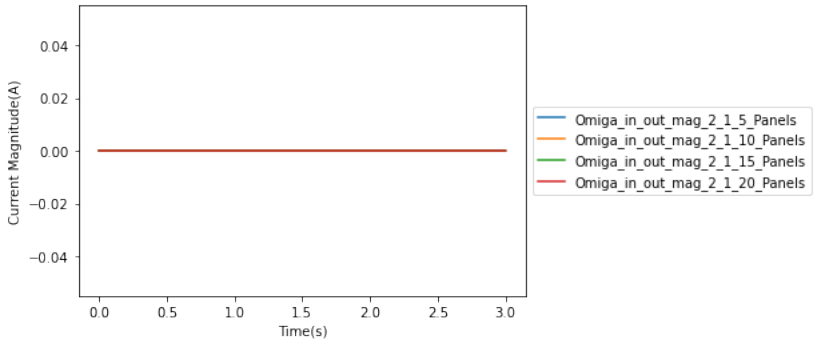

(**b**) $\Omega\_in\_out\_mag\_2\_1$

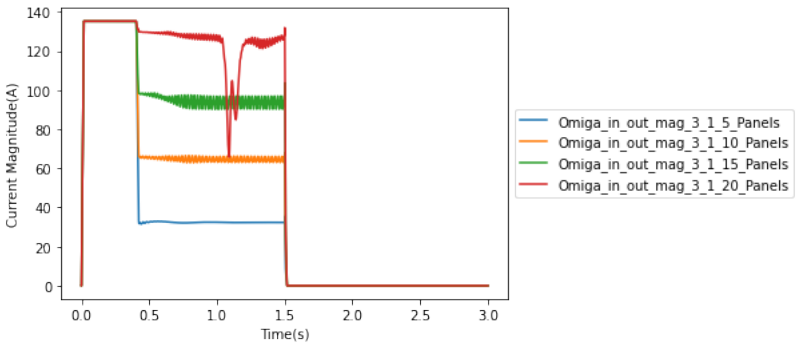

(**c**) $\Omega\_in\_out\_mag\_3\_1$

Figure C.19: Magnitude of decomposed current between current sources on bus 1 to current source 1 on bus 2 with LLLG fault under different level of DER penetration rate

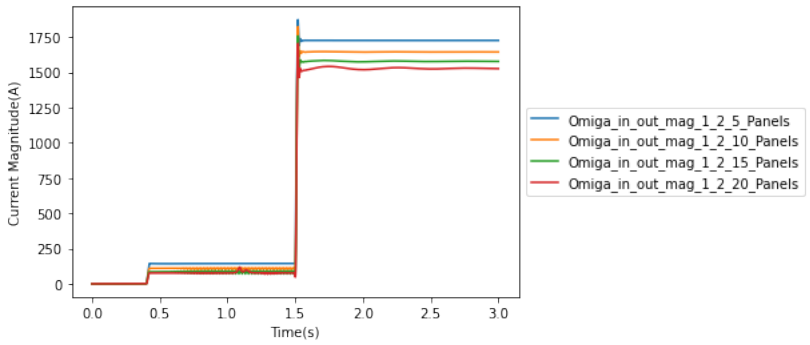

(**a**) $\Omega\_in\_out\_mag\_1\_2$

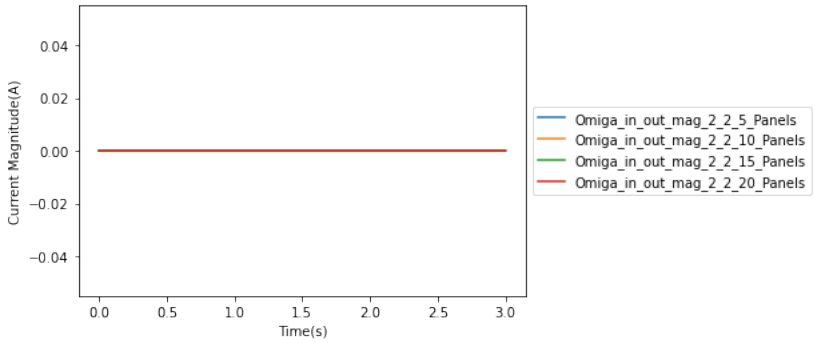

(**b**) $\Omega\_in\_out\_mag\_2\_2$

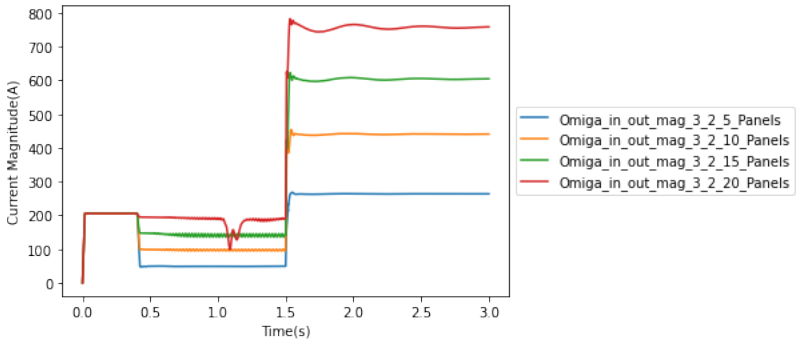

(**c**) $\Omega\_in\_out\_mag\_3\_2$

Figure C.20: Magnitude of decomposed current between current sources on bus 1 to current source 2 on bus 2 with LLLG fault under different level of DER penetration rate

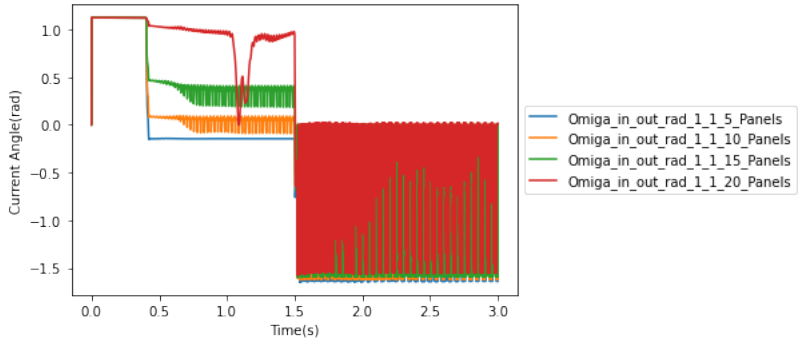

(**a**) $\Omega\_in\_out\_rad\_1\_1$

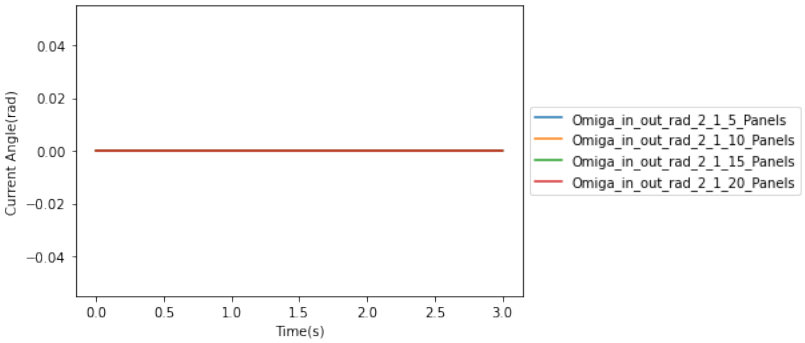

(**b**) $\Omega\_in\_out\_rad\_2\_1$

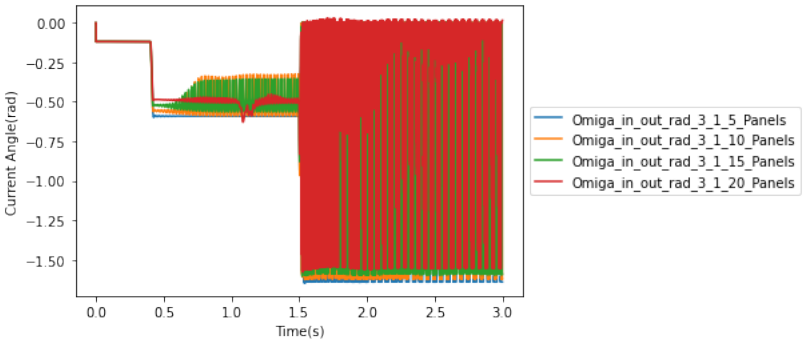

(**c**) $\Omega\_in\_out\_rad\_3\_1$

Figure C.21: Angle of decomposed current between current sources on bus 1 to current source 1 on bus 2 with LLLG fault under different level of DER penetration rate

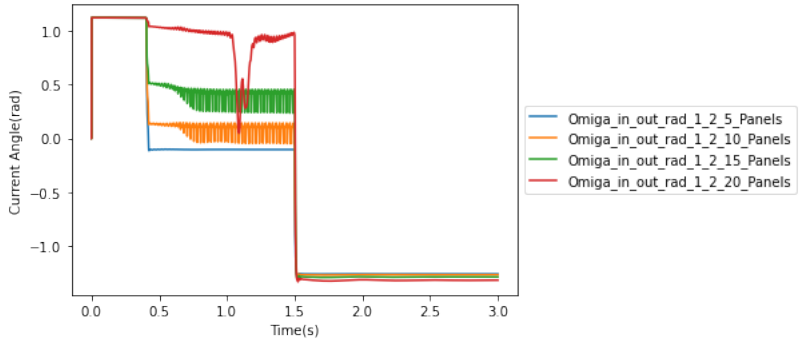

(**a**) $\Omega\_in\_out\_rad\_1\_2$

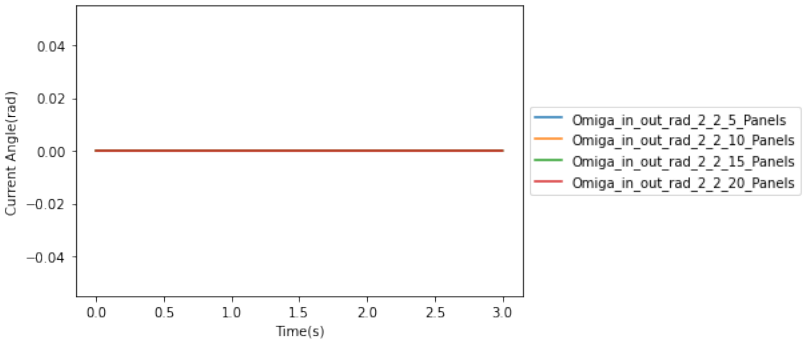

(**b**) $\Omega\_in\_out\_rad\_2\_2$

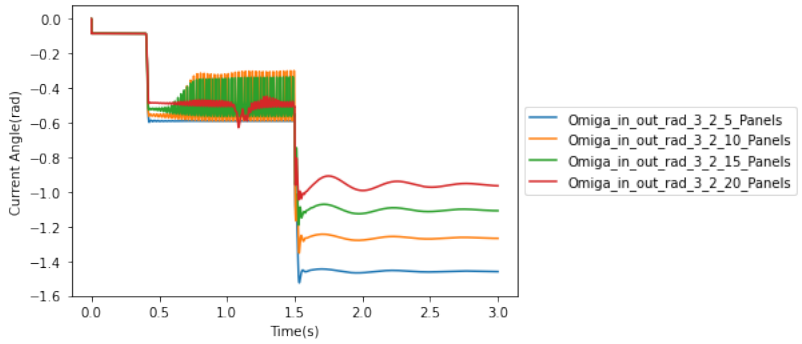

(**c**) $\Omega\_in\_out\_rad\_3\_2$

Figure C.22: Angle of decomposed current between current sources on bus 1 to current source 2 on bus 2 with LLLG fault under different level of DER penetration rate

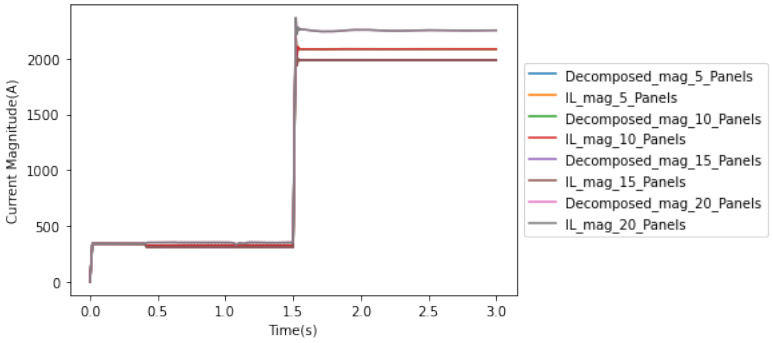

(**a**) Magnitude of I_L and the sum of the decomposed current between multiple current sources

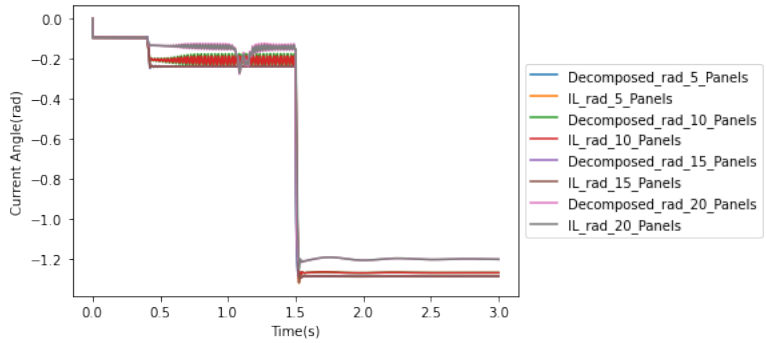

(**b**) Angle of I_L and the sum of the decomposed current between multiple current sources

Figure C.23: Magnitude and angle of I_L and the sum of the decomposed current between multiple current sources

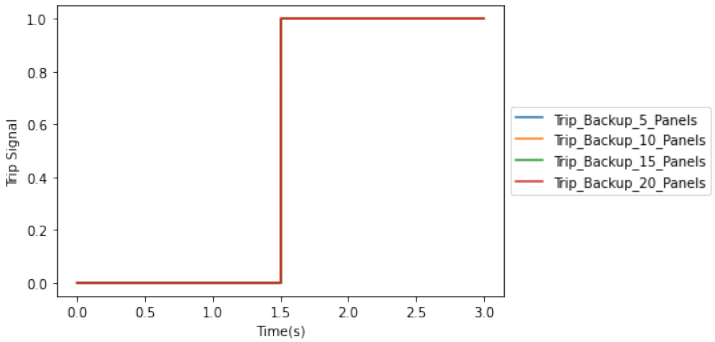

Figure C.24: EMTP-MATLAB backup protection interface trip signal

List of Abbreviations

CT	Current Transformer
DC	Direct Current
DER	Distributed Energy Resource
DT	Definite Time
EMS	Energy Management System
EMTP	Electromagnetic Transients Program
FCL	Fault Current Limiter
IED	Intelligent Electronic Device
IDMT	Inverse Definite Minimum Time
INST	Instantaneous
ITO	Inverse Time Overcurrent
LG	Line-Ground
LL	Line-Line
LLG	Line-Line-Ground
LLL	Line-Line-Line
LLLG	Line-Line-Line-Ground
LV	Low-Voltage
MV	Medium-Voltage
PMU	Phasor Measurement Unit

RMS	Root Mean Square
SCADA	Supervisory Control and Data Acquisition
TCC	Time Current Curve

Bibliography

[1] M. Ahmadi, N. Mithulananthan, and R. Sharma, "A review on topologies for fast charging stations for electric vehicles," in *2016 IEEE International Conference on Power System Technology (POWERCON)*, 2016, pp. 1–6.

[2] J. Parmar, "Total losses in power distribution and transmission lines," *Transmission and Distribution Electrical Engineering Portal (EEP)*, 2013.

[3] U. Shahzad, S. Kahrobaee, S. Asgarpoor *et al.*, "Protection of distributed generation: challenges and solutions," *Energy and Power Engineering*, vol. 9, no. 10, p. 614, 2017.

[4] X. Lin, Z. Liang, Y. Zheng, Y. Lin, and Y. Kang, "A current limiting strategy with parallel virtual impedance for three-phase three-leg inverter under asymmetrical short-circuit fault to improve the controllable capability of fault currents," *IEEE Transactions on Power Electronics*, vol. 34, no. 8, pp. 8138–8149, 2019.

[5] Z. Liang, X. Lin, Y. Kang, B. Gao, and H. Lei, "Short circuit current characteristics analysis and improved current limiting strategy for three-phase three-leg inverter under asymmetric short circuit fault," *IEEE Transactions on Power Electronics*, vol. 33, no. 8, pp. 7214–7228, 2018.

[6] S. Boljevic and M. F. Conlon, "The contribution to distribution network short-circuit current level from the connection of distributed generation," in

2008 43rd International Universities Power Engineering Conference, 2008, pp. 1–6.

[7] T. M. Masaud and R. D. Mistry, "Fault current contribution of renewable distributed generation: An overview and key issues," in *2016 IEEE Conference on Technologies for Sustainability (SusTech)*, 2016, pp. 229–234.

[8] P. Sudhakar, S. Malaji, and B. Sarvesh, "Reducing the impact of dg on distribution networks protection with reverse power relay," *Materials Today: Proceedings*, vol. 5, no. 1, pp. 51–57, 2018.

[9] H. Yang, F. Wen, and G. Ledwich, "Optimal coordination of overcurrent relays in distribution systems with distributed generators based on differential evolution algorithm," *International transactions on electrical energy systems*, vol. 23, no. 1, pp. 1–12, 2013.

[10] S. Cho, H. Shin, and J. Kim, "Study on coordination of protective relays between primary feeder and interconnecting transformer grounded by sfcl of wind farm," *IEEE Transactions on Applied Superconductivity*, vol. 22, no. 3, pp. 5 500 404–5 500 404, 2012.

[11] "Ieee guide for protective relay applications to transmission lines," *IEEE Std C37.113-2015 (Revision of IEEE Std C37.113-1999)*, pp. 1–141, 2016.

[12] S. Rahman, H. Aburub, M. Moghaddami, and A. I. Sarwat, "Reverse power flow protection in grid connected pv systems," in *SoutheastCon 2018*. IEEE, 2018, pp. 1–5.

[13] M. G. Adamiak, A. P. Apostolov, M. M. Begovic, C. F. Henville, K. E. Martin, G. L. Michel, A. G. Phadke, and J. S. Thorp, "Wide area protection—

technology and infrastructures," *IEEE Transactions on Power Delivery*, vol. 21, no. 2, pp. 601–609, 2006.

[14] R. C. Borges Hink, J. M. Beaver, M. A. Buckner, T. Morris, U. Adhikari, and S. Pan, "Machine learning for power system disturbance and cyber-attack discrimination," in *2014 7th International Symposium on Resilient Control Systems (ISRCS)*, 2014, pp. 1–8.

[15] T. S. Sidhu and M. Khederzadeh, "Series compensated line protection enhancement by modified pilot relaying schemes," *IEEE Transactions on Power Delivery*, vol. 21, no. 3, pp. 1191–1198, 2006.

[16] R. Mohanty and A. K. Pradhan, "A superimposed current based unit protection scheme for dc microgrid," *IEEE Transactions on Smart Grid*, vol. 9, no. 4, pp. 3917–3919, 2018.

[17] Liu Pei, Chen Deshu, Peng Hua, O. P. Malik, and G. S. Hope, "Analysis of an accelerated trip scheme for faults in the second zone of protection of a transmission line," *IEEE Transactions on Power Delivery*, vol. 5, no. 1, pp. 72–78, 1990.

[18] W. Tang, H. Yang, C. Tsai, and P. Lubicki, "Overcurrent protection strategies for distribution system with distributed energy resources and fault current limiters," in *2016 IEEE International Conference on Power System Technology (POWERCON)*, 2016, pp. 1–6.

[19] X. Dong, J. Wang, S. Shi, B. Wang, B. Dominik, and M. Redefern, "Traveling wave based single-phase-to-ground protection method for power distribution system," *CSEE Journal of Power and Energy Systems*, vol. 1, no. 2, pp. 75–82, 2015.

[20] K. A. Saleh, A. Hooshyar, and E. F. El-Saadany, "Ultra-high-speed traveling-wave-based protection scheme for medium-voltage dc microgrids," *IEEE Transactions on Smart Grid*, vol. 10, no. 2, pp. 1440–1451, 2019.

[21] Z. He, X. Liu, X. Li, and R. Mai, "A novel traveling-wave directional relay based on apparent surge impedance," *IEEE Transactions on Power Delivery*, vol. 30, no. 3, pp. 1153–1161, 2015.

[22] W. Fei, G. Ji, D. Sharma, and J. N. Jiang, "A new traveling wave representation for propagation of energy transients in power lines from a quantum perspective," in *2018 North American Power Symposium (NAPS)*, 2018, pp. 1–6.

[23] G. Zou and H. Gao, "A traveling-wave-based amplitude integral busbar protection technique," *IEEE Transactions on Power Delivery*, vol. 27, no. 2, pp. 602–609, 2012.

[24] J. Bertsch, C. Carnal, D. Karlson, J. McDaniel, and Khoi Vu, "Wide-area protection and power system utilization," *Proceedings of the IEEE*, vol. 93, no. 5, pp. 997–1003, 2005.

[25] S. M. Brahma and A. A. Girgis, "Development of adaptive protection scheme for distribution systems with high penetration of distributed generation," *IEEE Transactions on Power Delivery*, vol. 19, no. 1, pp. 56–63, 2004.

[26] P. R. Walsh and M. M. Price, "Reducing arc-flash hazards: Installing mv-controllable fuses on the secondary side of the transformer in a pumped storage plant," *IEEE Industry Applications Magazine*, vol. 23, no. 5, pp. 21–27, 2017.

[27] M. Kabiri and N. Amjady, "A new hybrid state estimation considering different accuracy levels of pmu and scada measurements," *IEEE Transactions on Instrumentation and Measurement*, vol. 68, no. 9, pp. 3078–3089, 2019.

[28] W. Fei and P. Moses, "Fault current tracing and identification via machine learning considering distributed energy resources in distribution networks," *Energies*, vol. 12, no. 22, p. 4333, 2019.

[29] W. Fei, P. Moses, and C. Davis, "Identification of smart grid attacks via state vector estimator and support vector machine methods," in *2020 Intermountain Engineering, Technology and Computing (IETC)*. IEEE, 2020, pp. 1–6.

[30] M. Cui, J. Wang, and B. Chen, "Flexible machine learning-based cyberattack detection using spatiotemporal patterns for distribution systems," *IEEE Transactions on Smart Grid*, vol. 11, no. 2, pp. 1805–1808, 2020.

[31] P. Wang and M. Govindarasu, "Multi-agent based attack-resilient system integrity protection for smart grid," *IEEE Transactions on Smart Grid*, vol. 11, no. 4, pp. 3447–3456, 2020.

[32] Y. Jia, L. Ying, D. Wang, and J. Zhang, "Defect prediction of relay protection systems based on lssvm-bndt," *IEEE Transactions on Industrial Informatics*, vol. 17, no. 1, pp. 710–719, 2021.

[33] M. Z. Ali, M. N. S. K. Shabbir, X. Liang, Y. Zhang, and T. Hu, "Machine learning-based fault diagnosis for single- and multi-faults in induction motors using measured stator currents and vibration signals," *IEEE Transactions on Industry Applications*, vol. 55, no. 3, pp. 2378–2391, 2019.

[34] H. R. Baghaee, D. Mlakić, S. Nikolovski, and T. Dragicević, "Support vector machine-based islanding and grid fault detection in active distribution networks," *IEEE Journal of Emerging and Selected Topics in Power Electronics*, vol. 8, no. 3, pp. 2385–2403, 2020.

[35] D. C. P. Barbosa, L. H. A. de Medeiros, M. T. de Melo, L. R. G. da Silva Lourenço Novo, M. d. S. Coutinho, M. M. Alves, H. B. D. T. Lott Neto, P. H. R. P. Gama, R. G. M. dos Santos, and V. L. Tarragô, "Machine learning approach to detect faults in anchor rods of power transmission lines," *IEEE Antennas and Wireless Propagation Letters*, vol. 18, no. 11, pp. 2335–2339, 2019.

[36] B. Luo, H. Wang, H. Liu, B. Li, and F. Peng, "Early fault detection of machine tools based on deep learning and dynamic identification," *IEEE Transactions on Industrial Electronics*, vol. 66, no. 1, pp. 509–518, 2019.

[37] G. Benmouyal, M. Meisinger, J. Burnworth, W. A. Elmore, K. Freirich, P. A. Kotos, P. R. Leblanc, P. J. Lerley, J. E. McConnell, J. Mizener, J. Pinto de Sa, R. Ramaswami, M. S. Sachdev, W. M. Strang, J. E. Waldron, S. Watansiriroch, and S. E. Zocholl, "Ieee standard inverse-time characteristic equations for overcurrent relays," *IEEE Transactions on Power Delivery*, vol. 14, no. 3, pp. 868–872, 1999.

[38] E. O. Schweitzer and B. Kasztenny, "Distance protection: Why have we started with a circle, does it matter, and what else is out there?" in *2018 71st Annual Conference for Protective Relay Engineers (CPRE)*. IEEE, 2018, pp. 1–19.

[39] P. Mahat, Z. Chen, B. Bak-Jensen, and C. L. Bak, "A simple adaptive overcurrent protection of distribution systems with distributed generation," *IEEE Transactions on Smart Grid*, vol. 2, no. 3, pp. 428–437, 2011.

[40] J. Ma, W. Ma, X. Wang, and Z. Wang, "A new adaptive voltage protection scheme for distribution network with distributed generations," *Canadian Journal of Electrical and Computer Engineering*, vol. 36, no. 4, pp. 142–151, 2013.

[41] T. Senarathna and K. U. Hemapala, "Review of adaptive protection methods for microgrids," *AIMS Energy*, vol. 7, no. 5, pp. 557–578, 2019.

[42] M. K. Neyestanaki and A. M. Ranjbar, "An adaptive pmu-based wide area backup protection scheme for power transmission lines," *IEEE Transactions on Smart Grid*, vol. 6, no. 3, pp. 1550–1559, 2015.

[43] V. Papaspiliotopoulos, G. Korres, V. Kleftakis, and N. Hatziargyriou, "Hardware-in-the-loop design and optimal setting of adaptive protection schemes for distribution systems with distributed generation," in *2017 IEEE Power Energy Society General Meeting*, 2017, pp. 1–1.

[44] S. Shen, D. Lin, H. Wang, P. Hu, K. Jiang, D. Lin, and B. He, "An adaptive protection scheme for distribution systems with dgs based on optimized thevenin equivalent parameters estimation," *IEEE Transactions on Power Delivery*, vol. 32, no. 1, pp. 411–419, 2017.

[45] E. Purwar, S. P. Singh, and D. N. Vishwakarma, "A robust protection scheme based on hybrid pick-up and optimal hierarchy selection of relays in the variable dgs-distribution system," *IEEE Transactions on Power Delivery*, vol. 35, no. 1, pp. 150–159, 2020.

[46] J. L. Blackburn and T. J. Domin, *Protective relaying: principles and applications*. CRC press, 2015.

[47] Y. G. Paithankar and S. Bhide, *Fundamentals of power system protection*. PHI Learning Pvt. Ltd., 2010.

[48] H. Ha and S. Subramanian, "Predicting the prospective fault level on distribution grids and its impact on protective relaying," in *2017 70th Annual Conference for Protective Relay Engineers (CPRE)*. IEEE, 2017, pp. 1–4.

[49] S. Hayes, D. Hou, and N. Fischer, "Understanding ground fault detection sensitivity and ways to mitigate safety hazards in power distribution systems," in *46th Annual Western Protective Relay Conference*, 2019.

[50] E. O. Schweitzer, B. Kasztenny, A. Guzmán, V. Skendzic, and M. V. Mynam, "Speed of line protection-can we break free of phasor limitations?" in *2015 68th Annual Conference for Protective Relay Engineers*. IEEE, 2015, pp. 448–461.

[51] K. Breitfelder and D. Messina, "Ieee 100: the authoritative dictionary of ieee standards terms," *Standards Information Network IEEE Press. v879*, 2000.

[52] "Ieee standard electrical power system device function numbers, acronyms, and contact designations," *IEEE Std C37.2-2008 (Revision of IEEE Std C37.2-1996)*, pp. 1–48, 2008.

[53] C. L. Fortescue, "Method of symmetrical co-ordinates applied to the solution of polyphase networks," *Transactions of the American Institute of Electrical Engineers*, vol. XXXVII, no. 2, pp. 1027–1140, 1918.

[54] J. Keller and B. Kroposki, "Understanding fault characteristics of inverter-based distributed energy resources," National Renewable Energy Lab.(NREL), Golden, CO (United States), Tech. Rep., 2010.

[55] H. Saad, J. Peralta, S. Dennetiere, J. Mahseredjian, J. Jatskevich, J. Martinez, A. Davoudi, M. Saeedifard, V. Sood, X. Wang *et al.*, "Dynamic averaged and simplified models for mmc-based hvdc transmission systems," *IEEE transactions on Power delivery*, vol. 28, no. 3, pp. 1723–1730, 2013.

[56] M. Daryabak, S. Filizadeh, J. Jatskevich, A. Davoudi, M. Saeedifard, V. Sood, J. Martinez, D. Aliprantis, J. Cano, and A. Mehrizi-Sani, "Modeling of lcc-hvdc systems using dynamic phasors," *IEEE Transactions on Power Delivery*, vol. 29, no. 4, pp. 1989–1998, 2014.

[57] J. Kays, A. Seack, T. Smirek, F. Westkamp, and C. Rehtanz, "The generation of distribution grid models on the basis of public available data," *IEEE Transactions on Power Systems*, vol. 32, no. 3, pp. 2346–2353, 2017.

[58] T. Runolfsson, "On the dynamics of three phase electrical energy systems," in *American Control Conference (ACC), 2016*. IEEE, 2016, pp. 6827–6832.

[59] V. Aravinthan, T. Balachandran, M. Ben-Idris, W. Fei, M. Heidari-Kapourchali, A. Hettiarachchige-Don, J. N. Jiang, H. Lei, C.-C. Liu, J. Mitra, M. Ni, M. Papic, M. Parvania, M. Sephary, C. Singh, A. Srivastava, A. Stefanov, H. Sun, and S. Tindemans, "Reliability modeling considerations for emerging cyber-physical power systems." in *2018 IEEE International Conference on Probabilistic Methods Applied to Power Systems (PMAPS)*. IEEE, August 2018, pp. 324–330.

[60] K. R. Davis, C. M. Davis, S. A. Zonouz, R. B. Bobba, R. Berthier, L. Garcia, and P. W. Sauer, "A cyber-physical modeling and assessment framework for power grid infrastructures," *IEEE Transactions on Smart Grid*, vol. 6, no. 5, pp. 2464–2475, 2015.

[61] W. Fei, J. N. Jiang, and D. Wu, "Impacts of modeling errors and randomness on topology identification of electric distribution network," in *2018 IEEE*

International Conference on Probabilistic Methods Applied to Power Systems (PMAPS). IEEE, August 2018, pp. 1–6.

[62] Z. Tian, W. Wu, and B. Zhang, "A mixed integer quadratic programming model for topology identification in distribution network," *IEEE Trans. Power Syst*, vol. 31, no. 1, pp. 823–824, 2016.

[63] A. Garces, "A linear three-phase load flow for power distribution systems," *IEEE Transactions on Power Systems*, vol. 31, no. 1, pp. 827–828, 2016.

[64] J. Yang, N. Zhang, C. Kang, and Q. Xia, "A state-independent linear power flow model with accurate estimation of voltage magnitude," *IEEE Transactions on Power Systems*, vol. 32, no. 5, pp. 3607–3617, 2017.

[65] W. Fei, G. Ji, D. Sharma, and J. N. Jiang, "A new traveling wave representation for propagation of energy transients in power lines from a quantum perspective," in *2018 North American Power Symposium (NAPS)*. IEEE, 2018, pp. 1–6.

[66] T. Yi, Y. Ji-Lai, and L. X. Lin, "An electrical dissecting method of ac branch with facts for ancillary service assessment," in *Power System Technology, 2004. PowerCon 2004. 2004 International Conference on*, vol. 1. IEEE, 2004, pp. 317–321.

[67] G. James, D. Witten, T. Hastie, and R. Tibshirani, *An introduction to statistical learning*. Springer, 2013, vol. 112.

[68] Y. Zhang, M. D. Ilic, and O. K. Tonguz, "Mitigating blackouts via smart relays: a machine learning approach," *Proceedings of the IEEE*, vol. 99, no. 1, pp. 94–118, 2010.

[69] W. Fei and P. Moses, "Modeling power distribution grids through current tracing method," in *2019 IEEE International Conference on Smart Energy Grid Engineering (SEGE)*. IEEE, 2019, pp. 196–200.

[70] C. Pavlatos and V. Vita, "Linguistic representation of power system signals," in *Electricity Distribution*. Springer, 2016, pp. 285–295.

[71] C. Pavlatos, V. Vita, A. C. Dimopoulos, and L. Ekonomou, "Transmission lines' fault detection using syntactic pattern recognition," *Energy Systems*, vol. 10, no. 2, pp. 299–320, 2019.

[72] C. Sammut and G. I. Webb, *Encyclopedia of machine learning and data mining*. Springer Publishing Company, Incorporated, 2017.

[73] S. Bolognani, N. Bof, D. Michelotti, R. Muraro, and L. Schenato, "Identification of power distribution network topology via voltage correlation analysis," in *Decision and Control (CDC), 2013 IEEE 52nd Annual Conference on*. IEEE, 2013, pp. 1659–1664.

DEDICATION

to

My mother

Zhengyan Wang

For

Encouraging me to follow my dreams